SELF-ASSEMBLED MOLECULAR RODS AND SQUARES WITH CHALCOGENADIAZOLE FRAMEWORK LIGANDS

MOHAMMAD ROKIB HASSAN
M.Sc., Jahangirnagar University, Bangladesh, 2003

A Thesis
Submitted to the School of Graduate Studies
Of the University of Lethbridge
In Partial Fulfillment of the
Requirements for the Degree

MASTER OF SCIENCE

Chemistry and Biochemistry
University of Lethbridge
LETHBRIDGE, ALBERTA, CANADA

SELF-ASSEMBLED MOLECULAR RODS AND SQUARES WITH CHALCOGENADIAZOLE FRAMEWORK LIGANDS

MOHAMMAD ROKIB HASSAN

Approved:

René T. Boeré Supervisor	Professor	Ph.D.	Date
Paul G. Hayes Thesis Examination Committee Member	Associate Professor	Ph.D.	Date
Michael Gerken Thesis Examination Committee Member	Associate Professor	Ph.D.	Date
Stephen J. Loeb External Examiner	Professor	Ph.D.	
Ken Vos Thesis Examination Committee	Professor	Ph.D.	Date
Peter Dibble Chair, Defence	Professor	Ph.D.	Date

To all prophets (especially Prophet Mohammad saas.) who sacrificed their lives showing mankind the right path of life

Abstract

During the attempts to carry out Suzuki coupling reactions, the σ-bonded Pd−C_{aryl} benzochalcogenadiazolyl complexes *trans*-[ClPd(PPh_3)$_2$($C_6H_2BrN_2E$)] (E = S, Se) were isolated. The corresponding bromo derivatives were also synthesized on purpose to investigate their activity in Stille coupling reactions. A head-to-tail dimer *trans*-[{ClPd(PPh_3)(μ-$C_6H_2BrN_2Se$)}$_2$] was synthesized from the thermolysis of *trans*-[ClPd(PPh_3)$_2$($C_6H_2BrN_2Se$)] in the presence of SeO_2. The reduction potentials of the mononuclear and dinuclear complexes were measured by cyclic voltammetry (CV) and square wave voltammetry (SWV).

4,7-*bis*(2/4-pyridyl)benzochalcogenadiazole ligands were synthesized by Stille coupling reactions and the 1,5-*bis*(4-pyridyl)naphthalene ligand was prepared by a Suzuki coupling reaction. Reactions of the labile complex [BrRe(CO)$_4$($NCMe$)] with 4,7-*bis*(4-pyridyl)benzochalcogenadiazole ligands in a 2:1 ratio afforded self-assembled molecular rods [{ReBr(CO)$_4$}$_2$(μ-4,7-*bis*(4-pyridyl)benzochalcogenadiazoles)]. Palladium directed molecular squares [(enPd)(μ-4,7-*bis*(4-pyridyl)benzochalcogenadiazole)]$_4$[PF_6]$_8$ were prepared by reactions of enPd(PF_6)$_2$ and 4,7-*bis*(4-pyridyl)benzochalco-genadiazoles in a 1:1 ratio. The optoelectronic properties of the ligands and the molecular rods were investigated by CV and SWV, and by luminescence spectroscopy. The optical properties of the square complexes were also studied by luminescence spectroscopy.

ACKNOWLEDGEMENTS

First and foremost, I would like to express my sincere gratitude to my supervisor Prof. René T. Boeré for the continuous support of my M.Sc. studies and research, for his patience, motivation, enthusiasm, and immense knowledge. His guidance helped me throughout the research and writing of this thesis.

Besides my advisor, I would like to thank the rest of my thesis committee members: Dr. Ken Vos, Dr. Michael Gerken, and Dr. Paul G. Hayes, for their encouragement, insightful comments, and hard questions.

Thanks to the funding agencies Natural Sciences and Engineering Research Council of Canada (NSERC) for chemicals I purchased for my research and Alberta Ingenuity Fund (AIF) for providing me with a Nanotechnology Scholarship.

My sincere thanks also go to Dr. Tracey L. Roemmele and Dr. Ozan Ciftci for helping me to learn voltammetric and fluorescence measurements. Thanks to Craig Wheaton for performing combustion analyses of my samples. I also thank Kris Fischer for his technical help and glass blowing.

To all of the members of the Dibble and Boeré labs, I thank you for assistance and fun in the lab. I also thank Susan Hill for her administrative help.

Thanks to Andrew Hudson for taking the images of my samples under UV and white light. I also thank Dr. Md. Kamar Ali for helping me plot the graphs.

I would like to thank Tony Montina for setting up the diffusion NMR experiment that I have been eagerly awaiting for almost three months and helping me to run the experiment.

Table of Contents

List of Tables

List of Figures

List of schemes

List of abbreviations

Å	Angstrom
AC	Alternating current
ax	axial
BINAP	2,2'-bis(diphenylphosphino)-1,1'-binaphthyl
CCD	Charge-coupled device
CV	Cyclic voltammetry
DPPP	Diphenylphosphinopropane
DPPF	Diphenylphosphinoferrocene
DC	Direct current
DOSY	diffusion ordered spectroscopy
eq	equatorial
ESI	Electro-spray ionization
GC	Glassy Carbon
Hz	Hertz
HSQC	Heteronuclear single quantum coherence
HMBC	Heteronuclear multiple bond coherence
IUPAC	International union of pure and applied chemistry
LED	Light emitting diode
MLCT	Metal to ligand charge transfer
MALDI MS	Matrix-assisted laser desorption ionization mass spectrometry
MM+	molecular mechanics+
nm	nanometer
NMR	Nuclear magnetic resonance
NALDI	Nano-assisted laser desorption ionization
OFET	organic field-effect transistor
PFG	pulsed field gradient
SCE	Saturated calomel electrode
SBI	Secondary bonding interaction
SWV	Square-wave voltammetry
V	Volt

Compound Numbering Scheme

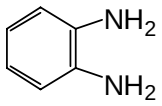

1

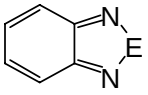

E = S, **2**
E = Se, **4**

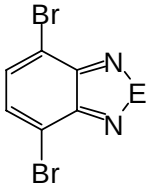

E = S, **3**
E = Se, **5**

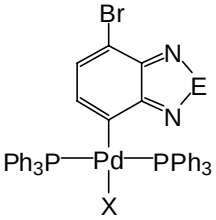

E = S; X = Cl, **6a**
E = S; X = Br, **6b**
E = Se; X = Cl, **7a**
E = Se; X = Br, **7b**

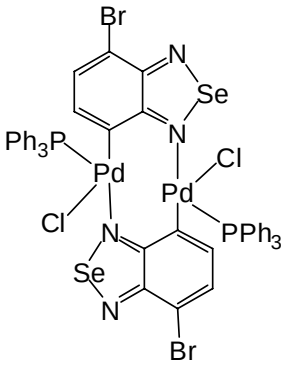

8

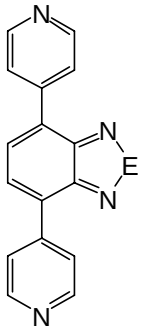

E = S, **9**
E = Se, **11**

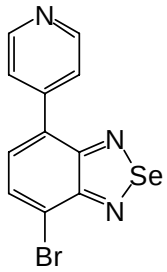

10

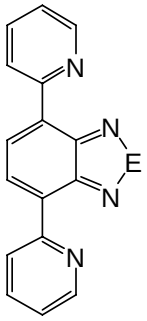

E = S, **12**
E = Se, **13**

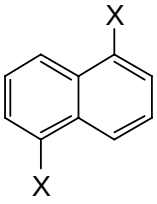

X = NH_2, **14**
X = Br, **15**

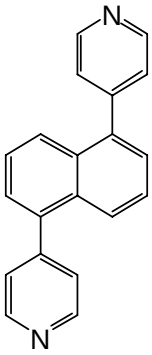

16

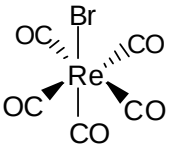

17

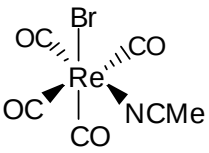

18

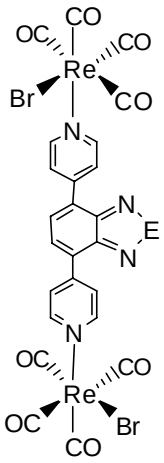

E = S, **19**
E = Se, **20**

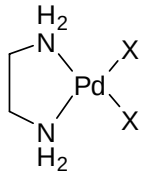

X = NO_3, **21**
X = PF_6, **22**

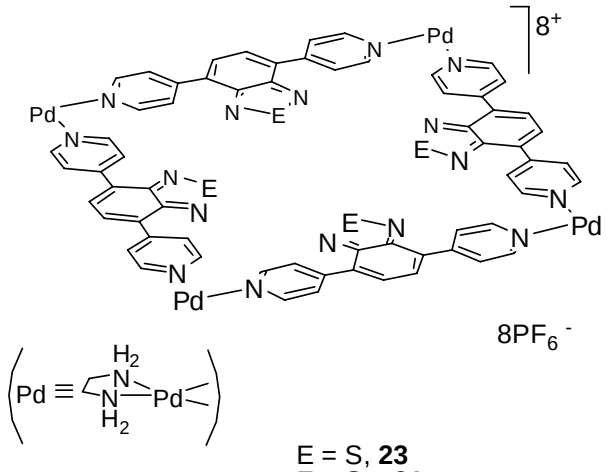

E = S, **23**
E = Se, **24**

Compounds **6**-**8**, **10**, **11**, **13**, **16**, **19**, **20**, **23** and **24** are novel.

CHAPTER ONE: INTRODUCTION

1.1 Introduction

There are two different well established approaches to building nanostructured materials: (i) "top-down" and (ii) "bottom-up" approaches.[1] In the top-down approach, a macrosized material is reduced in size to reach nanoscale dimensions, whereas in the bottom-up approach, molecular building blocks are assembled together to get the desired nanostructure. Self-assembled supramolecular architectures are constructed from relatively simple starting materials by combining complementary pairs of two molecular components. The use of metallic units as building blocks for making self-assemblies has emerged as a promising route towards functional metal-containing nanomaterials in bottom-up nanotechnology. The most fundamentally important aspect of the bottom-up approach is that the resulting nanostructures possess rich functions such as redox, optical, catalytic and magnetic properties heretofore unavailable in conventional materials.[1c] In this thesis, the synthesis of metal-directed self-assembled supramolecular complexes by applying the bottom-up approach will be discussed. In these self assemblies, redox-active heterocycles such as benzochalcogenadiazoles, are incorporated for the first time. The optoelectronic properties of the heterocyclic linkers as well as their assemblies are investigated to find their possible applications in material science. In this chapter, after a brief review of the literature relevant to the thesis topics, the theory behind the photonic and electrochemical methods used in this thesis will be discussed.

1.2 Chemistry of heterocyclic ring systems

1.2.1 Overview and scope

Over the last few decades, considerable advances have been made in the synthesis of redox-active heterocycles containing several Group 15 and 16 elements in search of their applications to materials science and biochemistry.[2] The purpose of this intensive research is to develop molecular conductors, superconductors and molecular magnets. Compared to the other heterocyclic systems, the S/Se,N heterocycles have been extensively explored and the driving force behind the development is their unique conducting and superconducting properties.[2e] These S/Se,N heterocycles include four-, five-, six-, seven- and eight-membered ring systems (Figure 1.1).[2e] Of greatest interest for applications to both conducting and magnetic systems are those species which have easily attainable and reversibly inter-convertible redox states. Indeed Group15/16 heterocycles are one of the most abundant compound classes where such special properties are observable.

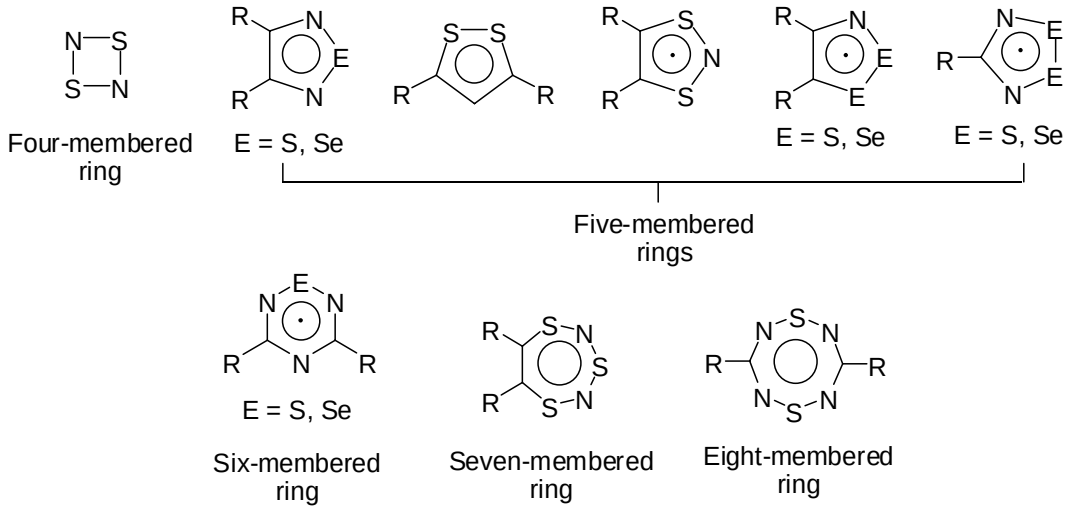

Figure 1.1 Different binary S/Se,N heterocyclic ring systems

1.2.2 2,1,3-chalcogenadiazoles

1.2.2.1 Synthesis of 2,1,3-chalcogenadiazoles

In addition to a number of general reviews,[2a, 3] the following specific aspects of the chemistry of C–N–E (E = S, Se) containing compounds have been the subject of comprehensive surveys: coordination chemistry,[4] electrochemistry,[2e] radical chemistry[2d,5] and magnetic properties[6]. Five-membered heterocycles have been by far the most studied, which include both diamagnetic and paramagnetic ring systems (Figure 1.1). However, the chemistry of 2,1,3-benzothiadiazole systems and their heavier chalcogen analogues has also been extensively investigated.[7, 8] 2,1,3-benzochalcogenadiazoles (E = S, Se) are usually synthesized by condensation reactions of sulfur halides or selenium dioxide with *o*-phenylenediamine (Figure 1.2).[7d, e, 8] The corresponding tellurium analog could also be synthesized by a condensation reaction of tellurium dioxide or tellurium tetrachloride with *o*-phenylenediamine (Figure 1.2).[9]

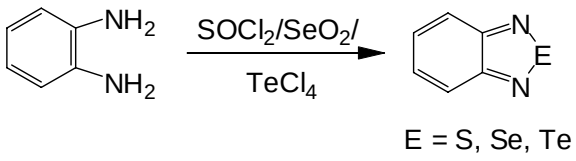

Figure 1.2 Synthesis of different benzofused chalcogenadiazole rings

1.2.2.2 Electrochemistry of 2,1,3-benzochalcogenadiazoles

In the neutral form, 2,1,3-benzochalcogenadiazoles are $2n + 2 = 10\pi$ ring systems where four electrons came from the =N–E–N= or –N=E=N− unit, indicating that they are incapable of forming neutral radicals. The redox processes of the benzothia- and selenadiazoles have been examined by electrochemistry demonstrating the stability of the mono-anion, where the −1/0 process involves addition/removal of electrons from the π-

LUMO (Figure 1.3).[2e] The redox process of the corresponding 2,1,3-benzotelluradiazole could not be examined by cyclic voltammetry due to low solubility.[10] The 0/+1 process was observed only for E = S which involves removal/addition of electrons from the π-HOMO (Figure 1.3).[2e] It should be noted that the −1/0 process for E = Se is +0.13 V more anodic compared to the analogous benzothiadiazole, indicating that the selenadiazole ring has a higher electron affinity, which makes it more easily reduced (Table 1.1). This is due to the larger polarizability of the selenium atom causing a lowering of the energy of the π-LUMO in the benzoselenadiazole ring.[11]

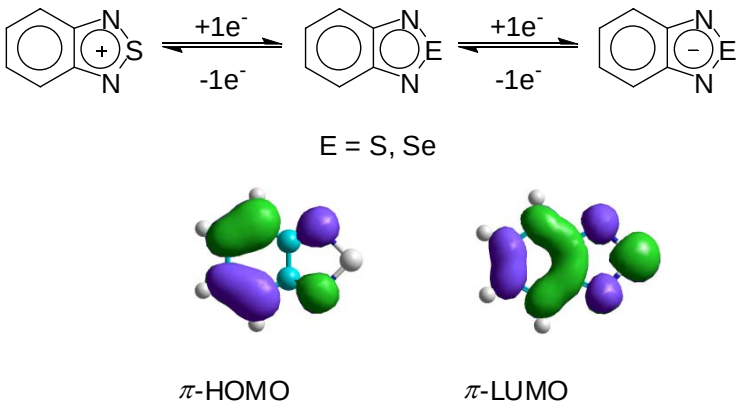

Figure 1.3 Redox processes in chalcogenadiazoles

Table 1.1 Electrochemical data for 2,1,3-benzothia- and selenadiazoles[2e]

Compound	Process[a]	Potentials (V)[b]	Comments[c]
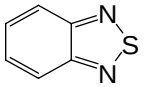	−2/−1	−2.88	IR at RT
	−1/0	−1.89	R at RT
	0/+1	+1.82	
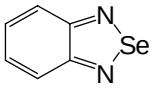	−2/−1	−2.68	IR at RT
	−1/0	−1.76	R at RT

[a]Expressed in terms of the redox couples relative to Fc as 0.0 V in accordance with current IUPAC recommendations. [b]Expressed as the half-wave potential from polarography for reversible systems, unless otherwise noted. The values are modified by a conversion constant of −0.380 V for GC electrode from SCE.[2f] [c]R = reversible; IR = irreversible

1.2.2.3 Secondary bonding interactions in 2,1,3-chalcogenadiazoles

In contrast to thiadiazoles, the heavier chalcogen analogues have more tendency to form associated structures through two antiparallel E---N secondary bonding interactions (SBIs) as a result of the high polarity of the E−N bonds, forming four-membered cyclic "supramolecular synthons" (Figure 1.4a). The 2,1,3-benzotelluradiazole has a polymeric structure and the Te−N distances within the monomeric units are 2.02(3) Å, typical of single bonds, while the intermolecular contacts are 2.76(4) Å.[12]

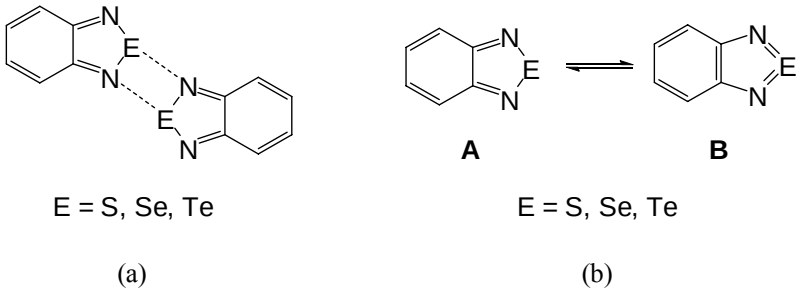

Figure 1.4 (a) Supramolecular synthons; (b) Resonance structures in benzochalcogenadiazoles

On the other hand, the short contact distances in selena- and thiadiazoles are 2.95(3) and 3.20(2) Å, respectively.[13] When the average SBI distances are compared to the sums of the corresponding van der Waals radii of the atoms, the two parameters change inversely with the SBIs in benzotelluradiazole being the strongest (Table 1.2). In addition to intermolecular interactions in the solid state, the relative importance of the two resonance structures A and B is an important issue in the structural determinations of selena- and telluradiazoles.[14a] The Se−N bond lengths fall within the range 1.78-1.81 Å and the Te−N bond lengths are 2.00-2.05 Å compared to single bond distances of 1.86 and 2.05 Å, respectively. Therefore it can be concluded that resonance structure **A** is more important

than **B** for the selenium and tellurium systems, which is consistent with weaker E−N π-bonds for the heavier chalcogens (Figure 1.4b).

Table 1.2 SBI Distances (Å) in 2,1,3-Chalcogenadiazoles

E	S	Se	Te
$r_{EvdW} + r_{NvdW}$[15]	3.35	3.45	3.65
E---$N_{(average)}$	3.20	2.95	2.76
% of E---N contact distance shortening	4.5	14.5	24.4

X-ray structure determinations of thiadiazoles indicate π-delocalization in the heterocyclic ring and, in the case of benzo derivatives, quinoidal character for the benzene ring, suggesting contributions from both resonance structures **A** and **B** (Figure 1.3b).[14b]

1.3 Metal-directed self-assembled supramolecular architectures

Over the last 15 years, major efforts have been dedicated to metal-directed self-assembly of discrete two- and three-dimensional structures using molecules with terminal pyridyl substituents.[16] This continuing interest is evidenced by the multitude of assemblies that have been reported in the recent literature.[16a,b] On the basis of this self-assembly strategy, numerous polygonal metallomacrocycles such as triangles, squares, pentagons, hexagons and molecular cages have been synthesized in the last decades.[16a,b] The interest in these supramolecular objects is partly aesthetic because these assemblies afford beautiful high-symmetries. However, the interest is also functional because the cavities of these metal-directed self-assemblies can accommodate various guest molecules offering new properties such as reactivity,[17a] selective aggregation[17b] and stable dinucleotide duplex formation[17c] which are not possible by traditional methods.

1.3.1 Ionic metal directed self-assembled molecular squares

The first crucial step towards the synthesis of self-assembled molecular squares is to design a metal center as a corner unit that can offer a 90^o coordination angle, and a linear ligand that can associate with the metal center to give the desired square assembly (Figure 1.5). The reason for selecting [enM$(NO_3)_2$] (M = Pd, Pt) as corner units is that it is a classical cis-chelated metal complex known for many years which affords a stable *cis*-capped metal unit. Thus, to form a square complex, four linear ligands such as 4,4′-bipyridine are necessary for bonding with four [enM(II)]$^{2+}$ units.

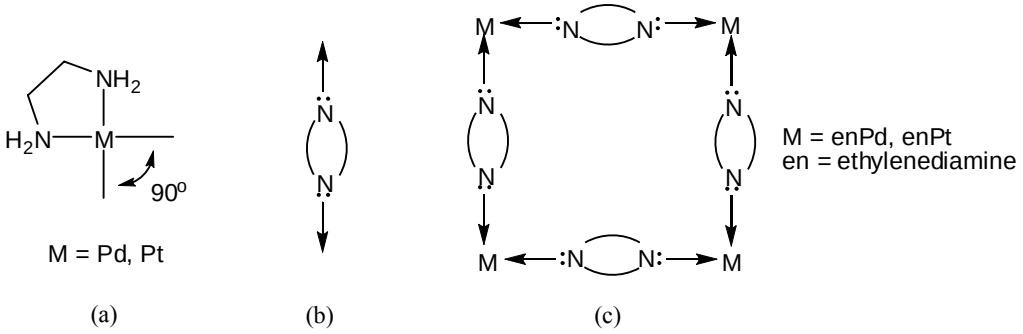

Figure 1.5 (a) 90^o Coordination angle in [enM$(NO_3)_2$], (b) Linear dipyridyl ligands, (c) metal square complex

Fujita and co-workers first demonstrated the synthesis of a palladium-directed molecular squares from the reaction of enPd$(NO_3)_2$ and 4,4′-bipyridine in an aqueous-alcohol solution in quantitative yield (Figure 1.6a).[18a] The formation of molecular squares was inferred by NMR spectroscopy which shows only two doublets in the aromatic region for pyridine ring protons without any proton signals for intermediate compounds. The proton signals are considerably downfield shifted due to the metal coordination compared to the free ligand. Later, the formation of the molecular square was proven by X-ray crystallography. They have investigated the mechanism for the square formation

suggesting that the cyclization is a thermodynamic controlled process where the product distributions only depend on the stability of the products themselves and occurred in a stepwise fashion (Figure 1.7).[19]

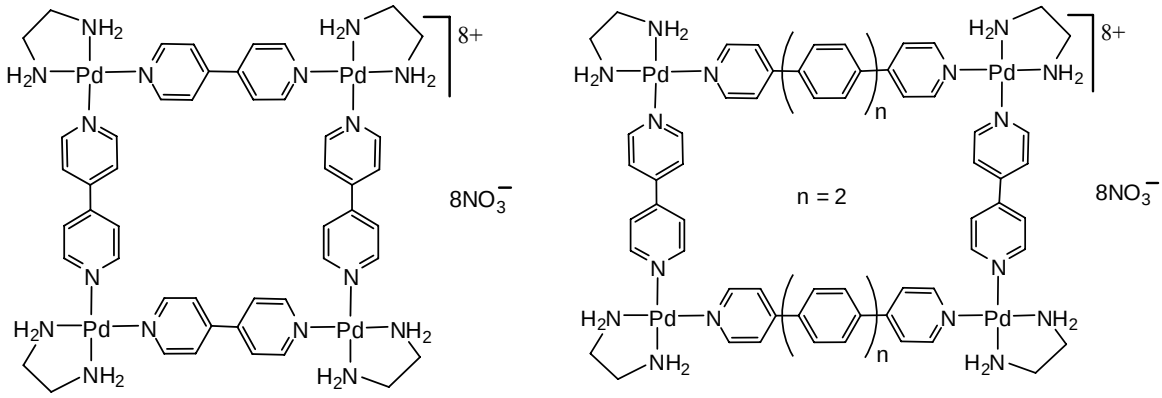

Figure 1.6 Palladium-directed molecular squares

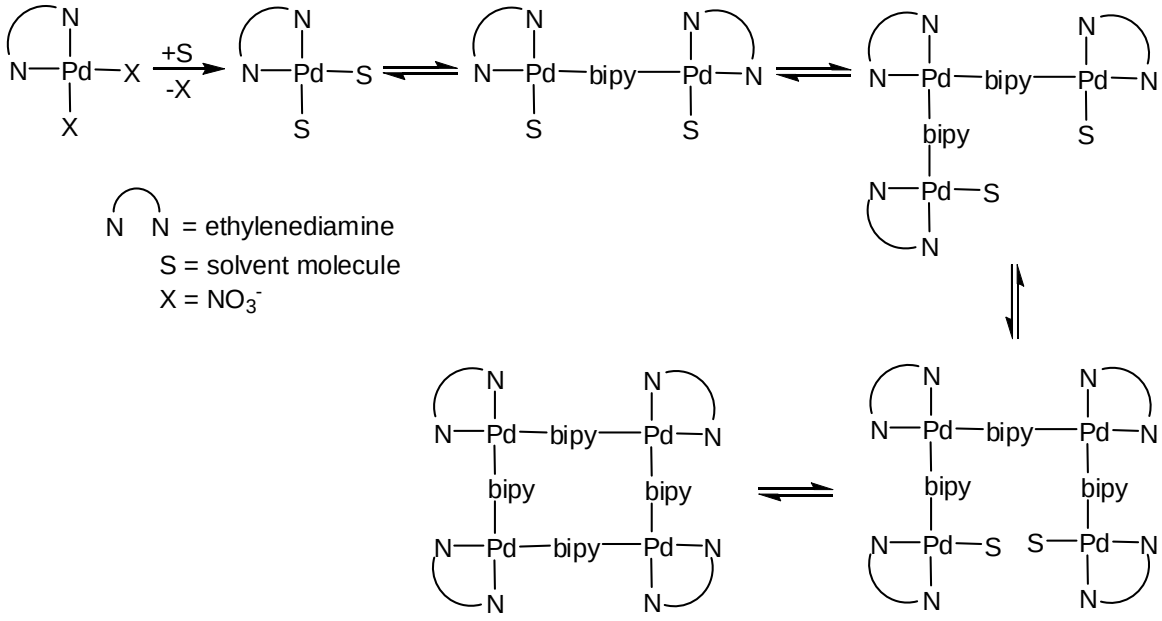

Figure 1.7 Proposed mechanism of molecular square formation (counter ions and charges are omitted for added clarity)

This is because of several reasons, namely: (i) aqueous solvent that causes hydrophobic effects, (ii) the open ligation sites are temporarily filled by weakly coordinated solvent molecules which keep the intermediates in solution, and (iii) the enthalpy released upon replacement of weak metal−solvent bonds with stronger metal−ligand bonds.[19a] A few years later, Fujita *et al.* also reported a new strategy for controlling a multicomponent assembly from two kinds of pyridine-based ligands (Figure 1.6b).[18b]

Since this initial work, the combination of palladium/platinum corner blocks and a variety of different pyridine-substituted ligands leading to the formation of molecular squares has been examined by many research groups.[20] The versatility of this approach was intensively developed by Stang and coworkers, who prepared organic soluble squares, chiral squares, crown-, ferrocene- and porphyrin-conjugated squares and hypervalent element-hybrid squares (Figure 1.8).[21]

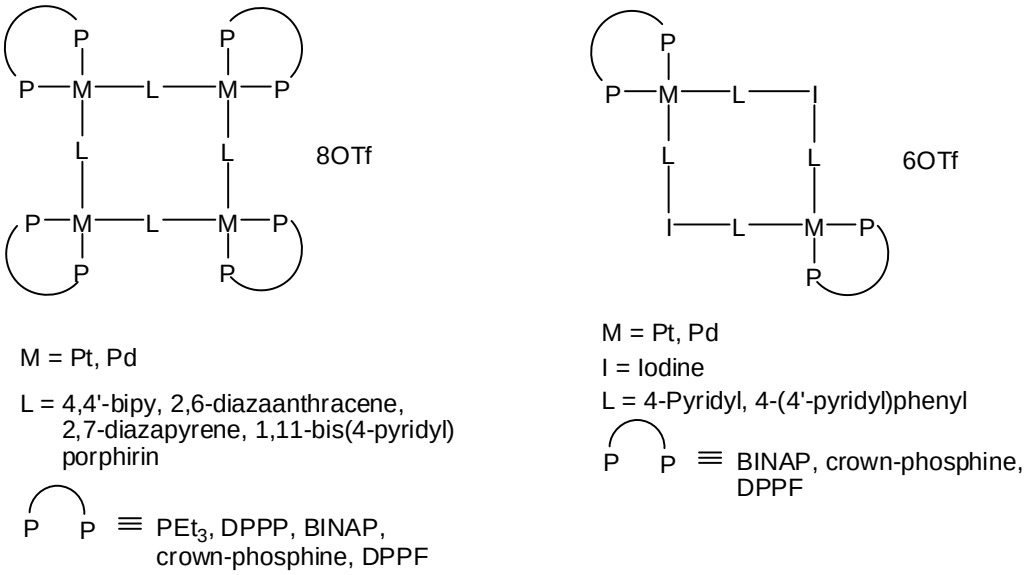

Figure 1.8 Organic soluble molecular squares (charges omitted)

This relies upon Pd(II) and Pt(II) as corners but with chelating diphosphine ligands in place of ethylenediamine to provide solubility in organic solvents and to enforce

subsequent *cis* coordination. With metal-directed chiral molecular squares, one could easily envision applications such as enantioselective catalysis, separation, or sensing.[19a] Very recently Quintela et al. have reported the synthesis of new dinuclear square and quadrangular metallocycles from the reaction of enM$(OTf)_2$ (M = Pd, Pt) with different pyridinium ligands and explored their catenation reactions with cyclophanes (Figure 1.9).[22]

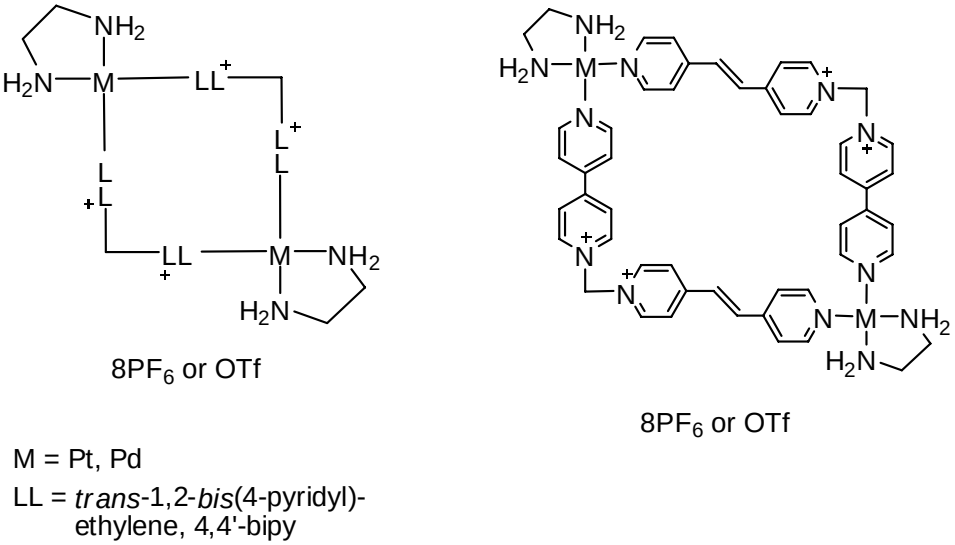

Figure 1.9 Dinuclear square and quadrangular metallocycles (charges omitted)

Thus, over the years several groups have designed and developed methods for the quantitative formation of molecular self-assemblies by mixing metal corner units and different pyridine-substituted organic ligands to make families of architectures, such as cages, bowls, boxes, tubes, catenanes and spheres.[16a, b]

1.3.2 Neutral metal-directed self-assembled molecular squares

Besides the synthesis of ionic self-assembled molecular complexes, considerable effort has been made in the past few years to prepare organometallic self-assemblies using metal carbonyls as corner units.[23] The first metal-containing neutral molecular squares

were reported in 1983 and the authors featured $M(CO)_4$ (M = Cr, Mo, W) as corner units and $P(OCH_2)_3P$ as linkers (Figure 1.10a).[23a] Neutral squares can also be obtained by linear difunctional ligands, and Leadbeater et al. first demonstrated the synthesis of such neutral homo- and heterometallic squares from the photochemical reaction of $M(CO)_6$ (M = Cr, Mo) and 4,4′-bipyridine (Figure 1.10b).[23b]

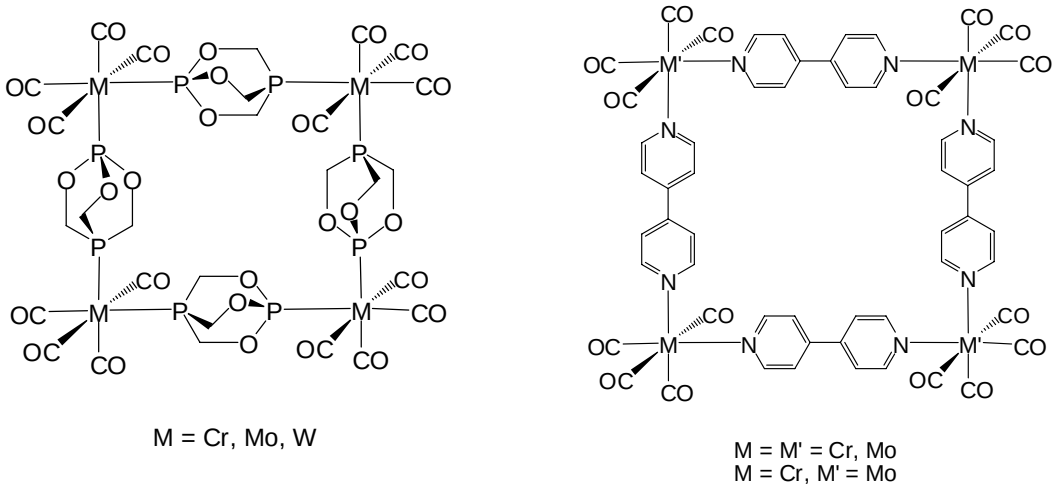

(a) (b)

Figure 1.10 Group 6 metal directed molecular squares

The purification of these squares often faces difficulties as they are air- and moisture-sensitive at room temperature and stick to silica. Hence, differential solubility effects were used as an effective purification method of the squares. Firstly, as the staring materials $M(CO)_6$ are soluble in non-polar solvent, the reaction mixture was washed a couple of times with hexane to remove $M(CO)_6$ from the mixture and then the recrystallization of the solid residues from dichloromethane leads to an effective purification of squares. As a consequence of instability of the metal-ligand dative bonds, most often it is not possible to observe the parent ion of the molecular square formation by mass spectrometry.[23b] However, it is possible to get a confirmatory mass for rhenium-

directed molecular squares by FAB-MS analyses, which is probably due to the high stability of the rhenium-ligand dative bond compared to the Group 6 metal squares.

Compared to Group 6 metal-directed molecular squares, a series of luminescent homometallic neutral molecular squares has been assembled by using $Re(CO)_5X$ (X = Cl, Br) as corner units.[23c-g] Hupp and co-workers first reported the synthesis of rhenium directed molecular squares containing pyrazine, 4,4′-bipyridine and 1,2-*bis*(4-pyridyl)ethylene as linkers in nearly quantitative yield (Figure 1.11a).[23c] They have also explored the synthesis of square complexes by using picolinoate and porphyrin based pyridyl ligands.[23g] A few years later, Lu and co-workers performed thorough mechanistic studies of the self-assembly process of rhenium-based molecular squares and synthesized rhenium macromolecules with mixed linker units (Figure 1.11b).[23d,e]

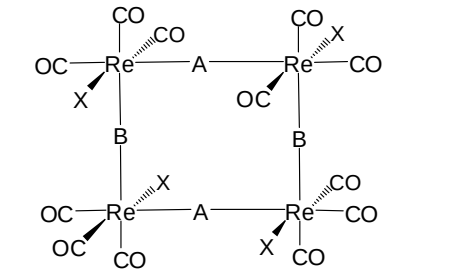

(a)

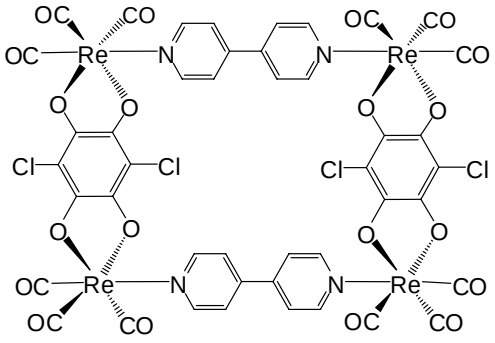

(b)

Figure 1.11 Rhenium-directed molecular squares

Rhenium-directed self-assembled complexes have attracted much attention due to the behavior of singlet and triplet metal-to-ligand charge transfer (MLCT) excited states which are key to their efficient use in photonic applications.[24] For example, upon optical excitation rhenium containing chromophores give MLCT singlet states and then, by

intersystem crossing (ISC) strongly phosphorescent triplet states are generated from the singlet states. Remarkably, almost all molecular squares, whether ionic or neutral, crystallize as one-dimensional channel-containing materials which lead to the formation of thin films, with square cavities defining the channel width. Microcrystallinity typically persists in thin films for smaller squares, whereas for larger squares such thin films are more typically amorphous.[19a] Very recently, MacLachlan and co-workers have observed the columnar aggregation of platinum-directed self-assembled molecular squares by π-π interactions even in solution.[25] This columnar aggregation facilitates the formation of amorphous thin films and hinders formation of crystalline materials.

1.4 Optoelectronic techniques

1.4.1 Voltammetry

Voltammetry is a type of electrochemical technique which deals with the study of electrode reactions and interfacial properties of redox-active substances with a view to characterizing electrochemical redox reactions. The objectives of electrochemistry include quantitative analysis of species of interest in biological systems (for example, brain electrochemistry) as well as for environmental monitoring.[26] Furthermore, voltammetry is used as a powerful tool to guide battery technology or fuel cell development research. Another important practical challenge which interests electrochemists is solar energy conversion, including the development of practical systems that mimic biological photosynthesis. Though the basic theory and practice of voltammetry is the same for all of these above mentioned applications, a variety of modifications and optimizations of the basic technique are essential for some of these applications.

The following information documented here is largely based on standard text book presentations.[26a-c] The common feature of all voltammetric experiments is that a potential perturbation is applied to the working electrode and the resulting current response associated with the redox process (transfer of one or more electrons) is measured as a function of potential. DC linear sweep, DC cyclic, square-wave, pulsed, AC and Fourier, and hydrodynamic voltammetries are considered as a family of techniques that belong to voltammetry. The important time-dependent aspect of both DC linear sweep and cyclic voltammetry (Figure 1.12) is the scan rate (ν) with which the potential of the working electrode is ramped as a function of time (dE/dt).

1.4.1.1 Cyclic voltammetry (CV)

Cyclic voltammetry is the most widely used technique by electrochemists who are interested in understanding the qualitative aspects of the mechanism of a Faradaic electrode process in the solution phase. It offers a rapid determination of *redox potentials* of the electro-active species. When the DC potential is swept linearly in one direction and then reversed at a fixed scan rate (ν), and a repetitive sequence is observed (Figure 1.12a), this technique is known as cyclic voltammetry. Experimentally, the potential is swept from an initial potential (E_1) to a second potential E_2 (Figure 1.13a). After reaching E_2, the potential returns to E_1 by sweeping in the reverse direction. At this point the scan might be halted and again reversed or continued to a third potential E_3 (Figure 1.12a). Graphically the resulting cyclic voltammogram displays the current dependence as a function of the potential difference between the reference and working electrodes (Figure 1.12b). Voltammetric measurements are carried out using an electrochemical cell made

up of three electrodes immersed in a solution containing the analyte and an excess of a nonreactive electrolyte called the supporting electrolyte (Figure 1.13b).

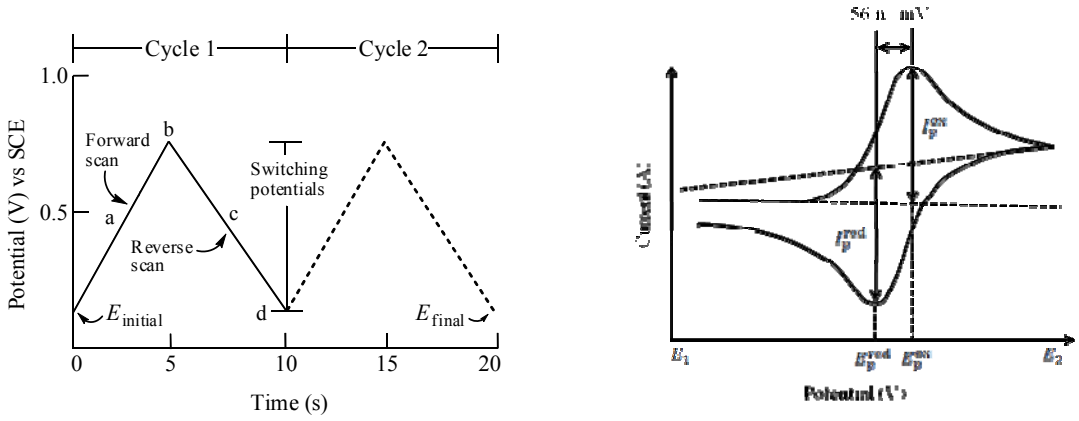

(a) (b)

Figure 1.12 (a) An example of a typical waveform used in DC voltammetric experiments. (b) Typical (ideal) cyclic voltammogram obtained for a reversible one-electron oxidation process at 25 °C "Adapted from Eklund, J. C.; Bond, A. M.; Alden, J. A.; Compton, R. G. *Adv. Phys. Org. Chem.* **1999**, *32*, 1"

The three electrodes are: (i) the working electrode where the redox reaction takes place, (ii) the reference electrode which provides calibration for the applied potential, and (iii) the auxiliary electrode, which is often a platinum wire that simply serves to conduct electricity from the signal source through the solution to the other electrodes. Most of the actual current flow occurs between the auxiliary and working electrodes, leaving the reference electrode essentially unchanged. A typical electrode reaction involves the transfer of charge between an electrode and a species in solution (eq. 1.1).

$$A_{soln} + e^- \underset{k_b}{\overset{E^o,\, k_f,\, \alpha}{\rightleftharpoons}} B_{soln} \qquad 1.1$$

Where, k is the heterogeneous rate constant (cm s^{-1}) for the forward and reverse reaction, E^o is the formal electrode potential, and α is the transfer coefficient. The electrode reaction, usually referred to as electrolysis, typically involves a series of steps: Reactant (A) moves to the interface by diffusion, migration or convection. The CV experiments are carried out under stationary solution conditions; hence, diffusion is the sole form of mass transport. Electron transfer can then occur between the electrode and reactant close to the electrode. Once the product (B) is formed by the heterogeneous electron-transfer reactions, it moves away from the electrode to allow fresh reactants to diffuse to the surface.

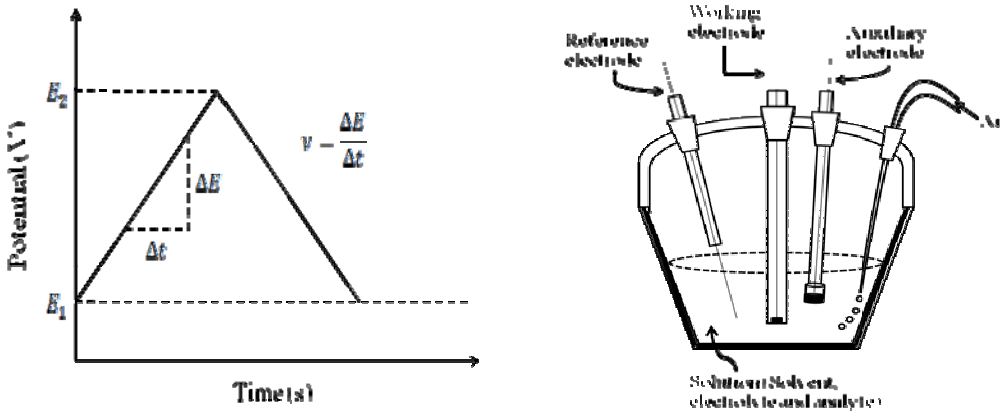

(a) (b)

Figure 1.13 (a) Potential-time profile used in a typical voltammetric experiment, (b) Typical cell design employed for CV studies in non-aqueous solution "Adapted from Eklund, J. C.; Bond, A. M.; Alden, J. A.; Compton, R. G. *Adv. Phys. Org. Chem.* **1999**, *32*, 1; Roemmele, T. L. *PhD thesis* 2009"

Normally homogeneous chemical reactions proceed with an electron-transfer step where the electron-transfers between the reacting species is taking place. Hence, a combination of both heterogeneous electron-transfer and homogeneous chemical reaction steps could

be observed in an electrochemical reaction mechanism. If the product B undergoes a first-order solution-phase chemical reaction with a rate constant of k^o:

$$\mathbf{C} \quad B \xrightarrow{k^o} C$$

then a complete description of the electrode process when the initial charge-transfer step is reversible is given by the reaction scheme:

$$\mathbf{E} \quad A + e^- \underset{}{\overset{E_1^o,\, k_1,\, \alpha_1}{\rightleftharpoons}} B$$

$$\mathbf{C} \quad B \xrightarrow{k^o} C$$

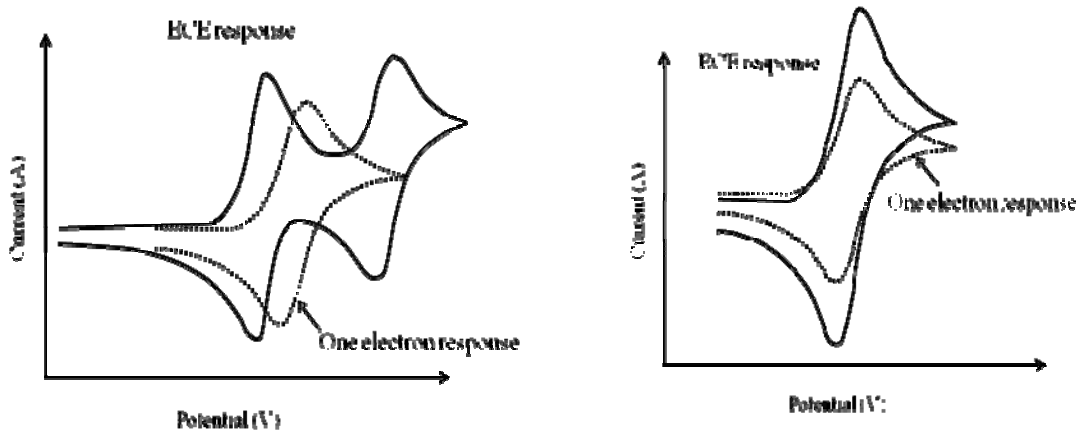

(a) (b)

Figure 1.14 Cyclic voltammograms associated with an oxidative **ECE** process (a) two resolved one electron transfer process, (b) single overall two electron transfer process "Adapted from Eklund, J. C.; Bond, A. M.; Alden, J. A.; Compton, R. G. *Adv. Phys. Org. Chem.* **1999**, *32*, 1"

This is referred to as the **EC** (or **E**rev**C**irrev) mechanism where the electrode step is labeled as **E** and the chemical step is labeled as **C**. The **EC** mechanism is the simplest example of a coupled homogeneous chemical reaction. A slightly more complex but

common electrode reaction mechanism encountered in voltammetric studies is the **ECE** (e.g. **E**rev**C**irrev**E**rev) mechanism. In **ECE** mechanism, the first step is similar to the **EC** process but the chemical reaction product C undergoes further electron transfer reaction giving product D and for reversible electron transfer process:

$$\mathbf{E} \quad C + e^- \overset{E_2^{\circ},\, k_2,\, \alpha_2}{\rightleftharpoons} D$$

For this ECE mechanism, the voltammogram may consist of either two resolved one electron transfer processes (Figure 1.14a) or a single overall two electron transfer process (Figure 1.14b).

1.4.1.2 Square-wave voltammetry (SWV)

Square-wave voltammetry is a large-amplitude differential technique that can be applied to both electro-kinetic and analytical measurements.[27] In SWV typically a symmetrical square-wave pulse superimposed on a base staircase potential, is applied to the working electrode (Figure 1.15a). The net current is obtained by taking the difference between the forward and reverse currents which are sampled at the end of the forward pulse and then at the end of the reverse pulse in each square-wave cycle. The peak height is directly proportional to the concentration of the electroactive species. Because of the very large modulation amplitude of the square-wave, the reverse pulses cause the reverse reaction of the product (of the forward pulse). Figure 1.15b, represents a dimensionless plot of the forward, reverse, and difference currents for a reversible process. The peak-shaped voltammogram is symmetric about the half-wave potential for reversible processes.

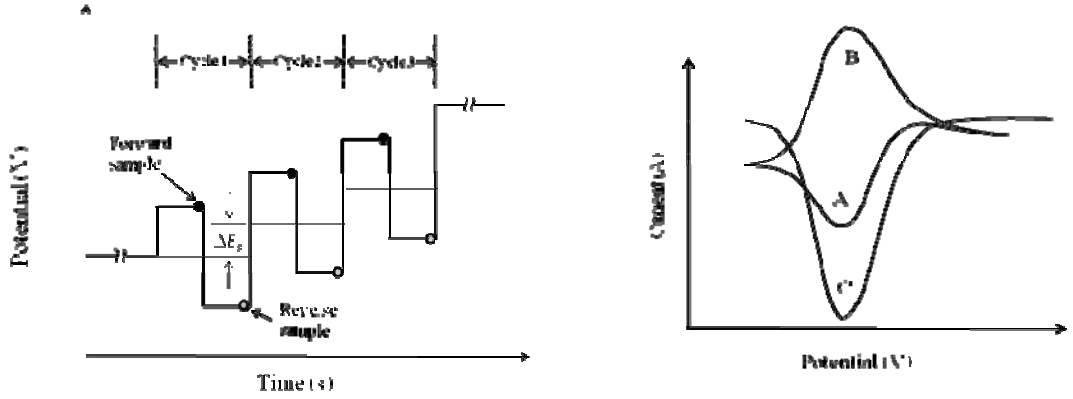

(a) (b)

Figure 1.15 (a) Waveform and measurement scheme for square wave voltammetry, (b) Square-wave voltammograms for reversible electron transfer: (curve A) forward current; (curve B) reverse current; (curve C) net current "Adapted from Wang, J. *Analytical electrochemistry*, 3rd Ed, New York: Wiley-VCH, 2006"

The net current is larger than either the forward or reverse components because it is the difference between them. Square-wave voltammetry is advantageous due to its speed. The effective scan rate ($f\Delta E_s$) is simply the multiplication of the frequency (in Hz) and the step height (Figure 1.15a). For example, if ΔE_s = 10 mV and f = 50 Hz, then the effective scan rate is 0.5 V/s. Hence a complete voltammogram can be recorded within a few seconds as the analysis time is significantly reduced, compared to the differential-pulse voltammetry which takes about 2-3 minutes.

1.4.2 Ultraviolet (UV) and Luminescence spectroscopy

1.4.2.1 UV spectroscopy

The topic under discussion is based on standard text book presentations.[28] Ultraviolet-visible spectroscopy (UV-Vis) refers to electronic spectroscopy which typically occurs

due to the absorption of light by a chromophore (atoms or molecules) in the ultraviolet-visible spectral region. The absorption of light which occurs in the visible range directly affects the perceived color of the chemicals involved.[28] As a result of energy absorption, atoms or molecules pass from a state of lower energy (the ground state) to a state of higher energy (the excited state) (Figure 1.16a) by electron excitation.

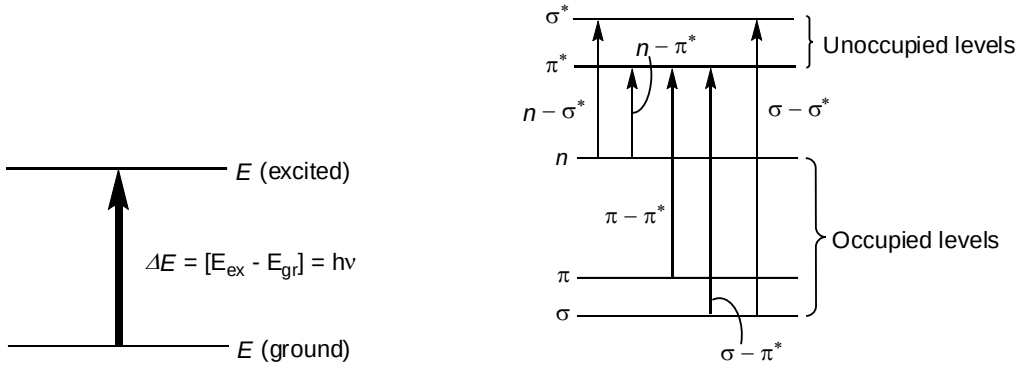

(a) (b)

Figure 1.16 (a) The excitation process, (b) Orbital energy level diagram and possible electronic transitions between the bonding (σ, π), non-bonding (n) and anti-bonding (σ^*, π^*) orbitals "Adapted from Pavia, D. L.; Lampman, G. M.; Kriz, G. S. *Introduction to Spectroscopy*, 3rd Ed, Thomson Brooks/Cole, 2001, 353"

The energy of the electromagnetic radiation absorbed by a chromophore is equal to the energy difference between the excited and ground states. In UV spectroscopy, the transitions that result in the absorption of electromagnetic radiation are taken place between different electronic energy levels. Normally the most probable transition occurs from the highest occupied molecular orbital (HOMO) to the lowest unoccupied molecular orbital (LUMO). For most molecules, the energy differences between electronic levels vary from 125 to 650 kJ/mol. Evidently, the energy required to carry out transitions from

the HOMO to the LUMO is less than the energy required to bring about a transition from a lower occupied energy level. This indicates that $n \rightarrow \pi^*$ transition has lower energy than $\pi \rightarrow \pi^*$ transition (Figure 1.16b). The choice of the solvent is crucial to perform UV experiments. For example, the solvent used for the experiments should not absorb ultraviolet radiation in the same region where the substance under investigation absorbs. Typically non-conjugated solvents are most suitable for this purpose avoiding the interference of the absorptions. Peaks resulting from $n \rightarrow \pi^*$ transitions are shifted to shorter wavelengths (*blue shift*) with increasing solvent polarity. This arises from increased solvation of the lone pair, which lowers the energy of the *n* orbital. On the other hand polar solvents shift the $\pi \rightarrow \pi^*$ transition to longer wavelength.

Many inorganic compounds show charge-transfer (CT) absorptions in addition to excitations that are either metal-centred or ligand-centred. To exhibit charge-transfer behavior, compounds should have two components where one shows electron donating properties and the other shows electron accepting properties. Metal-to-ligand charge-transfer (MLCT) transitions occur due to the transfer of electrons from the metal atom to the ligand.[28] This feature is most commonly observed in complexes with ligands having low-lying π^* orbitals, especially aromatic ligands. The transition occurs at low energy (longer wavelength) for a metal ion in low oxidation state where the *d* orbitals have relatively high energy.

1.4.2.2 Luminescence spectroscopy

The following treatment of luminescence is based on the description presented in J. R. Lakowicz, *Principles of Fluorescence Spectroscopy*, 4th Ed, Springer, 2006, Chapter 1.

Luminescence refers to the emission of light from any substance that takes place from electronically excited states. Depending on the nature of the excited state luminescence is classified into the categories: *fluorescence* and *phosphorescence*. The electron in the excited orbital (singlet state) caused by the absorption of light is paired by an opposite spin to the second electron in the ground state orbital indicating that returning to the ground state is spin allowed. As a result when the electron decays back to the ground state rapid emission of a photon takes place. This emission is known as fluorescence where the emission rate is 10^8 s^{-1}, indicating that the fluorescence lifetime is near about 10 ns. On the other hand, phosphorescence is the emission of light which occurs from triplet excited states. The lifetime of phosphorescence is usually longer than fluorescence and can range from milliseconds to seconds. This is because the electron in the triplet state has the same spin orientation as the ground state electron which causes to reduce the emission rate. Hence phosphorescent compounds glow for a while and slowly decays back to the ground state. Normally phosphorescence is not observed in fluid solutions at ambient temperature due to many deactivation processes that compete with emission, such as non-radiative decay and quenching processes.

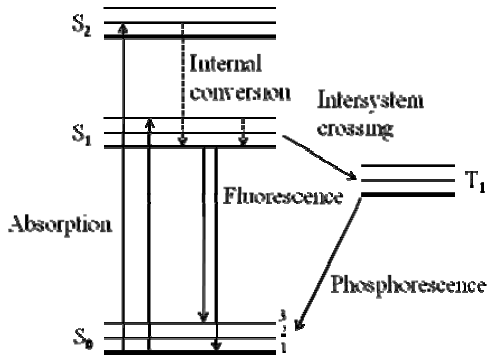

Figure 1.17 One form of a Jablonski diagram "Adapted from Lakowicz, J. R. *Principles of Fluorescence Spectroscopy*, 4th Ed, Springer, 2006, Chapter 1"

Transition metal-ligand complexes (TMLCs) display mixed singlet-triplet states with intermediate lifetimes of hundreds of nanoseconds to several microseconds. Figure 1.17 represents a Jablonski diagram where the singlet ground, first, and second electronic states are depicted by S_0, S_1, and S_2, respectively. The fluorophores can exist in a number of vibrational energy levels at each of the electronic energy levels depicted by 0, 1, 2, etc. The energy difference between the ground state S_0 and the first excited state S_1 is very large. Due to this large energy difference, thermal population of electrons to S_1 is not possible, and hence light is used to induce fluorescence instead.

Upon light absorption, a fluorophore is usually excited to higher vibrational levels of S_1 or S_2 electronic states and within a very short period of time molecules rapidly relax to the lowest vibrational level of S_1. This process of rapid relaxation is known as internal conversion which occurs within 10^{-12} s or less, and because of this rapid relaxation, emission spectra are usually independent of the excitation wavelength. This internal conversion is generally complete prior to emission. Hence, fluorescence emission results from the lowest energy vibrational state of S_1. This leads to a lower average energy of the emitted light compared to the absorbed light. This difference is known as the Stokes shift.

When molecules in S_1 undergo a spin conversion to the first triplet state T_1 then the emission from T_1 is known as phosphorescence. Generally the phosphorescence emissions occur at longer wavelength (lower energy) and lower intensity compared to the fluorescence emission. The spin conversion from S_1 to T_1 is called intersystem crossing. As the transition from T_1 to the singlet ground state is forbidden the phosphorescence emission rate is several orders of magnitude smaller than that for fluorescence. The

presence of heavy atoms such as bromine or iodine helps the molecules to be phosphorescent as heavy atoms facilitate intersystem crossing.

The intensity of fluorescence can be reduced by a process known as quenching, which can occur by different mechanisms. When the fluorophore in the excited state undergoes deactivation upon contact with some other molecule (quencher) in solution, the process is known as collisional quenching. In case of transition metal ligand complexes, fluorescence quenching occurs due to spin-orbit coupling and intersystem crossing which is facilitated by metal-to-ligand charge-transfer (MLCT).[29,30] Fluorescence quenching can also occur if the fluorophores form nonfluorescent complexes with quenchers, and by a variety of other non-molecular mechanisms, such as attenuation of the incident light by the fluorophore itself or other absorbing species present.

1.5 Thesis goals

The primary goal of this thesis is to establish a method for the synthesis of self-assembled supramolecular architectures by the coordination of pyridine-substituted ligands incorporating redox-active organic heterocycles, such as benzochalcogenadiazoles. The key steps involved in making these metal complexes are efficient syntheses of 4,7-*bis*(4-pyridyl)chalcogenadiazole ligands and then their incorporation into the molecular self assemblies. Chapters 2 and 3 describe how the conditions for the synthesis of 4,7-*bis*(4-pyridyl)benzothiadiazole were optimized and successfully extended to the analogous selenadiazole ring system. The main emphasis was to carry out comparative studies between the two ring systems. Chapters 4 and 5 describe the synthesis of novel self-assembled molecular rods and squares containing both benzothia- and selenadiazole ligands that have never been investigated before. The optoelectronic properties of the

ligands and their metal complexes are documented in chapter 6. Indeed, both the ligands and their self-assemblies show possibilities for developing new materials for electroluminescent, conducting and photovoltaic device applications. This thesis provides foundational and exploratory research for the preparation of metal-directed nanomaterials incorporating organic redox systems, thus opening a new branch of redox-active molecular assemblies that has never been reported previously in the literature.

References

1. (a) Siegel, R. W.; Hu, E; Roco, M. C. (Eds.), *Nanostructure Science and Technology-A Worldwide Study*. *Prepared under the guidance of the IWGN and NSTC*; WTEC: Loyola College, Maryland, 1999. (b) Mansoori, G. A. *Principles of Nanotechnology: Molecular Based Study of Condensed Matter in Small Systems*, World Scientific: New York, 2005. (c) Mansoori, G. A.; George, T. F.; Assoufid, L.; Zhang, G. *Molecular Building Blocks for Nanotechnology: from Diamondoids to Nanoscale Materials and Applications*, Springer: New York, 2007.

2. (a) Oakley, R. T. *Prog. Inorg. Chem.* **1988**, *36*, 299. (b) Chivers, T. *Chem. Rev.* **1985**, *85*, 341. (c) Parsons, S.; Passmore, J. *Acc. Chem. Res.* **1994**, *27*, 101. (d) Rawson, J. M.; McManus, G. D. *Coord. Chem. Rev.* **1999**, *189*, 135. (e) Boeré R. T.; Roemmele, T. L. *Coord. Chem. Rev.* **2000**, *210*, 369. (f) Pavlishchuk, V. V.; Addison A. W. *Inorg. Chim. Acta* **2000**, *298*, 97.

3. (a) Morris, J. L.; Rees, C. W. *Chem. Soc. Rev.* **1986**, *15*, 1. (b) Chivers, T. *Sulfur-Nitrogen Heterocycles*, in Haiduc, I.; Sowerby, D. B. (Eds.), *The Chemistry of Inorganic Homo- and Heterocycles, Academic Press, London,* **1987**, *Vol. 2*, p-793. (c) Oakley, R. T. *Can. J. Chem.* **1993**, *71*, 1775. (d) Chivers, T. *Sulfur-Nitrogen Heterocycles*, in King, R. B. (Ed.), *Encyclopedia of Inorganic Chemistry, 2nd Edition,* Wiley: Chichester, U.K., 2005, p-2028.

4. Banister, A. J.; May, I.; Rawson, J. M.; Smith, J. N. B. *J. Organomet. Chem.* **1998**, *550*, 241.

5. Cordes, A. W.; Haddon, R. C.; Oakely, R.T. *Heterocyclic Thiazyl and Selenazyl Radicals: Synthesis and Applications in Solid-state Architecture,* in Steudel, R. (Ed.), *The Chemistry of Inorganic Heterocycles,* Elsevier, 1992, p-295.

6. Rawson, J. M.; Palacio, F. Structure and Bonding, **2001**, *100*, 93.

7. (a) Gilchrist, T. L. *Heterocyclic Chemistry,* Pitman, London, 1985. (b) Daley, S. T. A. K.; Rees, C. W. *J. Chem. Soc., Perkin Trans. 1*, **1987**, 207. (c) Alicina, J. F.; Kowald, J. A., in Klaymann, D. L.; Günther, W. H. (Eds.), *Organic Selenium Compounds: Their Chemistry and Biology,* Wiley: Chichester, U.K., 1973, p-1050. (d) Nunn, A. J.; Ralph, J. T. *J. Chem. Soc.* **1965**, 6769. (e) Bird, C. W.; Cheeseman, G. W. H.; Sarsfiel, A. A. *J. Chem. Soc.* **1963**, 4767.

8. (a) Weinstock, L. M.; Davis, P.; Mulvey, D. M.; Schaeffer, J. C. *Angew. Chem., Int. Ed.* **1967**, *6*, 364. (b) Bertini, V. *Angew. Chem., Int. Ed.* **1967**, *6*, 563. (c) Bertini, V.; Lucchesini, F. *Synthesis*, **1982**, 681.

9. (a) Risto, M.; Reed, R. W.; Robertson, C. M.; Oilunkaniemi, R.; Laitinen, R. S. Oakley, R. T. *Chem. Commun.* **2008**, 3278. (b) Cozzolino, A. F.; Britten, J. F.; Vargas-Baca, I. *Cryst. Growth Des.* **2006**, *6*, 181.

10. Kovtonyuk, V. N; Makarov, A. Y.; Shakirov, M. M.; Zibarev, A. V. *Chem. Commun.* **1996**, 1991.

11. Suzuki, T.; Tsuji, T.; Miyashi, T.; Yamashita, Y. *J. Org. Chem.* **2001,** *66,* 8954.

12. Bertini, V.; Dapporto, P.; Lucchesini, F.; Sega, A.; Munno, A. D. *Acta Crystallogr., Sect. C* **1984**, *40*, 653.

13. (a) Mellini, M.; Merlino, S. *Acta Crystallogr., Sect. B* **1976**, *32*, 1074. (b) Cozzolino, A. F.; Vargas-Baca, I.; Mansour, S.; Mahmoudkhani, A. H. *J. Am. Chem. Soc.* **2005**, *127*, 3184 and references therein.

14. (a) Björgvinsson, M.; Roeskey, H. W. *Polyhedron* **1991**, *10*, 2353. (b) Gieren, M.; Beta, H.; Hübner, T.; Lamm, V.; Neidlein, R.; Droste, D. *Z. Naturforsch.* **1984**, *39B*, 485.

15. Bondi, A. *J. Phys. Chem.* **1964**, *68*, 441.

16. For recent reviews, see: (a) Northrop, B. H.; Zheng, Y. -R.; Chi, K. -W.; Stang, P. J. *Acc. Chem. Res.* **2009**, *42*, 1554. (b) Fujita, M.; Tominaga, M.; Hori, A.; Therrien, B. *Acc. Chem. Res.* **2005**, *38*, 369 and references therein. (c) Seidel, S. R.; Stang, P. J. *Acc. Chem. Res.* **2002**, *35*, 972. (d) Swiegers, G. F.; Malefetse, T. J. *Coord. Chem. Rev.* **2002**, *225*, 91. (e) Holliday, B. J.; Mirkin, C. A. *Angew. Chem., Int. Ed.* **2001**, *40*, 2022. (f) Cotton, F. A.; Lin, C.; Murillo, C. A. *Acc. Chem. Res.* **2001**, *34*, 759. (g) Leininger, S.; Olenyuk, B.; Stang, P. J. *Chem. Rev.* **2000**, *100*, 853. (h) Fujita, M. *Chem. Soc. Rev.* **1998**, *27*, 417. (i) Uller, E.; Demleitner, I.; Bernt, I.; Saalfrank, R. W. *Synergistic Effect of Serendipity and Rational Design in Supramolecular Chemistry*. In *Structure and Bonding*; Fujita, M. (Ed.), Springer: Berlin, 2000; Vol. 96, p 149. (j) Caulder, D. L.; Raymond, K. N. *J. Chem. Soc., Dalton Trans.* **1999**, 1185. (k) Caulder, D. L.; Raymond, K. N. *Acc. Chem. Res.* **1999**, *32*, 975. (l) Baxter, P. N. W.; Lehn, J. -M.; Baum, G.; Fenske, D. *Chem. Eur. J.* **1999**, *5*, 102. (m) Chambron, J. -C.; Dietrich-Buchecker, C.; Sauvage, J. -P. *Transition Metals as Assembling and Templating Species*. In *Comprehensive Supramolecular Chemistry*; Lehn, J.-M., Chair, E., Atwood, J. L., Davis, J. E. D., MacNicol, D. D., Vogtle, F. (Eds.), Pergamon Press: Oxford, 1996; Vol. 9, Chapter 2, p 43. (n) Baxter, P. N. W. *Metal Ion Directed Assembly of Complex Molecular*

Architectures and Nanostructures. In *Comprehensive Supramolecular Chemistry*; Lehn, J.-M., Chair, E., Atwood, J. L., Davis, J. E. D., MacNicol, D. D., Vogtle, F. (Eds.), Pergamon Press: Oxford, 1996; Vol. 9, Chapter 5, p 165.

17. (a) Murase, T.; Horiuchi, S.; Fujita, M. *J. Am. Chem. Soc.* **2010**, *132*, 2866 and references therein. (b) Yamauchi, Y.; Yoshizawa, M.; Akita, M. Fujita, M. *J. Am. Chem. Soc.* **2010**, *132*, 960 and references therein. (c) Dolain, C.; Hatakeyama, Y.; Sawada, T.; Tashiro, S.; Fujita, M. *J. Am. Chem. Soc.* **2010**, *132*, 5564 and references therein.

18. (a) Fujita, M.; Yazaki, J.; Ogura, K. *J. Am. Chem. Soc.* **1990**, *112*, 5645. (b) Yoshizawa, M.; Nagao, M.; Kumazawa, K.; Fujita, M. *J. Organomet. Chem.* **2005**, *690*, 5383.

19. (a) Dinolfo, P. H.; Sun, S. -S.; Hupp, J. T. *Moleculer squares, boxes, and cubes*. In *Encyclopedia of Supramolecular Chemistry*; Atwood, J. L.; Steed, J. W. (Eds.), Taylor & Francis: London, 2004, *2*, p 909. (b) Furlan, R. L. E.; Otto, S.; Sanders, J. K. M. *Proc. Natl. Acad. Sci. USA* **2002**, *99*, 4801.

20. (a) Lee, S. B.; Hwang, S.; Chung, D. S.; Yun, H.; Hong, J. -I. *Tetrahedron Lett.* **1998**, *39*, 873. (b) Ikeda, A.; Yoshimura, M.; Udzu, H.; Fukuhara, C.; Shinkai, S. *J. Am. Chem. Soc.* **1999**, *121*, 4296. (c) Johannessen, S. C.; Brisbois R. G. *J. Am. Chem. Soc.* **2001**, *123*, 3818.

21. (a) Stang, P. J.; Cao, D. H. *J. Am. Chem. Soc.* **1994**, *116*, 4981. (b) Olenyuk, B.; Whiteford, J. A.; Stang, P. J. *J. Am. Chem. Soc.* **1996**, *118*, 8221. (c) Stang, P. J.; Cao, D. H.; Chen, K.; Gray, G. M.; Muddiman, D. C.; Smith, R. D. *J. Am. Chem. Soc.* **1997**, *119*, 5163. (d) Stang, P. J.; Olenyuk, B.; Fan, J.; Arif, A. M. *Organometallics* **1996**, *15*, 904. (e) Stang, P. J.; Fan, J.; Olenyuk, B. *J. Chem. Soc., Chem. Commun.* **1997**, 1453.

22. (a) Blanco, V.; Chas, M.; Abella, D.; Peinador, C.; Quintela J. M. *J. Am. Chem. Soc.* **2007**, *129*, 13978. (b) Blanco, V.; Gutiérrez, A.; Platas-Iglesias, C.; Peinador, C.; Quintela, J. M. *J. Org. Chem.* **2009**, *74*, 6577. (c) Peinador, C.; Blanco, V.; Quintela, J. M. *J. Am. Chem. Soc.* **2009**, *131*, 920.

23. (a) Stricklen, P. M.; Volcko, E. J.; Verkade, J. G. *J. Am. Chem. Soc.* **1983**, *105*, 2494. (b) Cruse, H. A.; Leadbeater, N. E. *Inorg. Chem.* **1999**, *38,* 4149. (c) Slone, R. V.; Hupp, J. T.; Stern, C. L.; Albrecht-Schmitt, T. E. *Inorg. Chem.*, **1996**, *35*, 4096. (d) Rajendran, T.; Manimaran, B.; Lee, F. -Y.; Chen, P. -J.; Lin, S.-C.; Lee, G. -H.; Peng, S. -M.; Chen, Y. -J.; Lu, K. -L. *J. Chem. Soc*., *Dalton Trans*., **2001**, 3346. (e) Rajendran, T.; Manimaran, B.; Lee, F. -Y.; Lee, G.-H.; Peng, S. -M.; Wang, C. M.; Lu, K. -L. *Inorg. Chem.* **2000**, *39,* 2016. (f) Liao, R. -T.; Yang, W. -C.; Thanasekaran, P.; Tsai, C. -C.; Sathiyendiran, M.; Liu, Y. -H.; Rajendran, T.; Lin, H. -M.; Tseng, T. -W.; Lu, K. -L. *Chem. Commun.* **2008**, 3175. (g) Slone, R. V.; Benkstein, K. D.; Bélanger, S.; Hupp, J. T.; Guzei, I. A.; Rheingold, A. L. *Coord. Chem. Rev.* **1998**, *171*, 221.

24. Cannizzo, A.; Blanco-Rodríguez, A. M.; Nahhas, A. E.; Šebera, J.; Záliš, S.; Vlček, A. Jr.; Chergui, M. *J. Am. Chem. Soc.* **2008**, *130*, 8967.

25. Frischmann, P. D.; Guieu, S.; Tabeshi, R.; Maclachlan, M. J. *J. Am. Chem. Soc.* **2010**, *132*, 7668.

26. (a) Wang, J. *Analytical electrochemistry*, 3rd Ed, New York: Wiley-VCH, 2006. (b) Kissinger, P. T.; Heineman, W. R. *Laboratory techniques in electroanalytical chemistry*, 2nd Ed, New York: Marcel Dekker, Inc. 1996. (c) Bard, A. J.; Faulkner, L. R. *Electrochemical methods: fundamentals and applications*, 2nd Ed, New York: Wiley,

2001. (d) Harris, D. C. *Quantitative Chemical Analysis*; W. H. Freeman and Company: New York, 1995.

27. (a) Osteryoung, J.; O'Dea, J. J. *Square-wave voltammetry*. In *Electroanalytical chemistry*; Bard A. J. (Ed), Marcel Dekker, New York, 1986, *14*, p-209. (b) Eccles G. N. *Crit. Rev. A nal. Chem.* **1991**, *22*, 345. (c) Lovrić, M. *Square-wave voltammetry*. In *Electroanalytical methods*; Scholz, F. (Ed), Springer, New York, 2002, p-111. (d) de Souza, D.; Machado, S. A. S.; Avaca, L. A. *Quim. Nova*. **2003**, *26*, 81.

28. (a) Skoog, D. A.; Holler, F. J.; Crouch, S. R. *Principles of Instrumental Analysis*, 6th Ed, Thomson Brooks/Cole, 2007, 169. (b) Pavia, D. L.; Lampman, G. M.; Kriz, G. S. *Introduction to Spectroscopy*, 3rd Ed, Thomson Brooks/Cole, 2001, 353.

29. (a) Atkins, P. J.; Shriver, D. F. *Inorganic chemistry*, 3rd Ed, New York: Freeman, W. H. and CO, 1999. (b) Tarr, D. A.; Miessler, G. L. *Inorganic chemistry*, 2nd Ed, Englewood Cliffs, N. J: Prentice Hall, 1991.

30. Lakowicz, J. R. *Principles of Fluorescence Spectroscopy*, 4th Ed, Springer, 2006, Chapter 1.

CHAPTER TWO: ISOLATION OF Pd(II) COMPLEXES IN ATTEMPTED COUPLING REACTIONS

2.1 Introduction

Arylpalladium chemistry continues to be a subject of interest because of its involvement in so many palladium-catalyzed organic reactions.[1] Among the different palladium-catalyzed reactions, carbon-carbon coupling processes in organic synthesis on laboratory and industrial scale is a well established method for fine chemical synthesis.[2] Palladium(II) complexes of aryl halides, formed *in situ* during the catalytic reaction by the oxidative addition of aryl halide to Pd(0), have been documented as intermediates for carbon-carbon coupling reactions by several authors (Figure 2.1).[3]

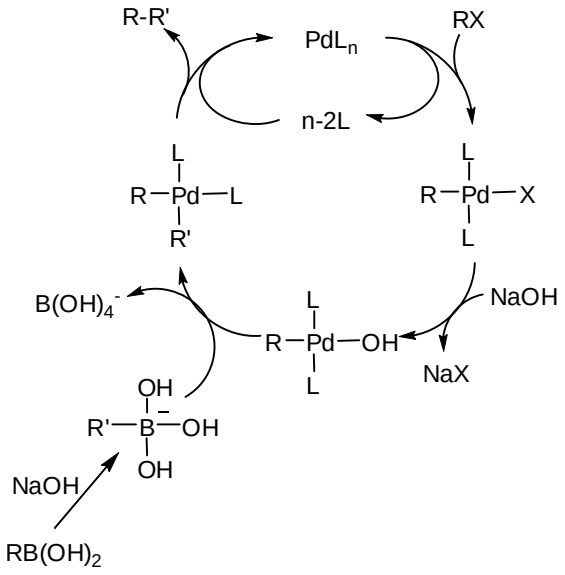

Figure 2.1 Mechanism of the Pd-catalyzed Suzuki coupling reaction[1c]

Recently, Beller and co-workers reported the catalytic cyanation of aryl halides using arylpalladium(II) complexes.[4] Palladium complexes with functionalized aryl ligands have also been synthesized to investigate their reactivity towards insertion reactions with

different substrates.[5] During the attempts to prepare 4,7-*bis*(4-pyridyl)benzo-chalcogenadiazoles (Figure 2.2) by Suzuki coupling reactions, we trapped an intermediate chalcogenadiazolyl palladium(II) complex and the palladium-promoted C–C coupling reaction was not observed. To our knowledge, however, no reports have been made in the literature concerning σ-bonded Pd–C_{aryl} benzochalcogenadiazolyl metal complexes. We thus decided to synthesize the chalcogenadiazolyl palladium complexes on purpose to investigate (i) their reactivity towards Stille coupling conditions, and (ii) the redox properties of the σ-bonded Pd–C_{aryl} benzochalcogenadiazolyl heterocycles (which will be discussed in Chapter 6).

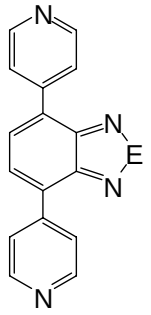

(E = S, **9**; Se, **11**)

Figure 2.2 4,7-*bis*(4-pyridyl)benzochalcogenadiazoles

2.2 Synthesis of 4,7-dibromo-2,1,3-benzochalcogenadiazoles

2.2.1 Synthesis of 4,7-dibromo-2,1,3-benzothiadiazole (**3**)

After reviewing the literature, a large scale synthesis of 2,1,3-benzothiadiazole (**2**) was found,[6a] which involves the treatment of commercially available *o*-phenylenediamine (**1**) with freshly distilled thionyl chloride in refluxing toluene for 3h (Scheme 2.1). Initially the diamine was not dissolved in toluene, and upon addition of thionyl chloride, afforded a yellow sludge. Soon after starting reflux, the sludge turned into a yellow solution with

some solids left and after refluxing for 2 h the solution became a clear amber color and refluxing was continued for one more hour to complete the reaction. Distillation first removed the toluene and excess thionyl chloride, then gave 2,1,3-benzothiadiazole (**2**) as a dark orange distillate which solidified to a pale yellow material on cooling. The yellow residue was dissolved in ethanol and reprecipitated with water, giving an off-white solid in 97% yield. Bromine was added to a solution of **2** followed by the addition of silver sulfate in concentrated sulfuric acid. The mixture was shaken at room temperature for 2 h and the precipitate of silver bromide filtered off using glass wool. Pouring the filtrate directly into ice-water gave an off-white precipitate which upon recrystallization from ethyl acetate gave 4,7-dibromo-2,1,3-benzothiadiazole (**3**) in 98% yield as thin white needles (Scheme 2.1).[6b] Formation of compound **2** and its dibromo derivative **3**, was confirmed by comparing the melting point, IR and ^{1}H NMR spectra with the literature data.[6]

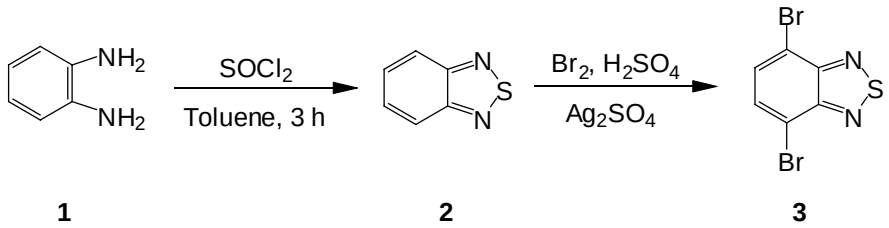

Scheme 2.1 Synthesis of 4,7-dibromo-2,1,3-benzothiadiazole (**3**)

2.2.2 Synthesis and molecular structure of 4,7-dibromo-2,1,3-benzoselenadiazole (**5**)

Synthesis of 2,1,3-benzoselenadiazole and its bromination has been known for many years and was first reported by Bird and co-workers in 1963.[6b] Following their report, we synthesized 2,1,3-benzoselenadiazole by adding an aqueous solution of selenium dioxide

to a solution of the diamine in a minimum volume of boiling 96% ethanol. The mixture was boiled for an additional 5-10 min and then cooled to room temperature, and the needle-like white crystals of 2,1,3-benzoselenadiazole were filtered off in 99% yield. Bromination was carried out following the same procedure as mentioned above for **2** affording **5** in 67% yield as yellow needles. Formation of both 2,1,3-benzoselenadiazole and the dibromo derivative was confirmed by comparing the melting point, IR and ^{1}H NMR spectra with the literature values (Scheme 2.2).[6b]

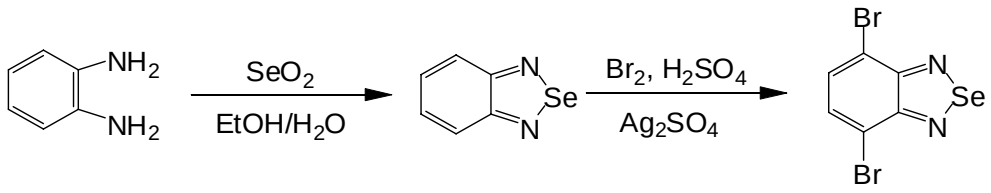

1 **4** **5**

Scheme 2.2 Synthesis of 4,7-dibromo-2,1,3-benzoselenadiazole (**5**)

The structures of 4,7-dibromo- and diiodobenzothiadiazole,[7a, b] and 4,7-dibromobenzo-telluradiazole[7c] were previously reported but the structure of the analogous benzoselenadiazole has not been reported. We therefore determined the structure of **5** by single-crystal X-ray diffraction methods. Suitable crystals of **5** were grown by slow evaporation of a dilute ethyl acetate solution at ambient temperature.

The molecular structure of **5** in the crystal is depicted in Figure 2.3, selected crystal data are listed in Table 2.1 and selected bond distances and angles are listed in the caption to the Figure 2.3. The full crystal reports are presented in the electronic Appendix. Similar to that of the corresponding sulfur and tellurium analogs,[7] compound **5** crystallizes in the monoclinic system with the centrosymmetric space group $P2_1/n$ except the asymmetric unit consists of only one molecule rather than the two observed for the sulfur analog.

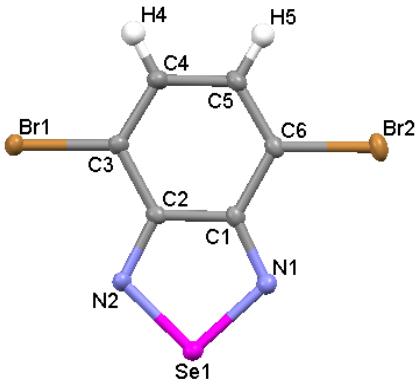

Figure 2.3 Molecular structure of **5**, selected bond lengths (Å) and angles (°): Br(1) –C(3) 1.894(2); Se(1) –N(1) 1.7950(19); Se(1) –N(2) 1.7962(18); N(1) –C(1) 1.329(3); N(2) –C(2) 1.332(3); C(1) –C(2) 1.440(6); C(1) –C(6) 1.442(5); C(2) –C(3) 1.428(6); C(3) –C(4) 1.371(6); C(5) –C(6) 1.360(6); C(5) –C(4) 1.423(6); N(1) –Se(1) –N(2) 94.20(9); C(1) –N(1) –Se(1) 106.90(14); C(2) –N(2) –Se(1) 106.46(14)

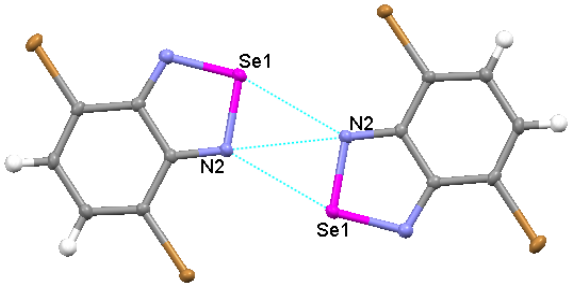

Figure 2.4 Side-by-side dimer arrangement within the crystal structure of **5**

Considerable shortening of the C(3)–C(4), C(5)–C(6), C(1)–N(1) and C(2)–N(2) bonds {av. 1.34(5) Å} in **5** is observed in comparison to the C(1)–C(2), C(2)–C(3), C(4)–C(5), C(1)–C(6), N(1)–Se(1) and N(2)–Se(1) bonds. Such double bond fixation suggests quinoidal character in the 2,1,3-benzoselenadiazole ring, and similar bond fixation phenomena are also found for the corresponding 2,1,3-benzothiadiazole and telluradiazole ring systems.[7]

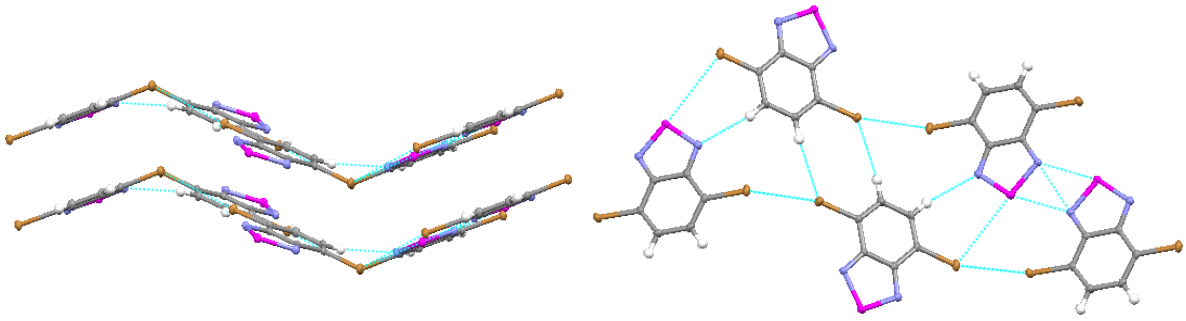

(a) (b)

Figure 2.5 Arrangement of molecules in zigzag layered sheets within the crystal structure of **5**, viewed (a) along *c* axis and (b) along *a* axis

Table 2.1 Crystal data and structure refinement for **5**

	5
Temperature (K)	173(2)
Crystal system	Monoclinic
Space group	$P2_1/n$
Unit cell dimensions	
a, Å	3.9378(2)
b, Å	18.3462(11)
c, Å	11.1358(7)
β, deg	95.0080(10)
Z	4
Goodness-of-fit on F^2	1.051
Final *R* indices [$I>2\sigma(I)$]	$R_1 = 0.0153$
	w$R_2 = 0.0367$
R indices (all data)	$R_1 = 0.0172$
	w$R_2 = 0.0373$

The crystal structure of **5** confirmed dimer formation (Figure 2.4) in the solid state by Se---N secondary bonding interactions (SBI) similar to that of the corresponding tellurium analog[7c, d] and the length of Se---N SBI distance {2.94(5) Å} is comparable with the length of Se---N SBI distance {2.95(0) Å} observed for 2,1,3-benzoselenadiazole[8] (See Table 1.2, Chapter 1). Similar to the corresponding tellurium analog, the dimers in the crystal of **5** appear to engage in SBIs with other molecules.[7c] Besides the Se---N SBI,

additional weak Se---Br {3.73(5) Å} and Br---Br {3.52(0) Å} long contacts gave one dimensional layered zigzag sheets (Figure 2.5) and the two contacts are shorter than the sum of the van der Waals radii (3.75(0) and 3.70(0) Å, respectively).[9]

2.3 Synthesis of *trans*-[XPd(PPh_3)$_2$($C_6H_2BrN_2E$)] (E = S, Se; X = Cl, Br)

2.3.1 Synthesis and characterization of *trans*-[XPd(PPh_3)$_2$($C_6H_2BrN_2S$)] (**6**)

In an attempt to synthesize 4,7-bis(4-pydiryl)benzothiadiazole, reaction of **3** and 4-pyridylboronic acid in the presence of a catalytic amount of [Pd(PPh_3)$_4$] was carried out in refluxing toluene for 24 h affording *trans*-[ClPd(PPh_3)$_2$($C_6H_2BrN_2S$)] (**6a**) in 14% yield as lemon yellow solids. Compound **6a** was formed by the oxidative addition of the C–Br bond of **3** to the Pd(0) center giving a σ-bonded Pd–C_{aryl} benzothiadiazolyl Pd(II) complex. Surprisingly, the molecule contains chlorine instead of the expected bromine bonded to the palladium, which most likely resulted from the ion exchange reactions during the workup with brine, a standard method for quenching the catalyst in a Suzuki coupling reaction. The presence of chlorine was confirmed by single crystal X-ray structure determination (see below).

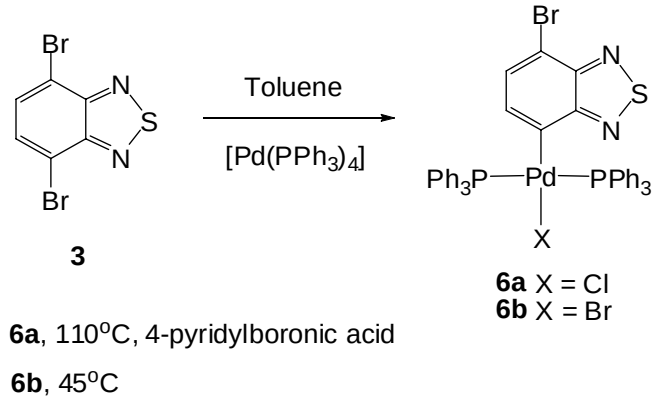

Scheme 2.3 Synthesis of *trans*-[XPd(PPh_3)$_2$($C_6H_2BrN_2S$)] (**6**)

Subsequently, the bromo analog **6b** was prepared by heating a toluene solution of **3** and $[Pd(PPh_3)_4]$ in 1:1 ratio at 45°C for 12 h giving *trans*-$[BrPd(PPh_3)_2(C_6H_2BrN_2S)]$ (**6b**) in 98% yield (Scheme 2.3). Compounds **6a** and **6b** have been characterized by spectroscopic methods together with single crystal X-ray diffraction studies on **6a**.

Table 2.2 ^1H and ^{31}P $\{^1H\}$ NMR data of **3**, **5-8** in $CDCl_3$[a]

Compounds	^1H NMR	^{31}P NMR
3	7.65 (s)	
5	7.72 (s)	
6a	7.62-7.56 (m), 7.32-7.27 (m), 7.22-7.17 (m) } PPh_3 6.94-6.90 (m)	23.06 (s)
6b	7.60-7.54 (m), 7.29-7.25 (m), 7.20-7.15 (m) } PPh_3 6.95-6.92 (m)	23.01 (s)
7a	7.63-7.57 (m), 7.32-7.26 (m), 7.22-7.17 (m) } PPh_3 6.82-6.76 (m)	22.99 (s)
7b	7.61-7.55 (m), 7.30-7.25 (m), 7.20-7.16 (m) } PPh_3 6.80-6.75 (m)	22.97 (s)
8	7.92-7.85 (m), 7.35-7.30 (m), 7.23-7.18 (m) } PPh_3 6.82 (d, J = 7.2 Hz) 6.74 (dd, J = 7.2, 3.3 Hz)	28.23 (s)

[a]All values are in ppm, with reference to TMS for ^1H and 85% H_3PO_4 for $^{31}P\{^1H\}$

The ^1H NMR spectra of **6a** and **6b** are highly similar except for subtle differences in chemical shifts. Both spectra show four multiplets due to the phenyl protons of the triphenylphosphine ligands and the benzothiadiazole ring protons in the range δ 6.95-6.90

ppm. The $^{31}P\{^{1}H\}$ NMR spectra show singlets at δ 23.06 ppm in **6a** and 23.01 ppm in **6b** indicating that each contains equivalent phosphorus environments (Table 2.2).

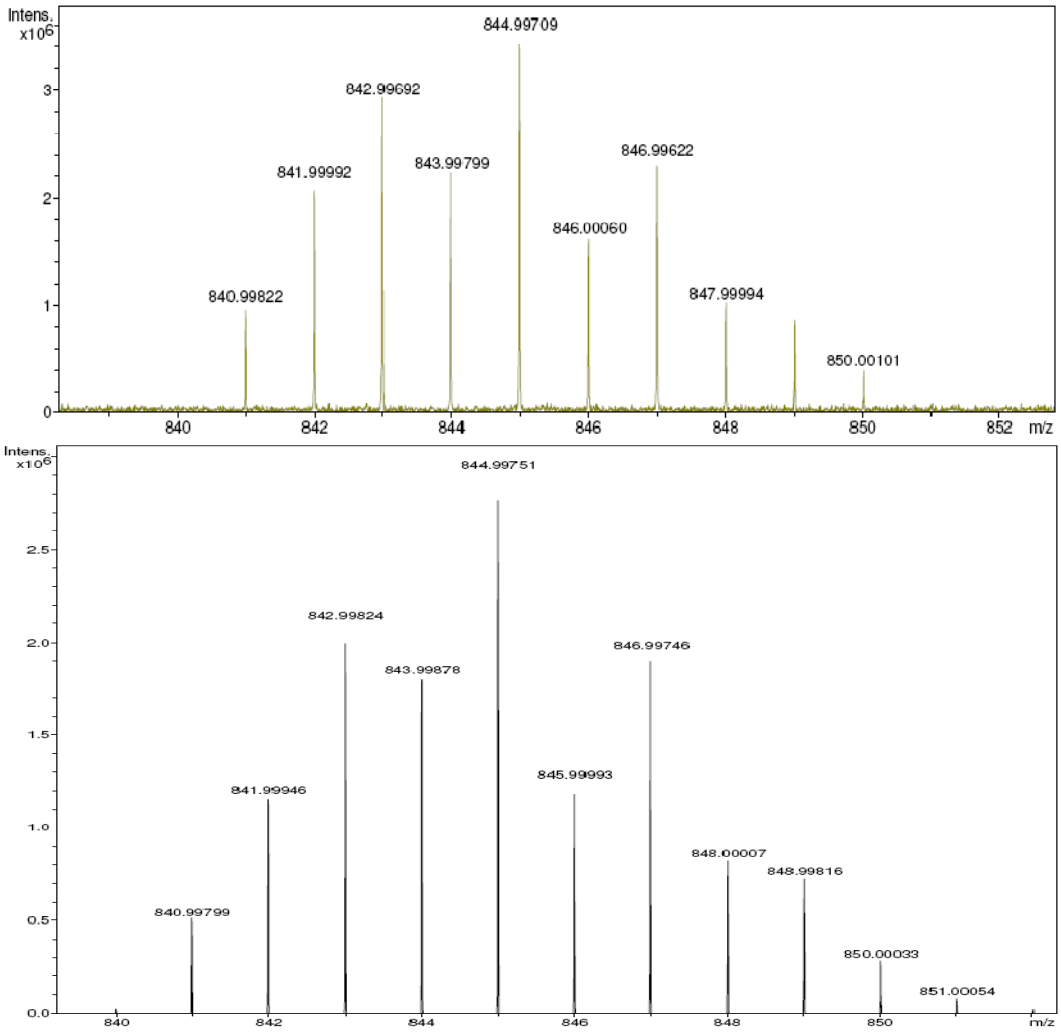

Figure 2.6 Observed (top) and theoretical (bottom) isotopic distribution for the cation $[Pd(PPh_3)_2(C_6H_2BrN_2S)]^+$ in high resolution MALDI MS for **6a**

The high resolution MALDI mass spectrum of **6a** consists of a cation peak at *m*/*z* 844.99709 due to loss of a chloride ion from the parent compound and matches the calculated value of 844.99751 for $^{12}C_{42}{}^{1}H_{32}{}^{81}Br^{14}N_2{}^{31}P_2{}^{106}Pd^{32}S^+$ (Figure 2.6). The low

resolution mass spectrum of **6b** also confirms the cation peak at *m*/*z* 845 due to loss of a bromide ion.

The single crystal molecular structure of **6a** is depicted in Figure 2.7, selected crystal data are given in Table 2.4 and selected bond distances and angles are listed in the caption to the Figure 2.7. The full crystal reports are presented in the electronic Appendix. The compound, as grown by slow diffusion of ethanol into chloroform at –4°C, was found to crystallize in the orthorhombic system with the centrosymmetric space group *P*nma and consists of a square planar organometallic Pd(II) centre exhibiting *trans*-disposed phosphine ligands.

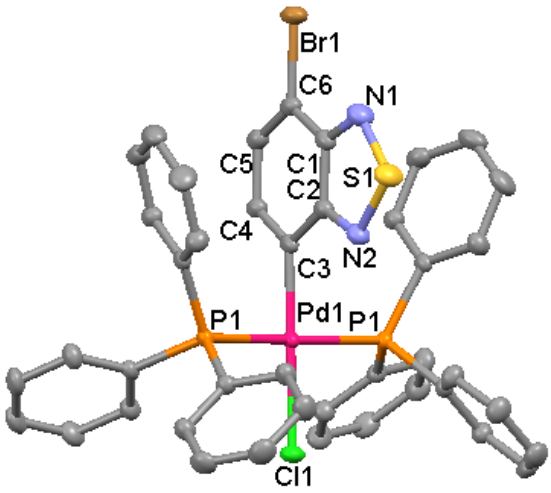

Figure 2.7 Molecular structure of **6a**, selected bond lengths (Å) and angles (°): Pd(1)–C(3) 2.006(4); Pd(1)–P(1) 2.3109(11); Pd(1)–Cl(1) 2.3945(11); S(1)–N(1) 1.618(5); S(1)–N(2) 1.628(4); N(1)–C(1) 1.331(7); N(2)–C(2) 1.335(6); C(1)–C(6) 1.411(7); C(1)–C(2) 1.446(6); C(2)–C(3) 1.417(6); C(3)–C(4) 1.376(7); C(4)–C(5) 1.437(7); C(5)–C(6) 1.346(7); P(1)#1–Pd(1)–P(1) 172.96(4); C(3)–Pd(1)–Cl(1) 179.69(14); N(1)–S(1)–N(2) 100.8(2)

Table 2.3 Comparison of bond lengths[a] in 5, 6a, 7b and 8

Compounds	C(1)–N(1)	C(2)–N(2)	C(2)–C(3)	C(3)–C(4)	C(5)–C(6)	C(1)–C(6)	C–Pd
5	1.329(3)	1.332(3)	1.428(6)	1.371(6)	1.360(6)	1.442(5)	
6a	1.331(7)	1.335(6)	1.417(6)	1.376(7)	1.437(7)	1.411(7)	2.006(4)
7b	1.338(15)	1.342(13)	1.426(15)	1.370(15)	1.398(17)	1.426(16)	2.032(11)
8	1.339(5)	1.331(5)	1.439(5)	1.370(5)	1.358(6)	1.425(5)	2.012(4)

[a]Bond lengths are measured in Angstroms (Å)

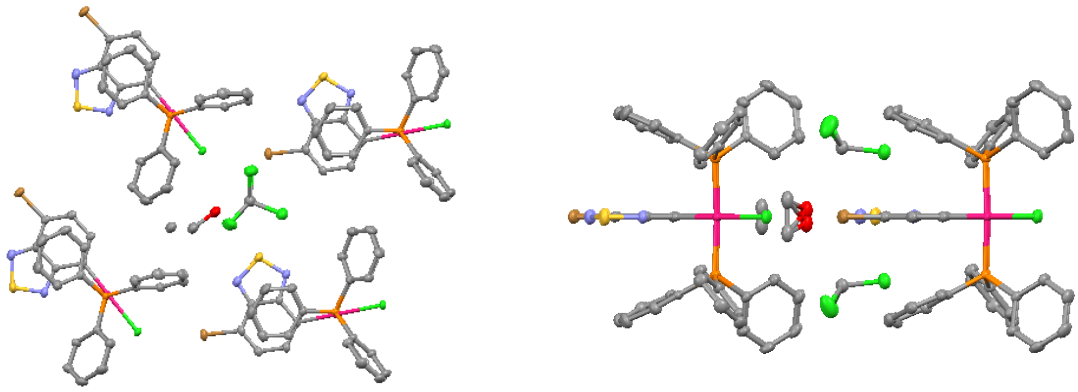

(a) (b)

Figure 2.8 Association of **6a** and solvent molecules viewed (a) along *b* axis and (b) along *c* axis

Table 2.4 Crystal data and structure refinement for **6a** and **7b**

	6a·EtOH·2CHCl$_3$	**7b**·2C$_2$H$_4$Cl$_2$
Temperature (K)	173(2)	173(2)
Crystal system	Orthorhombic	Orthorhombic
Space group	*P*nma	*P*nma
Unit cell dimensions		
a, Å	22.374	11.022(2)
b, Å	22.374(8)	15.261(3)
c, Å	9.580(4)	28.105(6)
$\alpha = \beta = \gamma$, deg	90	90
Z	4	4
Goodness-of-fit on F^2	1.066	1.109
Final *R* indices [$I>2\sigma(I)$]	$R_1 = 0.0397$	$R_1 = 0.0680$
	w$R_2 = 0.1160$	w$R_2 = 0.1411$
R indices (all data)	$R_1 = 0.0485$	$R_1 = 0.1249$
	w$R_2 = 0.1200$	w$R_2 = 0.1685$

The unit cell of **6a** includes solvent molecules in the lattice with two chloroform solvent molecules lying above and below the symmetry plane whereas an ethanol molecule lies on the symmetry plane. The two chloroform and ethanol molecules are surrounded by four molecules of **6a** (Figure 2.8).

The Pd–C bond distance {2.006(4) Å} in **6a** is comparable to the Pd–C bond distances {1.998(4)–2.016(3) Å} observed in [arylPd(PPh_3)$_2$Cl] complexes,[10] and {2.002(3)–2.026(5) Å} observed in [(2-phenylmercapto)arylPd(PPh_3)$_2$Br].[11] The Pd–Cl bond distance {2.3945(11) Å} is comparable to the Pd–Cl bond distances found in [arylPd(PPh_3)$_2$Cl] {2.4005(12)–2.407(1) Å} complexes.[10] The quinoidal character of the σ-bonded 2,1,3-benzothiadiazolyl ring in **6a** was also observed (Table 2.3).

2.3.2 Synthesis and characterization of *trans*-[XPd(PPh_3)$_2$($C_6H_2BrN_2Se$)] (**7**)

The corresponding selenium analog of **6a** containing a chloride ligand was also isolated as a lemon yellow solid from the attempt to carry out the Suzuki coupling reaction. The stoichiometric reaction of **5** and [Pd(PPh_3)$_4$] in toluene at 45^{o}C gave the bromo derivative *trans*-[BrPd(PPh_3)$_2$($C_6H_2BrN_2Se$)] (**7b**) in 98% yield (Scheme 2.4). Compounds **7a** and **7b** have been characterized by spectroscopic methods together with a single crystal X-ray diffraction study for **7b**.

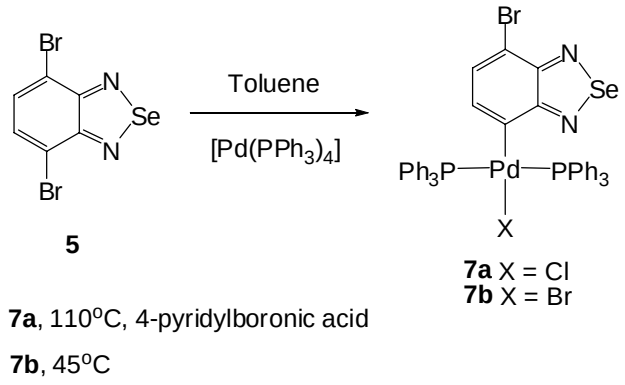

Scheme 2.4 Synthesis of *trans*-[XPd(PPh_3)$_2$($C_6H_2BrN_2Se$)] (**7**)

For the elemental analysis of **7b**, measured (C, 51.17; H, 3.32; N, 2.63%) and calculated values (C, 51.91; H, 3.32; N, 2.88%) are outside accepted standards: C and N but not H are found to be lower than the formula suggests. However, the X-ray crystallographic

analysis (discussed later in this section) indicates the presence of solvent of crystallization ($C_2H_4Cl_2$) in the lattice. Indeed, inclusion of this solvent into the molecular formula leads to lower C and N, but not H, content. The best match (C, 51.14; H, 3.32; N, 2.71%) fits for a ratio of 0.62 solvent molecules per metal complex, consistent with a crystal that has lost some but not all of the lattice solvent at the time the elemental analysis was performed.

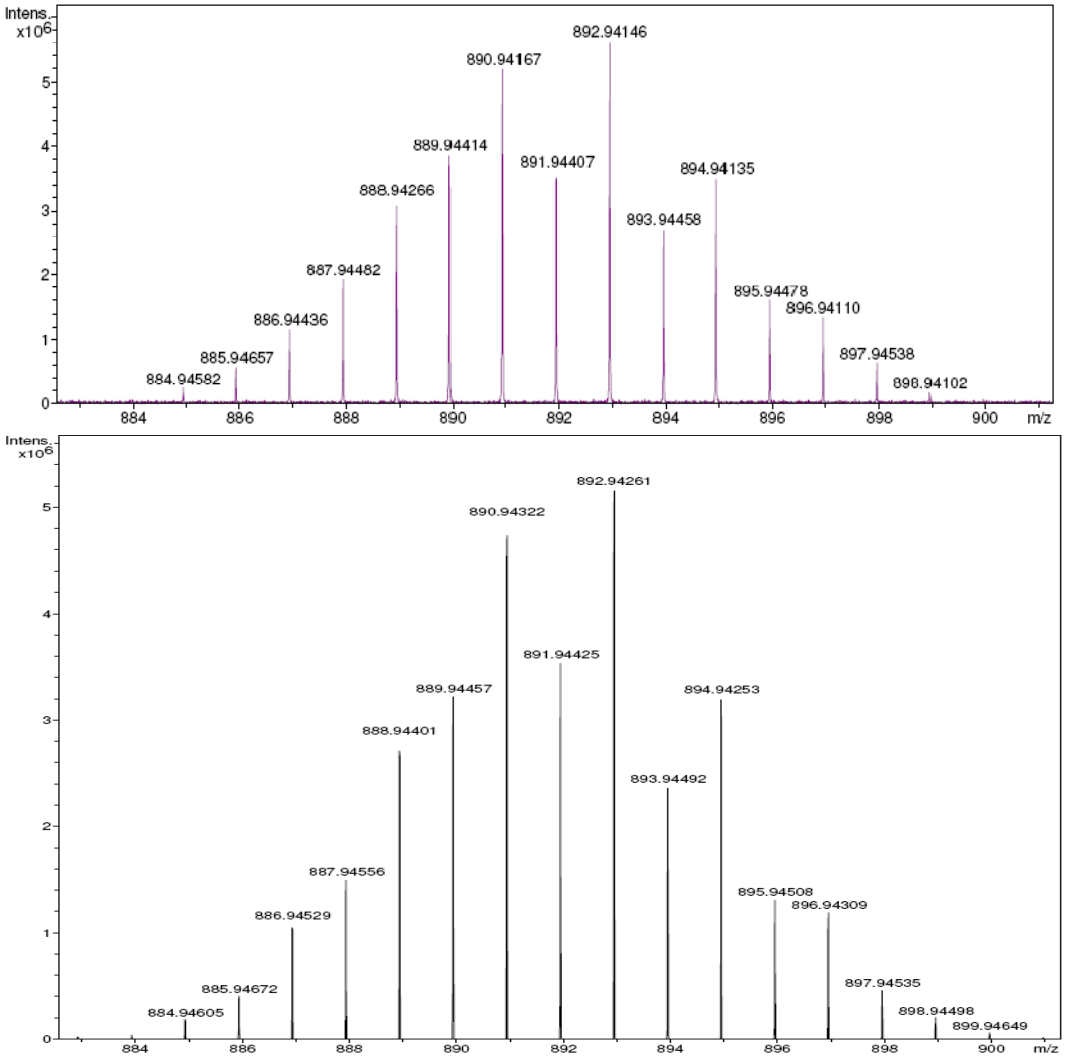

Figure 2.9 Observed (top) and theoretical (bottom) isotopic distribution for the cation $[Pd(PPh_3)_2(C_6H_2BrN_2Se)]^+$ in high resolution MALDI MS for **7b**

The ^{1}H NMR spectra of **7a** and **7b** show four multiplets due to the phenyl protons of the triphenylphosphine ligands and the benzoselenadiazole ring protons in the range δ 6.82-6.75 ppm (Table 2.2). The ^{31}P{^{1}H} NMR spectra show singlets at δ 22.99 ppm for **7a** and 22.97 ppm for **7b** indicating that each contains equivalent phosphorus environment (Table 2.2). The high resolution MALDI mass spectrum of **7b** consists of a cation peak at *m*/*z* 892.94146 due to the loss a bromide ion from the parent compound and matches with the calculated value of 892.94261 for $^{12}C_{42}{}^{1}H_{32}{}^{81}Br^{14}N_2{}^{31}P_2{}^{106}Pd^{80}Se^{+}$ (Figure 2.9).

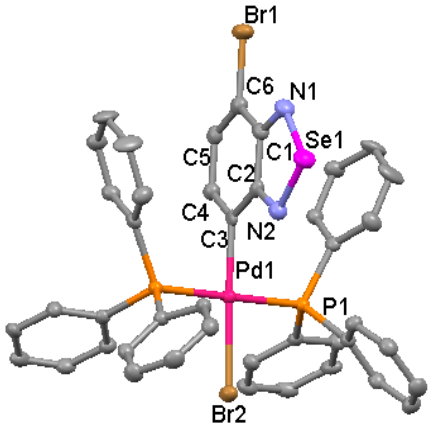

Figure 2.10 Molecular structure of **7b**, selected bond lengths [Å] and bond angles [^{o}]: Pd(1)–C(3) 2.032(11); Pd(1)–P(1) 2.3353(19); N(1)–C(1) 1.338(15); N(2)–C(2) 1.342(13); C(1)–C(6) 1.426(16); C(1)–C(2) 1.470(15); C(2)–C(3) 1.426(15), C(3)–C(4) 1.370(15); C(4)–C(5) 1.443(16); C(5)–C(6) 1.398(17); Pd(1)–Br(2) 2.5247(15); Se(1)–N(2) 1.794(10); Se(1)–N(1) 1.811(11); P(1)–Pd(1)–P(1)#1 179.54(11); C(3)–Pd(1)–Br(2) 175.8(3); N(2)–Se(1)–N(1) 94.1(4)

The single crystal molecular structure of **7b** is depicted in Figure 2.10, crystal data are listed in Table 2.4, and selected bond distances and angles are listed in the caption to the Figure 2.10. The structure has similar structural features of a square planar organometallic Pd(II) centre exhibiting *trans*-disposed phosphine ligands as observed for

6a. Similarly to that of **6a**, compound **7b** crystallizes in the orthorhombic system with the centrosymmetric space group *P*nma. The Pd–C bond distance {2.032(11) Å} is comparable to the Pd–C bond distance of {2.006(4) Å} found in **6a** and {2.026(5) Å} observed in [(2-phenylmercapto)arylPd(PPh_3)$_2$Br] complexes.[11]

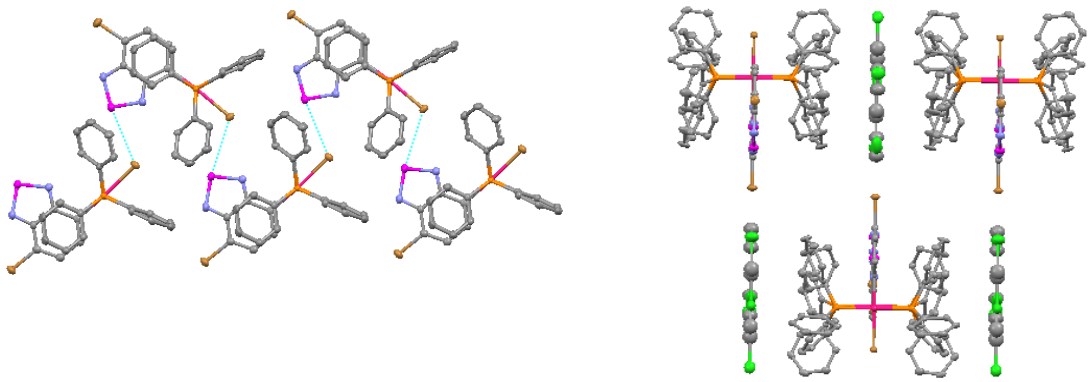

(a) (b)

Figure 2.11 Association of **7b** and solvent molecules observed (a) along *b* axis and (b) through *ac* axes

The Pd–Br {2.5247(15) Å} bond distance is comparable to the Pd–Br bond distance in *trans*-[Pd(2-PhC_6H_4S)Br(PPh_3)$_2$] {2.5296(3) Å}.[11a] Again the quinoidal character of the benzoselenadiazole ring was also observed as evidenced by similar bond fixation as found in **5** and **6a** (Table 2.3). Compound **7b** crystallizes with two dichloroethane molecules located on symmetry planes. Careful observation shows that **7b** forms an array of infinite ribbons along the *a* axis by SBI between the bromine and selenium atoms {3.637(2) Å} of two molecules and the contact distance is shorter than the sum of the van der Waals radii (3.75(0) Å) (Figure 2.11a).[9] In addition, compound **7b** forms two-dimensional infinite sheets repeatedly layered between the solvent molecules along the *ac* plane (Figure 2.11b).

2.4 Synthesis and characterization of *trans*-[{ClPd(PPh_3)(μ-$C_6H_2BrN_2Se$)}$_2$] (**8**)

Thermolysis of **7a** in the presence of SeO_2 gave a novel head-to-tail Pd(II) dimer *trans*-[{ClPd(PPh_3)(μ-$C_6H_2BrN_2Se$)}$_2$] (**8**) in 44% yield (Scheme 2.5). To the best of our knowledge, such σ-bonded Pd–C_{aryl} benzoselenadiazolyl head-to-tail dimerization is unprecedented and is believed to be formed by the combination of two molecules of **7a** after removing two triphenylphosphines. Compound **8** has been characterized by a combination of elemental analysis, IR, ^{1}H NMR, ^{31}P{^{1}H} NMR, mass spectral data, and single-crystal X-ray diffraction studies.

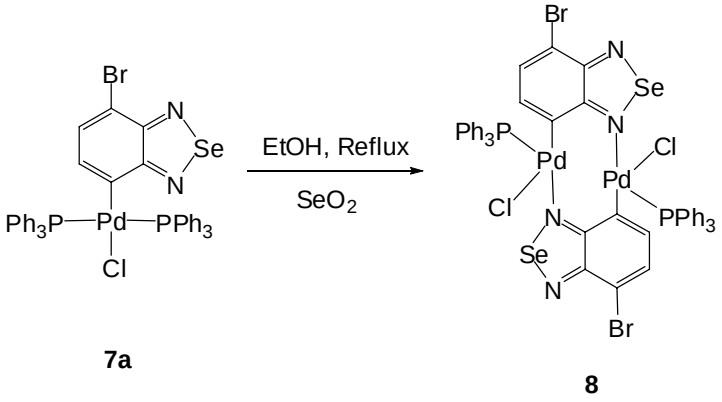

7a **8**

Scheme 2.5 Synthesis of *trans*-[{ClPd(PPh_3)(μ-$C_6H_2BrN_2Se$)}$_2$] (**8**)

Again, for the elemental analysis of **8**, measured (C, 42.80; H, 2.84; N, 3.99%) and calculated values (C, 43.33; H, 2.58; N 4.21%) are outside accepted standards: C but not H and N is found to be lower than the formula suggests. However, the X-ray crystallographic analysis (discussed later in this section) indicates the presence of solvent of crystallization ($CHCl_3$) in the lattice. Here too, inclusion of this solvent into the molecular formula leads to lower C but not H and N, content.

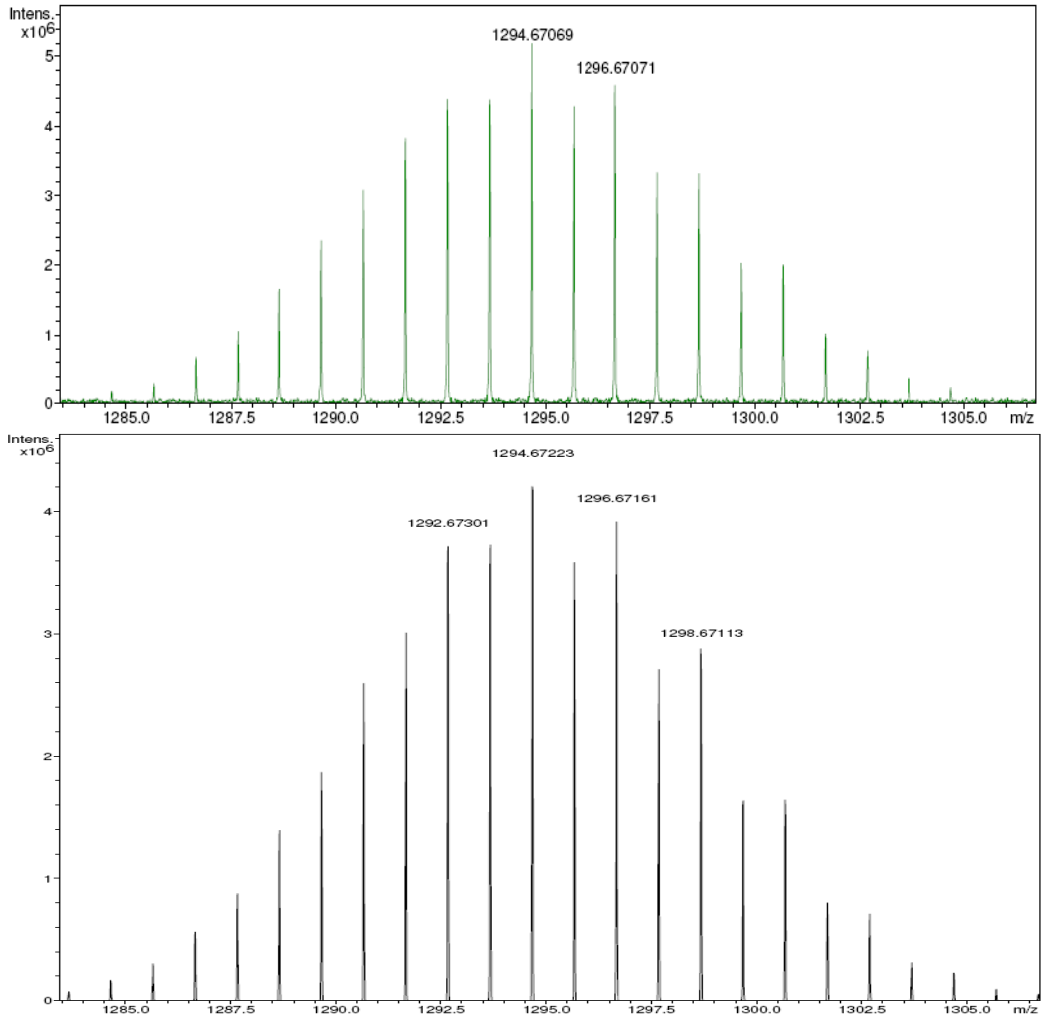

Figure 2.12 Observed (top) and theoretical (bottom) isotopic distribution for the cation $C_{48}H_{34}Br_2ClN_4P_2Pd_2Se_2^+$ in high resolution MALDI MS for **8**

The best match (C, 42.69; H, 2.56; N, 4.06%) fits for a ratio of 0.6 solvent molecules per metal complex which is consistent with a crystal that has lost some but not all of the lattice solvent at the time of analysis. In addition to the phenyl proton resonances of the triphenylphosphine, the ^{1}H NMR spectrum of **8** contains a doublet at δ 6.82 ppm and a doublet of doublets at δ 6.74 ppm assigned to the benzoselenadiazole ring protons (Table 2.2). The two phosphorus nuclei are chemically equivalent, and as expected, the $^{31}P\{^1H\}$ NMR spectrum of **8** shows a singlet at δ 28.23 ppm (Table 2.2). The mass spectrum

confirms the stoichiometry with a cation peak at *m*/*z* 1294.67069 after losing a chloride ion for **8** and matches with the calculated value of 1294.67223 for $^{12}C_{48}{}^{1}H_{34}{}^{81}Br_2{}^{35}Cl2{}^{14}N_4{}^{31}P_2{}^{106}Pd_2{}^{80}Se_2{}^{+}$ (Figure 2.12).

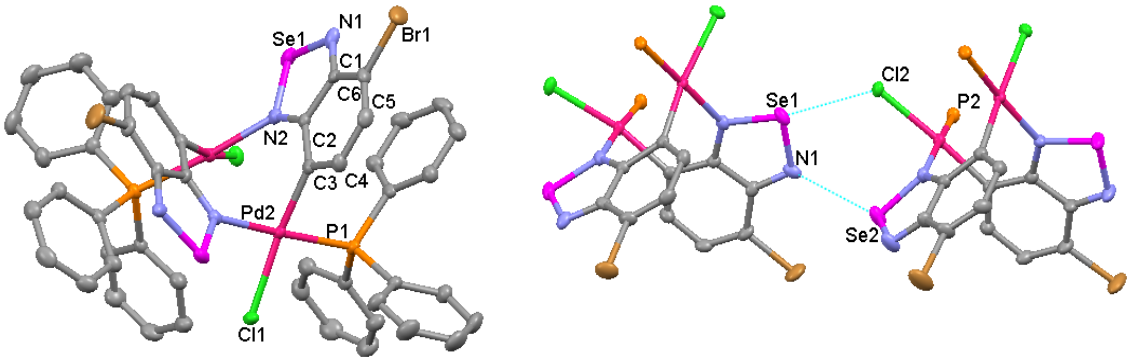

(a) (b)

Figure 2.13 (a) Molecular structure of one molecule of **8**·2.5$CHCl_3$ (hydrogen atoms are omitted for clarity), (b) Further association in the crystal structure of **8**·2.5$CHCl_3$ (phenyl rings of PPh_3 are omitted), selected bond lengths [Å] and bond angles [°]: Pd(1)–C(27)#1 2.012(4); Pd(1)–N(4) 2.088(3); Pd(1)–P(2) 2.2462(10); Pd(1)–Cl(2) 2.3641(10); Pd(2)–C(3) 1.992(4); Pd(2)–N(2) 2.090(3); Pd(2)–P(1) 2.2563(10); Pd(2)–Cl(1) 2.3863(10); Se(1)–N(1) 1.780(3); Se(1)–N(2) 1.796(3); Se(2)–N(3) 1.782(3); Se(2)–N(4) 1.792(3); N(4)–Pd(1)–P(2) 169.78(9); C(27)#1–Pd(1)–Cl(2) 177.09(11); N(2)–Pd(2)–P(1) 175.31(9); C(3)–Pd(2)–Cl(1) 168.91(11); N(1)–Se(1)–N(2) 92.83(15); N(3)–Se(2)–N(4) 92.87(15)

The single crystal molecular structure of **8** is depicted in Figure 2.13, selected crystal data are listed in Table 2.5, and selected bond distances and angles are listed in the caption to the figure. The full crystal reports are presented in the electronic appendix. The asymmetric unit of **8** appears to hold 2.5 equivalents of $CHCl_3$ solvent of crystallization,

as a result of huge solvent voids. One of these molecules appeared highly ordered, one is disordered by rotation about the molecular 3-fold axis with a reasonable disorder model, while one is disordered about a molecular 2-fold (i.e. shares a Wyckoff position with the Pd dimers). Thus there are in all 4 × 2.5 = 10 chloroform in the unit cell.

Table 2.5 Crystallographic data and structure refinement for **8** (after SQUEEZE)

	8·2.5$CHCl_3$
Temperature (K)	173(2)
Crystal system	Monoclinic
Space group	$P2_1/n$
Unit cell dimensions	
a, Å	18.0613(8)
b, Å	15.5096(7)
c, Å	21.0807(10)
β, deg	103.4100(10)
Z	4
Goodness-of-fit on F^2	1.056
Final *R* indices [$I>2\sigma(I)$]	R_1 = 0.0387
	wR_2 = 0.0875
R indices (all data)	R_1 = 0.0566
	wR_2 = 0.0926

While a reasonable disorder model was constructed, the resulting refinement suffered from a high R_{int} (5.1%); large residual peaks (7.5 $e^-\cdot Å^{-3}$) and a larger *R*-factor (R_1 = 11.0%). Therefore recourse was made to the Platon SQUEEZE routine to remove all the solvent from the unit cell.[12] This leads to a model presented here without solvent, which seems quite successful but still leads to certain artifacts, most noteworthy of which is the large hole in the final difference map 0.49 Å from Br(2). The structure of **8** has several special features from the crystallographic point of view. First of all, while $Z = 4$ is quite ordinary for $P2_1/n$, here there are four dimeric molecules in the unit cell containing a total of 8 Pd atoms. However, the asymmetric unit consists of two different "half dimers", in

different special locations within the unit cell. The two resulting kinds of dimers differ quite significantly in their Pd–Pd non-bonded separations. The dimer with the shorter Pd–Pd distance {3.1768(4) Å} is located on Wyckoff position 2*e* with site symmetry of 2, whereas the other with the *longer* Pd–Pd distance {3.2880(4) Å} is located on Wyckoff position 2*f*, also with site symmetry of 2.

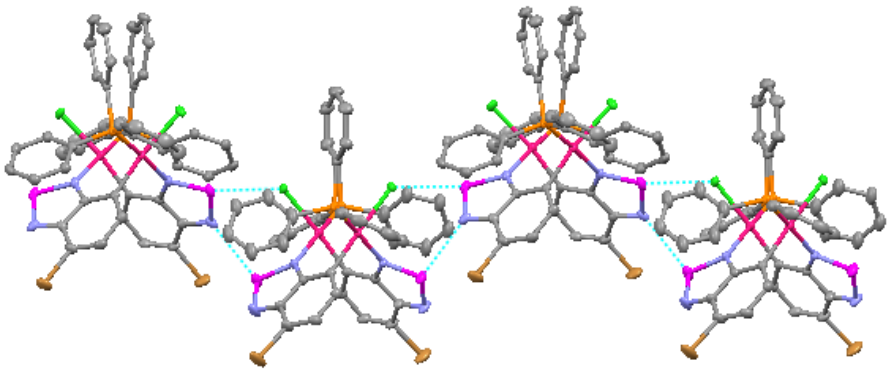

Figure 2.14 Ribbon growth in the crystals of **8** by SBI along the *a* axis

The Pd–C bond distances {Pd(1)–C(27)#1 2.012(4); Pd(2)–C(3) 1.992(4) Å} in two asymmetric units differ significantly from each other, and the Pd–C bond distance {Pd(2)–C(3)} is shorter than the Pd–C bond distance {2.032(11) Å} in **7b**. Similarly the Pd–Cl {Pd(1)–Cl(2) 2.3641(10); Pd(2)–Cl(1) 2.3863(10) Å} and Pd–P {Pd(1)–P(2) 2.2462(10); Pd(2)–P(1) 2.2563(10) Å} bond distances are also different and shorter than the Pd–Cl {2.3945(11) Å} and Pd–P {2.3109(11) Å} bond distances in **6a**. Another intriguing feature of the structure is the association of the two dimers (Figure 2.13b) by SBI between the Se---N {3.24(1) Å} and Se---Cl {3.06(9) Å}, and the two contacts are shorter than the sum of the van der Waals radii (3.45 and 3.66 Å, respectively). The Se---N contact distance is longer than the Se---N distance of {2.94(5) Å} found in **5** due to the

bulky nature of the molecule (Figure 2.13b). The secondary bonding interaction among the dimers continues along the *a* axis forming an infinite ribbon array (Figure 2.14).

2.5 Pd-promoted C–C coupling reactions

2.5.1 C–C coupling reactions of **6b**

To support the proposed mechanism of Pd-catalyzed C–C coupling reactions, simple tests were conducted to see if the oxidative addition products could function as intermediates for such coupling. Stoichiometric reactions of **6b** were carried out with 4-*tri*-butylstannylpyridine in refluxing toluene for two days affording a *bis*-coupling product 4,7-*bis*(4-pyridyl)benzothiadiazole. As the earlier attempts at Suzuki coupling reactions showed that $-B(OH)_2$ is not a sufficiently good leaving group, it was replaced by *tri*-butylstannyl groups which succeeded in the C–C coupling reaction. The reaction features were quite interesting in that both 1:1 and 1:2 ratio reactions gave only the *bis*-coupling product but the yield was higher when the correct stoichiometry was used (Scheme 2.6).

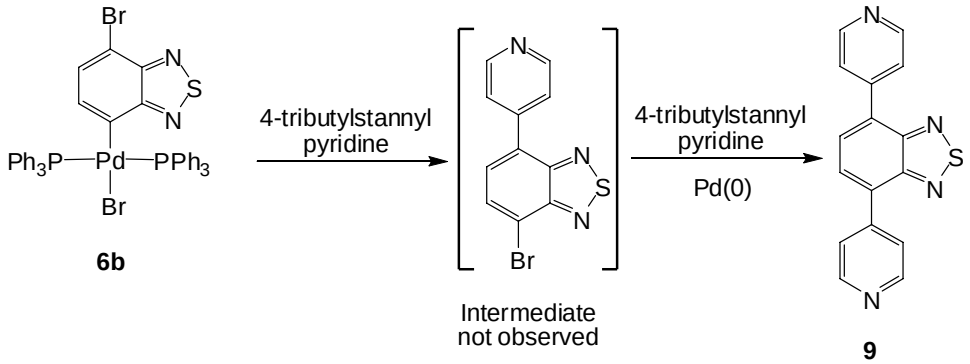

Scheme 2.6 Synthesis of 4,7-*bis*(4-pyridyl)benzothiadiazole (**9**)

This suggests that even though the first C–C coupling reaction is stoichiometric, the intermediate formed *in situ* rapidly undergoes a transmetallative coupling reaction with

excess 4-*tri*-butylstannylpyridine followed by further oxidative addition and transmetallation to give 4,7-*bis*(4-pyridyl)benzothiadiazole (**9**). The attempts to isolate the *mono*-coupling product by stopping the reaction even after 12 or 24 h and from lower-boiling solvents were unsuccessful. This is probably due to the fast transmetallative coupling reaction of the intermediate.

2.5.2 C–C coupling reactions of **7b**

Similar reactions of **7b** and 4-tributylstannylpyridine afforded *mono*- and *bis*-coupling products depending on the solvents used and the stoichiometry of the reactants. The intermediate *mono*-coupling product was isolated from the 1:1 ratio toluene reflux reaction whereas the *bis*-coupling product formation was observed in 1:2 ratio xylene reflux reaction (Scheme 2.7).

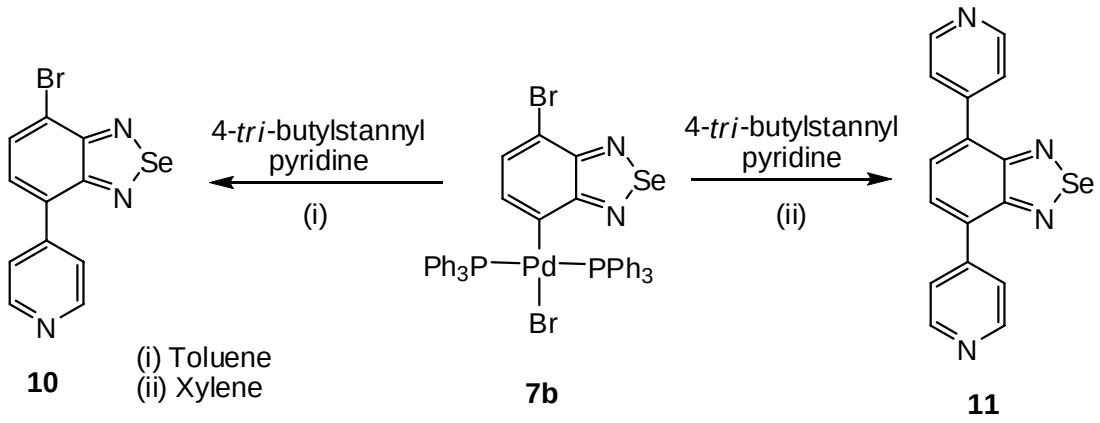

Scheme 2.7 Synthesis of 4,7-*bis*(4-pyridyl)benzoselenadiazole (**11**) and isolating the intermediate *mono*-coupling product (**10**)

This bolsters the proposed mechanism for the Stille coupling reaction[13] by confirming that the reaction proceeds in a stepwise manner. Thus, the isolated intermediate undergoes transmetallative coupling, followed by further oxidative addition and

transmetallation with excess 4-*tri*-butylstannylpyridine to give 4,7-*bis*(4-pyridyl)benzoselenadiazole (**11**). However, unlike the previous example, the second step appears to occur more slowly than the first resulting in isolable mono-addition product **10**. Further discussion of the optimized syntheses and characterization of 4,7-*bis*(2/4-pyridyl)benzochalcogenadiazoles is presented in chapter 3.

References

1. (a) Heck, R. F. *Palladium Reagents in Organic Synthesis*; Academic Press: New York, 1985. (b) Tsuji, J. *Palladium Reagents and Catalysts*; Wiley: Chichester, U.K., 1995. (c) Hartwig, J. F. *Angew. Chem., Int. Ed.* **1998**, *37*, 2046. (c) Kürti, L.; Czakó, B., *Strategic Applications of Named Reactions in Organic Synthesis*. Elsevier Academic Press: London, 2005.

2. (a) Vries, J. G. de *Can. J. Chem.* **2001**, *79*, 1086. (b) Beller, M.; Zapf, A.; Mägerlein, W. *Chem. Eng. Technol.* **2001**, *24*, 575. (c) Zapf, A.; Beller, M. *Top. Catal.* **2002**, *19*, 101.

3. (a) Suzuki, A. *Pure Appl. Chem.* **1991**, *63*, 419. (b) Miyaura, N.; Suzuki, A. *Chem. Rev.* **1995**, *95*, 2457.

4. Sundermeier, M.; Mutyala, S.; Zapf, A.; Spannenberg, A.; Beller, M. *J. Organomet. Chem.* **2003**, *684*, 50.

5. Vicente, J.; Abad, J. A.; López-Nicolás, R. -M.; Jones, P. G. *Organometallics* **2004**, *23*, 4325 and the references therein.

6. (a) Nunn, A. J.; Ralph, J. T. *J. Chem. Soc.* **1965**, 6769. (b) Bird, C. W.; Cheeseman, G. W. H.; Sarsfiel, A. A. *J. Chem. Soc.* **1963**, 4767.

7. (a) Tomura, M.; Yamashita Y. *Z. Kristallogr. New Cryst. Struct.* **2003**, *218*, 555. (b) Tomura, M.; Akhtaruzzaman, Md.; Suzuki, K.; Yamashita, Y. *Acta Crystallogr., Sec C: Cryst. Struct. Commun.* **2002**, *58*, o373. (c) Cozzolino, A. F.; Britten, J. F.; Vargas-Baca, I. *Cryst. Growth Des.* **2006**, *6*, 181. (d) Cozzolino, A. F.; Vargas-Baca, I. *J. Organomet. Chem.* **2007**, *692*, 2654.

8. Gomes, A. C.; Biswas, G.; Banerjee, A.; Duax, W. L. *Acta Crystallogr., Sec C: Cryst. Struct. Commun.* **1989**, *45*, 73.

9. Bondi, A. *J. Phys. Chem.* **1964**, *68*, 441.

10. (a) Schuster, O.; Raubenheimer, H. G. *Inorg. Chem.* **2006**, *45*, 7997. (b) Flemming, J. P.; Pilon, M. C.; Borbulevitch, O. Y.; Antipin, M. Y.; Grushin, V. V. *Inorg. Chim. Acta* **1998**, *280*, 87.

11. (a) Vicente, J.; Abad, J. A.; Nicolás, R. M. L.; Jones, P. G. *Organometallics* **2004**, *23*, 4325. (b) Retbøll, M.; Edwards, A. J.; Rae, A. D.; Willis, A. C.; Bennett, M. A.; Wenger, E. *J. Am. Chem. Soc.* **2002**, *124*, 8348. (c) Albert, J.; Granell, J.; Moragas, R.; Sales, J.; Bardia, M. F.; Solans, X. *J. Organomet. Chem.* **1995**, *494*, 95.

12. Sluis, P. V. D.; Spek, A. L. *Acta Cryst.* **1990**, *A46*, 194.

13. Stille, J. K. *Angew. Chem., Int. Ed.* **1986**, *25*, 508.

CHAPTER THREE: LIGAND SYNTHESIS BY STILLE COUPLING REACTION

3.1 Introduction

Over the last few decades, long π–conjugated molecules with rigid structures, such as molecules with pyridyl substituents at the terminal positions, have attracted much attention because they are expected to be precursors for the synthesis of molecular devices.[1] They form supramolecular architectures by the self-assembly with metals[2] exhibiting interesting properties, such as guest storage, luminescence,[3] redox activity,[4] and magnetism.[5] Recently, several papers have shown the synthesis of self-assembled molecular squares and square-grid polymers using 4,4′-bipyridine and analogous structural units that are significantly longer such as Py–X–Py (Py = 4-pyridyl, X = CH_2CH_2, S–S, CH=CH, C≡C, Ar) (Figure 3.1).[6]

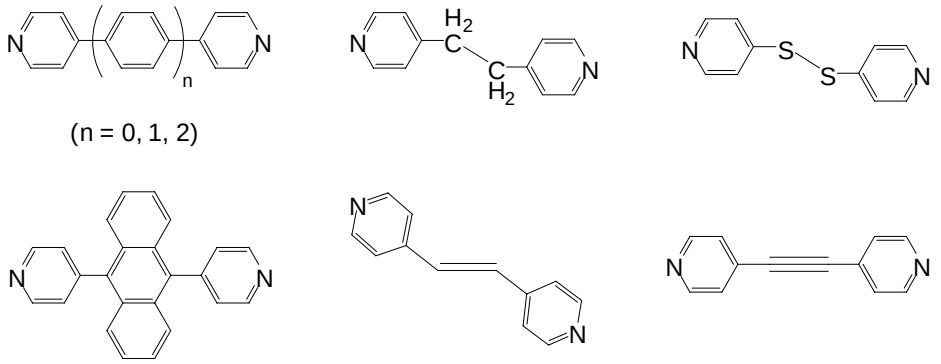

Figure 3.1 Different 4-pyridyl derivatives

2,1,3-benzochalcogenadiazoles are one of the more important classes of organic redox systems due to their high reduction potential, electron affinity and high fluorescence quantum yields, necessary for their utilization in light-emitting diode (LED) technology and have been investigated for a considerable time.[7] Over the past few years, several

reports have been documented on the derivatization of the parent 2,1,3-benzothiadiazole ring system by C−C coupling reactions in the presence of catalytic amounts of a palladium catalyst. Dupont and co-workers reported the synthesis of different aryl substituted 2,1,3-benzothiadiazoles by Suzuki coupling and Sonogashira cross-coupling reactions (Figure 3.2).[7]

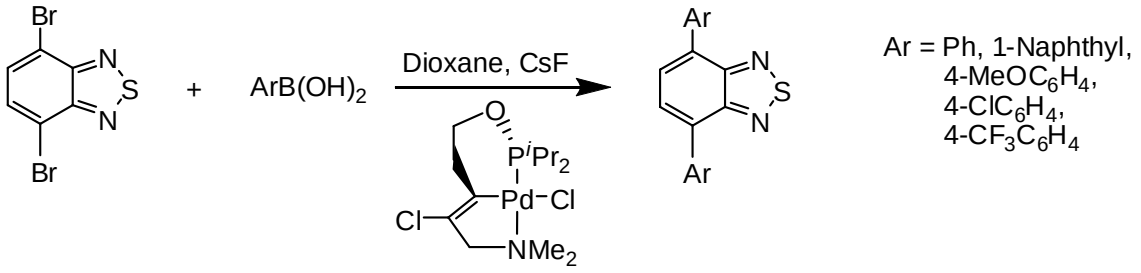

Suzuki Coupling

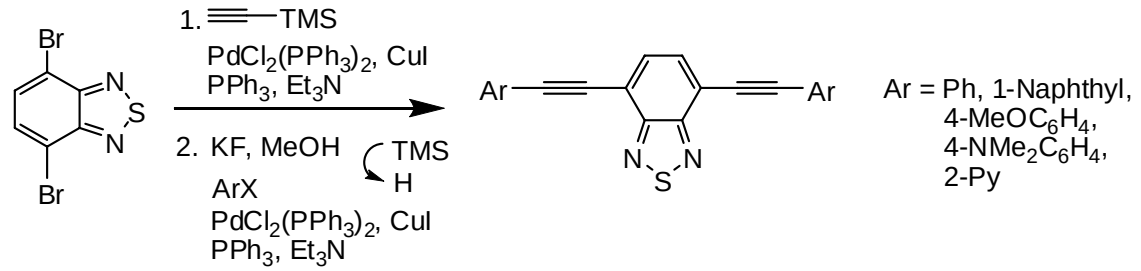

Sonogashira Cross-coupling

Figure 3.2 Synthesis of π–extended 2,1,3-benzothiadiazoles

Bipolar compounds containing peripheral diaryl amines and/or 4-*tert*-butylphenyl with 2,1,3-benzothiadiazole cores have also been synthesized and reported by Lin *et al*.[8] Very recently Qiu and co-workers have extended this thiadiazole chemistry by introducing naphtho-2,1,3-thiadiazole as a core and derivatized them with different aryl groups (Figure 3.3).[9] Several reports have demonstrated the application of π-extended

thiadiazole chemistry in the development of new materials for technological applications.[7-9]

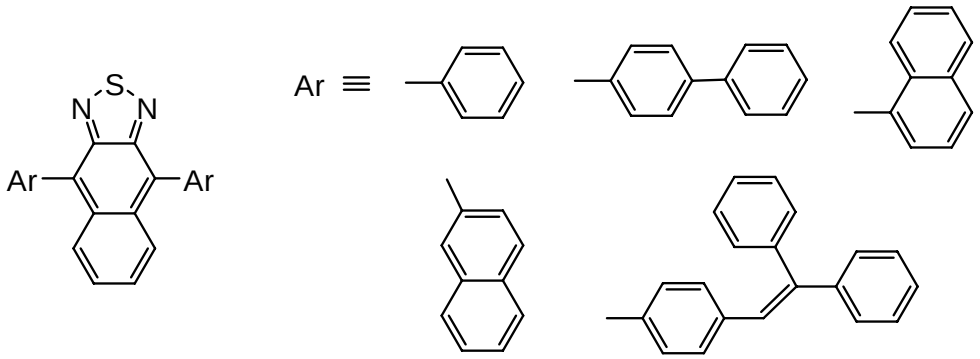

Figure 3.3 Synthesis of π–extended Naphtho-2,1,3-benzothiadiazoles

Compared to aryl derivatives the related pyridyl substituents are relatively unexplored. Very recently Yamashita and co-workers have demonstrated the synthesis of dipyridyl compounds containing a mono and bisbenzothiadiazole unit by Stille coupling and they also alkylated the nitrogen of the pyridyl rings.[10] The structures and properties of these dipyridyls were tuned by changing the nitrogen positions (positional isomers) and spacer groups (Figure 3.4).

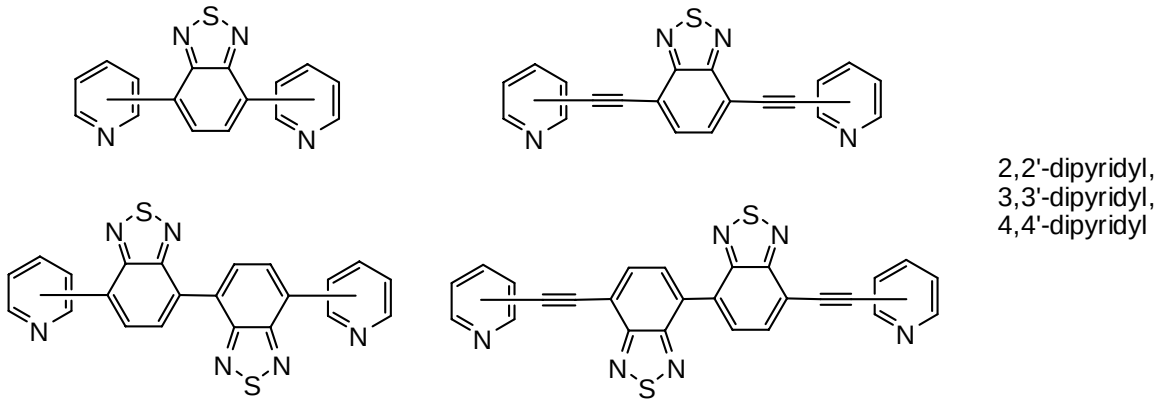

Figure 3.4 Synthesis of π–extended pyridyl-2,1,3-benzothiadiazoles

This group has also synthesized the thiazolyl derivatives of thiadiazoles and investigated their semiconducting responses by organic field-effect transistors (OFLETs) measurements (Figure 3.5).[11]

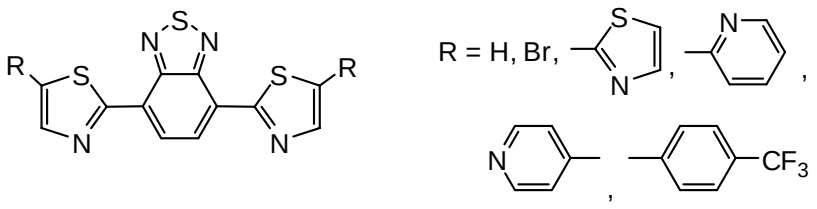

Figure 3.5 Synthesis of π–extended thiazolyl-2,1,3-benzothiadiazoles

3.2 Synthesis of 4,7-*bis*(4-pyridyl)-2,1,3-benzochalcogenadiazoles

3.2.1 Synthesis and characterization of 4,7-*bis*(4-pyridyl)-2,1,3-benzothiadiazole (**9**)

To produce **9**, the main challenge was to find an efficient catalytic process to carry out the targeted C–C coupling reaction. As mentioned in chapter 2, initial attempts to prepare **9** by a Suzuki coupling reaction were unsuccessful and switching to a Stille coupling reaction was found to work for these C–C coupling reactions. Following the literature method reported by Yamashita *et al.*,[10] the dipyridyl compound **9** was successfully prepared and the reaction conditions were modified by reducing the catalyst loading and increasing the duration of refluxing. According to the reported procedure, compound **9** was synthesized by refluxing a toluene solution of 4-*tri*-butylstannylpyridine and **3** in presence of 20% of catalyst loading of $Pd(PPh_3)_4$ overnight. On repeating the reaction under identical conditions to those of Yamashita *et al.*, low yields (<10%) of **9** were obtained. Thorough investigation of the reaction conditions either by reducing the

catalyst loading to 10 and 5%, or refluxing the reaction mixture for 3 to 7 days were undertaken which significantly improved the utility of this method in our hands.

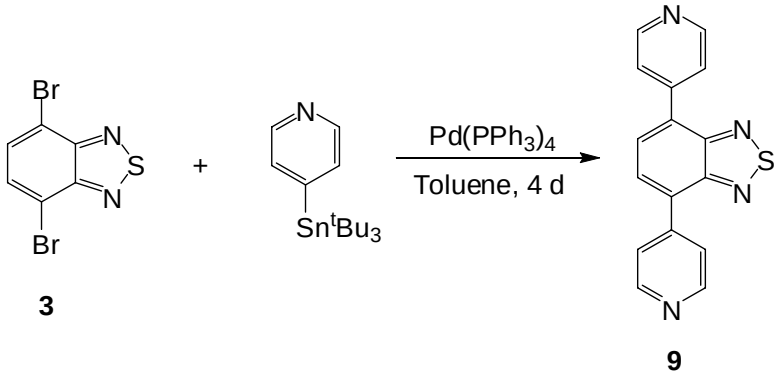

Scheme 3.1 Synthesis of 4,7-*bis*(4-pyridyl)-2,1,3-benzothiadiazole (**9**)

The best conditions determined to date consist of continuing the reflux for 4 days in the presence of 10% $Pd(PPh_3)_4$ catalyst to give compound **9** in 75% yield whereas at 5% catalyst loading the reflux must be continued for 7 days to give a yield of compound **9** was 50% (Scheme 3.1). It should also be noted that, though the single crystal X-ray structure of **9** was reported, the published NMR data cannot fit the reported structure and actually appears to be a gloss. Thus **9** was thoroughly characterized by spectroscopic methods, the results of which are reported here.

The ^{1}H NMR spectrum of **9** shows two doublets at δ 8.82 ppm (J = 6.0 Hz) and 7.94 ppm due to the four equivalent pyridyl ring protons, but the doublet at δ 7.94 ppm is overlapped by a singlet for the two equivalent benzothiadiazole ring protons (Figure 3.6). The presence of a total of ten hydrogens is evident from a 4:4:2 integration. The ^{13}C NMR spectrum has six distinct signals attributed to the six different carbon atoms in **9**. A full assignment of the ^{1}H and ^{13}C resonances of **9** was obtained by 2D shift-correlated

Heteronuclear Single Quantum Coherence (HSQC) and Heteronuclear Multiple Bond Coherence (HMBC) NMR experiments and is presented in the electronic appendix. The mass spectrum of **9** shows a molecular ion peak at m/z 290 as well as a fragment ion peak at m/z 212 due to the loss of one of the pyridyl rings.

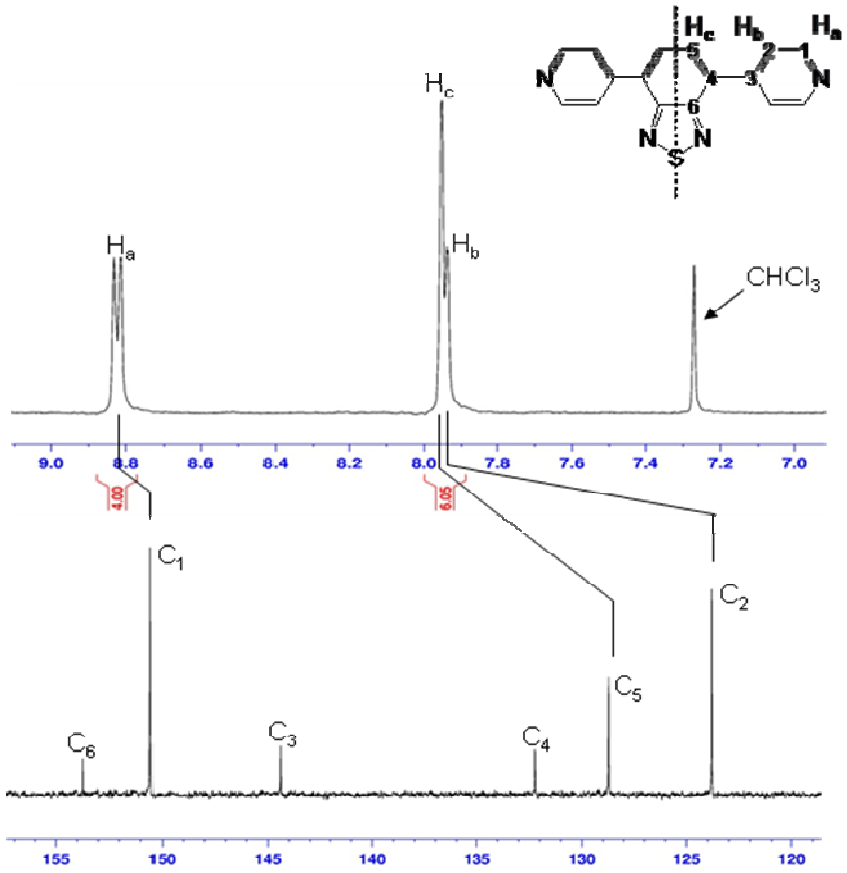

Figure 3.6 ^{1}H and ^{13}C NMR spectra of compound **9** (H_b, doublet)

3.2.2 Synthesis and characterization of 4-bromo-7-(4-pyridyl)-2,1,3-benzoselenadiazole (**10**)

Though the chemistry of π–extended 2,1,3-benzo- and naphthothiadiazoles has been investigated over the past few years, the corresponding selenadiazole ring system seems to have remained unexplored. Thus it was decided to synthesize the selenium analog of **9**.

Several attempts to synthesize 4,7-*bis*(4-pyridyl)-2,1,3-benzoselenadiazole following the optimized procedure for **9** were unsuccessful, and only the *mono*-coupled product was isolated (Scheme 3.2). Compound **10** obtained from the toluene reaction, was thoroughly characterized by spectroscopic methods together with a single crystal X-ray diffraction analysis.

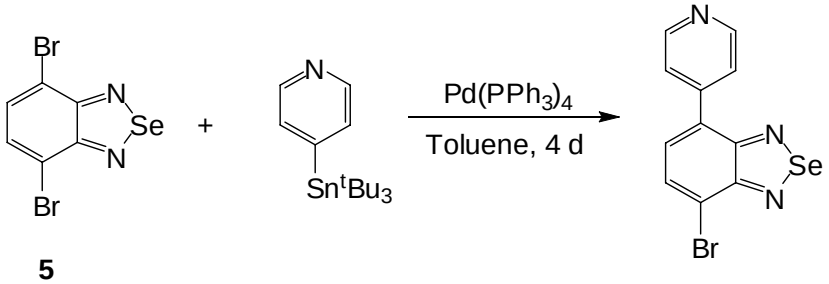

5 **10**

Scheme 3.2 Synthesis of 4-bromo-7-(4-pyridyl)-2,1,3-benzoselenadiazole (**10**)

Table 3.1 The full spectral assignment of **10** obtained by heteronuclear 2D shift-correlated HSQC and HMBC NMR experiments. Chemical shifts (δ in ppm) and the carbon-hydrogen correlation

	δ_C	δ_H	C-H	C-H	C-numbering
C					
1	157.6			H_5	
2	158.5			H_4	
3	132.7			$H_{8,\ 11,\ 4}$	
				H_5	
6	117.8			$H_{9,\ 10,\ 5}$	
7	144.5			H_5	
CH					
4	132.0	7.90	H_4		
5	129.2	7.53	H_5		
8,11	123.9	7.78	$H_{8,\ 11}$		
9,10	150.1	8.77	$H_{9,\ 10}$		

The ^{1}H NMR spectrum of **10** shows four doublets at δ 8.77, 7.90, 7.78 and 7.53 ppm. Two doublets at δ 8.77 ppm and 7.78 ppm with coupling constants of 6.4 Hz, each

integrating for two protons, are attributed to the pyridyl ring hydrogen atoms. Two other doublets at δ 7.90 ppm and 7.53 ppm integrate to one hydrogen atom each with coupling constant of 7.2 Hz, are attributed to the two different protons of the benzoselenadiazole ring. The ^{13}C NMR spectrum showed nine distinct signals attributed to the nine different carbon atoms in **10** (Table 3.1). A full assignment of the ^{1}H and ^{13}C resonances of **10** was obtained by 2D shift-correlated HSQC and HMBC NMR experiments and is presented in the electronic appendix.

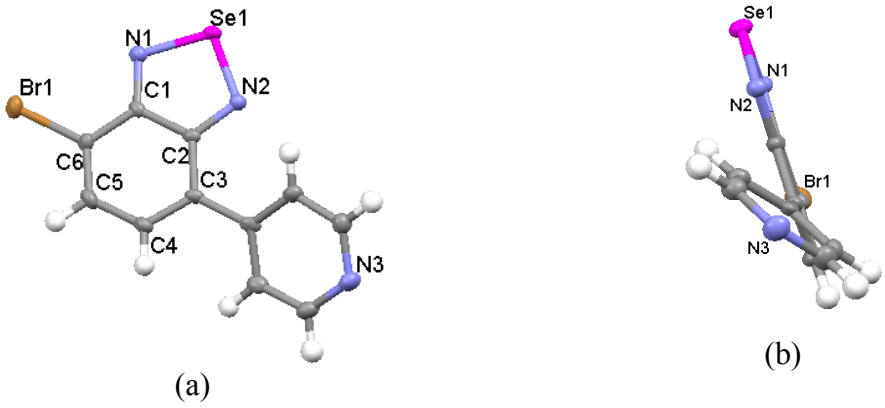

Figure 3.7 (a) Molecular structure of 4-bromo-7-(4-pyridyl)-2,1,3-benzothiadiazole (**10**), (b) Side view of **10**, selected bond lengths [Å] and bond angles [^{o}]: Se(1)–N(2) 1.783(6); Se(1)–N(1) 1.792(6); Br(1)–C(6) 1.879(7); N(1)–C(1) 1.315(9); N(2)–C(2) 1.329(9); C(2)–C(3) 1.445(9); C(3)–C(4) 1.364(10); C(4)–C(5) 1.415(11); C(5)–C(6) 1.359(11); C(1)–C(6) 1.419(9); N(2)–Se(1)–N(1) 93.9(3); C(1)–N(1)–Se(1) 106.6(5); C(2)–N(2)–Se(1) 106.9(5)

The single crystal molecular structure of **10** is depicted in Figure 3.7, selected crystal data are listed in Table 3.2, and selected bond distances and angles are listed in the caption to the Figure 3.7. The full crystal reports are presented in the electronic appendix. The structure consists of a 4-pyridyl group bonded to the aryl ring which formed by the

substitution of one bromine from the starting 4,7-bromobenzoselenadiazole (**4**). Similar to **5**, bond fixation is also observed, suggesting that after one pyridyl group is introduced the quinoidal character of the benzoselenadiazole is unperturbed (See Table 2.3, Chapter 2). The pyridyl ring is twisted and bent with respect to the benzoselenadiazole ring (Figure 3.7b) due to the steric hindrance and the dihedral angle between them is 36.1(6)^{o}.

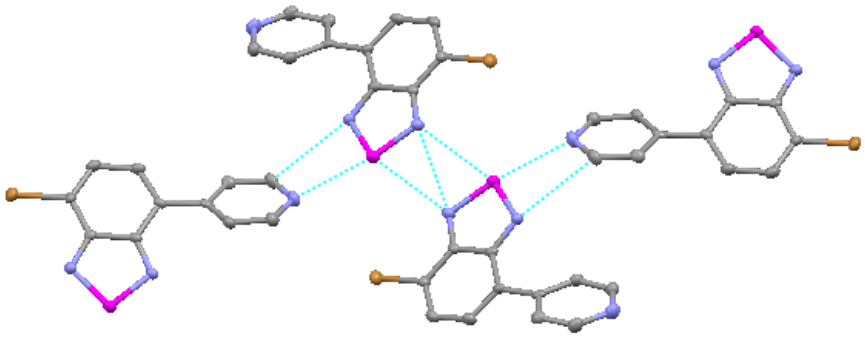

Figure 3.8 SBIs in the crystals of **10**

Table 3.2 Crystal data and structure refinement for **10**

	10
Temperature (K)	173(2)
Crystal system	Orthorhombic
Space group	Pbca
Unit cell dimensions	
a, Å	12.183(6)
b, Å	7.516(4)
c, Å	23.215(11)
$\alpha = \beta = \gamma$, deg	90
Z	8
Goodness-of-fit on F^2	1.138
Final *R* indices [$I>2\sigma(I)$]	$R_1 = 0.0526$
	$wR_2 = 0.1303$
R indices (all data)	$R_1 = 0.0735$
	$wR_2 = 0.1439$

The most intriguing structural features of **10** are the out-of-plane secondary bonding interactions (SBI) with the dihedral angle of 0.84(3)^{o}, which has never been observed before for chalcogenadiazole ring systems (Figure 3.8), with the contact distance of 3.12(8) Å (See Table 1.2, Chapter 1) longer than the SBI distance {2.94(5) Å} found in **5**. In addition, the SBI is extended by the presence of pyridyl rings and this Se---N short contact in the crystals of **10** helps to grow two dimensional zigzag sheets (Figure 3.8).

3.2.3 Synthesis and characterization of 4,7-*bis*(4-pyridyl)-2,1,3-benzoselenadiazole (**11**)

To obtain **11**, recourse was made to a higher boiling solvent, such as xylene which worked well and the duration of reflux could even be reduced to 4 h. In a typical experiment, a xylene solution (30 mL) of 4-*tri*-butylstannylpyridine and **5** containing 10% of $Pd(PPh_3)_4$ as catalyst was refluxed for 4 h, which afforded the expected 4,7-*bis*(4-pyridyl)-2,1,3-benzoselenadiazole (**11**) in 50% yield (Scheme 3.3). Attempts to grow single crystals for structure determination failed which perhaps due to the SBI leading to the formation of amorphous solids. Hence the characterization of **11** was entirely based on elemental analysis and spectroscopic methods, such as IR, NMR and mass spectroscopy.

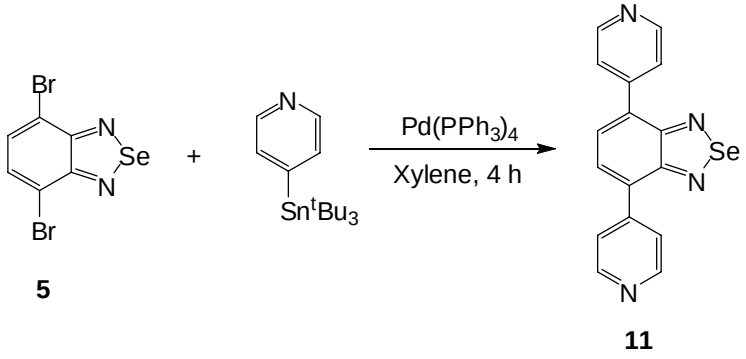

Scheme 3.3 Synthesis of 4,7-*bis*(4-pyridyl)-2,1,3-benzoselenadiazole (**11**)

The ^{1}H NMR spectrum of **11** shows two equal intensity doublets at δ 8.80 ppm and 7.86 ppm with coupling constants of 5.1 Hz, each integrating to four hydrogens, attributed to the two equivalent pyridyl ring protons and a singlet at δ 7.78 ppm due to the two equivalent protons of the benzoselenadiazole ring. As for the case of **9**, the ^{13}C NMR spectrum has six distinct signals attributed to the six different carbon atoms in **11** (Figure 3.9). A full assignment of the ^{1}H and ^{13}C resonances of **11** was obtained by heteronuclear 2D shift-correlated HSQC and HMBC NMR experiments and is presented in the electronic appendix. The mass spectrum of **11** shows a fragment ion peak at m/z 258 due to the loss of Se instead of giving a molecular ion peak as observed for **9**.

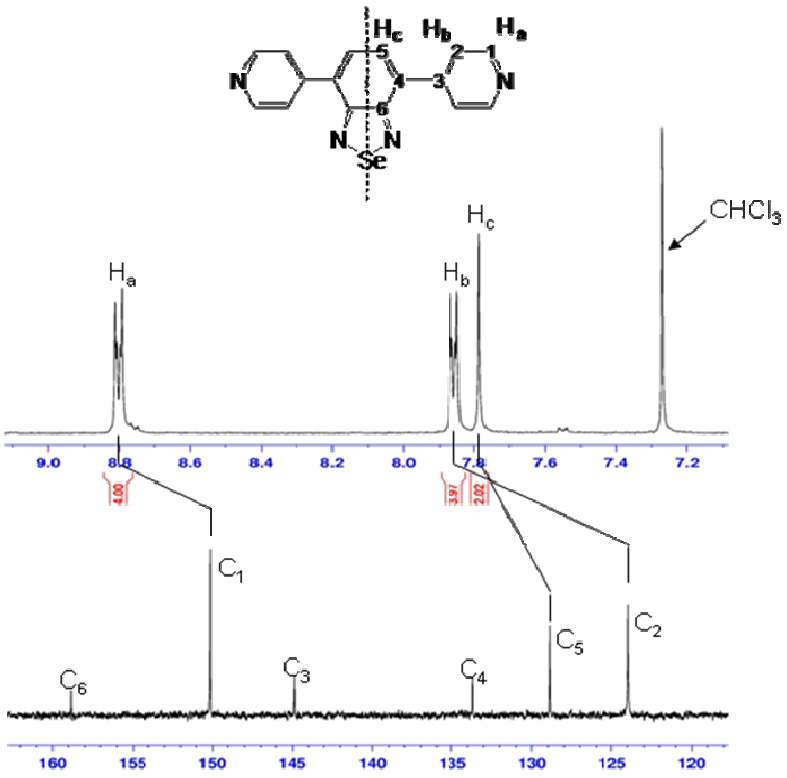

Figure 3.9 ^{1}H and ^{13}C NMR of compound **11**

3.3 Synthesis of 4,7-*bis*(2-pyridyl)-2,1,3-benzochalcogenadiazoles

3.3.1 Synthesis and characterization of 4,7-*bis*(2-pyridyl)-2,1,3-benzothiadiazole (**12**)

Though compound **12** was previously reported by Yamashita and co-workers,[10c] we decided to repeat the synthesis following the same procedure under identical condition that we optimized for **9**, as it would be a suitable candidate for synthesizing chelating metal complexes. Refluxing a toluene solution of 2-*tri*-butylstannylpyridine and **3** in the presence of 10% catalyst loading of $Pd(PPh_3)_4$ for 4 days afforded **12** in 42% yield (Scheme 3.4). The formation of compound **12** was confirmed by comparing the melting point and ^1H NMR data with the literature values.

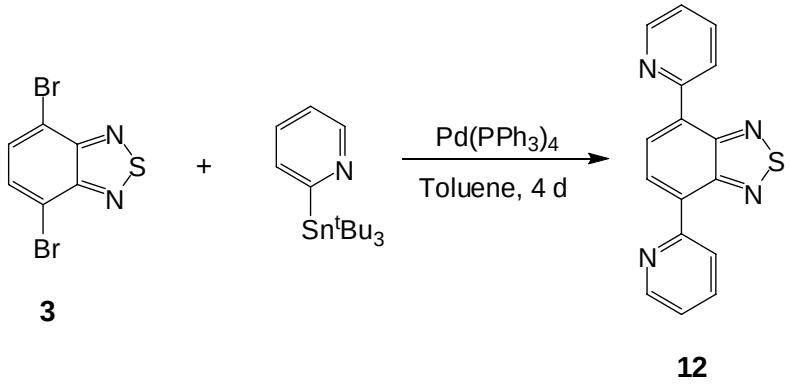

Scheme 3.4 Synthesis of 4,7-*bis*(2-pyridyl)-2,1,3-benzothiadiazole (**12**)

3.3.2 Synthesis and characterization of 4,7-*bis*(2-pyridyl)-2,1,3-benzoselenadiazole (**13**)

Earlier success with the synthesis of **11** helped us to extend our benzoselenadiazole chemistry by introducing 2-pyridyl groups in order to be able to compare the effect of the nitrogen position on the reduction potentials of the selenadiazole ring. Compound **13** was synthesized by repeating the reaction on a small scale under identical conditions as optimized for **11** using 2-*tri*-butylstannylpyridine instead, which gave **13** in 50% yield as

a yellow solid (Scheme 3.5). Compound **13** was characterized by a combination of spectroscopic methods and single-crystal X-ray diffraction studies.

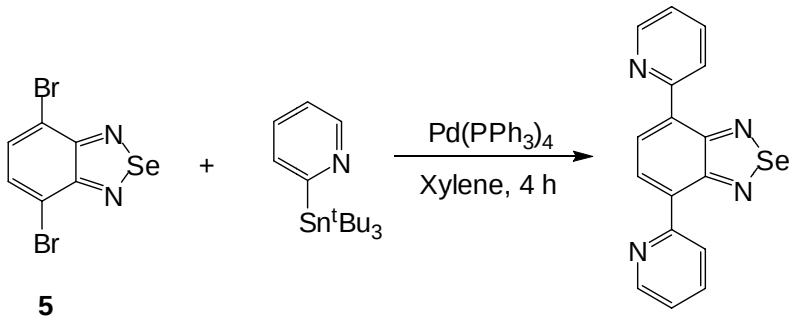

5 **13**

Scheme 3.5 Synthesis of 4,7-*bis*(2-pyridyl)-2,1,3-benzoselenadiazole (**13**)

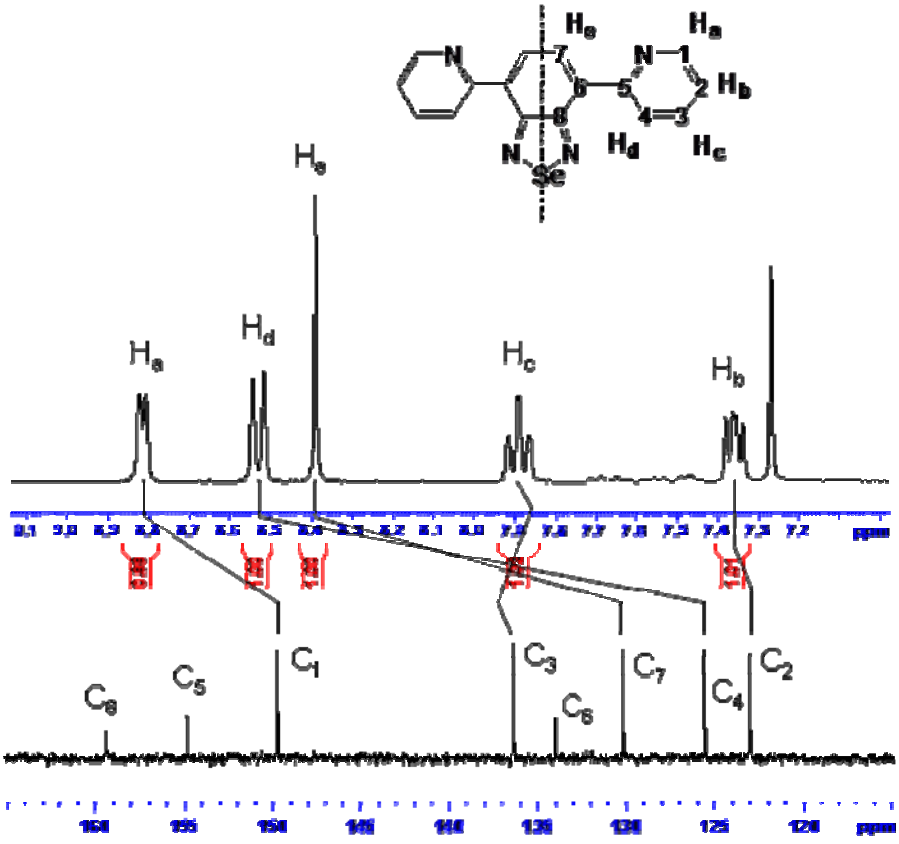

Figure 3.10 ^{1}H and ^{13}C NMR of compound **13**

The ^{1}H NMR spectrum of **13** shows five different proton signals at δ 8.82, 8.53, 8.39, 7.89 and 7.38-7.33 ppm, each integrating for two hydrogens, attributed to the two equivalent 2-pyridyl and benzoselenadiazole ring protons. The ^{13}C NMR spectrum has eight distinct signals attributed to the eight different carbon atoms in **13** (Figure 3.10). A full assignment of the ^{1}H and ^{13}C resonances of **13** was obtained by heteronuclear 2D shift-correlated HSQC and HMBC NMR experiments and is presented in the electronic appendix. As in the case of **11**, the EI mass spectrum of **13** shows a fragment ion peak at m/z 258 due to the loss of Se instead of giving a molecular ion peak at m/z 338.

The single-crystal molecular structure of **13** is depicted in Figure 3.11, crystal data are given in Table 3.3, and selected bond distances and angles are listed in the caption to the Figure 3.11. Compound **13** crystallizes in the monoclinic system with the centrosymmetric space group $P2_1/c$ and the asymmetric unit consists of two molecules.

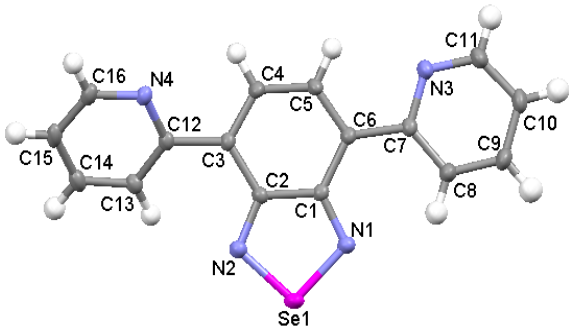

Figure 3.11 Molecular structure of 4,7-*bis*(2-pyridyl)-2,1,3-benzoselenadiazole (**13**), selected bond lengths [Å] and bond angles [^{o}]: C(1)–C(6) 1.443(2); C(1)–C(2) 1.465(2); C(2)–C(3) 1.440(2); C(3)–C(4) 1.359(2); C(4)–C(5) 1.410(2); C(5)–C(6) 1.369(2); Se(1)–N(2) 1.7749(15); Se(1)–N(1) 1.7796(15); Se(1A)–N(2A) 1.7802(14); Se(1A)–N(1A) 1.7826(14); N(2)–Se(1)–N(1) 94.82(7); N(2A)–Se(1A)–N(1A) 94.57(6); C(1)–N(1)–Se(1) 106.99(12); C(2)–N(2)–Se(1) 106.93(12)

The presence of two 2-pyridyl groups in the structure confirms C−C coupling on both sides of 4,7-dibromobenzoselenadiazole (**5**), and the 2-pyridyl rings are twisted and bent with respect to the benzoselenadiazole ring due to steric hindrance. The dihedral angles between pyridyl and benzoselenadiazole rings {25.6(3)^{o}, molecule 1; 32.5(2)^{o}, molecule 2} are different showing that the pyridyl rings are not twisted equally and for molecule 2, the value is essentially same as the dihedral angle {32.4(1)^{o}} found in the corresponding thiadiazole analog.[10c] As previously noted e.g. in the structure of **5**, the quinoidal character of the benzoselenadiazole ring is also observed as indicated by the fixation of certain bonds (See Table 2.3, Chapter 2).

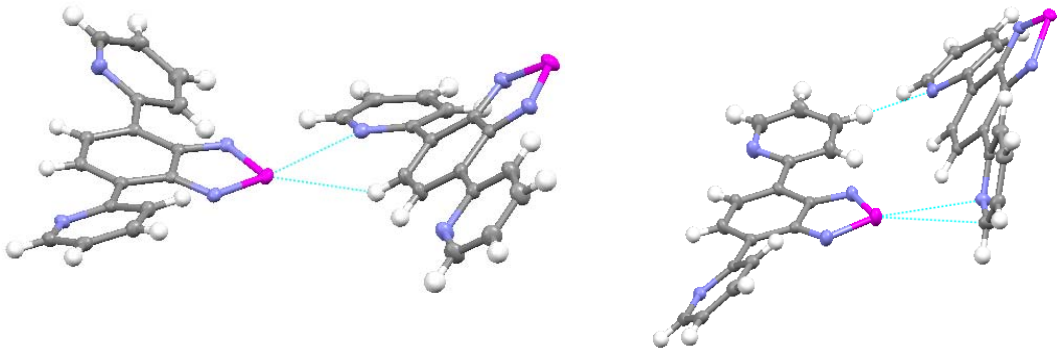

(a) (b)

Figure 3.12 Secondary bonding interactions (SBIs) of **13** in three dimensions (a) face-to-face and (b) sidewise

Though Se---N secondary bonding interactions between the selenadiazole rings are not observed in the crystal structure, perhaps because of the bulky pyridyl rings, the structure contains face-to-face and sidewise Se---N short contacts {3.21(4) and 3.38(8) Å} (See Table 1.2, Chapter 1) between the selenium atom of the selenadiazole ring and the nitrogen atom of the pyridyl ring (Figure 3.12). The % shortenings for the face-to-face and sidewise Se---N interactions (6.96 and 2.03) are significantly smaller than the Se---N

SBI (14.5) observed between the selenadiazole rings, indicating that the interactions are weak.

Table 3.3 Crystal data and structure refinement for **13**

	13
Temperature (K)	173(2)
Crystal system	Monoclinic
Space group	$P2_1/c$
Unit cell dimensions	
a, Å	15.3736(8)
b, Å	8.3764(4)
c, Å	20.5773(11)
β, deg	93.1210(10)
Z	8
Goodness-of-fit on F^2	1.030
Final *R* indices [$I>2\sigma(I)$]	$R_1 = 0.0235$
	w$R_2 = 0.0613$
R indices (all data)	$R_1 = 0.0296$
	w$R_2 = 0.0644$

3.4 Synthesis and characterization of 1,5-*bis*(4-pyridyl)naphthalene (**16**)

Literature review for molecules with 4-pyridyl structural units shows that over the past few decades, scientists around the world made and used several derivatives such as Py–X–Py (Py = 4-pyridyl, X = CH_2CH_2, S–S, CH=CH, C≡C, Ar) to prepare both self-assembled single molecules and extended solids.[6] However, the corresponding naphthalene derivatives are less explored. A few naphthalene derivatives, such as 1,8-*bis*(4-pyridyl)naphthalene[12a] and 4-(1-naphthyl)-2-phenylpyridine,[12b] have been reported, but no such results have been reported for 1,5-*bis*(4-pyridyl)naphthalene (**16**). The synthesis of **16** involves two steps from commercially available 1,5-diaminonaphthalene, the first of which has been reported earlier[13a] in which **14** was diazotized and brominated following a published procedure[13b] for the bromination of 2,6-diisopropylanilene ($DippNH_2$) to afford 1,5-dibromonaphthalene (**15**) in 14% yield. The formation of

compound **15** was confirmed by melting point and ^{1}H NMR spectroscopy comparing with the literature reported values.

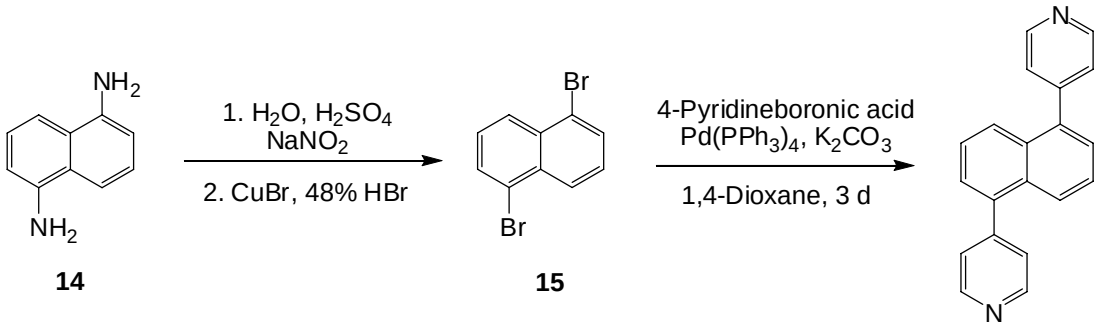

14 **15** **16**

Scheme 3.6 Synthesis of 1,5-*bis*(4-pyridyl)naphthalene (**16**)

Once the dibromo compound **15** was prepared, the corresponding 1,5-*bis*(4-pyridyl)naphthalene (**16**) was synthesized by a Suzuki coupling reaction, where a 1,4-dioxane solution of **15** and 4-pyridylboronic acid was refluxed for 3 days in the presence of a catalytic amount of [$Pd(PPh_3)_4$] (10%) and K_2CO_3 (Scheme 3.6). The solution was carefully transferred into a round-bottom flask and the solvent removed using a rotary evaporator under vacuum. The residue was dissolved in 30 mL of $CHCl_3$ giving a slightly black cloudy solution and treated twice with 20 mL of brine. The $CHCl_3$ layer was collected using a separatory funnel and removed under vacuum. The off-white solid was dissolved in a minimum amount of $CHCl_3$ and layered with ethanol affording **16** as colorless crystals in 44% yield. Compound **16** was characterized by spectroscopic methods together with a single-crystal X-ray diffraction study.

The ^{1}H NMR spectrum of **16** consists of four signals at δ 8.77, 7.91, 7.54 and 7.46 ppm attributed to the two equivalent 4-pyridyl and naphthalene ring protons (Figure 3.13). The ^{13}C NMR spectrum has eight distinct signals attributed to the eight different carbon atoms

in **16** (Figure 3.13). A full assignment of the ^{1}H and ^{13}C resonances of **16** was obtained by heteronuclear 2D shift-correlated HSQC and HMBC NMR experiments and is presented in the electronic appendix. The mass spectrum of **16** shows a molecular ion peak at m/z 282.

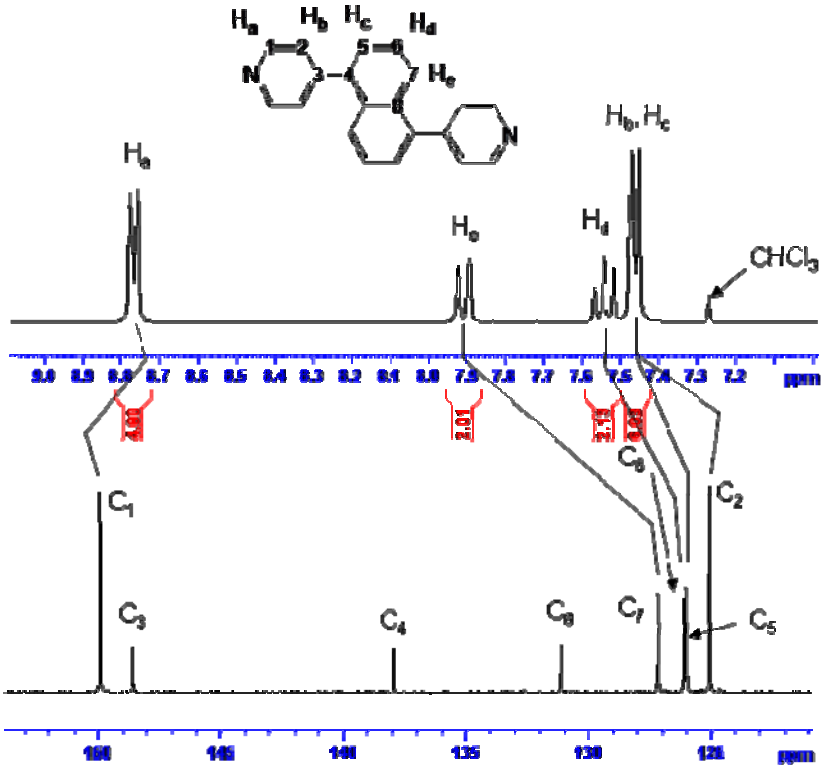

Figure 3.13 ^{1}H and ^{13}C NMR spectrum of compound **16**

The single-crystal molecular structure of **16** is depicted in Figure 3.14, crystal data are listed in Table 3.4, and selected bond distances and angles are given in the caption to the Figure 3.14. The full crystal reports are presented in the electronic appendix. The asymmetric unit of **16** contains half of the molecule with the centre of the molecule at an inversion site of the lattice.

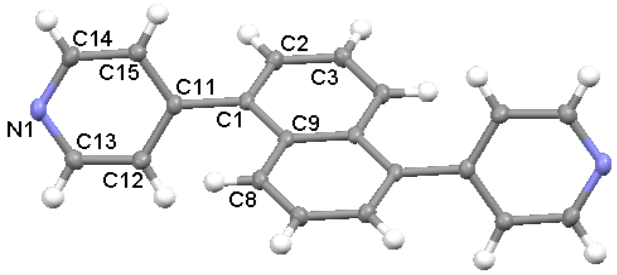

Figure 3.14 Molecular structure of 1,5-*bis*(4-pyridyl)naphthalene (**16**), selected bond lengths [Å] and bond angles [°]: N(1)–C(13) 1.3365(19); N(1)–C(14) 1.3396(19); C(1)–C(2) 1.372(2); C(1)–C(9) 1.4298(19); C(1)–C(11) 1.4952(17); C(2)–C(3) 1.4104(18); C(3)–C(8)#1 1.3670(19); C(13)–N(1)–C(14) 116.06(11); C(2)–C(1)–C(9) 119.84(11); C(2)–C(1)–C(11) 118.74(12); C(9)–C(1)–C(11) 121.41(11); C(1)–C(2)–C(3) 121.13(12)

Table 3.4 Crystal data and structure refinement for **16**

	16
Temperature (K)	173(2)
Crystal system	Monoclinic
Space group	$P2_1/n$
Unit cell dimensions	
a, Å	9.096(6)
b, Å	5.954(4)
c, Å	13.447(9)
β, deg	103.849(7)
Z	2
Goodness-of-fit on F^2	1.040
Final *R* indices [$I>2\sigma(I)$]	$R_1 = 0.0425$ $wR_2 = 0.1004$
R indices (all data)	$R_1 = 0.0555$ $wR_2 = 0.1075$

The molecule contains two 4-pyridyl groups at 1 and 5 positions of the naphthalene ring. The pyridyl rings are twisted because of the steric hindrance between the hydrogen atoms and the dihedral angle between the 4-pyridyl and naphthalene ring is 59.0(2)°. Bond fixation in the naphthalene ring is evident from the two different types of C−C bond

distances. The crystal structure of **16** shows π-π stacking interactions (between the pyridine rings), and T-interactions (between the pyridine and naphthalene rings). The packing diagram of **16** in the unit cell is shown in Figure 3.15, which shows that the molecules pack in criss-crossed layers. In three dimensions, the molecules are associated with non-classical C−H---N weak hydrogen bonding with an H---N distance {2.53(8) Å} shorter than 2.75 Å (van der Waals sum of H and N).[14] One layer, the center of Figure 3.15, forms C−H---N weak hydrogen bonds oriented rigorously in the [110] directions and along the ab planes at c = 0.5. The second layer (upper and lower in Figure 3.15) has the same structure but oriented in the [$\overline{1}10$] directions.

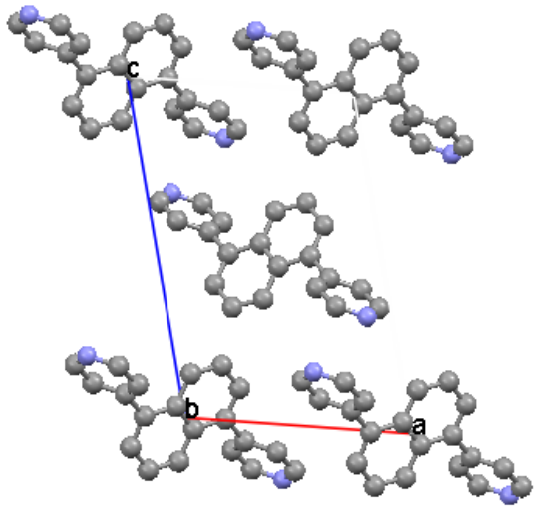

Figure 3.15 Perspective views of the crystal packing of **16** along *b* axis (hydrogen atoms are omitted for clarity)

References

1. (a) Tour, J. M. *Acc. Chem. Res*. **2000**, *33*, 791. (b) Tour, J. M. *Chem. Rev*. **1996**, *96*, 557. (c) Dirk, S. M.; Pric, D. W., Jr.; Chantean, S.; Kosynkin, P. V.; Tour, J. M. *Tetrahedron* **2001**, *57*, 5109. (d) Garnier, F. *Angew. Chem., Int. Ed.* **1989**, *28*, 513. (e) Roncali, J. *Chem. Rev*. **1992**, *92*, 711. (f) Chantean, S. H.; Tour. J. M. *Tetrahedron Lett.* **2001**, *42*, 3057.

2. (a) Zaman, M. B.; Smith, M. D.; Zur Loye, H.-C. *Chem. Commun*. **2001**, 2256. (b) Biradha, K.; Hongo, Y.; Fujita, M. *Angew. Chem., Int. Ed*. **2000**, *39*, 3843. (c) Carlucci, L.; Ciani, G.; Proserpio, D. M. *Dalton Trans*. **1999**, 1799.

3. Sakamoto, H.; Ishikawa, J.; Nakao, S.; Wada, H. *Chem. Commun*. **2000**, 2395.

4. (a) Slone, R. V.; Hupp, J. T.; Stem, C. L.; Albrecht-Schmitt, T. E. *Inorg. Chem*. **1996**, *35*, 4096. (b) Slone, R. V.; Hupp. J. T. *Inorg. Chem*. **1997**, *36*, 5422. (c) Slone, R. V.; Benkstein, K. D.; Belanger, S.; Hupp. J. T.; Guzei, I. A.; Rheingold, A. L. *Coord. Chem. Rev*. **1998**, *171*, 221. (d) Belanger, S.; Hupp, J. T.; Stern, C. L.; Slone, R. V.; Wastone, D. F.; Carrel, T. G. *J. Am. Chem. Soc*. **1999**, *121*, 557.

5. (a) Miller, J. S.; Epstein, A. J. *Angew. Chem., Int. Ed.* **1994**, *33*, 385. (b) McOuillan, F. S.; Berridge, T. E.; Chen, H.; Hamor, T. A.; Jones, C. J. *Inorg. Chem*. **1998**, *37*, 4959.

6. (a) Biradha, K.; Hongo, Y.; Fujita, M. *Angew. Chem., Int. Ed.* **2000**, *39*, 3843 and references therein. (b) Martin, G.; Andruh, M.; Madalan, A. M.; Blake, A. J.; Wilson, C.; Champness, N. R.; Schröder, M. *Cryst. Growth Des.* **2008**, *8*, 964 and references therein.

7. Neto, B. A. D.; Lopes, A. S. A.; Ebeling, G.; Gonçalves, R. S.; Costa, V. E. U.; Quina, F. H.; Dupont, J. *Tetrahedron* **2005**, *61*, 10975.

8. Thomas, J.; Lin, J. T.; Velusamy, M.; Tao, Y. –T.; Chuen, C. –H. *Adv. Func. Mat.* **2004**, *14*, 83.

9. Wei, P.; Duan, L.; Zhang, D.; Qiao, J. Wang, L.; Wang, R.; Dong, G.; Qiu, Y. *J. Mat. Chem.* **2008**, *18*, 806.

10. (a) Akhtaruzzaman, M.; Tomura, M.; Zaman, M. B.; Nishida, J. –I.; Yamashita, Y. *J. Org. Chem.* **2002**, *67*, 7813. (b) Akhtaruzzaman, M.; Tomura, M.; Nishida, J. –I.; Yamashita, Y. *Synth. Met.* **2003**, *137*, 873. (c) Akhtaruzzaman, M.; Tomura, M.; Nishida, J. –I.; Yamashita, Y. *J. Org. Chem.* **2004**, *69*, 2953.

11. Akhtaruzzaman, M.; Kamata, N.; Nishida, J. –I.; Ando, S.; Tada, H.; Tomura, M.; Yamashita, Y. *Chem. Commun*. **2005**, 3183.

12. (a) Mei, X.; Wolf, C. *Cryst. Eng. Comm.* **2006**, *8*, 377. (b) Mkhalid, I. A. I.; Coventry, D. N.; Albesa-Jove, D.; Batsanov, A. S.; Howard, J. A. K.; Perutz, R. N.; Marder, T. B. *Angew. Chem., Int. Ed.* **2006**, *45*, 489.

13. (a) Hodgson, H. H.; Whitehurst, J. S. *J. Chem. Soc*. **1947**, 80. (b) Masuda, J. D. MSc. Thesis **2002**, *Chapter 4*, p-65.

14. (a) Bondi, A. *J. Phys. Chem.* **1964**, *68*, 441. (b) Yue, W.; Tian, H. K.; Hu, N.; Geng, Y.; Wang, F. *Cryst. Growth Des.* **2008**, *8*, 2352.

CHAPTER FOUR: SELF-ASSEMBLED RHENIUM-RODS

4.1 Introduction

As mentioned in Chapter 1, there are numerous examples of neutral molecular squares containing metal carbonyls as corner units. Compared to the neutral squares, the synthesis of neutral self-assembled molecular rods is less explored. Recently Kühn *et al.* reported the synthesis of mixed metallic tetranuclear molecular rods $[(2,2'\text{-bipy})(CO)_3Re(4,4'\text{-bipy})]_2[M_2(O_2CR)_4](CF_3SO_3)_2$ (M = Mo, R = CF_3; M = Rh, R = CH_3) from the reaction of $[(2,2'\text{-bipy})(CO)_3Re(4,4'\text{-bipy})](CF_3SO_3)$ with $M_2(O_2CR)_4$ (Figure 4.1).[1]

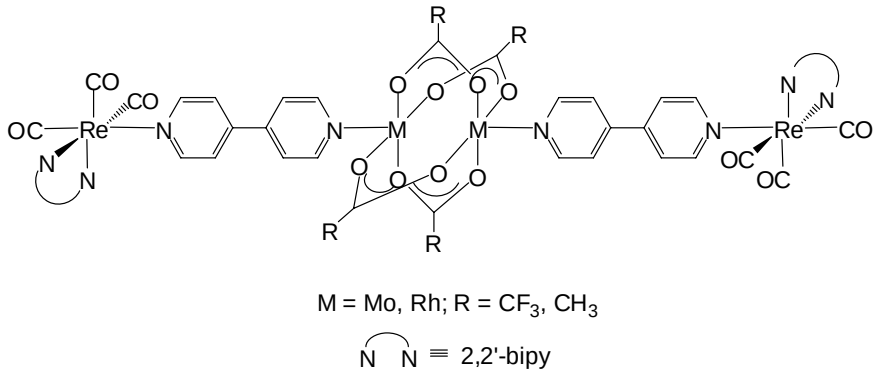

Figure 4.1 Tetranuclear mixed Re-Mo/Rh(acetate) molecular rod

4.2 Synthesis of [{$ReBr(CO)_4$}$_2$(μ-4,7-*bis*(4-pyridyl)benzochalcogenadiazoles)]

4.2.1 Synthesis and characterization of [{$ReBr(CO)_4$}$_2$(μ-4,7-*bis*(4-pyridyl)benzothia-diazole)] (**19**)

Though a variety of self-assembled squares and cages of rhenium have been synthesized in the last few years, a literature review shows only one example of a rhenium-directed molecular cage using triazine heterocycles,[2] but no such work incorporating

benzochalcogenadiazole ring systems has been reported. We thus decided to synthesize a molecular rod of rhenium-containing the 4,7-*bis*(4-pyridyl)benzothiadiazole (**9**) ligand following the procedure reported by Lu *et al.* for related systems.[3] According to the literature method, an activated complex [$ReBr(CO)_4(NCMe)$] (**18**) was synthesized by adding trimethylamine N-oxide dropwise to a dichloromethane solution of $BrRe(CO)_5$ (**17**) in the presence of acetonitrile. Once the labile complex **18** was formed, it was purified by passing the solution through a short silica column and then re-dissolving it in toluene. A solution of the 4,7-*bis*(4-pyridyl)benzothiadiazole (**9**) ligand dissolved in dichloromethane and toluene was added rapidly using a dropping funnel. The solution was stirred at 15°C for 30 min and stirring was continued for another 30 min at ambient temperature. The crude product was purified by silica gel column chromatography affording a novel dirhenium molecular rod [{$ReBr(CO)_4$}$_2$(μ-4,7-*bis*(4-pyridyl)benzothiadiazole)] (**19**) in 27% yield (Scheme 4.1).

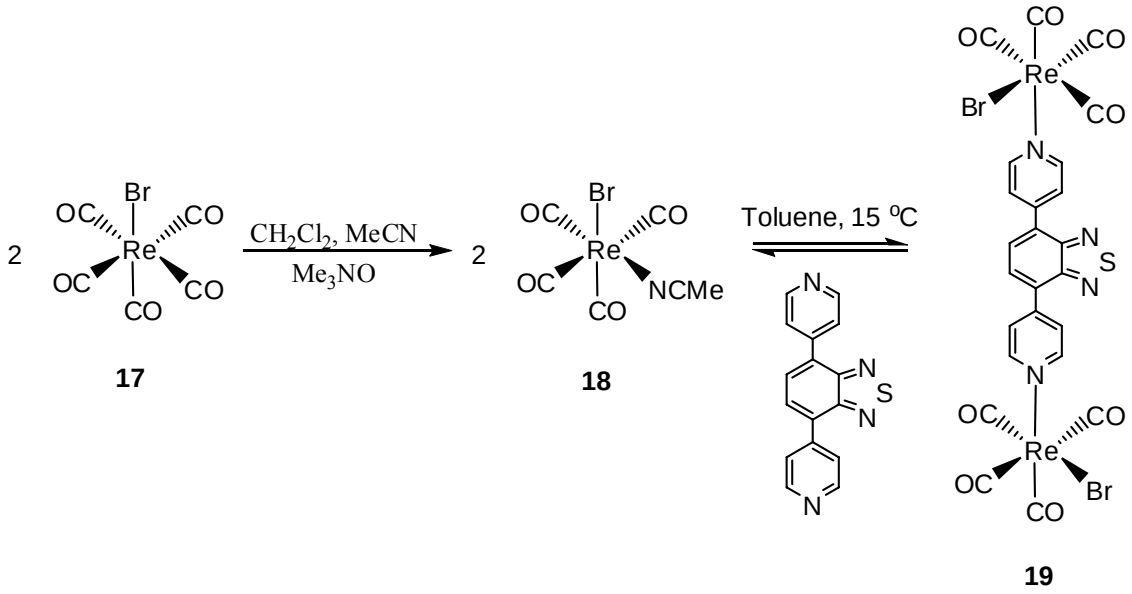

Scheme 4.1 Synthesis of [{$ReBr(CO)_4$}$_2$(μ-4,7-*bis*(4-pyridyl)benzothiadiazole)] (**19**)

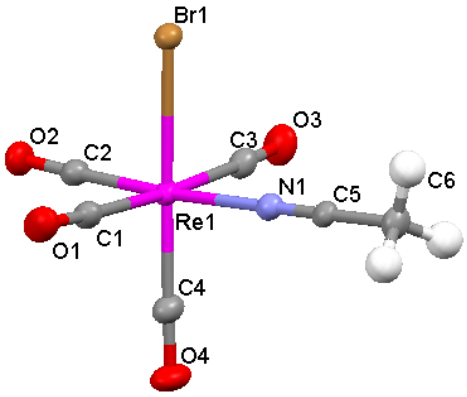

Figure 4.2 Molecular structure of [ReBr(CO)$_4$(NCMe)] (**18**), selected bond lengths [Å] and bond angles [^{o}]: Re(1)–N(1) 2.139(4); Re(1)–Br(1) 2.6125(5); N(1)–C(5) 1.129(6); C(5)–C(6) 1.446(6); N(1)–Re(1)–Br(1) 85.62(11)

Table 4.1 Crystal data and structure refinement for **18**

	18
Temperature (K)	173(2)
Crystal system	Triclinic
Space group	P-1
Unit cell dimensions	
a, Å	5.8624(4)
b, Å	7.2614(5)
c, Å	12.5469(8)
α, deg	94.1040(10)
β, deg	103.2590(10)
γ, deg	103.6670(10)
Z	2
Goodness-of-fit on F^2	1.062
Final *R* indices [$I>2\sigma(I)$]	R_1 = 0.0265
	wR_2 = 0.0674
R indices (all data)	R_1 = 0.0280
	wR_2 = 0.0680

A search of the Cambridge Structural Database (CSD) revealed no crystal structure of **18** even though it was known for many years, so we solved the structure by single-crystal X-ray diffraction analysis (Figure 4.2). The single-crystal molecular structure of **18** is depicted in Figure 4.2, crystal data are given in Table 4.1, and selected bond distances

and angles are listed in the caption to the Figure 4.2. The full crystal reports are presented in the electronic appendix. The compound has octahedral geometry containing a single rhenium atom with four carbonyl groups, a bromide and a coordinated acetonitrile ligand. The bromide and acetonitrile ligands are *cis* to each other.

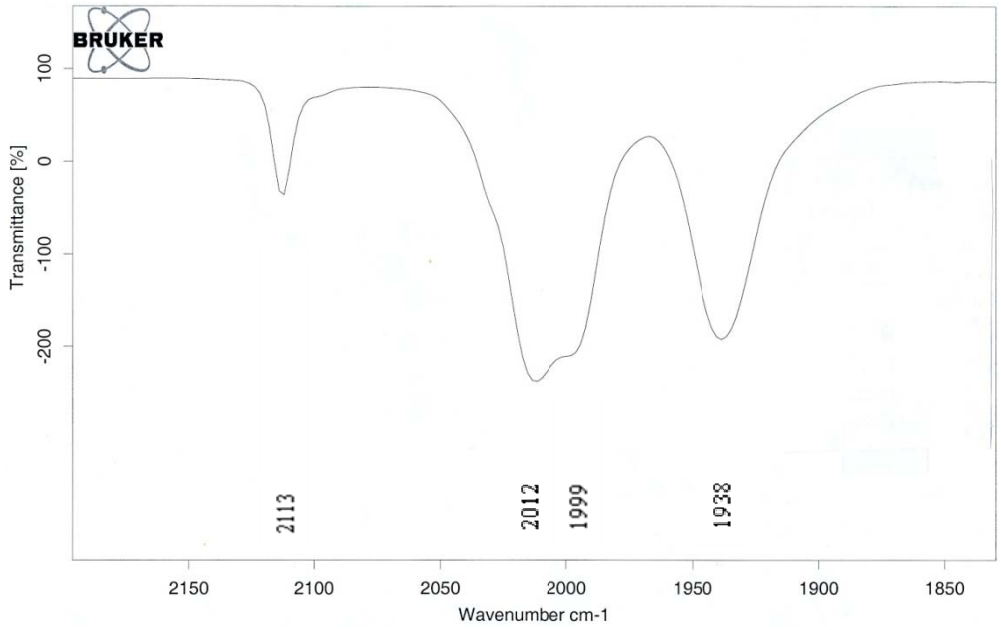

Figure 4.3 Infrared spectrum of compound **19** in the carbonyl (C≡O) region in CH_2Cl_2

Compound **19** has been characterized by a combination of spectroscopic methods (infrared and NMR) as well as elemental analysis and a single-crystal X-ray diffraction analysis. The pattern of the infrared spectrum of **19** in the carbonyl region is very similar to that of the previously reported [{$ReBr(CO)_4$}$_2$(μ-4,4′-bipy)] complex,[3] indicating the presence of four terminal carbonyls *cis* to each other (Figure 4.3). The ^{1}H NMR spectrum of **19** shows considerable downfield shifts of the proton signals and resolves the overlapped proton signals observed in the free ligand (Chapter 3) due to metal coordination (Figure 4.4). The doublet of the α-protons of the pyridyl ring adjacent to the rhenium center appears at δ 9.26 ppm (J = 5.7 Hz) and is shifted by 0.44 ppm compared

to the free ligand (Section 3.2.1). The doublet for the β-protons (δ 8.14 ppm, J = 5.7 Hz) and the singlet of the benzothiadiazole ring (δ 8.07 ppm) are resolved and integrate separately for four and two protons, respectively.

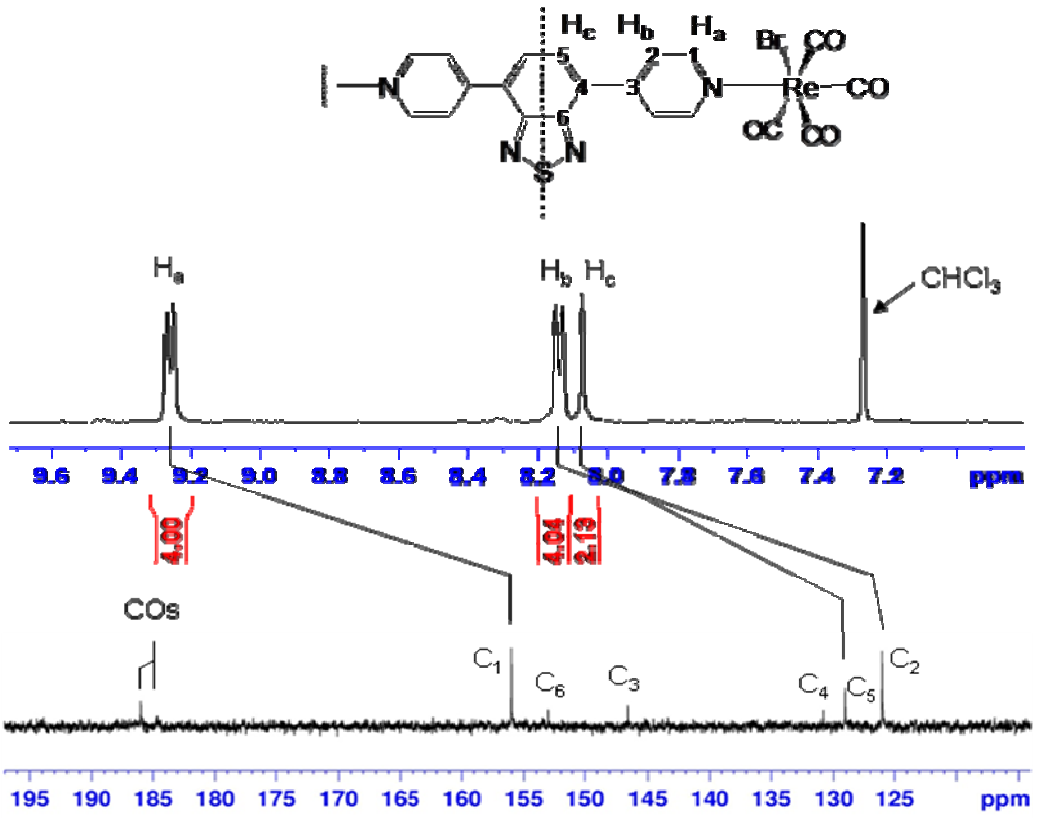

Figure 4.4 ^{1}H and ^{13}C NMR spectra of compound **19**

In addition to the carbon signals {δ 186.0 ppm (eq) and 184.2 ppm (ax)} of the CO ligands, the ^{13}C NMR spectrum has six distinct signals attributed to the six different carbon atoms in **19**, considerably shifted to downfield by roughly 3 ppm (Figure 4.4) compared to the free ligand (Chapter 3). A full spectral assignment of **19** was obtained by heteronuclear 2D shift-correlated HSQC and HMBC NMR experiments. It has not been possible to obtain confirmatory mass data for **19** by mass spectroscopy due to the Re–N dative bond dissociation.

Single-crystals of **19** were grown by slow diffusion of *n*-hexane into a dichloromethane solution at −4°C, affording two different colored needle-type crystals. We mounted both types of crystals to understand the mode of crystallization and the structure determination confirms that compound **19** crystallizes in two different morphologies. Compound **19a** crystallizes in the rhombohedral system with space group $R\bar{3}$ and a *Z* of 18, whereas **19b** crystallizes along with one dichloromethane solvent molecule in the triclinic system with the centrosymmetric space group $P\bar{1}$ and a *Z* of 2.

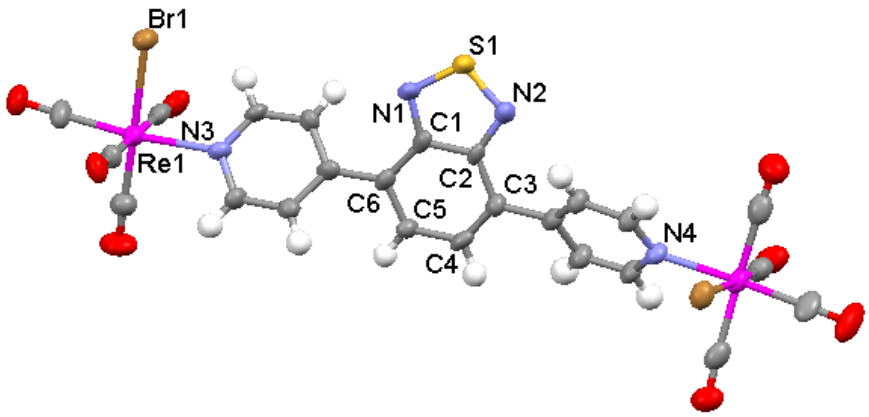

Figure 4.5 Molecular structure of **19a**, selected bond lengths [Å] and bond angles [°]: Re(1)–N(3) 2.244(13); Re(1)–Br(1) 2.6088(18); S(1)–N(1) 1.598(15); S(1)–N(2) 1.622(14); N(1)–C(1) 1.366(19); N(2)–C(2) 1.36(2); C(1)–C(2) 1.420(19); C(1)–C(6) 1.43(2); C(2)–C(3) 1.42(2); C(3)–C(4) 1.36(2); C(3)–C(12) 1.49(2); C(4)–C(5) 1.42(2); C(5)–C(6) 1.384(19); N(1)–S(1)–N(2) 101.2(7); N(3)–Re(1)–Br(1) 88.3(3)

The molecular structures of **19**(**a, b**) are depicted in Figures 4.5 and 4.6, crystal data are collected in Table 4.2, and selected bond distances and angles are listed in the captions to the Figures 4.5 and 4.6. The full crystal reports are presented in the electronic appendix. The structure consists of a molecular rod in which two $ReBr(CO)_4$ fragments are bridged

by a 4,7-*bis*(4-pyridyl)benzothiadiazole ligand. The coordination geometry at the Re atom is a distorted octahedron and the distortion is evident from reduction of the C–Re–N and C–Re–C trans angle from 180° in the idealized geometry to 173.6(6) and 177.5(7)° in **19a**, and to 175.4(5) and 177.1(6)^{o} in **19b**, respectively.

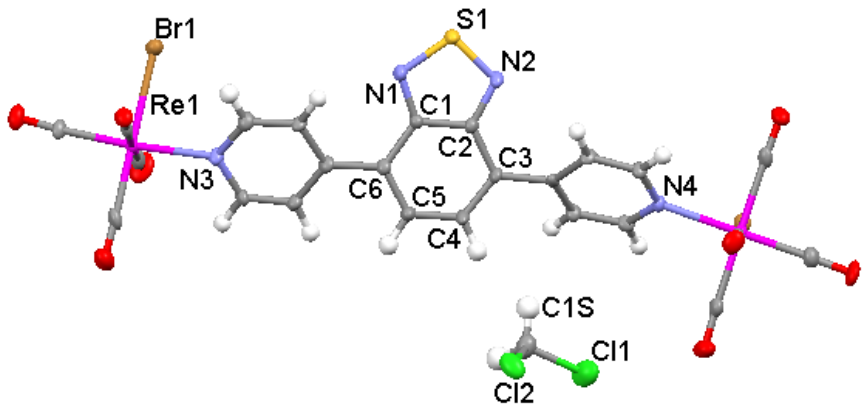

Figure 4.6 Molecular structure of **19b** showing the dichloromethane of solvation, selected bond lengths [Å] and bond angles [^{o}]: Re(1)–N(3) 2.205(11); Re(1)–Br(1) 2.6081(16); S(1)–N(2) 1.610(12); S(1)–N(1) 1.615(12); N(1)–C(1) 1.341(17); N(2)–C(2) 1.345(17); C(1)–C(2) 1.434(18); C(1)–C(6) 1.439(17); C(2)–C(3) 1.442(18); C(3)–C(4) 1.375(19); C(3)–C(12) 1.478(17); C(4)–C(5) 1.40(2); C(5)–C(6) 1.379(19); N(3)–Re(1)–Br(1) 85.9(3); N(2)–S(1)–N(1) 101.5(6)

The basic difference between the two structures is the twisting of both pyridyl rings with respect to the central benzothiadiazole ring. In **19a**, the two pyridyl rings are twisted in opposite direction like a cross with the dihedral angles of 36.4(4) and −33.7(2)^{o} (Figure 4.7a), whereas in **19b**, both pyridyl rings are slightly twisted in the same direction with the angles of 23.7(0) and 19.6(0)^{o} (Figure 4.9b). The quinoidal character of the benzothiadiazole ring remains unperturbed even after coordination of the terminal pyridyl rings to the rhenium atoms (See Table 2.3, Chapter 3).

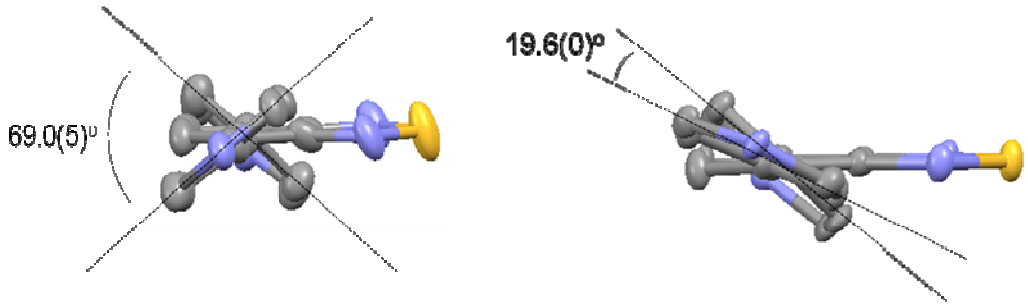

19a **19b**

Figure 4.7 The mode of twisting of the pyridyl rings in solid state forms of **19**

Table 4.2 Crystal data and structure refinement for **19**

	19a	**19b.CH_2Cl_2**
Temperature (K)	173(2)	173(2)
Crystal system	Rhombohedral	Triclinic
Space group	$R\bar{3}$	$P\bar{1}$
Unit cell dimensions		
a, Å	28.8050(16)	6.1496(13)
b, Å	28.8050(16)	15.569(3)
c, Å	21.754(2)	17.686(4)
α, deg	90	109.581(2)
β, deg	90	91.113(2)
γ, deg	120	99.489(2)
Z	18	2
Goodness-of-fit on F^2	1.046	1.131
Final *R* indices [$I>2\sigma(I)$]	$R_1 = 0.0691$	$R_1 = 0.0660$
	w$R_2 = 0.1708$	w$R_2 = 0.1880$
R indices (all data)	$R_1 = 0.1385$	$R_1 = 0.0718$
	w$R_2 = 0.2043$	w$R_2 = 0.1916$

4.2.2 Synthesis and characterization of [{$ReBr(CO)_4$}$_2$(*μ*-4,7-*bis*(4-pyridyl)benzo-selenadiazole)] (20)

A similar reaction to that mentioned above of the activated intermediate **18** with 4,7-*bis*(4-pyridyl)benzoselenadiazole ligand **11** yielded the analogous novel dirhenium molecular rod [{$ReBr(CO)_4$}$_2$(*μ*-4,7-*bis*(4-pyridyl)benzoselenadiazole)] **20** in 18% yield

(Scheme 4.2). Formation of compound **20** has been confirmed by spectroscopic methods such as infrared and NMR, as well as elemental analysis.

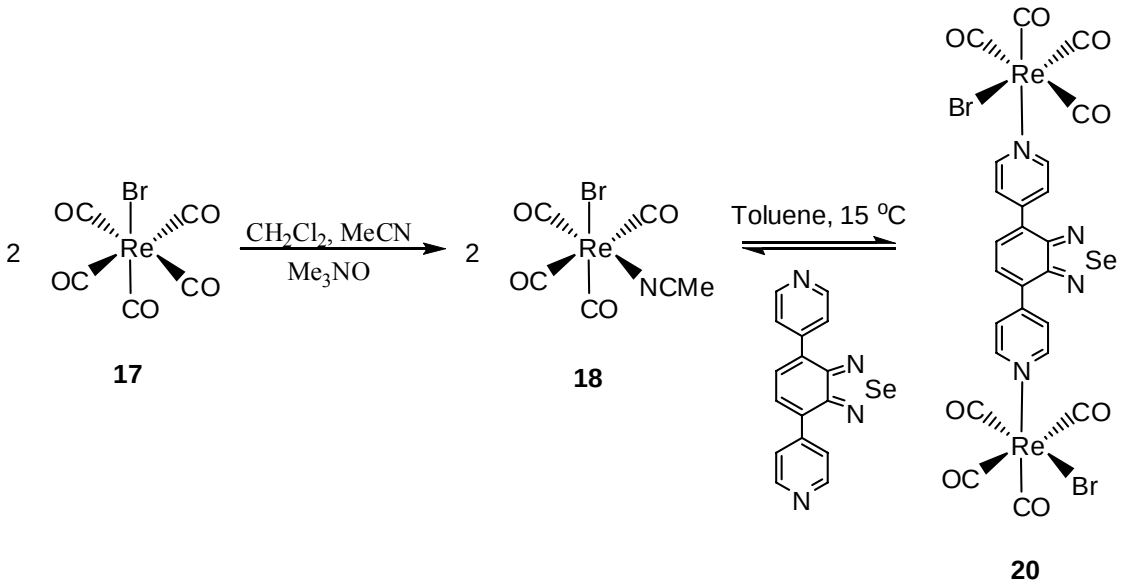

Scheme 4.2 Synthesis of [{ReBr(CO)$_4$}$_2$(μ-4,7-*bis*(4-pyridyl)benzoselenadiazole)] (**20**)

The pattern of the infrared spectrum of **20** in the carbonyl region is very similar to that of **19** and the analogous [{ReBr(CO)$_4$}$_2$(μ-4,4′-bipy)] complex,[3] indicating a similar arrangement of four terminal carbonyls *cis* to each other (Figure 4.8). The ^{1}H NMR spectrum of **20** shows considerable downfield shifts of the proton signals due to metal coordination (Figure 4.9), compared to those observed for the free ligand (Section 3.2.2).

The two equal intensity doublets at δ 9.20 ppm (J = 6.6 Hz) and 8.07 ppm (J = 6.6 Hz), each integrating for four hydrogens, are attributed to the coordinated pyridyl ring protons. The doublet of the α-protons of the pyridyl ring adjacent to the rhenium centers are shifted downfield by 0.40 ppm and the doublet of the β-protons is shifted by 0.21 ppm compared to the free ligand.

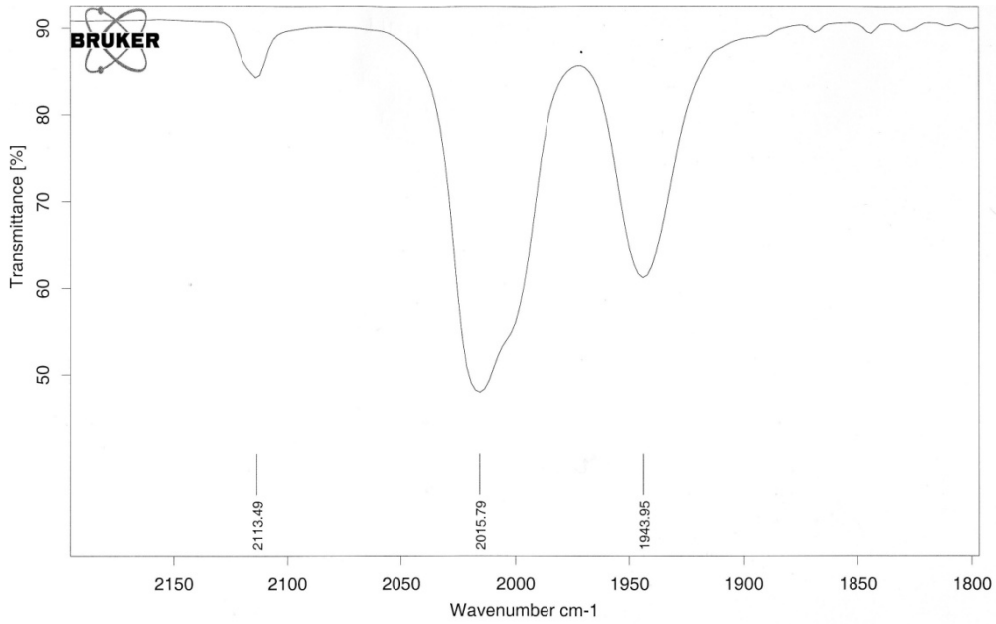

Figure 4.8 Infrared spectrum of compound **20** in the carbonyl (C≡O) in CH_2Cl_2 region

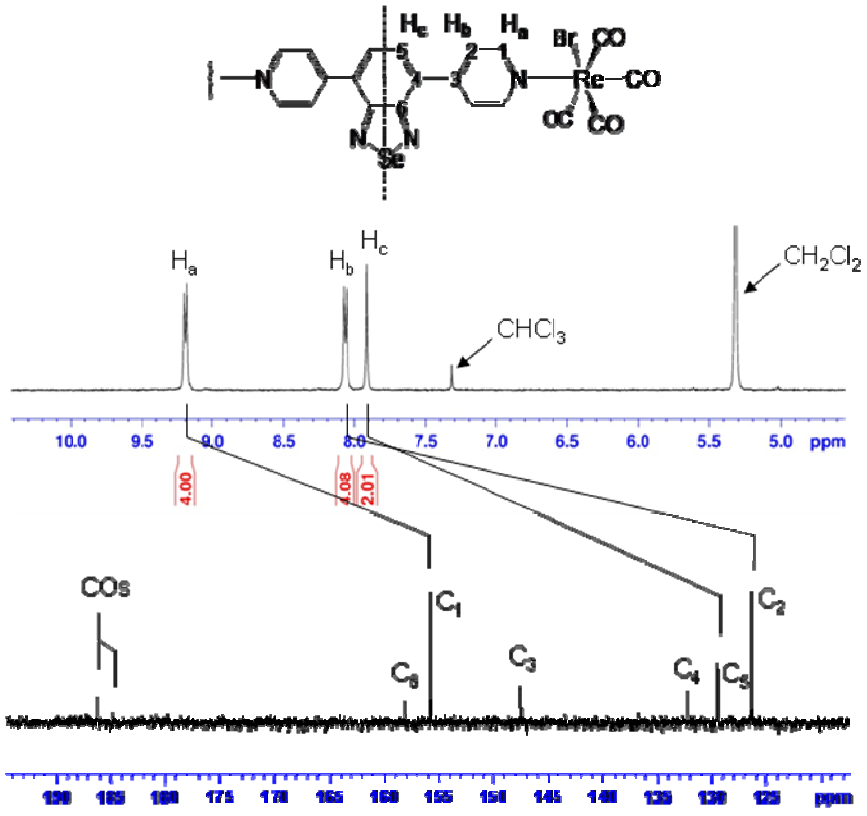

Figure 4.9 ^{1}H and ^{13}C NMR spectra of compound **20**

The singlet at δ 7.92 ppm due to the benzoselenadiazole ring protons is also shifted downfield by 0.14 ppm compared to the free ligand (Chapter 3). In addition to the carbon signals {δ 186.2 ppm (eq) and 185.0 ppm (ax)} of the CO ligands the ^{13}C NMR spectrum has six distinct signals attributed to the six different carbon atoms in **20** and the signals for the carbon atoms attached to the proton are shifted downfield compared to the free ligand (Figure 4.9). A full assignment of the ^{1}H and ^{13}C NMR resonances of **20** was obtained by heteronuclear 2D shift-correlated HSQC and HMBC NMR experiments. Similarly to that of **19**, it was not possible to obtain confirmatory mass data for **20** by mass spectroscopy due to the dissociation of Re–N dative bond.

References

1. Xue, W. -M.; Kühn, F. E.; Herdtweck, E. *Polyhedron* **2001**, *20*, 791.

3. Dinolfo, P. H.; Coropceanu, V.; Brédas, J. -L.; Hupp, J. T. *J. Am. Chem. Soc.* **2006**, *128*, 12592.

2. Rajendran, T.; Manimaran, B.; Lee, F. -Y.; Lee, G.-H.; Peng, S. -M.; Wang, C. M.; Lu, K. -L. *Inorg. Chem.* **2000**, *39,* 2016.

CHAPTER FIVE: SELF-ASSEMBLED PALLADIUM-SQUARES

5.1 Introduction

As mentioned in Chapter 1, numerous examples of ionic group 10 (Pd, Pt) metal-directed molecular squares incorporating different pyridine-substituted ligands have been reported based on the dominant square-planar coordination geometry of these M^{2+} metal ions. To our knowledge, no such ligands to date have incorporated heterocyclic rings, except porphyrins which contains pyrrole subunits. The synthesis of chalcogenadiazole-based molecular squares is the subject of this chapter.

5.2 Synthesis of [(enPd)(μ-4,7-*bis*(4-pyridyl)benzochalcogenadiazole)]$_4$[PF_6]$_8$

5.2.1 Synthesis and characterization of [(enPd)(μ-4,7-*bis*(4-pyridyl)benzothiadiazole)]$_4$ [PF_6]$_8$ (**23**)

The synthesis of palladium-directed molecular squares was attempted using the previously introduced 4,7-*bis*(4-pyridyl)benzothiadiazole (**9**) ligand by a self-assembly reaction conducted at slightly elevated temperatures. Making the self-assembled molecular squares using **9** was not straightforward and it took considerable effort to optimize the reaction conditions. In a typical reaction, enPd(NO_3)$_2$ (**21**) was treated with KPF_6 in a mixture of acetonitrile and water (0.7/0.3 mL, v/v) at 50^{o}C to carry out ion-exchange to give [enPd($MeCN$)$_2$]$^{2+}$ (**22**). Formation of **22** was confirmed by comparing IR and $^{31}P\{^1H\}$ NMR spectroscopy with the literature values.[1] Complex **22** was then allowed to react with **9** in a mixture of acetonitrile and water (0.7/0.3 mL, v/v) at 50^{o}C without any further purification to afford a pale yellow solution with some insoluble

materials. The solution was filtered to remove insoluble materials and removal of the solvents under vacuum afforded a pale yellow solid. The solid was then washed twice with water and quenched with dichloromethane affording metal complex **23** in 88% yield (Scheme 5.1). The formation of complex **23** is thermodynamic in nature. This is evident from similar ambient temperature reactions which lead to the formation of insoluble polymeric materials. The complex **23** was characterized by spectroscopic methods (IR, NMR), elemental analysis and mass spectrometry together with diffusion ordered spectroscopy (DOSY) NMR experiments.

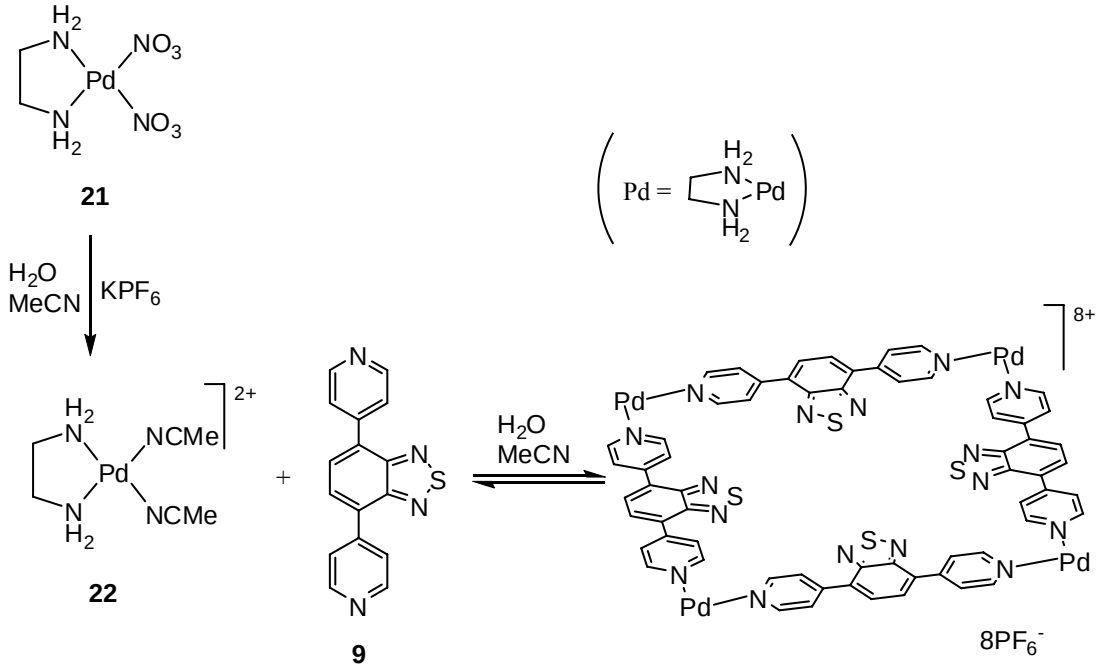

Scheme 5.1 Synthesis of [(enPd)(μ-4,7-*bis*(4-pyridyl)benzothiadiazole)]$_4$[PF_6]$_8$ (**23**)

The ^{1}H NMR spectrum of **23** in the aromatic region shows a small downfield shift of the proton signals due to metal coordination (Figure 5.1), compared to those observed for free ligand **9** (Chapter 3). The spectral lines at RT are broadened compared to the free ligand (Section 3.2.1) or the Re rod molecules (Section 4.2.1) indicating slowed re-

orientational motion in these large complexes. However, the signals are not split further, indicating that there is still relatively free rotation about the Pd-N and aryl-aryl bonds. The two equal intensity doublets at δ 8.90 ppm (J = 5.7 Hz) and 8.27 ppm (J = 5.7 Hz) are attributed to the coordinated pyridyl ring protons. The doublet of the α-protons of the pyridyl ring adjacent to the palladium center is shifted downfield by 0.08 ppm and the doublet of the β-protons is shifted by 0.33 ppm compared to the free ligand (Chapter 3). The singlet at δ 8.11 ppm due to the benzoselenadiazole ring protons is also shifted downfield by 0.16 ppm compared to the free ligand. The two equal intensity singlets in the aliphatic region at δ 4.33 ppm and 2.90 ppm are attributed to the NH_2 and CH_2 protons of the coordinated ethylenediamine ligands, which are considerably broader due to chelate-ring-twisting dynamic effects.

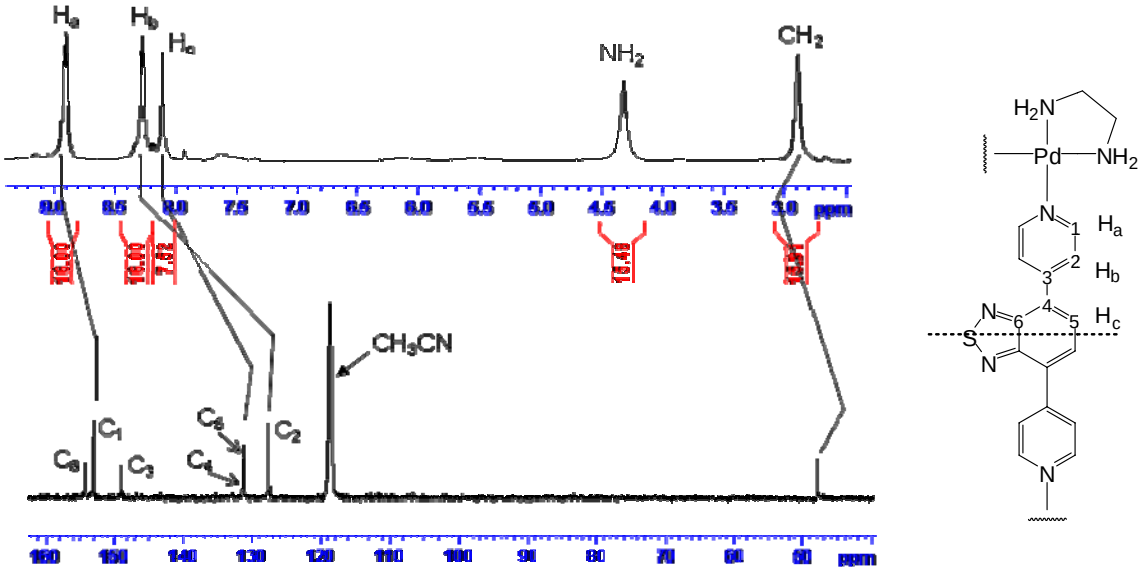

Figure 5.1 ^{1}H and ^{13}C NMR spectra of complex **23**

The integration of the proton signals of ligand **9** versus ethylenediamine indicates the 1:1 complexation of **9** and the palladium corner unit. The NMR spectra showed reasonable

purity of complex **23** indicating the presence of a single primary species. Besides the 4,7-*bis*(4-pyridyl)benzothiadiazole and ethylenediamine proton signals, the spectrum contains some additional, very broadened, signals of low integration at unusual chemical shifts (5 - 8 ppm). This is probably due to the presence of some minor species within the cavity such as water or organic solvents which can be expected for such larger size molecular complexes. There is little evidence of impurities in the neighborhood of ligand signals; however, careful drying of bulk material is warranted before conducting subsequent analyses. The ^{13}C NMR spectrum has seven distinct signals attributed to the seven different carbon atoms of the coordinated **9** and ethylenediamine ligands (Figure 5.1). The full spectral assignment of **23** is obtained by heteronuclear 2D shift-correlated HSQC and HMBC NMR experiments and is presented in the electronic appendix.

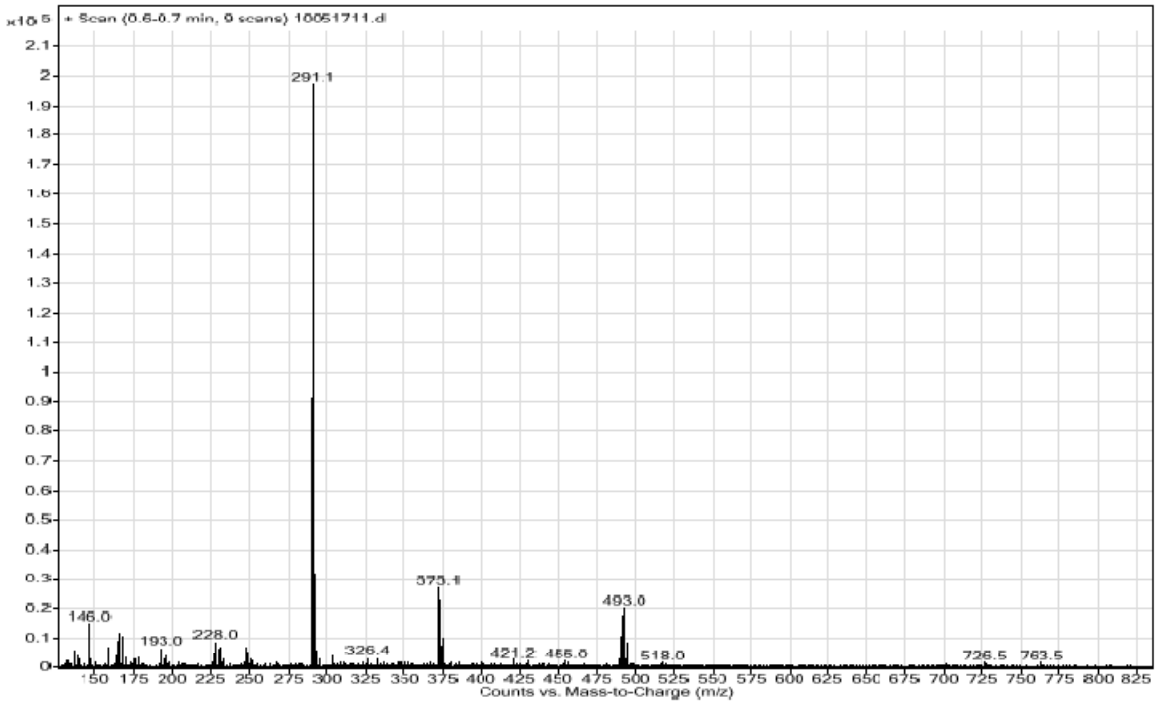

Figure 5.2 ESI mass spectrum of complex **23**, showing the most abundant peak at *m/z* 291 for a (ligand, $M+H)^+$ response for ligand **9** in assembly **23**

The element percentages obtained from C,H,N combustion analysis of repeatedly purified **23** fit well (0.02 - 0.15% deviations) with the calculated values for the proposed molecular assembly and are reported in Chapter 8. As mentioned in Chapter 1, in most cases the mass spectrometric characterization of larger size molecular assemblies fail because of rapid decomposition. However, some papers demonstrate the characterization of Pt-directed molecular assembly by ESI-MS but no mass data have been reported for the corresponding Pd macrocycles.[2] This is probably due to the more labile nature of the Pd−N coordinative bond compared to the Pt−N bond. The mass spectrometric analysis of **23** was attempted by ESI- and NALDI-MS but no clear confirmatory results were obtained for molecular assembly formation except indicating the presence of ligand **9** as follows.

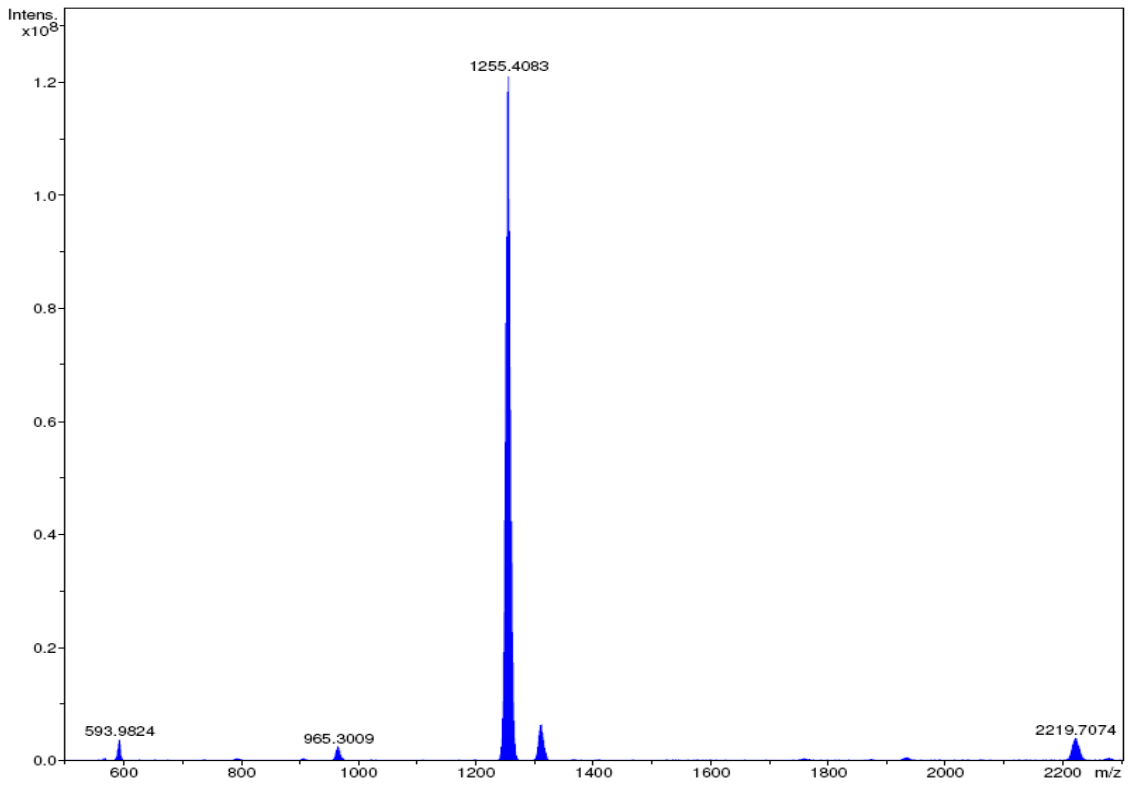

Figure 5.3 NALDI (no matrix) mass spectrum of complex **23**

The ESI-MS showed a $(M+H)^+$ (m/z 291.1) response for the ligand **9** with some additional peaks at higher m/z values for some unknown species which could not be assigned (Figure 5.2). The NALDI-MS showed cluster ion peaks at *m*/*z* 2219.7074 and 1255.4080. While a reasonable fragment could be assigned to the peak at *m*/*z* 2219.7074 for a $[M{\cdot}8PF_6 - (4S, 4PF_6 \text{ and en})]^+$ (calculated value, 2219.0421) ion and the peak at *m*/*z* 1255.4083 for a $[C_{34}H_{32}N_{12}Pd_2P_3F_{18}]^+$ (calculated value, 1254.9862) ion (Figure 5.3), the discrepancy between the observed and calculated values is far too high for the error limits of the FT-ICR instrument used for this analysis. This miss-match is in addition to the unusual fragmentation required for the above peak assignments. Instead, the peak cluster centered on 1255.4 u is likely due to a higher-order clusters of the type $[Pd_xen_y(PF_6)_z]^+$ (see below) although an exact fit has not been obtained; the isotope pattern at least suggests the presence of multiple palladium atoms ($x \geq 4$).

5.2.2 Synthesis and characterization of [(enPd)(*μ*-4,7-*bis*(4-pyridyl)benzoselenadiazole)]$_4$[PF$_6$]$_8$ (**24**)

A similar reaction of **22** with 4,7-*bis*(4-pyridyl)benzoselenadiazole (**11**) as mentioned above yielded an analogous novel self-assembled molecular square [(enPd)(*μ*-4,7-*bis*(4-pyridyl)benzo-selenadiazole)]$_4$[PF$_6$]$_8$ (**24**) in 82% yield (Scheme 5.2). Formation of assembly **24** has been determined by spectroscopic methods (IR, NMR), elemental analysis and mass spectrometry) together with DOSY NMR experiments.

The ^{1}H NMR spectrum of **24** in the aromatic region shows usual downfield shifts of the proton signals due to the metal coordination (Figure 5.4), compared to those observed for free ligand (Section 3.2.3). The proton signals of the heterocyclic ligands are also relatively sharp while those from the ethylenediamine are considerably broadened, just as

observed for **23**. The two equal intensity doublets at δ 8.95 ppm (J = 6.6 Hz) and 8.27 ppm (J = 6.6 Hz) are attributed to the coordinated pyridyl ring protons. The doublet of the α-protons of the pyridyl ring adjacent to palladium center was shifted downfield by 0.15 ppm and the doublet of the β-protons is shifted by 0.41 ppm compared to the free ligand. The singlet at δ 8.01 ppm due to the benzoselenadiazole ring protons is also shifted downfield by 0.23 ppm compared to the free ligand (Figure 5.4). The two broad equal intensity singlets in the aliphatic region at δ 4.38 ppm and 2.97 ppm are attributed to the NH_2 and CH_2 protons of the coordinated ethylenediamine ligands.

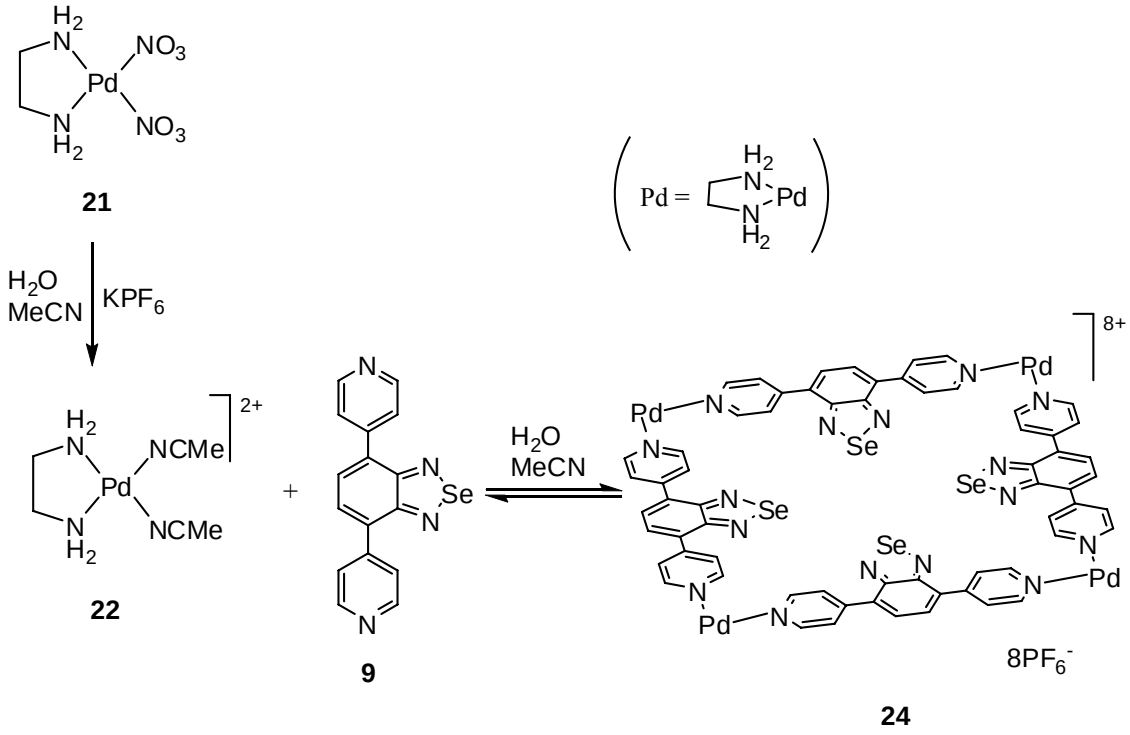

Scheme 5.2 Synthesis of [(enPd)(μ-4,7-*bis*(4-pyridyl)benzoselenadiazole)]$_4$[PF_6]$_8$ (**24**)

As in the case of **23**, the integration of the proton signals in **24** indicates 1:1 complexation of ligand **11** and the palladium corner units. The ^{1}H NMR spectrum of **24** strongly supports the presence of a single species. Minor impurities in the heterocyclic ligand

region are the only obvious additional signals except for a very broad resonance around 6 ppm, are possibly from cavity guests. The ^{13}C NMR spectrum has seven distinct signals attributed to the seven different carbon atoms of the coordinated **11** and ethylenediamine ligands (Figure 5.4). A full assignment of the ^{1}H and ^{13}C resonances of **24** was obtained by heteronuclear 2D shift-correlated HSQC and HMBC NMR experiments and is presented in the electronic appendix.

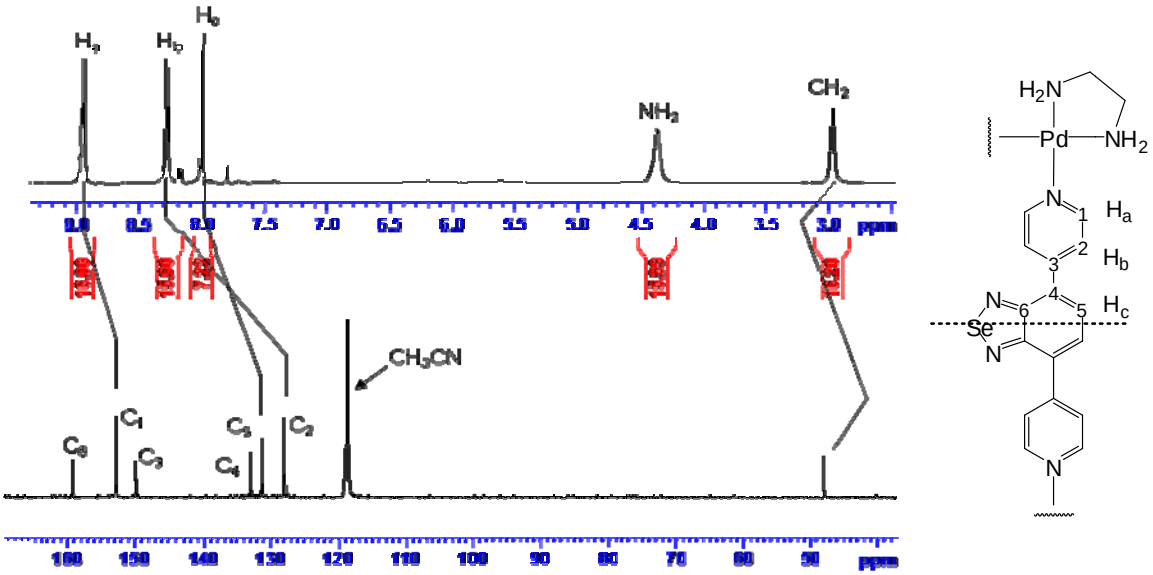

Figure 5.4 ^{1}H and ^{13}C NMR spectra of complex **24**

The combustion analysis of rigorously dried samples of **24** is also an excellent fit to the proposed formula (deviations of 0.07 to 0.22%) in support of the proposed molecular assembly (see Chapter 8). The ESI- and NALDI-MS analyses of **24** showed very similar features to those observed for **23**. The ESI-MS showed a most abundant peak at 339 which corresponds to a $(M+H)^{+}$ response of ligand **11** resulting from decomposition of the molecular assembly **24**. Some additional peaks were also observed at higher m/z

values but these could not be assigned to propose any reasonable ions from the larger cluster (Figure 5.5).

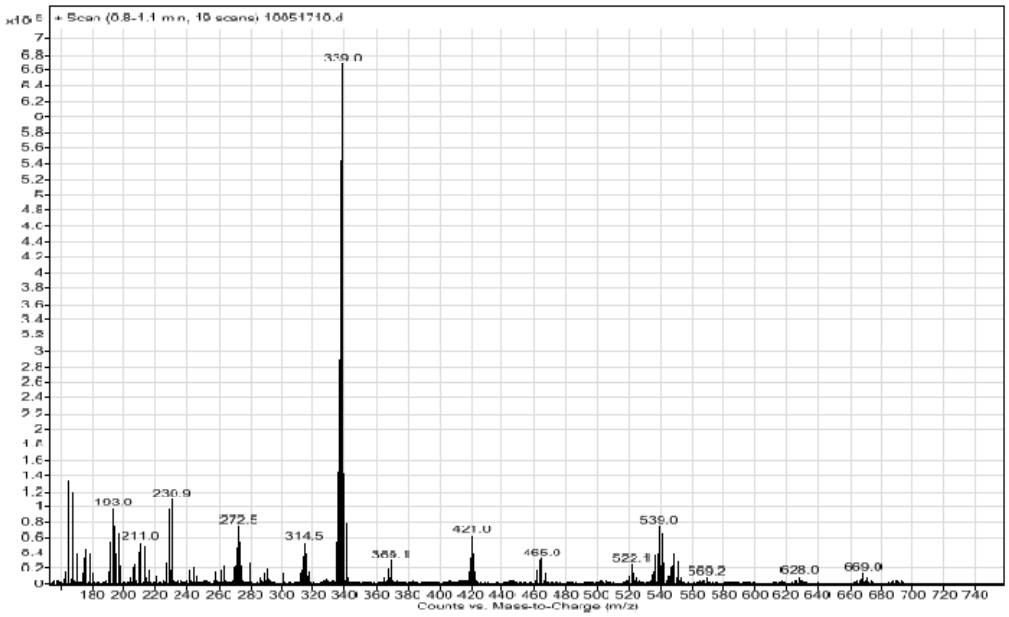

Figure 5.5 ESI mass spectrum of complex **24**, showing the most abundant peak at m/z 339 for a (ligand, $M+H)^+$ response for ligand **11** in assembly **24**

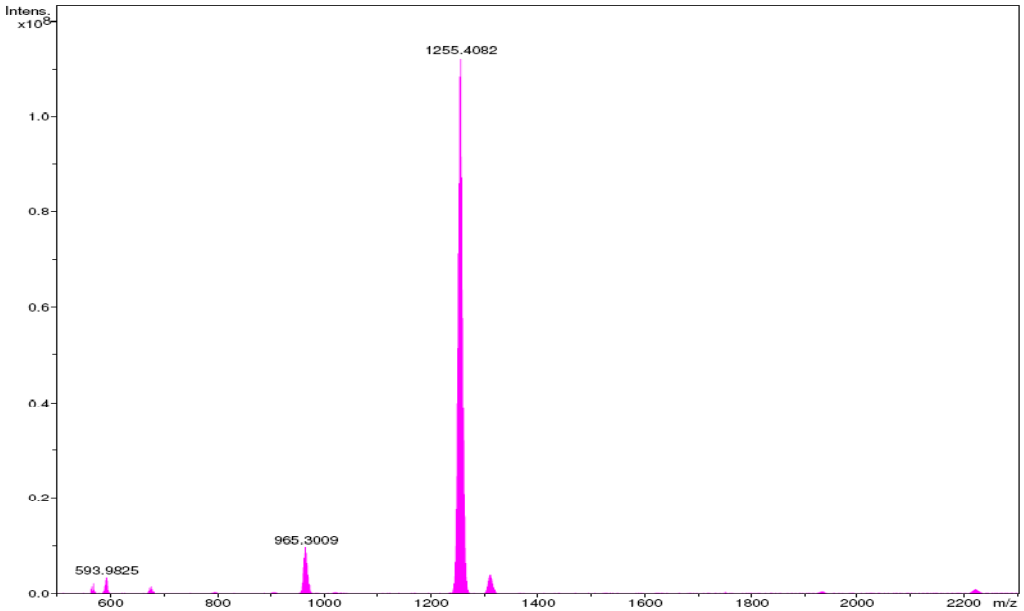

Figure 5.6 NALDI (no matrix) mass spectrum of complex **24**

Interestingly the NALDI-MS of complex **24** showed cluster ion peaks that appeared at the same *m*/*z* (2219.7087, 1255.4082) values as observed for complex **23** (Figure 5.6), even though the ESI-MS obtained on the same samples clearly distinguishes between the two different ligands present in complexes **23** and **24**. This result lends support to the notion that the observed peak(s) result from some sort of cluster of the type $[Pd_xen_y(PF_6)_z]^+$ which does not depend on the heterocyclic ligands.

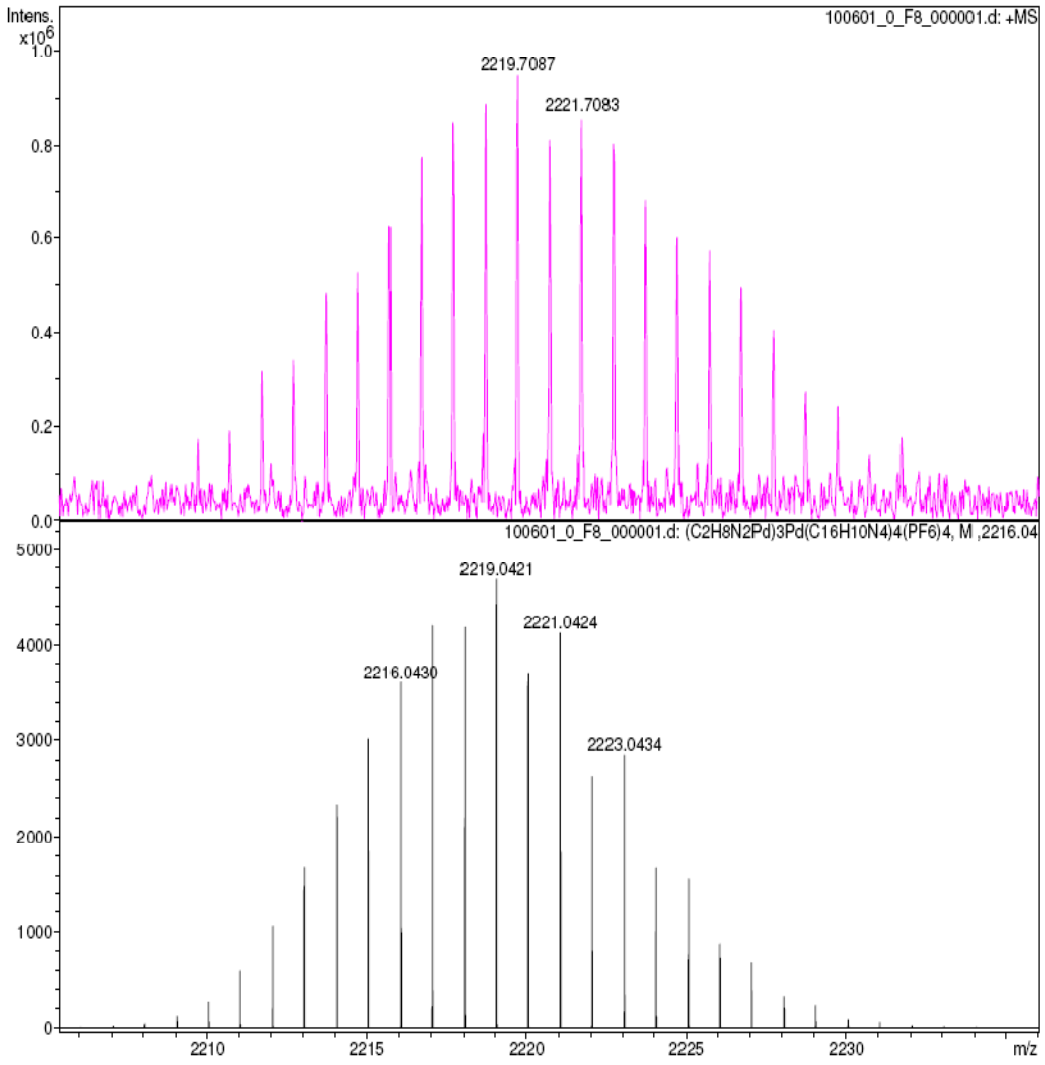

Figure 5.7 Observed (top) and theoretical (bottom) isotopic distribution for the cation $[C_{70}H_{64}F_{24}N_{22}P_4Pd_4]^+$ in NALDI-MS for **24**

5.3 Hyperchem MM+ molecular models

As mentioned in Chapter 1, self-assembled molecular squares tend to form thin films and for larger squares the films have a very high tendency to be amorphous. During the attempts of crystallization thin film formation of complexes **23** and **24** was also observed suggesting the amorphous nature of these complexes (Figure 5.8).

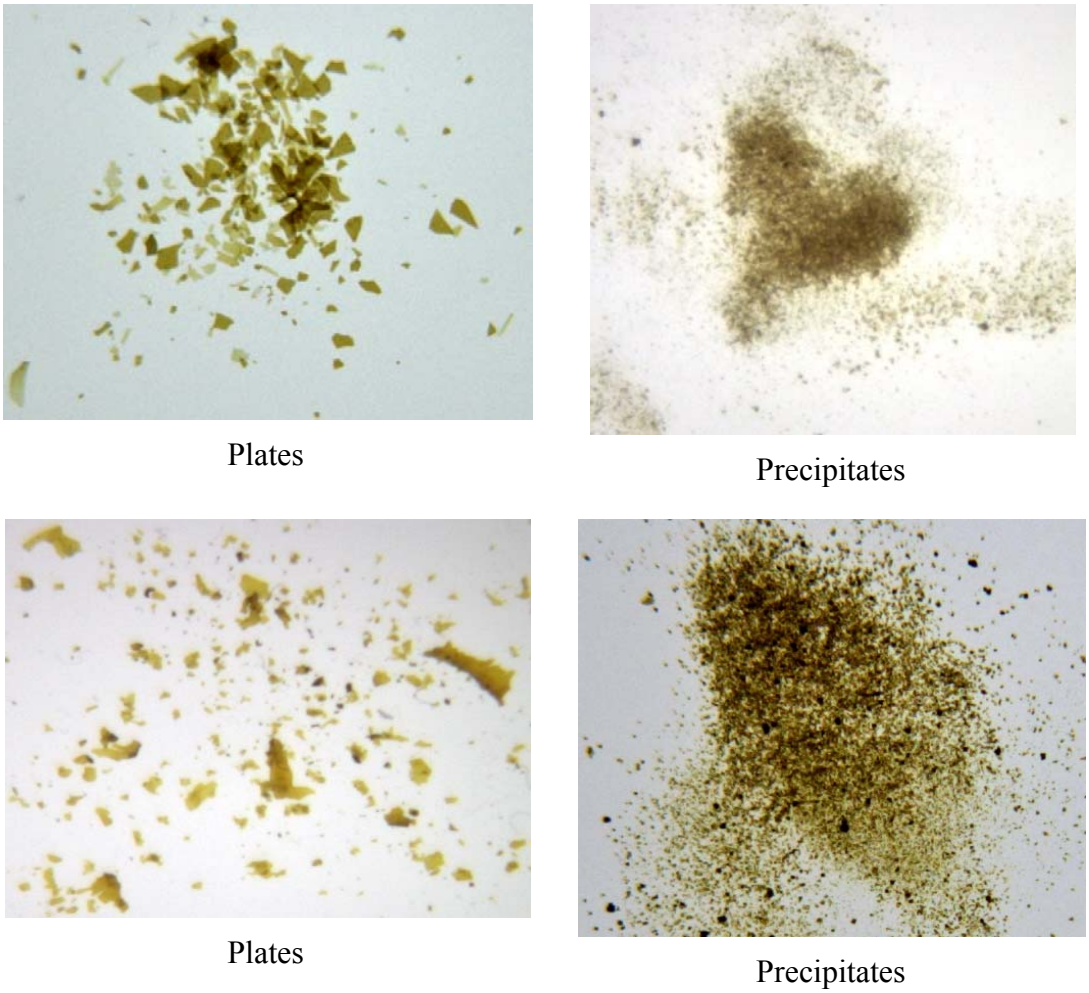

Figure 5.8 Molecular square **23** (top) and **24** (bottom) visualized under visible light and photographed by CCD camera

The amorphous nature of these complexes is evident from the X-ray diffraction experiments. Many good looking specimens of **23** and **24** were screened on the single-

crystal X-ray diffractometer. The remarkable thing about all these experiments was the complete absence of even a single diffraction peak given that such strong X-ray scatterers as palladium and selenium are present in these molecules.

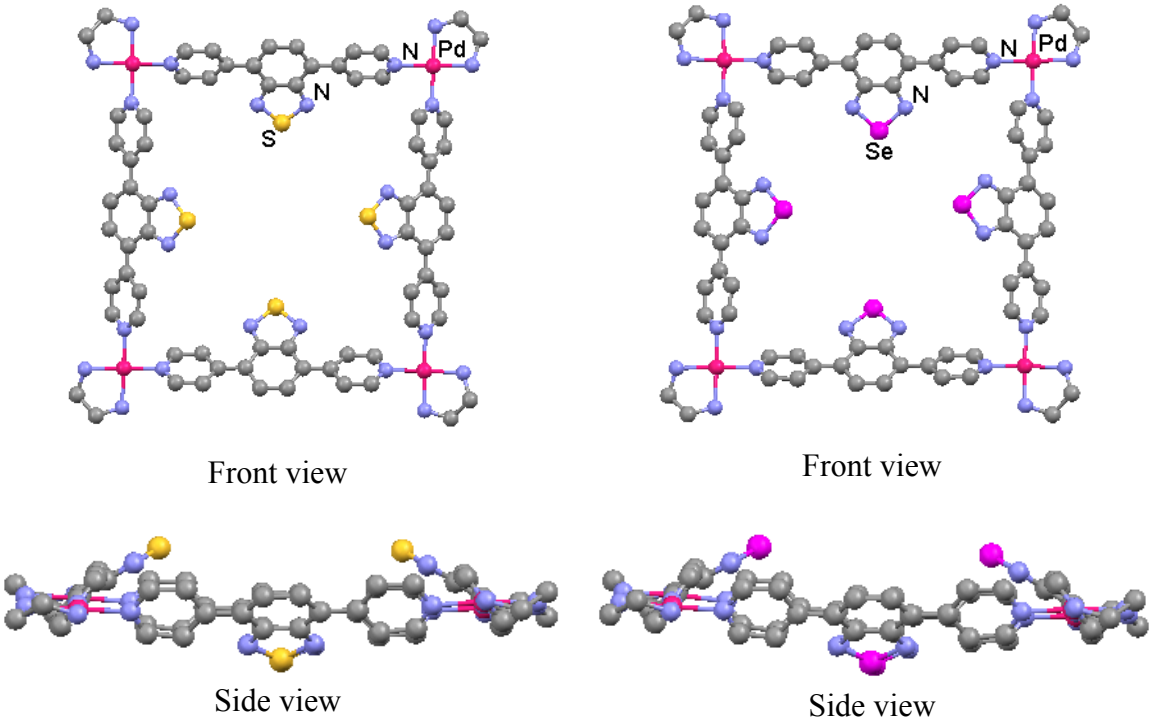

Figure 5.9 Ball and Stick models of **23** (left) and **24** (right)

Hence MM+ molecular mechanics calculations were undertaken in the program HyperChem™ on complexes **23** and **24** to learn more about their structures. The low energy models exhibit almost a planar conformation except for twisting of the thiadiazole/selenadiazole rings with dihedral angles of 31.59^{o} (top) and 33.38^{o} (bottom) in **23** and 29.50^{o} (top) and 30.04^{o} (bottom) in **24** with respect to the molecular plane (Figure 5.9). Both complexes **23** and **24** have the same outer length of 2.25 nm (Figure 5.10) including van der Waals radii. When the ligands, especially the benzochalco-genadiazole rings, approach in close proximity (i.e. pointed towards each other) the

internal cavities of **23** and **24** are 0.92 and 0.89 nm (Figure 5.10) excluding van der Waals radii. On the other hand for parallel arrangement of the ligands (i.e. twisted perpendicular to the molecular plane) within the molecules of **23** and **24** leads to the same, larger, internal cavity size of 1.52 nm.

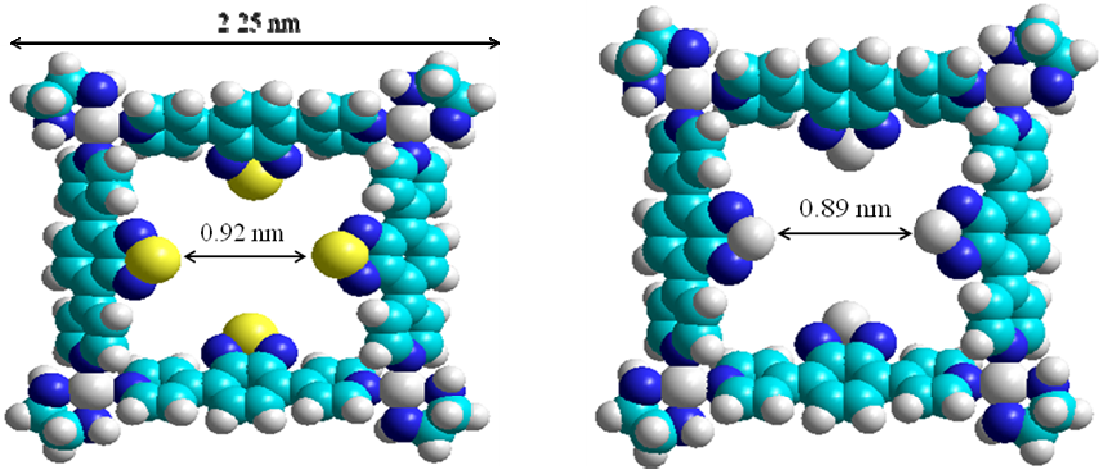

23 **24**

Figure 5.10 Space-filled models of **23** (left) and **24** (right) showing the molecular and internal cavity sizes

5.4 Analysis of molecular sizes of complexes **23** and **24** by DOSY NMR experiments

As discussed earlier, although the mass spectrometric analysis of complexes **23** and **24** reveals the presence of two different ligands, the confirmatory molecular cation or any other identifiable cluster ion peak which might confirm the proposed cluster composition could not be obtained by a variety of gently-ionizing mass spectrometry approaches. In addition, structural characterization by X-ray crystallography was not possible because of amorphous thin film formation. Hence, molecular size estimations for complexes **23** and **24** in solution were attempted using DOSY NMR experiments. Such "diffusion

spectroscopy" is basically obtained by pulsed field gradient (PFG) NMR experiments on the basis of the self-diffusion coefficient *D* of a molecule.

On the assumption of a simple hydrodynamic behavior for spherical objects, molecular size information can be obtained from the Stokes-Einstein equation:

$$D = \frac{k_B T}{6\pi\eta r_{hyd}} \qquad 5.1$$

where T is the absolute temperature, k_B is Boltzmann's constant, r_{hyd} is the hydrodynamic radius and η is the solvent viscosity. According to this equation, there is an inverse relationship between D and both, hydrodynamic radius and the solution viscosity. This results in a qualitative understanding that larger size molecules (or aggregates, such as small metal aqua ions) will have larger values of r_{hyd} and hence, will diffuse slower. This is a standard approach for obtaining approximate molecular size information on supramolecular assemblies where characterization by traditional methods (mass and X-ray) fails. Notably, molecular size calculations by DOSY NMR spectroscopy has previously been applied to characterize dendrimers and metallo-dendrimers,[3] gold nanoparticles,[4] and ion pairing in metal complexes [3b] and aggregation[5]. Very recently DOSY NMR spectroscopy has also been used to calculate molecular sizes of self-assembled molecular triangles, squares, rectangles and cages.[6]

The DOSY measurements of molecular assemblies **23** and **24** gave diffusion coefficients D from measurements of different ^{1}H NMR signals from the heterocyclic (H_a, H_b, H_c) and the ethylenediamine ligands (CH, NH) coordinated to the palladium atom (Table 5.1). The intriguing features of these measurements are (i) very similar D values are obtained from NMR signals of both framework chalcogenadiazole and ethylenediamine

ligands, which provides powerful evidence that these belong to a single component in solution. (ii) The molecular assemblies do not appear to be fluxional by the way of dissociation, and (iii) the average *D* values of **23** and **24** are very similar, as expected for essentially isostructural molecular squares differing only by the chalcogen atoms that are expected to be in the interior of the assembly.

Table 5.1 Molecular Diffusion coefficients[a] ($\times 10^{-10}$ m^2sec^{-1})

Compds	*D* in *d*-acetonitrile (experimental)					Average *D*	*D* in *d*-DMSO (corrected)
	N_2E ligands[b]			en ligands			
	H_a	H_b	H_c	NH	CH		
23	4.94 ±0.002	5.00 ±0.006	5.01 ±0.006	4.87 ±0.005	4.91 ±0.008	4.94 ±0.004	0.91 ±0.007
24	4.88 ±0.01	4.93 ±0.008	4.84 ±0.003	4.81 ±0.006	4.87 ±0.009	4.86 ±0.006	0.90 ±0.006

[a]The solvent viscosities were obtained from CRC hand book of Chemistry and Physics, 88th Eds, 2007-08, p 6-191. [b]Using the proton labeling for NMR spectra as defined in Figure 5.1 and 5.4.

The hydrodynamic radii of **23** (r_{hyd} 1.20; r_{calc} 1.46 nm) and **24** (r_{hyd} 1.22; r_{calc} 1.48 nm) calculated by using eq. 5.1 are comparable with the values reported by Stang and co-workers for molecular rectangles [(1,8-*bis*(*trans*-$Pt(PEt_3)_2$anthracene)$_2$(4,4′-bipy)$_2$][NO_3]$_4$ (r_{hyd} 1.15 nm; r_{calc} 1.19 nm), triangles [(2,9-*bis*(*trans*-$Pt(PEt_3)_2$phenanthrene)$_3$(4,4′-bipy)$_3$][NO_3]$_6$ (r_{hyd} 1.65 nm; r_{calc} 1.35 nm) and cages [(1,8-*bis*(*trans*-$Pt(PEt_3)_2$anthracene)$_3$(tris(4-pyridyl)methanol)$_2$][NO_3]$_6$ (r_{hyd} 1.28 nm; r_{calc} 0.95 nm).[6b] Though these molecules have different structures and are not squares, their sizes do not vary too much compared to complexes **23** and **24**. This restricts the possibility for complexes **23** and **24** to have polymeric structures. Because, for polymeric structures the diffusion coefficients would be much smaller than what observed for complexes **23** and **24**. Very recently, Hupp and co-workers have determined the size of large tetrametallic molecular squares by diffusion NMR experiments.[6a] They have developed a method to

calculate the sizes of molecular assemblies having oblate spheroid molecular shapes in a more sophisticated way. According to the Hupp approach, the diffusion coefficients of well characterized molecular species comprising a series of ligands (L = pyrazine, 4,4′-bipy, 1,4-phenylene diisonicotinate and 4-pyridylporphyrin) and their metal corners $\{Re(CO)_3ClL_2\}$ and squares $\{(Re(CO)_3ClL)_4\}$ were measured. To estimate the molecular size of an unknown complex, a calibration curve (D vs $1/r_{mod}$) was generated using the measured D values of the above mentioned known standards with theoretical radii (r_{mod}) where the slope of the fit was forced through zero (eq. 5.2).

$$D^{DMSO} = 22.7 \times 1/r_{mod} + 0 \qquad 5.2$$

To obtain r_{mod}, the complexes under investigation were approximated by the equivalent encapsulating sphere using the vander Waals radius at the widest point (equatorial radius) (Figure 5.11).[6a] Hence the radius of the unknown complex was determined for the measured D value using the slope of the best fit (eq. 5.2) and compared with the theoretical molecular radius.

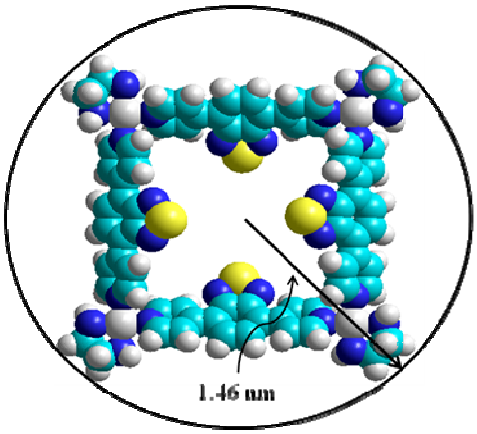

Figure 5.11 Approximation of molecular radius for complex **23** along the longest axis within the molecule (oblate spheroid approximation)

This approach for estimating the molecular size developed by Hupp, is found to be more relevant and realistic to estimate the sizes of complexes **23** and **24** as they are expected to be square assemblies having the same spheroid shapes. As the solvent viscosity has an inverse relationship with the diffusion coefficient, it was essential to switch the D^{CH_3CN} values to D^{DMSO} to fit to Hupp's data. Switching to D^{DMSO}, was done by using eq. 5.3 derived from eq. 5.1 assuming that $r_{hyd}^{CH_3CN} \cong r_{hyd}^{DMSO}$.

$$D_2 = \frac{\eta_1 D_1}{\eta_2} \qquad 5.3$$

The molecular radii on this empirical scale (i.e. r_{mod}) of complexes **23** (2.49 nm) and **24** (2.52 nm) were obtained by using the slope of the best-fit line from the equation 5.2 as reported by Hupp and co-workers.[6a] In comparison, the theoretical radii (calculated from the low energy MM+ space-filled models as mentioned above) for **23** and **24** are 1.46 and 1.48 nm, respectively. This indicates that they are in the size range expected for larger size molecular assembiles and the values are definitely smaller than the radius that would be for a polymeric structure. Disappointingly, the fit between r_{calc} and r_{mod} from Hupp´s calibration curve for **23** and **24** are not as good as expected. In fact, the agreement between r_{calc} and r_{hyd} is better. However, hydrodynamic radii are not true molecular sizes, so agreement should not be overemphasized. Perhaps the conversion of D^{CH_3CN} to D^{DMSO} is not as valid as assumed.

In conclusion, diffusion NMR experiments provide evidence that **23** and **24** are very similar in size, that they do not appear to be labile in solution and that their sizes are in approximately the right range for the claimed molecular squares. While this estimation is

not a definite proof of a square M_4L_4 unit rather than other possible shapes such as M_3L_3 triangles or M_5L_5 pentagons, it should also be remembered that squares are commonly observed using the same metal corners (enPd) and similar pillar ligands. Other geometries in this class of molecular structures apparently do not form readily.

References

1. (a) Guerrero, A.; Jalon, F. A.; Manzano, B. R.; Claramunt, R. M.; Cabildo, P.; Infantes, L.; Cano, F. H.; Elguero, J. *Chem. Heterocycl. Comp.* **2003**, *39*, 1396. (b) Herberhold, M.; Akkus, N.; Milius, W. *Z. Naturforsch.* **2003**, *58b*, 528.

2. (a) Blanco, V.; Chas, M.; Abella, D.; Peinador, C.; Quintela J. M. *J. Am. Chem. Soc.* **2007**, *129*, 13978. (b) Blanco, V.; Gutiérrez, A.; Platas-Iglesias, C.; Peinador, C.; Quintela, J. M. *J. Org. Chem.* **2009**, *74*, 6577. (c) Peinador, C.; Blanco, V.; Quintela, J. M. *J. Am. Chem. Soc.* **2009**, *131*, 920.

3. (a) Young, J. K.; Baker, G. R.; Newkome, G. R.; Morris, K. F.; Johnson, C. S., Jr. *Macromolecules* **1994**, *27*, 3464. (b) Ruegger, H.; Pregosin, P. S. *Helv. Chim. Acta* **2001**, *84*, 2833 and references therein.

4. Terrill, R. H.; Postlethwaite, T. A.; Chen, C. H.; Poon, C. D.; Terzis, A.; Chen, A. D.; Hutchison, J. E.; Clark, M. R.; Wignall, G.; Londono, J. D.; Superfine, R.; Falvo, M.; Johnson, C. S.; Samulski, E. T.; Murray, R. W. *J. Am. Chem. Soc.* **1995**, *117*, 12537.

5. Burini, A.; Fackler, J. P.; Gallassi, R.; Macchioni, A.; Omary, M. A.; Rawashdeh-Omary, M. A.; Pietroni, B. R.; Sabatani, S.; Zuccaccia, C. *J. Am. Chem. Soc.* **2002**, *124*, 4570.

6. (a) Otto, W. H.; Keefe, M. H.; Splan, K. E.; Hupp, J. T.; Larive, C. K. *Inorg. Chem.* **2002**, *41*, 6172. (b) Megyes, T.; Jude, H.; Grósz, T.; Bakó, I.; Randai, T.; Tárkányi, G.; Pálinkás, G.; Stang, P. J. *J. Am. Chem. Soc.* **2005**, *127*, 10731.

7. Peinador, C.; Blanco, V.; Quintela, J. M. *J. Am. Chem. Soc.* **2009**, *131*, 920.

CHAPTER SIX: OPTOELECTRONIC CHARACTERIZATION OF LIGANDS AND THEIR METAL COMPLEXES

6.1 Introduction

As mentioned in chapter 3, benzochalcogenadiazoles typically have high reduction potentials, electron affinity and luminescent properties. They are useful ring systems which have been derivatized with various substituents to modify their suitability for materials applications.[1-3] In this chapter, some optoelectronic properties of the compounds containing benzochalcogenadiazole ring systems previously introduced in this thesis are described. The measurements were important from the point of view of investigating the effects of the different substituent and heavier chalcogens as well as the metal centers on the reduction potentials and the luminescent properties.

6.2 CV and SWV of 4,7-dibromo-2,1,3-benzochalcogenadiazoles (**3**, **5**) and their metal complexes (**6b**, **7b**, **8**)

As mentioned in Chapter 1, the electrochemistry of benzochalcogenadiazole ring systems and their derivatives have previously been studied by various electrochemical methods. However, the electrochemistry of the the dibromo compounds **3** and **5** have apparently not been reported. Therefore they were studied by cyclic voltammetry (CV) and square-wave voltammetry (SWV) in CH_3CN and CH_2Cl_2 solvents over scan rates of 0.05-1.00 V s^{-1} and 0.10 V s^{-1}, at a temperature of 21±1°C. Potential data are reported on the IUPAC-recommended scale *versus* the ferrocene/ferrocenium redox couple as an internal standard at 0.00 V; literature data have been converted to this scale where necessary using established conversion factors, but it should be kept in mind that this introduces

some uncertainty due to the different junction potentials. Voltammetric results for **3** and **5** are reported in Table 6.1 and representative CVs obtained in CH_3CN at a scan rate of 0.2 V s^{-1}, are shown in Figure 6.1.

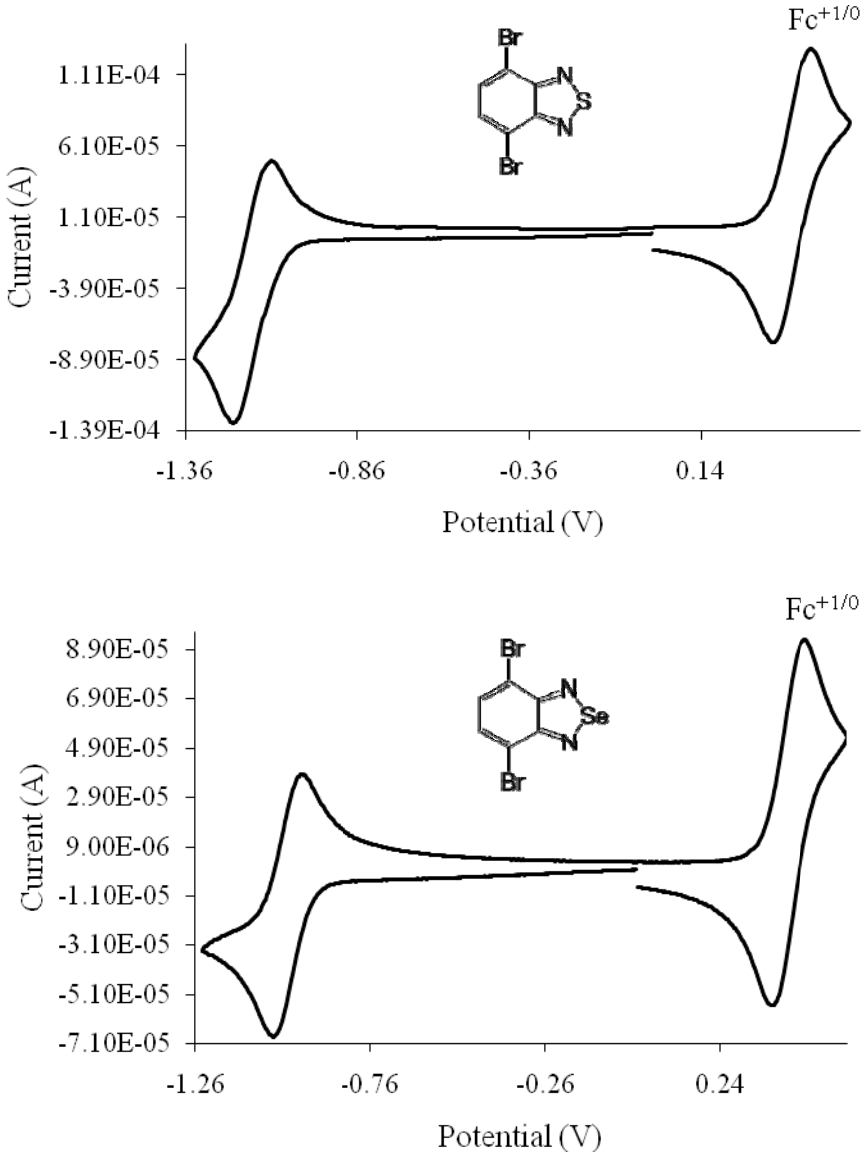

Figure 6.1 Cyclic voltammograms of 2.71 and 1.49 mM solutions of **3** (top, 2.81 mM Fc) and **5** (bottom, 1.55 mM Fc) in CH_3CN (0.1 M [$^nBu_4N$][PF_6]), ν = 0.2 V s^{-1}, T = 21°C. The voltage scale is nominal and has not been corrected to Fc = 0.0 V

Both compounds, in CH_3CN solutions with $[^nBu_4N][PF_6]$ as the supporting electrolyte, gave rise to a single reduction process which appears to involve one electron (by comparing the peak currents with those of the ferrocene internal standard present at the same concentration) as expected for benzochalcogenadiazole radical anion formation (See Chapter 1). The same processes in CH_2Cl_2/electrolyte solution are distinctly less reversible (Table 6.1) and independent of scan rate. Though further discussion will focus on voltammetry in CH_3CN/0.1 M $[^nBu_4N][PF_6]$ the data obtained from CH_2Cl_2 will be compared when necessary.

The reduction process for **3** in CH_3CN/electrolyte solution displays quasi-reversibility with anodic (E_p^{a1}) to cathodic (E_p^{c1}) peak-to-peak separation (ΔE_{pp}) of 110±1 mV, whereas **5** displays close to electrochemically reversible behavior with a peak-to-peak separation (ΔE_{pp}) of 80±1 mV. Compared to the parent benzothiadiazole (−1.89 V) and benzoselenadiazole (−1.76 V) rings (See Table 1.1, Chapter 1), the reduction potentials of **3** (−1.57 V) and **5** (−1.43 V) are less cathodic by +0.32 and +0.33 V, respectively. This is probably due to the inductive effect of the bromine atoms in **3** and **5**. These results are also supported by PM3 molecular orbital calculations showing that the energy levels of LUMOs (−2.12 eV for **3** and −2.13 eV for **5**) are lower than those observed for benzothiadiazole (−1.81 eV) and benzoselenadiazole (−1.82 eV). The reduction potential of **5** is less cathodic than **3** by +0.14 V suggesting that the selenadiazole ring in **5** is easier to reduce than the thiadiazole ring in **3**, and a similar influence was also observed in a comparative study of benzothiadiazole and benzoselenadiazole rings (ΔE = +0.13 V). This is probably due to the larger polarizability of the selenium atom.[4] The reduction potentials of **3** (−1.58 V) and **5** (−1.43 V) for the −1/0 process measured by SWV, are in

good agreement with the values observed by CV as expected for reversible or close-to-reversible processes.

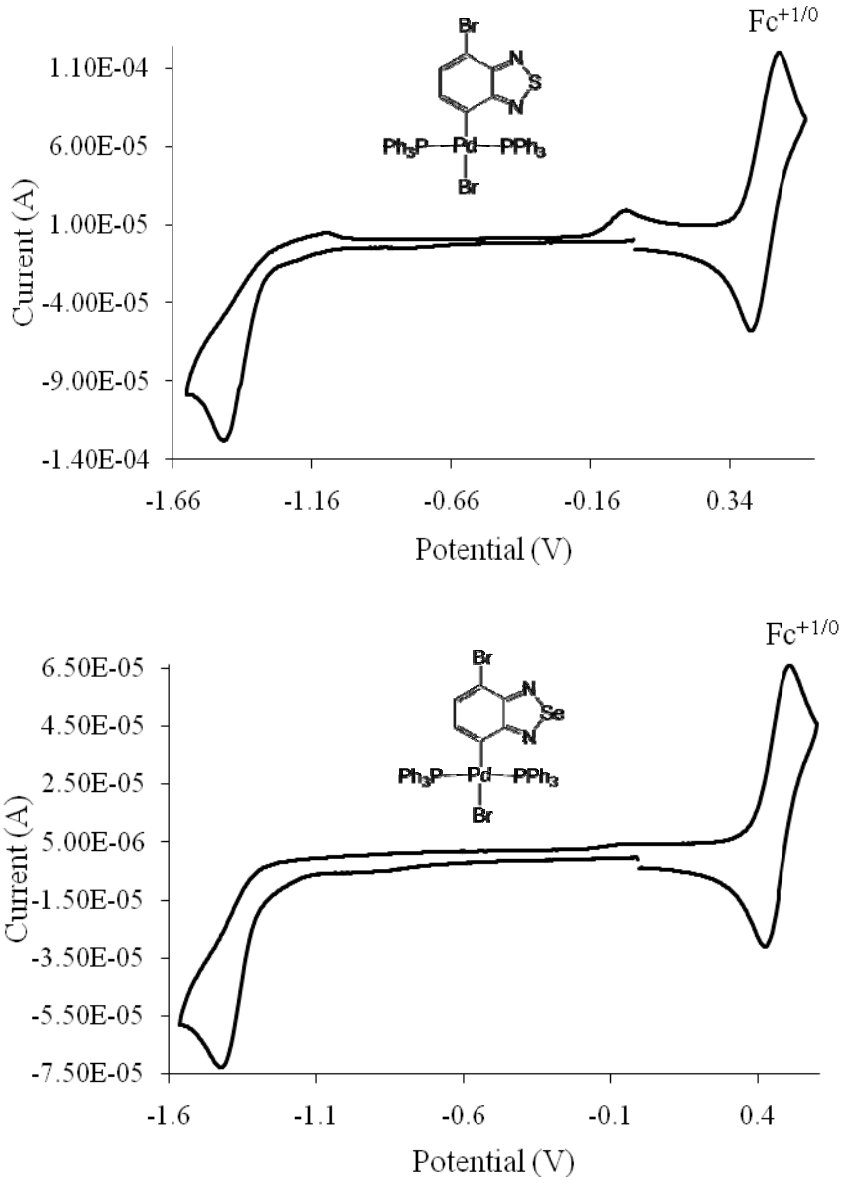

Figure 6.2 Cyclic voltammograms of 2.01 and 1.19 mM solutions of **6b** (top, 2.12 mM Fc) and **7b** (bottom, 1.19 mM Fc) in CH_3CN (0.1 M [$^nBu_4N$][PF_6]), ν = 0.2 V s^{-1}, T = 21^oC. The potential was first swept in the negative direction and the voltage scale is nominal and has not been corrected to Fc = 0.0 V

CVs of the monomeric palladium arene complexes **6b** and **7b** show irreversible reduction processes at −1.94 and −1.89 V (in CH_3CN), respectively and at −2.29 and −2.08 V (in CH_2Cl_2), respectively versus Fc/Fc^+ (Table 6.1, Figure 6.2) that also appear to involve a single-electron transfer by comparison of the cathodic peak currents with those of the Fc internal standard. Though the Pd monomers show irreversible reduction processes it is hard to comment on the reversibility of the reduction potentials of the Pd dimer **8** because of the presence of some residual dioxygen from insufficient purging of the electrolyte solution. In the case of this compound, the electrochemical studies could not be repeated with more rigorous purging due to insufficient amount of sample (and efforts to repeat the synthesis of **8** have so far been unsuccessful). However, the voltammogram of **8** shows two irreversible processes at −2.07 and −1.57 V versus Fc/Fc^+ in CH_2Cl_2 (Table 6.1).

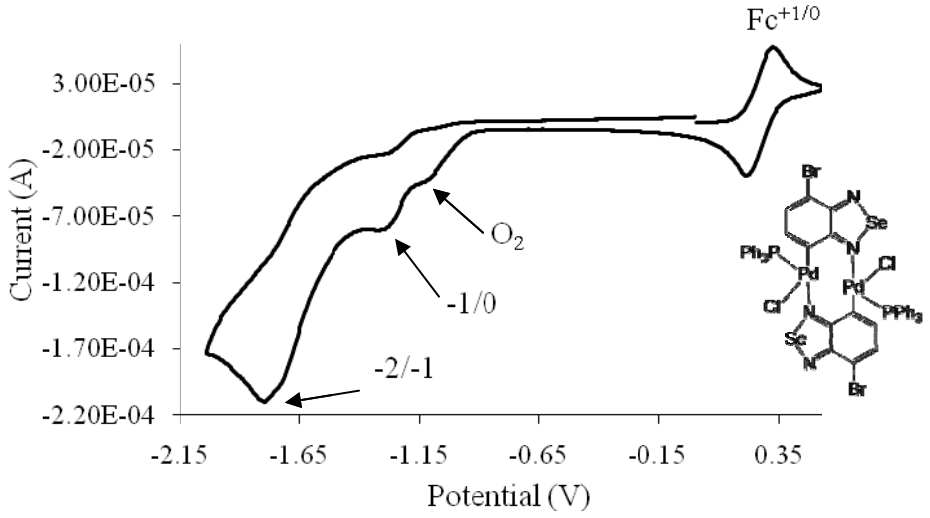

Figure 6.3 Cyclic voltammogram of 1.59 mM solution of **8** in CH_2Cl_2 (0.4 M $[^nBu_4N][PF_6]$, 2.11 mM Fc), $\nu = 0.2$ V s^{-1}, T = 21°C. The potential was first swept in the positive direction and the voltage scale is nominal and has not been corrected to Fc = 0.0 V

Table 6.1 CV and SWV data obtained for 3, 5, 6b, 7b, 8, 9, 11, 12, 13, 19 and 20[a] (in CH_3CN or CH_2Cl_2)

Compounds		CV[b]							SWV[b]	
		Conc (mM)	E_p^{a1} (V)	E_p^{c1} (V)	E_m [c] (V)	E_p^{a2} (V)	E_p^{c2} (V)	E_n [d] (V)	E_1 (V)	E_2 (V)
3	mCH_3CN	2.71	−1.51	−1.62	−1.57				−1.58	
	mCH_2Cl_2	3.54		1.76					1.70	
5	mCH_3CN	1.49	−1.39	−1.47	−1.43				−1.43	
	mCH_2Cl_2	2.39		1.62					1.53	
6b[e]	mCH_3CN	2.01		1.94					1.91	
	mCH_2Cl_2	2.07		−2.29						
7b[e]	mCH_3CN	1.19		1.89					1.85	
	mCH_2Cl_2	2.18		−2.08						
8[e]	mCH_2Cl_2	1.59		2.07			1.57		-	
9		2.07	−2.00	−2.11	−2.05	−1.62	−1.52	−1.57	−2.11	−1.63
11		1.66	1.96	2.06	2.01	1.46	1.54	1.50	2.02	1.51
12		2.11	2.17	2.30	2.24	1.50	1.69	1.64	2.25	1.66
13		2.22	−2.09	−2.28	−2.19	−1.51	−1.60	−1.56	−2.21	−1.58
19		2.03	1.50	1.59	1.55	1.23	1.32	1.28	1.56	1.29
20		1.18	−1.48	−1.57	−1.53	−1.21	−1.29	−1.25	−1.53	−1.25

[a] CV and SWV obtained at a GC electrode at $\nu = 0.2$ and $\nu = 0.1$ V s^{-1}, and $T = 21 \pm 1$ °C, Fc reference is corrected.
[b] Precision of data 0.01 V and accuracy 0.001 V
[c] $E_m = [E_p^{a1} + E_p^{c1}]/_2 \approx E^{0}_{(1)}$, [d] $E_n = [E_p^{a2} + E_p^{c2}]/_2 \approx E^{0}_{(2)}$, [e] irreversible process.

Table 6.2 Oxidation potentials for **19** and **20**[a] (in CH_3CN)

Compounds	CV				SWV		
	Conc.mM	E_p^a (V)	E_p^a (V)	E_p^a (V)	E_p (V)	E_p (V)	E_p (V)
19	2.03	1.06	1.40	1.57	1.02	1.29	1.50
20	1.18	1.05	1.39	1.54	1.02	1.28	1.47

[a] irreversible process.

The second reduction process is attributed to the reduction of two selenadiazole rings in dimer **8** (Figure 6.3, two electrons at the same potential) whereas the first process may be an impurity associated with reduction of oxygen (such as liberated chloride anions). As observed also for the "ligand" heterocycles **3** and **5,** the selenadiazole ring in **7b** is less cathodic by 0.05 V than the thiadiazole ring in **6b**. Square-wave voltammograms of **6b** (−1.91 V) and **7b** (−1.85 V) fit well with the values of the reduction potentials measured by CV. Interestingly the reduction potentials for both thiadiazole and selenadiazole rings in **6b** and **7b** are more cathodic (−0.32 and −0.42 V in CH_3CN, respectively; −0.53 and −0.46 V in CH_2Cl_2, respectively) compared to the same ring systems in **3** and **5**. This suggests that replacing one bromine atom by the palladium metal makes the benzochalcogenadiazole rings more difficult to reduce. This is indicative of a smaller inductive effect of the Pd atom which has lower electronegativity (2.20) than a bromine atom (2.96).

6.3 CV and SWV of 4,7-*bis*(2/4-pyridyl)benzochalcogenadiazoles (**9**, **11**, **12**, **13**) and rhenium complexes (**19**, **20**)

Over the past few years several authors investigated the electrochemical properties of different aryl substituted benzothiadiazole systems for the purpose of applications in materials science.[1-3] Recently Yamashita and co-workers reported nominal voltage data for the first reduction process of several pyridine substituted benzothiadiazoles but the detailed voltammetric behavior was apparently not investigated nor were the corresponding Se analogs prepared by them.[3] Hence, a thorough comparative study of the voltammetric responses between pyridine substituted S and Se ligands while free and coordinated to the metal center was performed and the results are presented here.

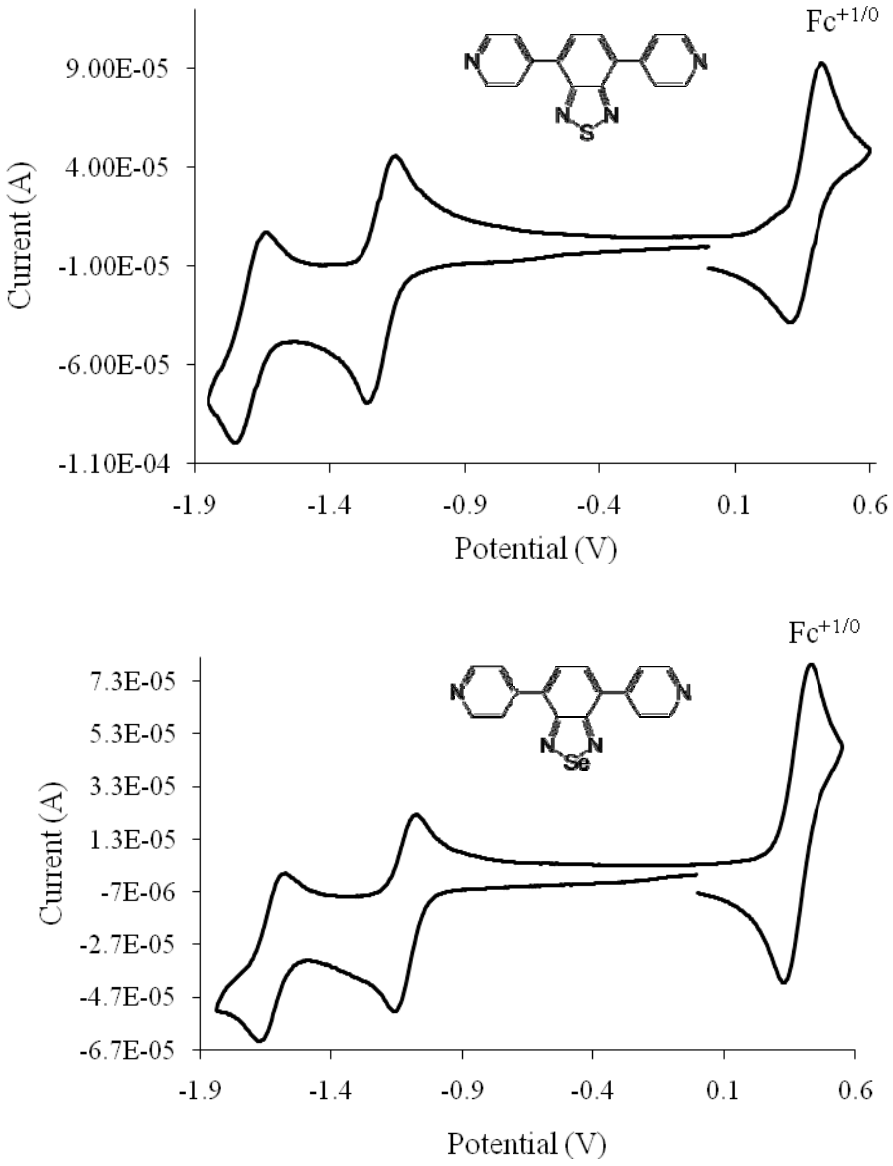

Figure 6.4 Cyclic voltammograms of 2.07 and 1.66 mM solutions of **9** (top, 2.05 mM Fc) and **11** (bottom, 1.68 mM Fc) in CH_3CN (0.1 M [$^nBu_4N$][PF_6]), ν = 0.2 V s^{-1}, T = 21°C. The potential was first swept in the negative direction and the voltage scale is nominal and has not been corrected to Fc = 0.0 V

Cyclicvoltammograms and square-wave voltammograms of all ligands (**9**, **11**, **12**, **13**) and metal complexes (**19**, **20**) showed two resolved one electron reduction processes in CH_3CN solutions with [$^nBu_4N$][PF_6] as the supporting electrolyte (Table 6.1).

The voltammetric studies were performed over scan rates of 0.1-1.0 V s^{-1} (CV) and 0.10 V s^{-1} (SWV) at a temperature of 21±1°C. Representative CVs obtained in CH_3CN at a scan rate of 0.20 V s^{-1} are shown in Figure 6.4 for **9** and **11**, Figure 6.5 for **12** and **13** and Figure 6.6 for **19** and **20**.

The first reduction process is attributed to benzochalcogenadiazole radical anion formation. This displayed quasi-reversible behavior for all ligands and metal complexes over the potential range −1.25 to −1.64 V verses Fc/Fc^+ except for **11** and **20** which exhibited close to electrochemically reversible behavior with anodic (E_p^{a2}) to cathodic (E_p^{c2}) peak-to-peak separation (ΔE_{pp}) of 80±1 mV. The reduction potentials for **9** (−1.57 V) and **12** (−1.64 V) are comparable with the previously reported values of −1.57 and −1.63 V for the same compounds.[3c] Again, comparison between S and Se systems in ligands and metal complexes suggests that the reduction potential for the Se system is less cathodic. For metal complexes **19** and **20**, the first reduction potentials are also shifted to more positive values, suggesting that the benzochalcogenadiazole rings of the ligands can more easily be reduced in the coordinated form than in the free ligands.

This is probably due to dative bond formation where electron density is shifted to the metal center from the nitrogen atom increasing the positive character (electron affinity) of the ligands. The second reduction process also display quasi-reversible behavior for **9**, **11** and their metal complexes (**19**, **20**) occurring over the potential range −1.53 to −2.24 V verses Fc/Fc^+. The second reduction process for **12** and **13** showed a very small return wave at moderate-to-slow scan rates, which remain unchanged in peak current height with increasing scan rate. PM3 calculations indicate that the second process involves the Singly Occupied Molecular Orbital (SOMO) of the radical anion produced in step 1.

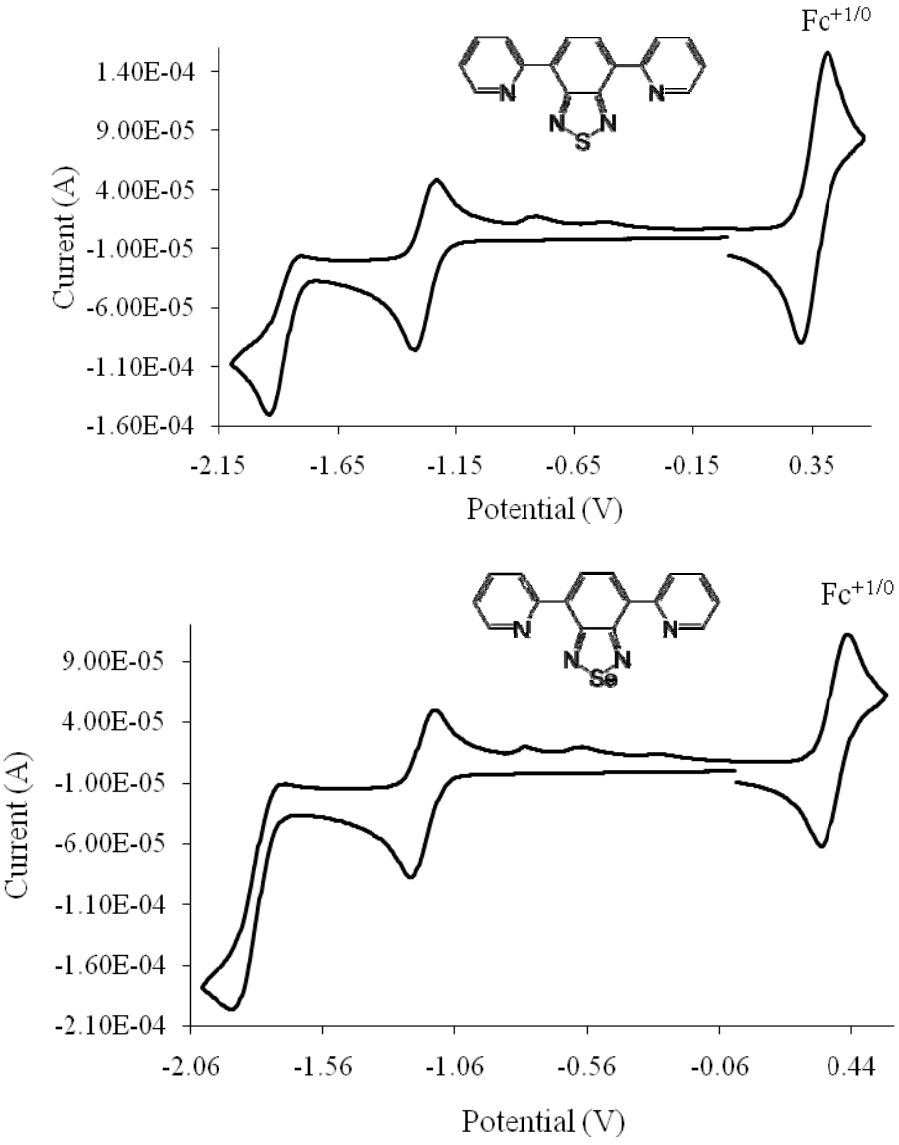

Figure 6.5 Cyclic voltammograms of 2.11 and 2.22 mM solutions of **12** (top, 2.50 mM Fc) and **13** (bottom, 2.37 mM Fc) in CH_3CN (0.1 M [$^nBu_4N$][PF_6]), ν = 0.2 V s^{-1}, T = 21^oC. The potential was first swept in the negative direction and the voltage scale is nominal and has not been corrected to Fc = 0.0 V. The asterisks show small additional re-oxidation peaks that are not observed for CVs reversed above -1.6 V on the (nominal) horizontal scales

The inductive electron delocalizing influence of the 4-pyridyl substituents is clearly indicated by the much more facile second reductions in the case of these compounds

compared to the simple halide or metal substituents in **3**-**7**, for which a second reduction could not be observed within the accessible solvent window.

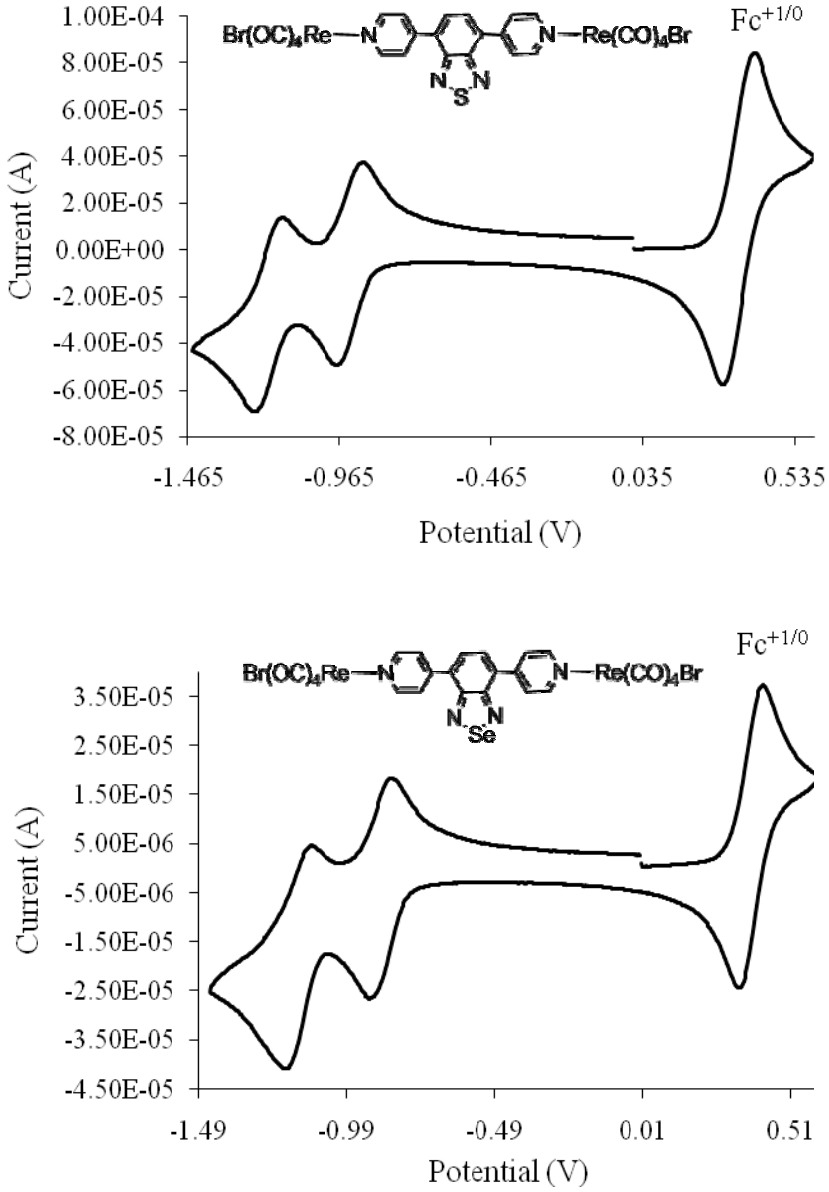

Figure 6.6 Cyclic voltammograms of 2.03 and 1.18 mM solutions of **19** (top, 2.05 mM Fc) and **20** (bottom, 1.17 mM Fc) in CH_3CN (0.1 M [$^nBu_4N$][PF_6]), ν = 0.2 V s^{-1}, T = 21^{o}C. The potential was first swept in the negative direction and the voltage scale is nominal and has not been corrected to Fc = 0.0 V

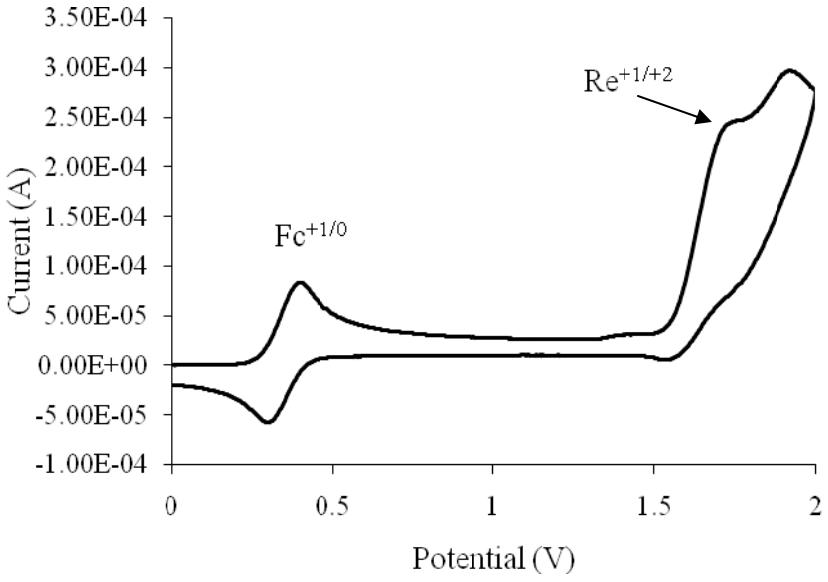

Figure 6.7 Cyclic voltammogram (oxidation potentials) of **19** in CH_3CN (0.1 M $[^nBu_4N][PF_6]$), $\nu = 0.2$ V s^{-1}, T = 21°C. The voltage scale is nominal and has not been corrected to Fc = 0.0 V

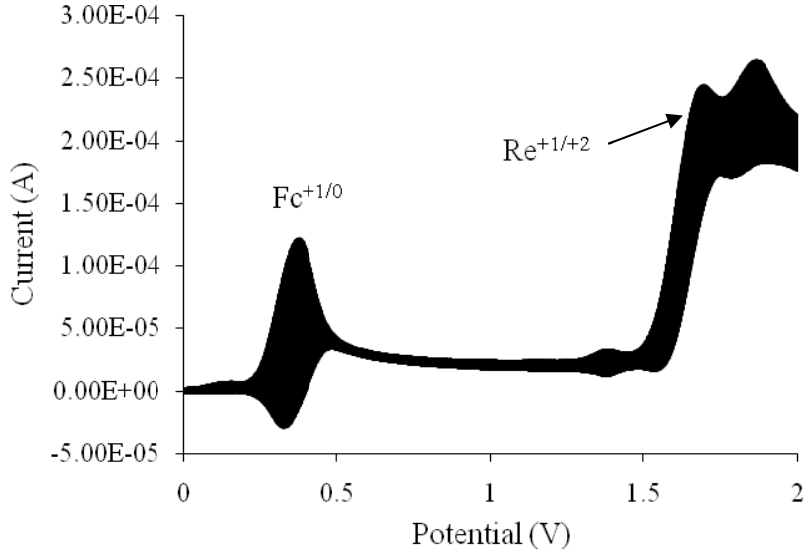

Figure 6.8 Square-wave voltammogram (oxidation potentials) of **19** in CH_3CN (0.1 M $[^nBu_4N][PF_6]$), $\nu = 0.1$ V s^{-1}, T = 21°C. The voltage scale is nominal and has not been corrected to Fc = 0.0 V

In the case of metal complexes the second reduction potentials are shifted significantly in the positive direction by 0.5 V for **19** and 0.48 V for **20**, indicating that the second reduction of the ligands are more easily accessible in the coordinated form. The first and second reduction potentials for **9** and **11** are less cathodic compared to the values observed for **12** and **13**. These results are supported by PM3 molecular orbital calculations showing that the energy levels of LUMOs (−2.37 eV for **9** and −2.38 eV for **11**) are lower than those observed for **12** (−1.80 eV) and **13** (−1.81 eV). After scans sufficiently cathodic to include the irreversible second reduction processes for **12** and **13**, additional small anodic peaks are observed which are probably due to re-oxidation of some decomposed species from the second process; these additional small peaks were absent when the scans were reversed directly after the first process. There were no significant changes in the peak height of the first reduction process observed for all ligands and metal complexes when the first process was observed alone. The SWVs of all the ligands and metal complexes showed two reduction peaks and potentials are in good agreement with the values measured by CVs.

The Re complexes **19** and **20** showed two oxidation processes in the potential region from +1.47 to +1.57 V with very small return waves (Figure 6.7, Table 6.2). Though the return waves are not seen clearly in CV, they can be seen in SWV (Figure 6.7). The first oxidation process appeared at +1.40 V for **19**, and at +1.39 V for **20**, which can be assigned to the $Re^{+1/+2}$ oxidation processes at both rhenium centers, accounting for the large current values which are approximately twice as great as for the Fc standard.[5a] The second oxidation wave may correspond to further oxidation of Re^{+2} species formed at the electrode (possibly Re^{+3} species) but while this oxidation behavior is common for

rhenium compounds, the processes observed here are poorly defined with only small current values.[5b, c] The oxidation potentials observed by SWV were consistent with the values measured by CV experiments.

6.4 Photophysical properties of 4,7-*bis*(2/4-pyridyl)benzochalcogenadiazoles (**9**, **11**, **13**) and their metal complexes (**19**, **20**, **23**, **24**)

6.4.1 Electronic Absorption Spectroscopy

The electronic absorption spectra for the 4,7-*bis*(2/4-pyridyl)benzochalcogenadiazole ligands and metal complexes were determined in CH_3CN solutions. The absorption data are listed in Table 6.3. The electronic spectra of the free ligands **9**, **11** and **13** have three main bands arising from $\pi-\pi^*$ and $n-\pi^*$ transitions (Figure 6.9).

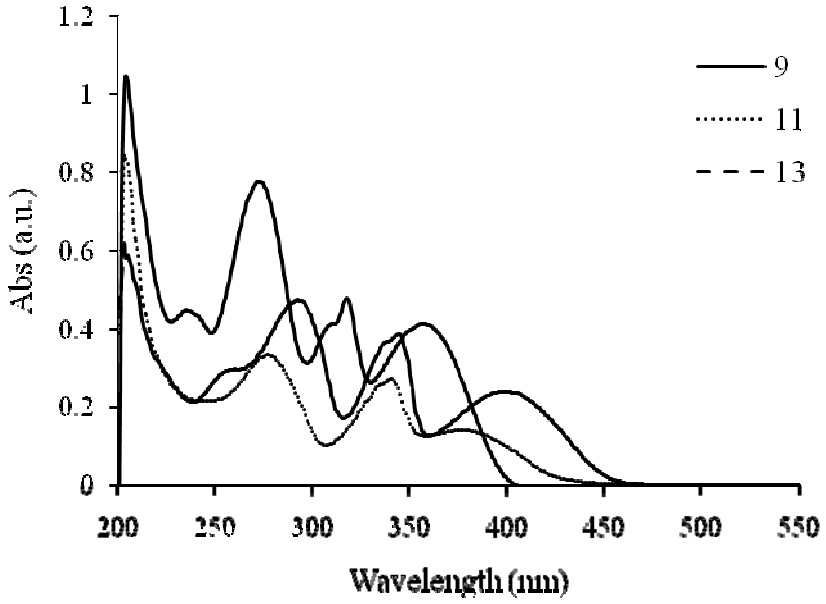

Figure 6.9 Electronic absorption spectra of **9**, **11** and **13**

By comparing compounds **9** and **11**, the absorption maxima are red shifted on going from S to Se by about 20 nm. The absorption maxima for **13** are further red shifted compared

to those observed for **11** when the nitrogen position is changed from 4 to 2. This can be explained by a more coplanar structure increasing the conjugation in **13** compared to **11**.[3c] The rhenium complexes **19** and **20** have four absorption bands instead of the three observed for the corresponding free ligands **9** and **11** (Figure 6.10).

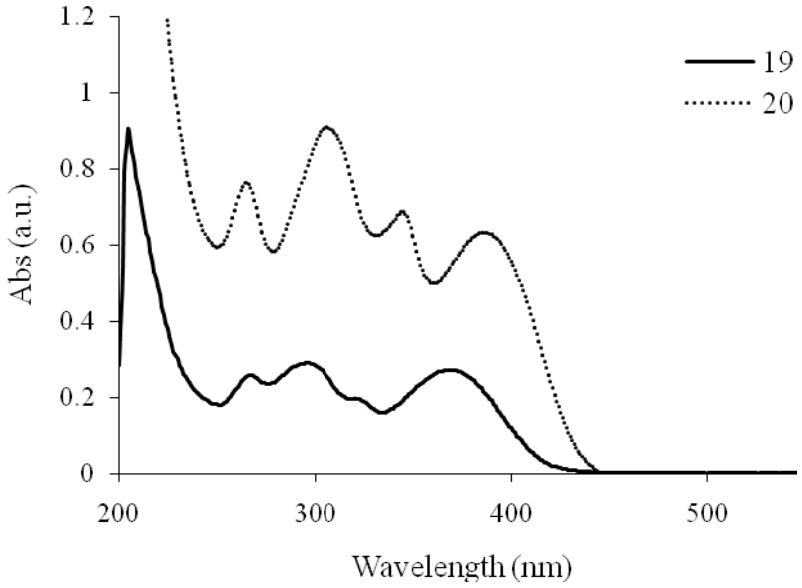

Figure 6.10 Electronic absorption spectra of **19** and **20**

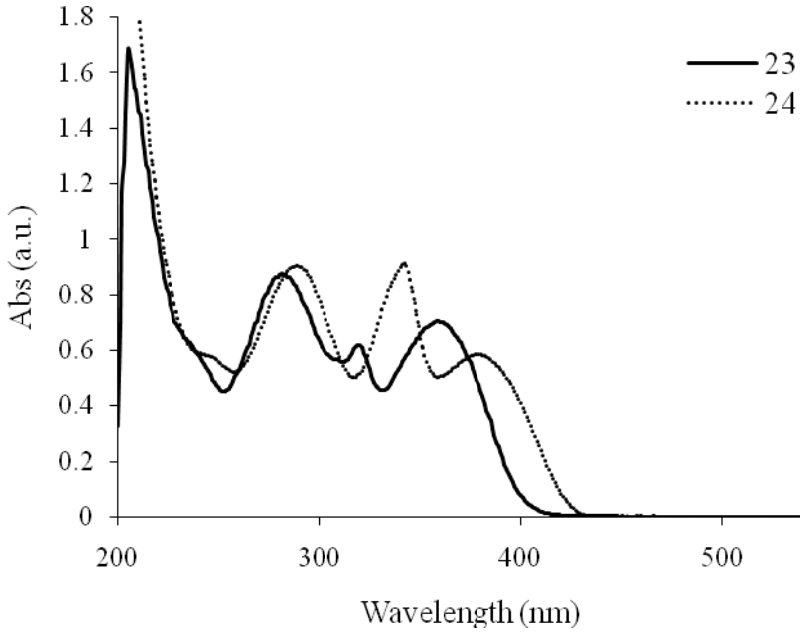

Figure 6.11 Electronic absorption spectra of **23** and **24**

Table 6.3 UV and luminescence data of 9, 11, 13, 19, 20, 23 and 24 in CH_3CN

Compounds	λ_{abs} (nm)	λ_{ex} (nm)	Fluorescence λ_{em} (nm)	Stokes shift (nm)	Phosphorescence λ_{em} (nm)
9	272, 318, 357	357	443	86	514
11	276, 340, 377	377	443	66	525
13	292, 344, 398	398	498	100	607
19	267, 296, 325, 368	368	412	44	535
20	265, 300, 345, 386	386			554
23	281, 319, 359	359	440	81	519
24	288, 342, 379	379			560

The additional absorption band at 267 and 265 nm for **19** and **20** arises due to the dπ(Re)→pπ*(ligand) MLCT. Compared to those of free ligands **9** and **11** the absorption bands due to the π–π* and n–π* transitions for the rhenium complexes are red shifted by about 30 nm. Similarly to the free ligands the absorption maxima are red shifted by changing sulfur to selenium in the rhenium complexes by about 20 nm.

The spectra of palladium squares **23** and **24** are shown in Figure 6.11, which consist of three absorption bands at 281, 319 and 359 for **23**, and 288, 242 and 379 for **24**. Compared to the free ligands the absorption bands are effectively unchanged (values differ on average by ~2 nm). The effect of changing sulfur to selenium on the absorption bands which causes to shift the bands to the longer wavelength (red shift) was also observed in the squares. By comparing the absorption spectra of sulfur compounds to the analogous selenium compounds in either free ligands (**9**, **11**) or in molecular rods (**19**, **20**) and squares (**23**, **24**), it has been found that the low energy absorption band is consistently red shifted by ~20 nm.

6.4.2 Luminescence Spectroscopy

Luminescence spectra have been recorded for the ligands (**9**, **11**, **13**) and the metal complexes (**19**, **20**, **23**, **24**) in CH_3CN solution. The room temperature emission data are listed in Table 6.3. All three ligands **9**, **11** and **13** display emissions from both fluorescence and phosphorescence (Figure 6.12) which can easily be distinguished by the wavelengths of the emission maxima and the intensities. As mentioned in Chapter 1, the phosphorescence emissions occur at higher wavelengths and the intensity is several orders of magnitude smaller compared to the fluorescence emission. The sulfur ligand **9** exhibited efficient fluorescence in solution compared to the selenium ligands **11** and **13**.

This is due to the heavy atom effect; because the selenium atoms in **11** and **13** are considerably heavier than the sulfur atom in **9** (sulfur precedes while selenium antecedes the first transition series). As mentioned in Chapter 1, heavy atoms facilitate the molecule to be phosphorescent by efficient spin-orbit coupling which serves to quench fluorescence. As mentioned earlier, although the low energy absorption band is red shifted on going from sulfur to selenium in **9** and **11**, interestingly the fluorescence emission maxima were found to be independent of this heavier chalcogen effect and appeared at 443 nm in both. As a result the sulfur ligand **9** has a larger Stokes shift (87 nm) compared to the selenium ligand **11** (66 nm).

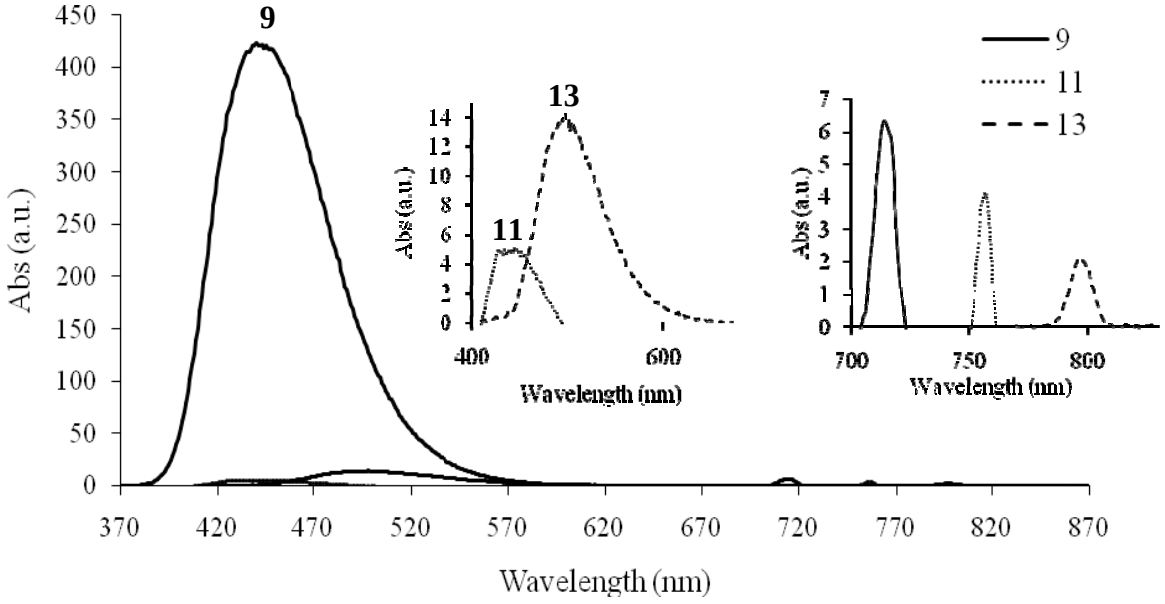

Figure 6.12 Luminescence spectra of **9**, **11** and **13**. The insets show fluorescence emissions of **11** and **13** (upper left) and phosphorescence emissions of **9**, **11** and **13** (upper right), with expanded *y* axes

However, similar to the effect on the wavelengths of the absorption maxima, on changing the nitrogen position from 4 to 2 in **13**, the emission maxima are red shifted by 55 nm

with larger Stokes shift (100 nm) perhaps due to increased conjugation caused by more coplanarity of the 2-pyridyl rings with respect to the benzoselenadiazole ring than in **11**.[3c] Though the heavier chalcogen has no effect on the fluorescence band energy, the phosphorescence emission maxima are red shifted on going from S in **9** to Se in **11**. Also the phosphorescence emission maxima are red shifted by 40 nm for changing the nitrogen position from 4 to 2 in **13**. Upon coordination to the metals in rhenium rods **19** and **20**, the fluorescence of the ligands is either partly or fully reduced as a result of efficient quenching (Figure 6.13). For heavy transition metal complexes, as mentioned in Chapter 1, quenching occurs due to spin-orbit coupling and rapid intersystem crossing.[6]

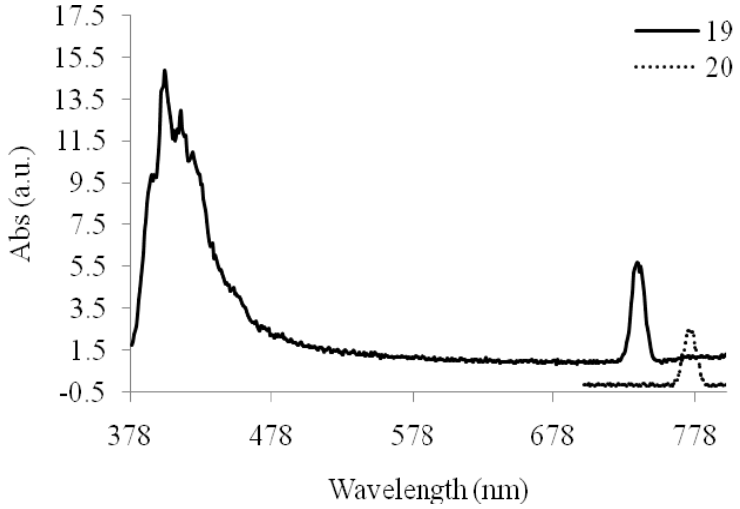

Figure 6.13 Luminescence spectra of **19** and **20**

In the case of compounds **19** and **20**, this can be explained as the optical excitation for the rhenium coordinated ligands to yield short-lived MLCT singlet states, from which the strongly phosphorescent triplet states are populated by intersystem crossing thus reducing the fluorescence intensity.[6] Figure 6.14 displays the fluorescence emission of ligands and metal complexes in solution showing that the fluorescence intensity is greatly reduced in **19** and fully reduced in **20**. Similarly to that of free ligands **9** and **11**, the effect of heavior

chalcogen shifting the phosphorescent emission to longer wavelength was also observed in molecular rods **19** and **20**. The palladium square **23** exhibits efficient fluorescence as observed for the free ligand and the emission maximum is red shifted by 2 nm compared to the free ligand (Figure 6.15).

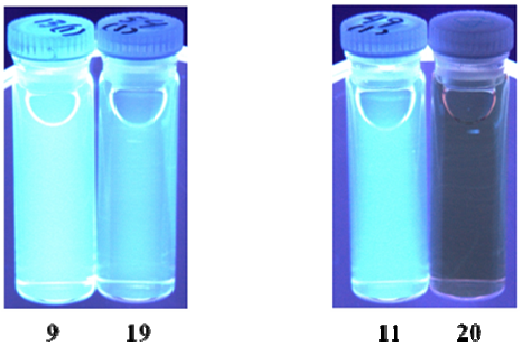

Figure 6.14 Visualization of 1 μM solutions of S ligand **9** and rhenium rod **19** (left), and Se ligand **11** and rhenium rod **20** (right) under UV irradiation (260 nm)

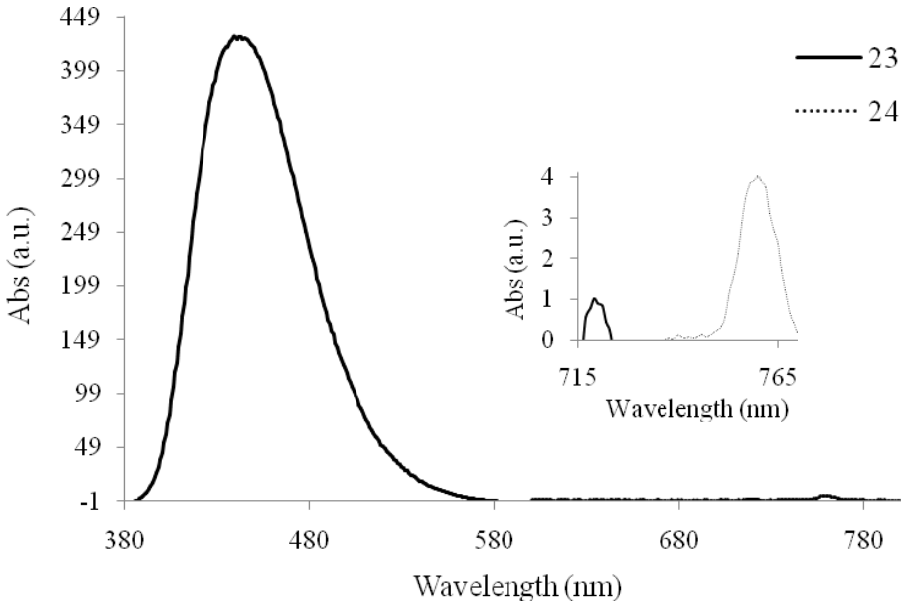

Figure 6.15 Luminescence spectra of **23** and **24**. Inset: phosphorescence emissions of **23** and **24** with expanded *y* axis

The strong fluorescence emission of **23** was also observed in the solid state for both thin plate and precipitate (Figure 6.16). Similarly to that of **9**, the square exhibits phosphorescent emission which is red shifted by 5 nm compared to **9**. The spectrum of square **24** displays only phosphorescent emission (Figure 6.17). This indicates that though the ligand **11** has weak fluorescence, this is fully quenched by Palladium spin-orbit coupling effects (Figure 6.17). Thus **24** may be of interest for applications requiring only phosphorescence.

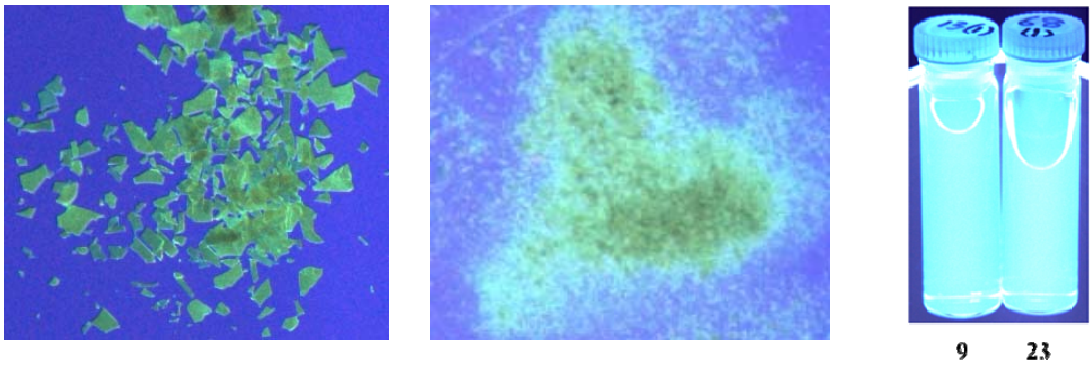

Figure 6.16 Fluorescence emissions of **23** in thin film (left), precipitate (middle) and in solution (right) under UV light (260 nm excitation)

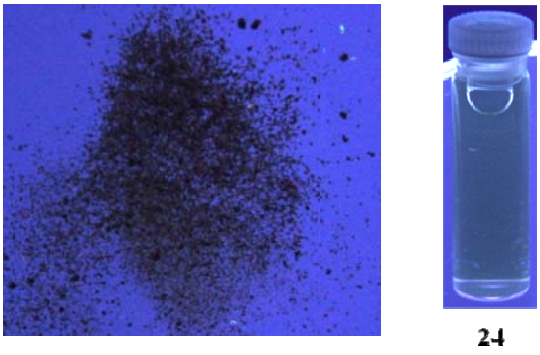

Figure 6.17 Visualization of square **24** in precipitate (left), and in solution (right) under UV light (260 nm excitation)

References

1. (a) Suzuki, T.; Yamashita, Y.; Kabuto, C.; Miyashi, T. *J. Chem. Soc., Chem. Commun.* **1989**, 1102. (b) Yamashita, Y.; Eguchi, J.; Suzuki, T.; Kabuto, C.; Miyashi, T.; Tanaka, S. *Angew. Chem., Int. Ed.* **1990**, *29*, 643. (c) Yamashita, Y.; Suzuki, T.; Mukai, T.; Saito, G. *J. Chem. Soc., Chem. Commun.* **1985**, 1044. (d) Hirayama, M.; Terasaka, T.; Itasaka, M.; Suzuki, T.; Yamashita, Y.; Miyashi, T. *Chem. Lett.* **1995**, 837. (e) Yamashita, Y.; Tomura, M. *J. Mater. Chem.* **1998**, *8*, 1933.

2. (a) Neto, B. A. D.; Lopes, A. S. A.; Ebeling, G.; Gonçalves, R. S.; Costa, V. E. U.; Quina, F. H.; Dupont, J. *Tetrahedron* **2005**, *61*, 10975. (b) Thomas, J.; Lin, J. T.; Velusamy, M.; Tao, Y. –T.; Chuen, C. –H. *Adv. Func. Mat.* **2004**, *14*, 83. (c) Wei, P.; Duan, L.; Zhang, D.; Qiao, J. Wang, L.; Wang, R.; Dong, G.; Qiu, Y. *J. Mat. Chem.* **2008**, *18*, 806.

3. (a) Akhtaruzzaman, M.; Tomura, M.; Zaman, M. B.; Nishida, J. –I.; Yamashita, Y. *J. Org. Chem.* **2002**, *67*, 7813. (b) Akhtaruzzaman, M.; Tomura, M.; Nishida, J. –I.; Yamashita, Y. *Synth. Met.* **2003**, *137*, 873. (c) Akhtaruzzaman, M.; Tomura, M.; Nishida, J. –I.; Yamashita, Y. *J. Org. Chem.* **2004**, *69*, 2953. (d) Akhtaruzzaman, M.; Kamata, N.; Nishida, J. –I.; Ando, S.; Tada, H.; Tomura, M.; Yamashita, Y. *Chem. Commun*. **2005**, 3183.

4. Suzuki, T.; Tsuji, T.; Miyashi, T.; Yamashita, Y. *J. Org. Chem.* **2001,** *66,* 8954.

5. (a) Pelleteret, D.; Fletcher, N. C.; Doherty, A. P. *Inorg. Chem.* **2007**, *46*, 4386. (b) Dehghanpour, S.; Khalaj, M.; Mahmoudi, A. *Inorg. Chem. Commun.* **2009**, *12*, 231. (c) Moya, S. A.; Pastene, R.; Schmidt, R.; Guerrero, J.; Sartori, R. *Polyhedron* **1992**, *11*, 1661.

6. Cannizzo, A.; Blanco-Rodríguez, A. M.; Nahhas, A. E.; Šebera, J.; Záliš, S.; Vlček, A. Jr.; Chergui, M. *J. Am. Chem. Soc.*, **2008**, *130*, 8967. (b) Masuhara, H.; Shioyama, H.; Saito, T.; Hamada, K.; Yasoshima, S.; Mataga, N. *J. Phys. Chem.* **1984**, *88*, 5868.

CHAPTER SEVEN: CONCLUSIONS

7.1 Conclusions

The goals of this thesis were the synthesis of molecular assemblies incorporating redox-active organic heterocycles such as benzochalcogenadiazoles and to find their possible application for developing new materials for electroluminescent, conducting and photovoltaic devices based on their optoelectronic analysis. While these goals are in principle quite simple, it was found that achieving them turned out to be very challenging. Nevertheless some significant steps have been made towards meeting these goals. Much of the work reported here was quite exploratory and no compounds of this class have ever been prepared in the supervisor's laboratory.

The results reported in this thesis can be divided into three main sections as follows: (i) the synthesis of 4,7-*bis*(2/4-pyridyl)benzochalcogenadiazole ligands and the preliminary results obtained during the attempts to prepare the ligands, (ii) synthesis of self-assembled molecular complexes using 4,7-*bis*(4-pyridyl)benzochalcogenadiazole ligands, and (iii) a comparative study of the optoelectronic properties of the ligands as well as the metal complexes.

Mononuclear Pd(II) complexes (**6**, **7**) of 4,7-dibromobenzochalcogenadiazole were synthesized. The reactivity of these mononuclear Pd(II) complexes towards the Stille coupling reactions was investigated giving the desired coupling products. In the case of the thiadiazole ring system, only a *bis*-coupled product was isolated from both 1:1 and 1:2 fold reactions but the yield was higher when the correct stoichiometry was used. On

the other hand, for the selenadiazole ring system, it has been found that both *mono*- and *bis*-coupling products can be isolated depending on the solvent used for the reaction. A dinuclear Pd(II) complex (**8**) was synthesized where the σ-bonded ($Pd-C_{aryl}$) benzoselenadiazole rings are coordinated in a head-to-tail fashion. However, its preparation was not found to be repeatable, unfortunate as structures of this type are quite rare. The solid state structures of 4,7-dibromobenzoselenadiazole and the palladium complexes reveal that secondary bonding interactions as well as the solvent molecules in the lattice play important roles on molecular aggregation giving one and two-dimensional sheets and chains. The redox properties of the 4,7-dibromobenzochalcogenadiazole and their Pd(II) complexes were also measured to investigate the effect of the σ-bonded palladium center to the heterocycles. Both the dibromo compounds undergo one electron reduction showing quasi-reversible and reversible behavior for the thiadiazole and selenadiazole rings, respectively. On the other hand, cyclic voltammograms of mononuclear Pd(II) complexes show one electron irreversible reduction whereas for the dimer, it shows simultaneous two electron reduction for two selenadiazole rings. In comparison, the reduction potentials of the Pd(II) complexes are more cathodic than the dibromo compounds due to the lower inductive effect of the Palladium atom.

The conditions for the synthesis of 4,7-*bis*(2/4-pyridyl)benzothiadiazoles (**9**, **12**) were modified and optimized, and a general method for the synthesis of corresponding 4,7-*bis*(2/4-pyridyl)benzoselenadiazoles (**11**, **13**) was developed. All dipyridyl compounds undergo two resolved one electron reductions showing quasi-reversible behaviors. The reduction potentials of the 4-pyridine substituted compounds (**9**, **11**) are less cathodic than the 2-pyridine substituted compounds (**12**, **13**). Though the luminescence spectra of

all dipyridyl compounds show fluorescence and phosphorescence emissions, the fluorescence intensity is much smaller for the selenadiazole than the thiadiazole ring compounds.

Novel self-assembled molecular rods of rhenium (**19**, **20**) containing redox-active 4,7-*bis*(4-pyridyl)benzochalcogenadiazole ligands were prepared. The molecular structure determinations revealed that the thiadiazole-ring-containing rod molecule (**19**) crystallizes in two different morphologies. Similarly to that of ligands (**9**, **11**), the rod molecules undergo two resolved one electron reductions and the potentials are less cathodic compared to the free ligands. The separation between the two reduction processes of the rod molecules is smaller than those observed for the free ligands. In addition to the reduction processes the rod molecules undergo two electron oxidations due to the two Re(I) metal centers. The luminescence spectra of the rod molecules show that the fluorescence is quenched due to the MLCT. Because of MLCT, there is a significant decrease in the fluorescence intensity of **19** whereas for **20** the intensity is completely reduced to give phosphorescence emission only. Palladium directed self-assembled molecular squares (**23**, **24**) were prepared using 4,7-*bis*(4-pyridyl)benzochalco-genadiazole ligands. The MM+ calculations of the squares reveal the internal cavity of 0.92 nm for **23** and 0.89 nm for **24**. The low energy model shows that the benzochalcogenadiazole rings are twisted av. 31.1^{o} above and below the molecular square plane. The molecular radii of squares **23** (2.49 nm) and **24** (2.52 nm) obtained from DOSY NMR experiments are not in good fit with the theoretical values of 1.46 and 1.48 nm, respectively, but in the size ranges expected for square structure.

Square **23** emits both fluorescence and phosphorescence whereas the square **24** emits only phosphorescence.

In general, cyclic voltammograms of selenadiazole ring containing compounds show that the reduction potential is less cathodic than the corresponding thiadiazole ring compounds due to the larger polarizability of selenium atoms. The effect of the heavier chalcogen is also observed lowering the intensity of the fluorescence emission for selenadiazole ring containing compounds compared to thiadiazole ring compounds as a consequence of quenching through spin-orbit coupling.

7.2 Future Work

There are aspects of these projects that have opened doors for further exploration. The corresponding tellurium analog can be synthesized through the conversion of the 4,7-*bis*(2/4-pyridyl)benzothia- and selenadiazole ligands back into a diamine by well-established procedures followed by condensation with $TeCl_4$.

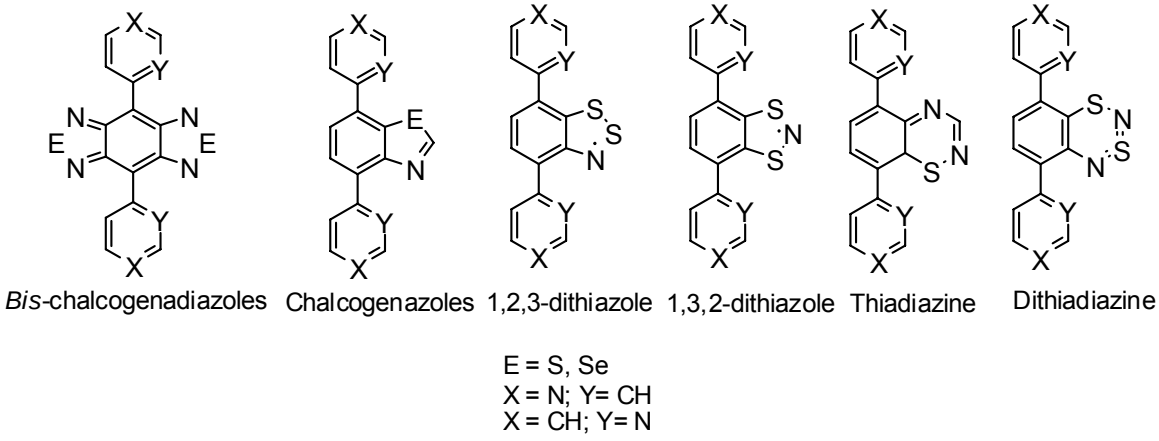

Figure 7.1 Proposed ligands incorporating different heterocycles

Similarly following the same experimental protocols as reported for 4,7-*bis*(2/4-pyridyl)benzothia- and selenadiazole ligands, pyridine substituted ligands incorporating other heterocycles such as *bis*-chalcogenadiazoles, chalcogenazoles, dithiazoles, thiadiazines and dithiadiazoles are worthy synthetic targets (Figure 7.1).

Chelating metal complexes could be synthesized by using 4,7-*bis*(2-pyridyl)benzochacogenadiazole ligands. This would help to investigate the effect of the chelated metal center on the reduction potentials and luminescent properties of the ligands, and to compare the results with those of self-assembled molecular rods and squares. The method for the synthesis of molecular rods using 4,7-*bis*(4-pyridyl)benzo-chacogenadiazole ligands could be explored to other metal carbonyls such as group 6 and 8 metal carbonyls. By making a series of molecular rods using different metal carbonyls would allow for a thorough study on the effect of the different metal centers on the redox potentials and luminescent properties of the ligands, and for developing materials for optoelectronic devices.

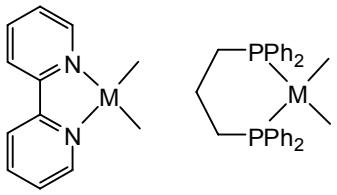

Figure 7.2 Different chelating ligands at the metal corner units

Platinum-directed self-assembled molecular squares of 4,7-*bis*(4-pyridyl)benzo-chacogenadiazoles could be synthesized following the same procedure as mentioned for palladium squares in chapter 5. This might help to get better mass spectral data as the Pt–N bond is less labile than Pd–N. Besides this, different chelating ligands such as 2,2′-

bipyridine or phosphines could be used instead of ethylenediamine at the metal corner units (Figure 7.2).

Finally the synthesis of neutral molecular squares using 4,7-*bis*(4-pyridyl)benzochacogenadiazoles could also be explored by use of suitable neutral corner fragments. Though the electrochemical studies of both 4,7-*bis*(2/4-pyridyl)benzochacogenadiazole ligands and the molecular rods of 4,7-*bis*(4-pyridyl)benzochacogenadiazoles were performed by cyclic voltammetry, showing reversibility on the two resolved one-electron reduction processes, the benzochalcogenadiazolyl radical anions have yet to be characterized by electron paramagnetic resonance (EPR) spectroscopy.

CHAPTER EIGHT: EXPERIMENTAL DETAILS

Experimental

General procedures. Solvents were dried and either distilled or purified using a solvent purification system (MBraun). Spectra for NMR spectroscopy were recorded on a 300 MHz Bruker Avance II spectrometer (^{1}H 300.138 MHz, ^{13}C{^{1}H} 75.468 MHz, ^{31}P{^{1}H} 121.495 MHz) and referenced relative to either $SiMe_4$ through the residual solvent resonance(s) for ^{1}H and ^{13}C{^{1}H} or external 85% H_3PO_4 for ^{31}P{^{1}H}. FT-IR spectra were recorded on a Bruker ALPHA FT infrared spectrometer. Elemental analyses were performed using an Elementar Americas Vario MicroCube instrument. NALDI (no matrix) and MALDI-TOF mass spectra were obtained on a Bruker ProFLEX III spectrometer using 2-[(2*E*)-3-(4-*tert*-Butylphenyl)-2-methylprop-2-enylidene] malononitrile (DCTB) as the matrix by the University of Alberta Mass Spectrometry Laboratory. ESI-MS were obtained on an orthogonal acceleration TOF (oaTOF) spectrometer by the University of Alberta Mass Spectrometry Laboratory, and EI-MS were obtained on a Varian 4000 GC mass spectrometer (Hayes research facility, University of Lethbridge) with solid insertion (chromatoprobe) analysis capabilities. Electrochemical grade tetrabutylammonium hexafluorophosphate [^{n}Bu$_4$N][PF_6] (Fluka) was used for CV experiments as the supporting electrolyte and was kept in a dessicator prior to use. Ferrocene (Fc) was sublimed prior to use.

DOSY NMR experiments. DOSY NMR experiments were carried out on a 300 MHz Bruker Avance II spectrometer (^{1}H 300.138 MHz) instrument. Diffusion coefficients *D*

were obtained from ^{1}H-NMR spectra measured with the bipolar pulse pair longitudinal encode decode (BPPLED) pulse sequence. The spectra were recorded using a 2 mm capillary tube held in a 5 mm Nalorac inverse probe at 25°C with an actively shielded z-gradient coil designed for pulsed-field gradient experiments. The diffusion experiments were carried out with the gradient strength amplitudes of 2 and 95%, a diffusion time Δ, of 0.1 s, a diffusion gradient δ, of 1.8 ms, and a longitudinal eddy current delay (LED), of 5 ms. The data were processed and the diffusion coefficients were calculated using *eddosy* editor software.

Voltammetry. Cyclic voltammograms were obtained at 20 ± 2 ^{o}C in both CH_3CN and CH_2Cl_2 solutions containing 0.1 and 0.4 M [$^{n}Bu_4N$][PF_6], as the supporting electrolyte. These solutions were purged with dry nitrogen for 10 min directly before use, and were kept under a blanket of nitrogen during all experiments. Square wave and cyclic voltammetry measurements were performed with a Princeton Applied Research PARSTAT 2273 potentiostat. The voltammetry cell design has been described previously (Chapter 1). Initial background scans characterized the size of the accessible electrochemical window and provided an estimate of the likely background current. The CVs were obtained over scan rates of 0.05-20 V s^{-1}. The potentials for **1-5** are reported versus the operative formal potential, $E^{0/}_{Fc^{0/+}}$, for the Fc/Fc^{+} redox couple, which was used as an internal standard. The 3.0 mm BASi glassy carbon (GC) electrode was used as a working electrode and polished with an Al_2O_3 (Buehler, 0.05 μm) slurry on a clean polishing cloth, rinsed with distilled water, and dried with tissue paper prior to use.[1]

Molecular orbital calculations. The molecular orbital calculations were performed for neutral molecules by semi empirical methods (PM3) using HyperChem™ 8.0.6 on

Intel(R) Core(TM)2 Quad CPU Q 6600 @ 2.40 GHz processor and Microsoft Windows XP. For geometry optimization, the Polak-Ribiere algorithm (conjugate gradient) was used with an RMS gradient cut-off of 0.1 kcal/(Å mol). The axial sites on the Pd were blocked by adding fluorine because of MM+'s inability to prevent tetrahedral geometries.

X-ray crystallography. Suitable crystals of **5**, **6a**, **7b**, **8**, **10**, **13**, **16**, **18** and **19** were selected, coated in dry Paratone 8277 oil and mounted on a glass fiber. Diffraction data were collected on a Bruker Apex II diffractometer using monochromated MoK_α radiation (λ = 0.71073 Å) and a KRYO-FLEX liquid nitrogen vapor cooling device at –100°C. The data were corrected for Lorentz and polarization effects, and an empirical absorption correction was applied to the net intensities. The structures were solved by direct methods and refined by least-squares methods on F^2 using the SHELXTL program package.[2] After full-matrix least-squares refinement of the non-hydrogen atoms with anisotropic thermal parameters, hydrogen atoms were placed in calculated positions (C–H = 0.99 Å). The isotropic thermal parameters of the hydrogen atoms were fixed at 1.2 times that of the corresponding carbon. In the final refinements, the hydrogen atoms were riding on the respective carbon atoms.

Reaction of 4,7-dibromobenzothiadiazole (3) with $Pd(PPh_3)_4$: To a toluene solution (40 mL) of 4,7-dibromobenzothiadiazole (**3**, 100 mg, 0.34 mmol) was added $Pd(PPh_3)_4$ (393 mg, 0.34 mmol) and the reaction mixture was heated at 45°C for 12 h. The solvent was removed *in vacuo* and the residue was washed twice with ethanol (10 mL). Recrystallisation from chloroform/ethanol afforded compound *trans*-$[BrPd(PPh_3)_2(C_6H_2BrN_2S)]$ (**6b**) (308 mg, 98%) as pale yellow crystals. **6b:** Anal. Calc. for $C_{43}H_{33}Br_2Cl_3N_2P_2PdS$: C, 49.45; H, 3.18; N, 2.68. Found: C, 49.50; H, 3.44; N,

2.51%. Melting point: 225-226°C. IR: 1567 w, 1479 m, 1431 s, 1178 m, 1095 s, 916 s, 740 s, 689 vs cm^{-1}. ^{1}H NMR ($CDCl_3$): δ 7.60-7.54 (m, 12H), 7.29-7.25 (m, 6H), 7.20-7.15 (m, 12H), 6.95-6.92 (m, 2H). $^{31}P\{^{1}H\}$ NMR ($CDCl_3$): δ 23.01 (s). High resolution MALDI MS: *m*/*z* 844.99709 (calcd. for $C_{42}H_{32}BrN_2P_2PdS^+$ 844.99751). **6a:** IR: 1569 w, 1480 m, 1433 s, 1180 m, 1095 s, 921 s, 742 s, 690 vs cm^{-1}. ^{1}H NMR ($CDCl_3$): δ 7.62-7.56 (m, 12H), 7.32-7.27 (m, 6H), 7.22-7.17 (m, 12H), 6.94-6.90 (m, 2H). $^{31}P\{^{1}H\}$ NMR ($CDCl_3$): δ 23.06 (s). Low resolution MALDI MS: *m*/*z* 845.

Reaction of 4,7-dibromobenzoselenadiazole (5) with $Pd(PPh_3)_4$: A similar reaction as above between 4,7-dibromobenzoselenadiazole (**5**, 100 mg, 0.29 mmol) and $Pd(PPh_3)_4$ (339 mg, 0.29 mmol) in toluene (40 mL) followed by identical purification and crystallization yielded compound *trans*-[$BrPd(PPh_3)_2(C_6H_2BrN_2Se)$] (**7b**) (418 mg, 98%) as pale yellow crystals. **7b**: Anal. Calc. for $C_{42}H_{32}Br_2N_2P_2PdSe$: C, 51.91; H, 3.32; N, 2.88. Found: C, 51.17; H, 3.32; N, 2.63%. Melting point: 242-244°C. IR: 1568 w, 1480 m, 1432 s, 1172 m, 1093 s, 921 s, 748 s, 688 vs cm^{-1}. ^{1}H NMR ($CDCl_3$): δ 7.61-7.55 (m, 12H), 7.30-7.25 (m, 6H), 7.20-7.16 (m, 12H), 6.80-6.75 (m, 2H). $^{31}P\{^{1}H\}$ NMR ($CDCl_3$): δ 22.97 (s). MALDI MS: *m*/*z* 892.94146 (calcd. for $C_{42}H_{32}BrN_2P_2PdSe^+$ 892.94261). **7a:** IR: 1570 w, 1482 m, 1433 s, 1184 m, 1096 s, 921 s, 749 s, 692 vs cm^{-1}. ^{1}H NMR ($CDCl_3$): δ 7.63-7.57 (m, 12H), 7.32-7.26 (m, 6H), 7.22-7.17 (m, 12H), 6.82-6.76 (m, 2H). $^{31}P\{^{1}H\}$ NMR ($CDCl_3$): δ 22.99 (s).

Thermolysis of 7a: An ethanol solution (25 mL) of **7a** (50 mg, 0.051 mmol) and SeO_2 (6 mg, 0.051 mmol, dissolved in a minimum amount of water, 1 mL) was boiled for 30 min, which afforded a yellow precipitate. Recrystallisation from chloroform/ethanol followed by washing the precipitate with ethanol (2 mL) gave *trans*-[{$ClPd(PPh_3)(\mu$-

$C_6H_2BrN_2Se)\}_2$] (**8**) (33 mg, 44%) as pale yellow crystals. Anal. Calc. for $C_{48}H_{34}Br_2Cl_2N_4P_2Pd_2Se_2$: C, 43.33; H, 2.58; N 4.21. Found: C, 42.80; H, 2.84; N, 3.99%. Melting point: 297°C (dec.). IR: 1567 w, 1480 m, 1461 m, 1432 s, 1328 m, 1307 m, 1180 s, 1095 s, 934 s, 816 vs, 688 vs cm^{-1}. ^1H NMR ($CDCl_3$): δ 7.92-7.85 (m, 12H), 7.35-7.30 (m, 6H), 7.23-7.18 (m, 12H), 6.82 (d, J = 7.2 Hz, 2H), 6.74 (dd, J = 7.2, 3.3 Hz, 2H). $^{31}P\{^1H\}$ NMR ($CDCl_3$): δ 28.23 (s). MALDI MS: m/z 1294.67069 (calcd. for $C_{48}H_{34}Br_2ClN_4P_2Pd_2Se_2^+$ 1294.67223).

Reactions of 6b with 4-*tri*-butylstannylpyridine: (i) A toluene solution of **6b** (300 mg, 0.325 mmol) and 4-*tri*-butylstannylpyridine (120 mg, 0.325 mmol) was heated to reflux for 2 d. The resulting mixture was extracted with chloroform followed by quenching with aqueous ammonia. The extract was washed with brine and dried over anhydrous $MgSO_4$. The solvent was removed under reduced pressure and the residue was purified by column chromatography on silica gel with chloroform/ethanol as the eluent to give **9** (20 mg, 21%) as a lemon yellow solid. (ii) A similar reaction of **6b** with two equivalents of 4-*tri*-butylstannylpyridine (240 mg, 0.650 mmol) followed by a similar work up afforded **9** (61 mg, 65%).

Reaction of 7b with 4-*tri*-butylstannylpyridine: (i) A similar reaction as above between **7b** (300 mg, 0.309 mmol) and 4-*tri*-butylstannylpyridine (83 mg, 0.309 mmol) in toluene was refluxed for 2 d, followed by similar purification gave the intermediate **10** (10 mg, 10%) as a yellow solid. (ii) A similar reaction of **7b** with two equivalents of 4-*tri*-butylstannylpyridine (170 mg, 0.634 mmol) in refluxing xylene for 4 h, followed by a similar work up yielded **11** (13 mg, 12%).

4,7-*bis*(4-pyridyl)benzothiadiazole (9; Modified literature preparation**):** To a toluene solution (10 mL) of **3** (600 mg, 2.04 mmol) was added $Pd(PPh_3)_4$ (236 mg, 0.204 mmol) and 4-*tri*-butylstannylpyridine (1938 mg, 5.26 mmol) and the reaction mixture was heated to reflux for 4 days. The resulting mixture was extracted with chloroform followed by quenching with aqueous ammonia. The extract was washed with brine and dried over anhydrous $MgSO_4$. The solvent was removed under reduced pressure and the residue was purified by column chromatography on silica gel with chloroform/ethanol as the eluent to give 4,7-*bis*(4-pyridyl)benzothiadiazole (**9**) (450 mg, 75%) as a lemon yellow solid. Anal. Calc. for $C_{16}H_{10}N_4S$: C, 66.18; H, 3.47; N 19.29. Found: C, 66.14; H, 3.62; N, 19.02%. Melting point: 255-256^oC. IR: 1592 s, 1582 s, 1543 m, 1408 s, 885 m, 814 vs, 711 s, 546 s, 518 s cm^{-1}. ^1H NMR ($CDCl_3$): δ 8.82 (d, J = 6.0 Hz, 4H), 7.95 (s, 2H), 7.94 (d, J = 6.0 Hz, 4H). ^{13}C NMR ($CDCl_3$): δ 153.7, 150.6, 144.4, 132.2, 128.7, 123.8. MS: m/z 290 $[M]^+$. The m.p. agrees with the literature report, but the NMR in the original report appears to be wrong.[3]

4,7-*bis*(2-pyridyl)benzothiadiazole (12; Modified literature preparation**):** A similar reaction of **3** (300 mg, 1.02 mmol), $Pd(PPh_3)_4$ (120 mg, 0.103 mmol) and 2-*tri*-butylstannylpyridine (938 mg, 2.55 mmol) as above followed by a similar work up afforded 4,7-*bis*(2-pyridyl)benzothiadiazole (**12**) (126 mg, 42%). Melting point: 144-146^oC. ^1H NMR ($CDCl_3$): δ 8.83 (d, J = 4.2 Hz, 2H), 8.70 (d, J = 7.8 Hz, 2H), 8.61 (s, 2H), 7.91 (t, J = 7.8 Hz, 2H), 7.39-7.32 (m, 2H), in agreement with the literature report.[3]

4-bromo-7-(4-pyridyl)benzoselenadiazole (10): A similar reaction as above between **5** (100 mg, 0.293 mmol) and 4-*tri*-butylstannylpyridine (140 mg, 0.38 mmol) in toluene, followed by similar purification and crystallization from chloroform/ethanol yielded **10**

(28 mg, 27%) as pale yellow needles. Anal. Calc. for $C_{11}H_6BrN_3Se$: C, 38.97; H, 1.78; N, 12.39. Found: C, 39.07; H, 1.70; N, 12.18%. Melting point: 211-213^oC. IR: 1521 w, 1472 w, 1455 w, 1142 m, 1103 s, 852 s, 634 m, 547 vs cm^{-1}. ^1H NMR ($CDCl_3$): δ 8.77 (d, J = 6.4 Hz, 2H), 7.90 (d, J = 7.2 Hz, 1H), 7.78 (d, J = 6.4 Hz, 2H), 7.53 (d, J = 7.2 Hz, 1H). ^{13}C NMR ($CDCl_3$): δ 158.5, 157.6, 150.1, 144.5, 132.7, 132.0, 129.2, 123.9, 117.8. MS: m/z 258 $[M\text{-}Se]^+$.

4,7-*bis*(4-pyridyl)benzoselenadiazole (11): To a xylene solution (30 mL) of **5** (300 mg, 0.880 mmol) was added $Pd(PPh_3)_4$ (234 mg, 0.202 mmol) and 4-*tri*-butylstannylpyridine (760 mg, 2.06 mmol) and the reaction mixture was heated to reflux for 3 h. The resulting mixture was extracted with chloroform (80 mL) followed by quenching with aqueous ammonia. The extract was washed with brine and dried over anhydrous $MgSO_4$. The solvent was removed under reduced pressure and the residue was purified by column chromatography on silica gel with chloroform/ethanol as the eluent to give 4,7-*bis*(4-pyridyl)benzoselenadiazole (**11**) (112 mg, 38%) as a yellow solid. Anal. Calc. for $C_{16}H_{10}N_4Se$: C, 56.98; H, 2.98; N, 16.61. Found: C, 56.68; H, 2.92; N, 16.53%. Melting point: 277-280^oC. IR: 1585 s, 1538 m, 1414 s, 1366 m, 1291 m, 1216 m, 1069 m, 997 m, 818 vs cm^{-1}. ^1H NMR ($CDCl_3$): δ 8.80 (d, J = 5.1 Hz, 4H), 7.86 (d, J = 5.1 Hz, 4H), 7.78 (s, 2H). ^{13}C NMR ($CDCl_3$): δ 158.8, 150.1, 144.9, 133.7, 128.9, 124.0. MS: m/z 258 $[M\text{-}Se]^+$.

4,7-*bis*(2-pyridyl)benzoselenadiazole (13): A similar reaction of **5** (100 mg, 0.293 mmol), $Pd(PPh_3)_4$ (78 mg, 0.067 mmol) and 2-*tri*-butylstannylpyridine (243 mg, 0.660 mmol) as above followed by similar work up afforded 4,7-*bis*(2-pyridyl)benzoselenadiazolediazole (**13**) (50 mg, 50%) as a yellow solid. Anal. Calc. for $C_{16}H_{10}N_4Se$: C,

56.92; H, 3.01; N, 16.67. Found: C, 57.04; H, 2.79; N, 16.50%. Melting point: 158-160°C. IR: 1581 s, 1566 m, 1530 m, 1460 s, 1431 s, 1051 m, 993 m, 934 m, 857 m, 769 vs, 736 vs cm^{-1}. ^1H NMR ($CDCl_3$): δ 8.82 (d, J = 4.8 Hz, 2H), 8.53 (d, J = 7.8 Hz, 2H), 8.39 (s, 2H), 7.89 (dt, J = 7.8, 1.5 Hz, 2H), 7.38-7.33 (m, 2H). ^{13}C NMR ($CDCl_3$): δ 159.4, 154.8, 149.8, 136.7, 134.1, 130.2, 125.6, 123.0. MS: m/z 258 $[M\text{-}Se]^+$.

1,5-*bis*(4-pyridyl)naphthalene (16): 1,5-diaminonaphthalene (**14**, 2 g, 0.0126 mol) was diazotized with $H_2SO_4/NaNO_2$ and slowly added to a solution of CuBr (5 g, 0.0349 mol) in 48% HBr (75 mL) and H_2O (75 mL). 1,5-dibromonaphthalene (**15**) was extracted with $CHCl_3$ and the solution was dried over anhydrous $MgSO_4$. The solvent was removed under vacuum and the resulting off-white solid was crystallized from chloroform (yield: 0.5 g, 14%).[4] A mixture of **15** (0.37 g, 1.3 mmol), $Pd(PPh_3)_4$ (0.15 g, 0.13 mmol), K_2CO_3 (1.073 g, 7.8 mmol) and 4-pyridineboronic acid (0.48 g, 3.9 mmol) in 1,4-dioxane (40 mL) was refluxed under N_2 for 3 days. After removal of 1,4-dioxane, the resulting mass was worked up with chloroform/water and recrystallization from chloroform/methanol afforded 1,5-*bis*(4-pyridyl)naphthalene (**16**) (yield: 0.160 g, 44%). Anal. Calc. for $C_{20}H_{14}N_2$: C, 85.08; H, 4.99; N, 9.92. Found: C, 84.71; H, 4.76; N, 9.90%. Melting point: 110-112°C. IR: 1589 s, 1542 m, 1585 m, 1437 s, 1409 s, 1312 m, 1261 s, 1183 vs, 1119 vs, 1070 vs, 992 s 799 vs cm^{-1}. ^1H NMR ($CDCl_3$): δ 8.77 (d, J = 6.0 Hz, 4H), 7.91 (d, J = 8.7 Hz, 2H), 7.54 (t, J = 7.2 Hz, 2H), 7.46 (d, J = 6.3 Hz, 6H). ^{13}C NMR ($CDCl_3$): δ 149.9, 148.6, 138.0, 131.1, 127.2, 126.1, 126.0, 125.0. MS: m/z 282 $[M]^+$.

Synthesis of [{ReBr(CO)$_4$}$_2$(μ-4,7-*bis*(4-pyridyl)benzothiadiazole)] (19): To a solution of $ReBr(CO)_5$ (**17**, 406 mg, 1.00 mmol) in CH_2Cl_2 (100 mL) and acetonitrile (1 mL) at 0°C was added a solution of Me_3NO (75 mg, 1.00 mmol) in CH_2Cl_2 (50 mL). The

mixture was stirred at 0°C for 1 h and filtered through a short column of silica gel. The solvent was removed under vacuum and the residue, [ReBr(CO)$_4$(NCMe)] (**18**), was redissolved in toluene (100 mL). To the resultant solution at 15°C was added dropwise a solution of **9** (146 mg, 0.5 mmol) in toluene (50 mL) and CH_2Cl_2 (20 mL). Stirring was continued for 30 mins at 15°C and another 30 mins at ambient temperature, and the completion of the reaction was checked by TLC and IR spectroscopy. The solvent was removed under vacuum and the residue was chromatographed on a silica gel column by use of CH_2Cl_2 with a few drops (5-10) of ethyl acetate as eluent to afford the pale yellow shiny compound [{ReBr(CO)$_4$}$_2$(μ-4,7-*bis*(4-pyridyl)benzothiadiazole)] (**19**) (150 mg, 27%).[5] Anal. Calc. for $C_{24}H_{10}N_4SO_8Re_2Br_2$: C, 27.54; H, 0.96; N, 5.35. Found: C, 27.54; H, 1.07; N, 5.22%. Melting point: 280°C (decomposed). IR: 2113 m, 2012 vs, 1999 vs, 1938 vs cm^{-1}. ^{1}H NMR ($CDCl_3$): δ 9.26 (d, J = 5.7 Hz, 4H), 8.14 (d, J = 5.7 Hz, 4H), 8.07 (s, 2H). ^{13}C NMR ($CDCl_3$): δ {186.0, 184.2 (CO)}, 156.0, 153.0, 146.5, 130.8, 129.1, 126.0.

Synthesis of [{ReBr(CO)$_4$}$_2$(μ-4,7-*bis*(4-pyridyl)benzoselenadiazole)] (20): A similar reaction as above between **18**, obtained from **17** (203 mg, 0.50 mmol), and **11** (85 mg, 0.25 mmol) in a mixture of toluene (80 mL) and CH_2Cl_2 (20 mL) followed by similar purification and crystallization yielded compound [{ReBr(CO)$_4$}$_2$(μ-4,7-*bis*(4-pyridyl)-benzoselenadiazole)] (**20**) (53 mg, 18%) as pale yellow crystals. Anal. Calc. for $C_{24}H_{10}N_4SeO_8Re_2Br_2$: C, 26.36; H, 0.92; N, 5.12. Found: C, 26.70; H, 1.04; N, 5.12%. Melting point: 267°C (decomposed). IR: 2113 w, 2016 vs, 2000 vs, 1944 vs cm^{-1}. ^{1}H NMR (CD_2Cl_2): δ 9.20 (d, J = 6.6 Hz, 4H), 8.07 (d, J = 6.6 Hz, 4H), 7.92 (s, 2H). ^{13}C NMR (CD_2Cl_2): δ {186.2, 185.0 (CO)}, 158.1, 155.7, 147.5, 132.3, 129.5, 126.4.

Synthesis of [(enPd)(μ-4,7-*bis*(4-pyridyl)benzothiadiazole)]$_4$[PF$_6$]$_8$ (23): To a MeCN/d.H_2O (0.7/0.3 mL, v/v) solution of enPd$(NO_3)_2$ (**21**) (17.4 mg, 0.06 mmol) was added KPF_6 (22.0 mg, 0.12 mmol) and the solution was heated at 50^{o}C for 30 mins to give enPd$(PF_6)_2$ (**22**). Then **9** (17.5 mg, 0.06 mmol) was added to the resulting solution of **22** formed *in situ* and continued heating at 50^{o}C for another 45 mins. Any insoluble materials were filtered off and the solvents were removed under vacuum giving a pale yellow powder. The pale yellow powder was washed twice with distilled water (20 mL) and CH_2Cl_2 (5 mL). The powder was then dried for 12 h under vacuum to remove water and re-dissolved in acetonitrile. The removal of solvent under vacuum afforded [(enPd)(μ-4,7-*bis*(4-pyridyl)benzothiadiazole)]$_4$[PF$_6$]$_8$ (**23**) (30 mg, 88%). Anal. Calc. for $C_{72}H_{72}F_{48}N_{24}P_8Pd_4S_4$: C, 28.95; H, 2.43; N, 11.25. Found: C, 29.10; H, 2.57; N, 11.23%. Melting point: 245^{o}C (dec). IR: 1614 m, 1436 m, 1141 w, 1058 w, 818 vs, 736 s, 554 vs, 523 s cm^{-1}. ^{1}H NMR ($CDCl_3$): δ 8.90 (d, J = 5.7 Hz, 16H), 8.27 (d, J = 5.7 Hz, 16H), 8.11 (s, 8H), 4.33 (s, 16H, NH_2), 2.90 (s, 16H, CH_2). ^{13}C NMR ($CDCl_3$): δ 154.3, 153.1, 149.1, 131.4, 131.2, 128.0, 48.1 (en).

Synthesis of [(enPd)(μ-4,7-*bis*(4-pyridyl)benzoselenadiazole)]$_4$[PF$_6$]$_8$ (24): A similar reaction as above between **22** obtained **21** (17.4 mg, 0.06 mmol) and **11** (20.4 mg, 0.06 mmol) in a mixture of acetonitrile (0.7 mL) and H_2O (0.3 mL) followed by similar purification and crystallization yielded assembly [(enPd)(μ-4,7-*bis*(4-pyridyl)benzo-selenadiazole)]$_4$[PF$_6$]$_8$ (**24**) (31 mg, 82%) as a yellow solid. Anal. Calc. for $C_{72}H_{72}F_{48}N_{24}P_8Pd_4Se_4$: C, 27.24; H, 2.28; N, 10.59. Found: C, 27.46; H, 2.37; N, 10.52%. Melting point: 252^{o}C (dec). IR: 1613 m, 1435 m, 1138 w, 1058 w, 817 vs, 739 s, 553 vs cm^{-1}. ^{1}H NMR (CD_2Cl_2): δ 8.95 (d, J = 6.6 Hz, 16H), 8.27 (d, J = 6.6 Hz, 16H), 8.01 (s,

8H), 4.38 (s, 16H, NH_2), 2.97 (s, 16H, CH_2). ^{13}C NMR (CD_2Cl_2): δ 159.3, 152.9, 149.9, 133.1, 131.3, 128.1, 48.1 (en).

References

1. Taken with gratitude from "Roemmele, T. L.; Konu, J.; Boeré, R. T.; Chivers, T. *Inorg. Chem.* **2009**, *48*, 9454."

2. (a) G.M. Sheldrick, SHELXS-97, Program for Crystal Structure Determination; University of Göttingen: Göttingen, Germany, 1997. (b) G.M. Sheldrick, SHELXL-97, Program for Crystal Structure Refinement; University of Göttingen: Göttingen, Germany, 1997.

3. Akhtaruzzaman, M.; Tomura, M.; Nishida, J. –I.; Yamashita, Y. *J. Org. Chem.* **2004**, *69*, 2953.

4. (a) Hodgson, H. H.; Whitehurst, J. S. *J. Chem. Soc*. **1947**, 80. (b) Masuda, J. D. MSc. Thesis **2002**, *Chapter 4*, p-65.

5. Rajendran, T.; Manimaran, B.; Lee, F. -Y.; Lee, G.-H.; Peng, S. -M.; Wang, C. M.; Lu, K. -L. *Inorg. Chem.* **2000**, *39,* 2016.

Self-assembled molecular rods and squares with chalcogenadiazole framework ligands

MOHAMMAD ROKIB HASSAN
M.Sc., Jahangirnagar University, Bangladesh, 2003

A Thesis
Submitted to the School of Graduate Studies
Of the University of Lethbridge
In Partial Fulfillment of the
Requirements for the Degree

MASTER OF SCIENCE

Appendices

Appendix one: Full crystallographic data of **5**

Table 1 Crystal data and structure refinement for **5**

Identification code	rb08043	
Empirical formula	$C_6H_2Br_2N_2Se$	
Formula weight	340.88	
Temperature	173(2) K	
Wavelength	0.71073 Å	
Crystal system	Monoclinic	
Space group	P2(1)/n	
Unit cell dimensions	a = 3.9378(2) Å	α = 90°.
	b = 18.3462(11) Å	β = 95.0080(10)°.
	c = 11.1358(7) Å	γ = 90°.
Volume	801.42(8) $Å^3$	
Z	4	
Density (calculated)	2.825 Mg/m^3	
Absorption coefficient	14.584 mm^{-1}	
F(000)	624	
Crystal size	0.34 x 0.14 x 0.08 mm	
Theta range for data collection	2.15 to 26.37°.	
Index ranges	-4<=h<=4, -22<=k<=22, -13<=l<=13	
Reflections collected	10350	
Independent reflections	1617 [R(int) = 0.0287]	
Completeness to theta = 25.00°	100.0 %	
Absorption correction	Semi-empirical from equivalents	
Max. and min. transmission	0.3810 and 0.0823	
Refinement method	Full-matrix least-squares on F^2	
Data / restraints / parameters	1617 / 0 / 101	
Goodness-of-fit on F^2	1.052	
Final R indices [I>2sigma(I)]	R1 = 0.0153, wR2 = 0.0367	
R indices (all data)	R1 = 0.0172, wR2 = 0.0373	
Extinction coefficient	0.0012(3)	
Largest diff. peak and hole	0.383 and -0.457 $e.Å^{-3}$	

Table 2 Atomic coordinates (x 10^4) and equivalent isotropic displacement parameters ($Å^2$ x 10^3) for **5**. U(eq) is defined as one third of the trace of the orthogonalized U^{ij} tensor

	x	y	z	U(eq)
Br(1)	12092(1)	2005(1)	8403(1)	28(1)
Br(2)	7147(1)	5315(1)	6656(1)	24(1)
Se(1)	6669(1)	4028(1)	10503(1)	21(1)
N(1)	8582(5)	3245(1)	9870(2)	23(1)
N(2)	6624(5)	4556(1)	9143(2)	19(1)
C(1)	9089(5)	3413(1)	8738(2)	19(1)
C(2)	8014(5)	4138(1)	8338(2)	18(1)
C(3)	8521(6)	4361(1)	7134(2)	19(1)
C(4)	9958(6)	3896(1)	6373(2)	24(1)
C(6)	10599(6)	2947(1)	7897(2)	21(1)
C(5)	11008(6)	3180(1)	6759(2)	24(1)

Table 3 Bond lengths [Å] and angles [°] for **5**

Br(1)-C(6)	1.894(2)	N(1)-C(1)-C(6)	125.9(2)
Br(2)-C(3)	1.894(2)	N(1)-C(1)-C(2)	115.96(19)
Se(1)-N(1)	1.7950(19)	C(6)-C(1)-C(2)	118.16(19)
Se(1)-N(2)	1.7962(18)	N(2)-C(2)-C(3)	124.4(2)
N(1)-C(1)	1.329(3)	N(2)-C(2)-C(1)	116.46(19)
N(2)-C(2)	1.332(3)	C(3)-C(2)-C(1)	119.11(19)
C(1)-C(6)	1.435(3)	C(4)-C(3)-C(2)	120.3(2)
C(1)-C(2)	1.455(3)	C(4)-C(3)-Br(2)	121.86(17)
C(2)-C(3)	1.432(3)	C(2)-C(3)-Br(2)	117.80(16)
C(3)-C(4)	1.360(3)	C(3)-C(4)-C(5)	120.8(2)
C(4)-C(5)	1.432(3)	C(3)-C(4)-H(4)	119.6
C(4)-H(4)	0.9500	C(5)-C(4)-H(4)	119.6
C(6)-C(5)	1.361(3)	C(5)-C(6)-C(1)	120.6(2)
C(5)-H(5)	0.9500	C(5)-C(6)-Br(1)	120.32(17)
		C(1)-C(6)-Br(1)	119.04(16)
N(1)-Se(1)-N(2)	94.20(9)	C(6)-C(5)-C(4)	120.9(2)
C(1)-N(1)-Se(1)	106.90(14)	C(6)-C(5)-H(5)	119.5
C(2)-N(2)-Se(1)	106.46(14)	C(4)-C(5)-H(5)	119.5

Symmetry transformations used to generate equivalent atoms:

Table 4 Anisotropic displacement parameters ($Å^2$ x 10^3) for **5**. The anisotropic displacement factor exponent takes the form: $-2\pi^2 [h^2 a^{*2} U^{11} + ... + 2 h k a^* b^* U^{12}]$

	U^{11}	U^{22}	U^{33}	U^{23}	U^{13}	U^{12}
Br(1)	31(1)	16(1)	38(1)	-1(1)	1(1)	3(1)
Br(2)	30(1)	19(1)	22(1)	5(1)	6(1)	2(1)
Se(1)	27(1)	20(1)	16(1)	0(1)	5(1)	-2(1)
N(1)	27(1)	20(1)	21(1)	0(1)	3(1)	-2(1)
N(2)	23(1)	17(1)	17(1)	0(1)	5(1)	-2(1)
C(1)	19(1)	16(1)	21(1)	0(1)	1(1)	-4(1)
C(2)	18(1)	17(1)	18(1)	-3(1)	2(1)	-3(1)
C(3)	22(1)	16(1)	20(1)	1(1)	4(1)	-2(1)
C(4)	31(1)	22(1)	20(1)	-2(1)	6(1)	-2(1)
C(6)	21(1)	13(1)	27(1)	-2(1)	1(1)	-1(1)
C(5)	28(1)	20(1)	25(1)	-6(1)	6(1)	2(1)

Table 5 Hydrogen coordinates ($x\ 10^4$) and isotropic displacement parameters ($Å^2\ x\ 10^3$) for **5**

	x	y	z	U(eq)
H(4)	10271	4049	5575	29
H(5)	12003	2863	6213	29

Table 6 Torsion angles [°] for **5**

N(2)-Se(1)-N(1)-C(1)	0.51(16)
N(1)-Se(1)-N(2)-C(2)	-0.70(16)
Se(1)-N(1)-C(1)-C(6)	179.37(18)
Se(1)-N(1)-C(1)-C(2)	-0.2(2)
Se(1)-N(2)-C(2)-C(3)	-178.80(18)
Se(1)-N(2)-C(2)-C(1)	0.7(2)
N(1)-C(1)-C(2)-N(2)	-0.4(3)
C(6)-C(1)-C(2)-N(2)	-180.0(2)
N(1)-C(1)-C(2)-C(3)	179.2(2)
C(6)-C(1)-C(2)-C(3)	-0.4(3)
N(2)-C(2)-C(3)-C(4)	-179.9(2)
C(1)-C(2)-C(3)-C(4)	0.6(3)
N(2)-C(2)-C(3)-Br(2)	0.4(3)
C(1)-C(2)-C(3)-Br(2)	-179.11(15)
C(2)-C(3)-C(4)-C(5)	-0.3(3)
Br(2)-C(3)-C(4)-C(5)	179.38(17)
N(1)-C(1)-C(6)-C(5)	-179.6(2)
C(2)-C(1)-C(6)-C(5)	0.0(3)
N(1)-C(1)-C(6)-Br(1)	-0.6(3)
C(2)-C(1)-C(6)-Br(1)	178.94(15)
C(1)-C(6)-C(5)-C(4)	0.3(3)
Br(1)-C(6)-C(5)-C(4)	-178.64(17)
C(3)-C(4)-C(5)-C(6)	-0.1(4)

Symmetry transformations used to generate equivalent atoms:

Appendix two: Full crystallographic data of **6a**

Table 1 Crystal data and structure refinement for **6a**

Identification code	rb08046	
Empirical formula	$C_{46}H_{40}BrCl_7N_2OP_2PdS$	
Formula weight	1165.32	
Temperature	173(2) K	
Wavelength	0.71073 Å	
Crystal system	Orthorhombic	
Space group	Pnma	
Unit cell dimensions	a = 22.374 Å	α = 90°.
	b = 22.374(8) Å	β = 90°.
	c = 9.580(4) Å	γ = 90°.
Volume	4796(2) $Å^3$	
Z	4	
Density (calculated)	1.614 Mg/m^3	
Absorption coefficient	1.758 mm^{-1}	
F(000)	2336	
Crystal size	0.28 x 0.16 x 0.14 mm^3	
Theta range for data collection	1.82 to 27.62°.	
Index ranges	-29<=h<=29, -28<=k<=28, -12<=l<=12	
Reflections collected	66472	
Independent reflections	5681 [R(int) = 0.0508]	
Completeness to theta = 25.25°	100.0 %	
Absorption correction	Semi-empirical from equivalents	
Max. and min. transmission	0.7846 and 0.6434	
Refinement method	Full-matrix least-squares on F^2	
Data / restraints / parameters	5681 / 0 / 296	
Goodness-of-fit on F^2	1.066	
Final R indices [I>2sigma(I)]	R1 = 0.0397, wR2 = 0.1160	
R indices (all data)	R1 = 0.0485, wR2 = 0.1200	
Largest diff. peak and hole	4.009 and -1.169 e.$Å^{-3}$	

Table 2 Atomic coordinates (x 10^4) and equivalent isotropic displacement parameters ($Å^2$ x 10^3) for **6a**. U(eq) is defined as one third of the trace of the orthogonalized U^{ij} tensor

	x	y	z	U(eq)
Pd(1)	-142(1)	2500	4078(1)	21(1)
Br(1)	2519(1)	2500	681(1)	43(1)
Cl(1)	-1059(1)	2500	5368(1)	34(1)
S(1)	1938(1)	2500	5454(2)	48(1)
P(1)	-105(1)	1469(1)	4198(1)	22(1)
N(2)	1225(2)	2500	5116(5)	36(1)
N(1)	2212(2)	2500	3891(5)	45(1)
C(1)	1744(2)	2500	3031(5)	32(1)
C(2)	1171(2)	2500	3728(5)	28(1)
C(3)	623(2)	2500	2987(5)	28(1)
C(4)	668(2)	2500	1555(5)	31(1)
C(5)	1234(2)	2500	848(5)	34(1)
C(6)	1753(2)	2500	1559(5)	33(1)
C(7)	-181(1)	1244(1)	6010(3)	27(1)
C(8)	165(2)	1545(2)	6999(3)	34(1)
C(9)	139(2)	1384(2)	8402(4)	43(1)
C(10)	-240(2)	926(2)	8810(4)	44(1)
C(11)	-588(2)	634(2)	7850(4)	41(1)
C(12)	-559(2)	789(2)	6440(4)	32(1)
C(13)	586(1)	1111(1)	3621(3)	25(1)
C(14)	1006(2)	882(2)	4534(4)	36(1)
C(15)	1548(2)	660(2)	4027(5)	50(1)
C(16)	1670(2)	665(2)	2628(5)	48(1)
C(17)	1253(2)	887(2)	1706(4)	41(1)
C(18)	711(2)	1107(1)	2193(4)	32(1)
C(19)	-683(1)	1080(1)	3223(3)	26(1)
C(20)	-620(2)	475(2)	2905(4)	36(1)
C(21)	-1069(2)	183(2)	2170(4)	43(1)
C(22)	-1576(2)	483(2)	1752(4)	43(1)
C(23)	-1642(2)	1080(2)	2049(4)	41(1)

C(24)	-1197(1)	1381(2)	2783(3)	32(1)
Cl(1S)	1767(1)	1358(1)	7995(1)	55(1)
Cl(2S)	2760(1)	869(1)	9540(1)	63(1)
Cl(3S)	2807(1)	907(1)	6552(1)	86(1)
C(1S)	2552(2)	1274(2)	8048(4)	47(1)
O(1S)	3206(2)	2384(4)	6906(5)	60(2)
C(2S)	3555(4)	2207(5)	5703(10)	60(2)
C(3S)	4030(4)	2659(4)	5338(9)	60(2)

Table 3 Bond lengths [Å] and angles [°] for **6a**

Pd(1)-C(3)	2.006(4)	C(14)-C(15)	1.398(5)
Pd(1)-P(1)#1	2.3109(11)	C(14)-H(14)	0.9500
Pd(1)-P(1)	2.3109(11)	C(15)-C(16)	1.367(6)
Pd(1)-Cl(1)	2.3945(11)	C(15)-H(15)	0.9500
Br(1)-C(6)	1.907(5)	C(16)-C(17)	1.376(6)
S(1)-N(1)	1.618(5)	C(16)-H(16)	0.9500
S(1)-N(2)	1.628(4)	C(17)-C(18)	1.390(5)
P(1)-C(7)	1.815(3)	C(17)-H(17)	0.9500
P(1)-C(19)	1.817(3)	C(18)-H(18)	0.9500
P(1)-C(13)	1.827(3)	C(19)-C(20)	1.394(5)
N(2)-C(2)	1.335(6)	C(19)-C(24)	1.399(4)
N(1)-C(1)	1.331(7)	C(20)-C(21)	1.390(5)
C(1)-C(6)	1.411(7)	C(20)-H(2)	0.9500
C(1)-C(2)	1.446(6)	C(21)-C(22)	1.377(6)
C(2)-C(3)	1.417(6)	C(21)-H(3)	0.9500
C(3)-C(4)	1.376(7)	C(22)-C(23)	1.374(6)
C(4)-C(5)	1.437(7)	C(22)-H(4)	0.9500
C(4)-H(20)	0.9500	C(23)-C(24)	1.392(5)
C(5)-C(6)	1.346(7)	C(23)-H(5)	0.9500
C(5)-H(19)	0.9500	C(24)-H(6)	0.9500
C(7)-C(12)	1.387(4)	Cl(1S)-C(1S)	1.768(4)
C(7)-C(8)	1.396(5)	Cl(2S)-C(1S)	1.756(4)
C(8)-C(9)	1.393(5)	Cl(3S)-C(1S)	1.747(4)
C(8)-H(8)	0.9500	C(1S)-H(1S)	1.0000
C(9)-C(10)	1.387(6)	O(1S)-C(2S)	1.447(11)
C(9)-H(9)	0.9500	O(1S)-H(1S1)	0.8400
C(10)-C(11)	1.370(6)	C(2S)-C(3S)	1.508(13)
C(10)-H(10)	0.9500	C(2S)-H(2S1)	0.9900
C(11)-C(12)	1.396(5)	C(2S)-H(2S2)	0.9900
C(11)-H(11)	0.9500	C(3S)-H(3S1)	0.9800
C(12)-H(12)	0.9500	C(3S)-H(3S2)	0.9800
C(13)-C(14)	1.382(5)	C(3S)-H(3S3)	0.9800
C(13)-C(18)	1.396(5)		

C(3)-Pd(1)-P(1)#1	89.74(2)	C(8)-C(7)-P(1)	117.6(2)
C(3)-Pd(1)-P(1)	89.74(2)	C(9)-C(8)-C(7)	120.5(3)
P(1)#1-Pd(1)-P(1)	172.96(4)	C(9)-C(8)-H(8)	119.8
C(3)-Pd(1)-Cl(1)	179.69(14)	C(7)-C(8)-H(8)	119.8
P(1)#1-Pd(1)-Cl(1)	90.28(2)	C(10)-C(9)-C(8)	119.2(3)
P(1)-Pd(1)-Cl(1)	90.28(2)	C(10)-C(9)-H(9)	120.4
N(1)-S(1)-N(2)	100.8(2)	C(8)-C(9)-H(9)	120.4
C(7)-P(1)-C(19)	107.00(14)	C(11)-C(10)-C(9)	120.8(3)
C(7)-P(1)-C(13)	104.24(14)	C(11)-C(10)-H(10)	119.6
C(19)-P(1)-C(13)	103.67(14)	C(9)-C(10)-H(10)	119.6
C(7)-P(1)-Pd(1)	108.75(11)	C(10)-C(11)-C(12)	120.3(3)
C(19)-P(1)-Pd(1)	115.32(11)	C(10)-C(11)-H(11)	119.9
C(13)-P(1)-Pd(1)	116.92(10)	C(12)-C(11)-H(11)	119.9
C(2)-N(2)-S(1)	106.7(3)	C(7)-C(12)-C(11)	119.9(3)
C(1)-N(1)-S(1)	106.0(4)	C(7)-C(12)-H(12)	120.1
N(1)-C(1)-C(6)	127.4(5)	C(11)-C(12)-H(12)	120.1
N(1)-C(1)-C(2)	114.3(5)	C(14)-C(13)-C(18)	118.8(3)
C(6)-C(1)-C(2)	118.3(4)	C(14)-C(13)-P(1)	123.2(3)
N(2)-C(2)-C(3)	125.3(4)	C(18)-C(13)-P(1)	117.9(2)
N(2)-C(2)-C(1)	112.3(4)	C(13)-C(14)-C(15)	120.1(3)
C(3)-C(2)-C(1)	122.4(4)	C(13)-C(14)-H(14)	119.9
C(4)-C(3)-C(2)	115.9(4)	C(15)-C(14)-H(14)	119.9
C(4)-C(3)-Pd(1)	125.6(4)	C(16)-C(15)-C(14)	120.6(4)
C(2)-C(3)-Pd(1)	118.5(3)	C(16)-C(15)-H(15)	119.7
C(3)-C(4)-C(5)	122.3(5)	C(14)-C(15)-H(15)	119.7
C(3)-C(4)-H(20)	118.8	C(15)-C(16)-C(17)	119.9(4)
C(5)-C(4)-H(20)	118.8	C(15)-C(16)-H(16)	120.1
C(6)-C(5)-C(4)	121.5(5)	C(17)-C(16)-H(16)	120.1
C(6)-C(5)-H(19)	119.3	C(16)-C(17)-C(18)	120.2(4)
C(4)-C(5)-H(19)	119.3	C(16)-C(17)-H(17)	119.9
C(5)-C(6)-C(1)	119.6(4)	C(18)-C(17)-H(17)	119.9
C(5)-C(6)-Br(1)	123.4(4)	C(17)-C(18)-C(13)	120.4(3)
C(1)-C(6)-Br(1)	117.0(4)	C(17)-C(18)-H(18)	119.8
C(12)-C(7)-C(8)	119.4(3)	C(13)-C(18)-H(18)	119.8
C(12)-C(7)-P(1)	123.0(2)	C(20)-C(19)-C(24)	119.0(3)

C(20)-C(19)-P(1)	120.4(2)	Cl(3S)-C(1S)-Cl(1S)	110.5(2)
C(24)-C(19)-P(1)	120.6(2)	Cl(2S)-C(1S)-Cl(1S)	110.0(2)
C(21)-C(20)-C(19)	119.6(3)	Cl(3S)-C(1S)-H(1S)	108.8
C(21)-C(20)-H(2)	120.2	Cl(2S)-C(1S)-H(1S)	108.8
C(19)-C(20)-H(2)	120.2	Cl(1S)-C(1S)-H(1S)	108.8
C(22)-C(21)-C(20)	120.8(4)	O(1S)-C(2S)-C(3S)	112.4(8)
C(22)-C(21)-H(3)	119.6	O(1S)-C(2S)-H(2S1)	109.1
C(20)-C(21)-H(3)	119.6	C(3S)-C(2S)-H(2S1)	109.1
C(23)-C(22)-C(21)	120.2(3)	O(1S)-C(2S)-H(2S2)	109.1
C(23)-C(22)-H(4)	119.9	C(3S)-C(2S)-H(2S2)	109.1
C(21)-C(22)-H(4)	119.9	H(2S1)-C(2S)-H(2S2)	107.9
C(22)-C(23)-C(24)	119.8(3)	C(2S)-C(3S)-H(3S1)	109.5
C(22)-C(23)-H(5)	120.1	C(2S)-C(3S)-H(3S2)	109.5
C(24)-C(23)-H(5)	120.1	H(3S1)-C(3S)-H(3S2)	109.5
C(23)-C(24)-C(19)	120.5(3)	C(2S)-C(3S)-H(3S3)	109.5
C(23)-C(24)-H(6)	119.8	H(3S1)-C(3S)-H(3S3)	109.5
C(19)-C(24)-H(6)	119.8	H(3S2)-C(3S)-H(3S3)	109.5
Cl(3S)-C(1S)-Cl(2S)	109.8(2)		

Symmetry transformations used to generate equivalent atoms: #1 x,-y+1/2,z

Table 4 Anisotropic displacement parameters ($Å^2$ x 10^3) for **6a**. The anisotropic displacement factor exponent takes the form: $-2\pi^2 [h^2 a^{*2} U^{11} + ... + 2 h k a^* b^* U^{12}]$

	U^{11}	U^{22}	U^{33}	U^{23}	U^{13}	U^{12}
Pd(1)	17(1)	22(1)	24(1)	0	-1(1)	0
Br(1)	31(1)	47(1)	52(1)	0	14(1)	0
Cl(1)	22(1)	47(1)	34(1)	0	4(1)	0
S(1)	28(1)	72(1)	43(1)	0	-7(1)	0
P(1)	21(1)	22(1)	23(1)	1(1)	-2(1)	-2(1)
N(2)	25(2)	42(2)	42(2)	0	-3(2)	0
N(1)	29(2)	55(3)	52(3)	0	-2(2)	0
C(1)	25(2)	28(2)	45(3)	0	-1(2)	0
C(2)	26(2)	25(2)	34(2)	0	4(2)	0
C(3)	24(2)	19(2)	40(2)	0	2(2)	0
C(4)	31(2)	27(2)	36(2)	0	7(2)	0
C(5)	37(3)	30(2)	36(3)	0	8(2)	0
C(6)	33(2)	27(2)	37(3)	0	10(2)	0
C(7)	28(2)	26(2)	26(1)	2(1)	0(1)	1(1)
C(8)	38(2)	36(2)	28(2)	1(1)	-2(1)	-7(1)
C(9)	50(2)	49(2)	29(2)	1(2)	-5(2)	-5(2)
C(10)	55(2)	52(2)	26(2)	8(2)	3(2)	3(2)
C(11)	42(2)	39(2)	41(2)	12(2)	8(2)	-5(2)
C(12)	31(2)	31(2)	33(2)	3(1)	-1(1)	-4(1)
C(13)	24(1)	20(1)	31(2)	-1(1)	-1(1)	-1(1)
C(14)	34(2)	40(2)	35(2)	-1(2)	-4(1)	6(2)
C(15)	33(2)	57(2)	59(3)	-3(2)	-11(2)	15(2)
C(16)	30(2)	46(2)	68(3)	-12(2)	7(2)	4(2)
C(17)	44(2)	36(2)	42(2)	-3(2)	14(2)	-1(2)
C(18)	32(2)	28(2)	34(2)	1(1)	4(1)	1(1)
C(19)	25(1)	29(2)	23(1)	0(1)	-3(1)	-5(1)
C(20)	39(2)	29(2)	40(2)	1(1)	-9(2)	-5(1)
C(21)	53(2)	33(2)	43(2)	-6(2)	-6(2)	-14(2)
C(22)	42(2)	53(2)	34(2)	-3(2)	-10(2)	-20(2)
C(23)	32(2)	53(2)	38(2)	2(2)	-12(2)	-7(2)

C(24)	30(2)	35(2)	30(2)	0(1)	-6(1)	-3(1)
Cl(1S)	44(1)	64(1)	57(1)	3(1)	0(1)	3(1)
Cl(2S)	61(1)	76(1)	53(1)	0(1)	-9(1)	12(1)
Cl(3S)	76(1)	130(1)	51(1)	-23(1)	1(1)	33(1)
C(1S)	45(2)	51(2)	46(2)	-3(2)	3(2)	2(2)
O(1S)	41(2)	83(5)	54(2)	2(2)	-7(2)	-1(2)
C(2S)	41(2)	83(5)	54(2)	2(2)	-7(2)	-1(2)
C(3S)	41(2)	83(5)	54(2)	2(2)	-7(2)	-1(2)

Table 5 Hydrogen coordinates (x 10^4) and isotropic displacement parameters ($Å^2$ x 10^3) for **6a**

	x	y	z	U(eq)
H(20)	312	2500	1014	37
H(19)	1243	2500	-143	41
H(8)	420	1862	6712	41
H(9)	379	1586	9072	51
H(10)	-260	814	9765	53
H(11)	-849	324	8145	49
H(12)	-799	584	5777	38
H(14)	927	876	5508	44
H(15)	1835	503	4660	60
H(16)	2040	516	2293	58
H(17)	1337	891	734	49
H(18)	423	1254	1551	38
H(2)	-273	263	3190	43
H(3)	-1026	-229	1954	52
H(4)	-1880	277	1255	52
H(5)	-1991	1287	1756	49
H(6)	-1243	1794	2986	38
H(1S)	2740	1679	8091	57
H(1S1)	3406	2327	7635	89
H(2S1)	3285	2154	4893	71
H(2S2)	3747	1817	5896	71
H(3S1)	4123	2631	4340	89
H(3S2)	4391	2579	5885	89
H(3S3)	3883	3062	5550	89

Table 6 Torsion angles [°] for **6a**

C(3)-Pd(1)-P(1)-C(7)	127.68(17)
Cl(1)-Pd(1)-P(1)-C(7)	-52.63(11)
C(3)-Pd(1)-P(1)-C(19)	-112.18(17)
C(3)-Pd(1)-P(1)-C(13)	10.06(17)
Cl(1)-Pd(1)-P(1)-C(13)	-170.25(12)
N(1)-S(1)-N(2)-C(2)	0.0
N(2)-S(1)-N(1)-C(1)	0.0
S(1)-N(1)-C(1)-C(6)	180.0
S(1)-N(1)-C(1)-C(2)	0.0
S(1)-N(2)-C(2)-C(3)	180.0
S(1)-N(2)-C(2)-C(1)	0.0
N(1)-C(1)-C(2)-N(2)	0.0
C(6)-C(1)-C(2)-N(2)	180.0
N(1)-C(1)-C(2)-C(3)	180.0
C(6)-C(1)-C(2)-C(3)	0.0
N(2)-C(2)-C(3)-C(4)	180.0
C(1)-C(2)-C(3)-C(4)	0.0
N(2)-C(2)-C(3)-Pd(1)	0.0
C(1)-C(2)-C(3)-Pd(1)	180.0
P(1)#1-Pd(1)-C(3)-C(4)	-93.509(19)
P(1)-Pd(1)-C(3)-C(4)	93.509(19)
P(1)#1-Pd(1)-C(3)-C(2)	86.491(19)
P(1)-Pd(1)-C(3)-C(2)	-86.491(19)
C(2)-C(3)-C(4)-C(5)	0.0
Pd(1)-C(3)-C(4)-C(5)	180.0
C(3)-C(4)-C(5)-C(6)	0.0
C(4)-C(5)-C(6)-C(1)	0.0
C(4)-C(5)-C(6)-Br(1)	180.0
N(1)-C(1)-C(6)-C(5)	180.0
C(2)-C(1)-C(6)-C(5)	0.0
N(1)-C(1)-C(6)-Br(1)	0.0
C(2)-C(1)-C(6)-Br(1)	180.0
C(19)-P(1)-C(7)-C(12)	8.7(3)

C(13)-P(1)-C(7)-C(12)	-100.7(3)
Pd(1)-P(1)-C(7)-C(12)	133.9(3)
C(19)-P(1)-C(7)-C(8)	-171.8(3)
C(13)-P(1)-C(7)-C(8)	78.8(3)
Pd(1)-P(1)-C(7)-C(8)	-46.6(3)
C(12)-C(7)-C(8)-C(9)	1.1(5)
P(1)-C(7)-C(8)-C(9)	-178.5(3)
C(7)-C(8)-C(9)-C(10)	-0.8(6)
C(8)-C(9)-C(10)-C(11)	-0.1(6)
C(9)-C(10)-C(11)-C(12)	0.7(6)
C(8)-C(7)-C(12)-C(11)	-0.5(5)
P(1)-C(7)-C(12)-C(11)	179.0(3)
C(10)-C(11)-C(12)-C(7)	-0.4(6)
C(7)-P(1)-C(13)-C(14)	-16.3(3)
C(19)-P(1)-C(13)-C(14)	-128.1(3)
Pd(1)-P(1)-C(13)-C(14)	103.8(3)
C(7)-P(1)-C(13)-C(18)	168.2(2)
C(19)-P(1)-C(13)-C(18)	56.3(3)
Pd(1)-P(1)-C(13)-C(18)	-71.8(3)
C(18)-C(13)-C(14)-C(15)	0.9(5)
P(1)-C(13)-C(14)-C(15)	-174.6(3)
C(13)-C(14)-C(15)-C(16)	0.0(6)
C(14)-C(15)-C(16)-C(17)	-0.5(7)
C(15)-C(16)-C(17)-C(18)	0.1(6)
C(16)-C(17)-C(18)-C(13)	0.9(5)
C(14)-C(13)-C(18)-C(17)	-1.4(5)
P(1)-C(13)-C(18)-C(17)	174.4(3)
C(7)-P(1)-C(19)-C(20)	-76.0(3)
C(13)-P(1)-C(19)-C(20)	33.8(3)
Pd(1)-P(1)-C(19)-C(20)	162.9(2)
C(7)-P(1)-C(19)-C(24)	103.8(3)
C(13)-P(1)-C(19)-C(24)	-146.3(3)
Pd(1)-P(1)-C(19)-C(24)	-17.3(3)
C(24)-C(19)-C(20)-C(21)	-0.4(5)
P(1)-C(19)-C(20)-C(21)	179.4(3)

C(19)-C(20)-C(21)-C(22)	-0.1(6)
C(20)-C(21)-C(22)-C(23)	0.4(6)
C(21)-C(22)-C(23)-C(24)	-0.3(6)
C(22)-C(23)-C(24)-C(19)	-0.2(5)
C(20)-C(19)-C(24)-C(23)	0.5(5)
P(1)-C(19)-C(24)-C(23)	-179.3(3)

Symmetry transformations used to generate equivalent atoms:
#1 x,-y+1/2,z

Appendix three: Full crystallographic data of **7b**

Table 1 Crystal data and structure refinement for **7b**

Identification code	rb09030a	
Empirical formula	$C_{46}H_{40}Br_2Cl_4N_2P_2PdSe$	
Formula weight	1169.72	
Temperature	173(2) K	
Wavelength	0.71073 Å	
Crystal system	Orthorhombic	
Space group	*P*nma	
Unit cell dimensions	a = 11.022(2) Å	α = 90°.
	b = 15.261(3) Å	β = 90°.
	c = 28.105(6) Å	γ = 90°.
Volume	4727.7(18) $Å^3$	
Z	4	
Density (calculated)	1.643 Mg/m^3	
Absorption coefficient	3.181 mm^{-1}	
F(000)	2312	
Crystal size	0.213 x 0.179 x 0.128 mm^3	
Theta range for data collection	1.98 to 27.51°.	
Index ranges	-14<=h<=14, -19<=k<=19, -36<=l<=36	
Reflections collected	62310	
Independent reflections	5617 [R(int) = 0.1033]	
Completeness to theta = 25.25°	99.9 %	
Absorption correction	Semi-empirical from equivalents	
Max. and min. transmission	0.6863 and 0.5506	
Refinement method	Full-matrix least-squares on F^2	
Data / restraints / parameters	5617 / 0 / 280	
Goodness-of-fit on F^2	1.109	
Final R indices [I>2sigma(I)]	R1 = 0.0680, wR2 = 0.1411	
R indices (all data)	R1 = 0.1249, wR2 = 0.1685	
Largest diff. peak and hole	2.215 and -1.493 e.$Å^{-3}$	

Table 2 Atomic coordinates (x 10^4) and equivalent isotropic displacement parameters ($Å^2$ x 10^3) for **7b**. U(eq) is defined as one third of the trace of the orthogonalized U^{ij} tensor

	x	y	z	U(eq)
Pd(1)	10294(1)	2500	3571(1)	25(1)
Br(1)	5343(1)	2500	5028(1)	47(1)
Br(2)	11972(1)	2500	2960(1)	39(1)
Se(1)	5861(1)	2500	3259(1)	47(1)
P(1)	10287(2)	970(1)	3573(1)	24(1)
N(1)	5519(9)	2500	3889(4)	43(3)
N(2)	7474(9)	2500	3346(3)	39(2)
C(1)	6583(10)	2500	4119(4)	32(3)
C(2)	7674(10)	2500	3817(4)	27(2)
C(3)	8856(10)	2500	4023(4)	27(2)
C(4)	8949(11)	2500	4510(4)	34(3)
C(5)	7893(11)	2500	4813(4)	35(3)
C(6)	6720(11)	2500	4623(4)	36(3)
C(7)	10147(6)	550(5)	2961(2)	26(2)
C(8)	9251(7)	933(5)	2674(3)	31(2)
C(9)	9074(8)	637(6)	2214(3)	38(2)
C(10)	9785(8)	-41(6)	2034(3)	41(2)
C(11)	10694(8)	-400(6)	2306(3)	41(2)
C(12)	10874(7)	-121(5)	2776(3)	33(2)
C(13)	9065(7)	415(5)	3907(3)	29(2)
C(14)	8008(8)	106(6)	3689(3)	43(2)
C(15)	7085(8)	-250(8)	3962(3)	61(3)
C(16)	7172(8)	-300(8)	4447(3)	53(3)
C(17)	8223(8)	15(6)	4671(3)	40(2)
C(18)	9142(7)	367(6)	4402(3)	33(2)
C(19)	11648(7)	481(5)	3841(2)	27(2)
C(20)	11709(7)	-449(5)	3910(3)	32(2)
C(21)	12726(7)	-820(6)	4124(3)	37(2)
C(22)	13698(8)	-286(7)	4268(3)	42(2)
C(23)	13643(8)	603(7)	4201(3)	41(2)

C(24)	12627(7)	997(6)	3983(3)	32(2)
Cl(1S)	5020(4)	7500	3526(2)	79(1)
Cl(2S)	2515(5)	7500	2349(3)	117(2)
C(1S)	3570(20)	7500	3155(9)	125(4)
C(2S)	3880(20)	7500	2686(9)	125(4)
Cl(3S)	5106(5)	7500	1474(2)	84(1)
Cl(4S)	2944(5)	7500	183(2)	94(2)
C(3S)	3710(20)	7500	1050(9)	125(4)
C(4S)	4280(20)	7500	642(9)	125(4)

Table 3 Bond lengths [Å] and angles [°] for **7b**

Pd(1)-C(3)	2.032(11)	C(14)-C(15)	1.385(12)
Pd(1)-P(1)	2.3353(19)	C(14)-H(8)	0.9500
Pd(1)-P(1)#1	2.3353(19)	C(15)-C(16)	1.369(12)
Pd(1)-Br(2)	2.5247(15)	C(15)-H(9)	0.9500
Br(1)-C(6)	1.897(12)	C(16)-C(17)	1.403(12)
Se(1)-N(2)	1.794(10)	C(16)-H(10)	0.9500
Se(1)-N(1)	1.811(11)	C(17)-C(18)	1.376(11)
P(1)-C(19)	1.837(8)	C(17)-H(11)	0.9500
P(1)-C(7)	1.841(7)	C(18)-H(12)	0.9500
P(1)-C(13)	1.847(8)	C(19)-C(24)	1.394(11)
N(1)-C(1)	1.338(15)	C(19)-C(20)	1.434(11)
N(2)-C(2)	1.342(13)	C(20)-C(21)	1.393(11)
C(1)-C(6)	1.426(16)	C(20)-H(14)	0.9500
C(1)-C(2)	1.470(15)	C(21)-C(22)	1.406(12)
C(2)-C(3)	1.426(15)	C(21)-H(15)	0.9500
C(3)-C(4)	1.370(15)	C(22)-C(23)	1.371(13)
C(4)-C(5)	1.443(16)	C(22)-H(16)	0.9500
C(4)-H(24)	0.9500	C(23)-C(24)	1.410(11)
C(5)-C(6)	1.398(17)	C(23)-H(17)	0.9500
C(5)-H(23)	0.9500	C(24)-H(18)	0.9500
C(7)-C(12)	1.401(11)	Cl(1S)-C(1S)	1.91(3)
C(7)-C(8)	1.403(10)	Cl(2S)-C(2S)	1.78(3)
C(8)-C(9)	1.385(11)	C(1S)-C(2S)	1.36(3)
C(8)-H(2)	0.9500	C(1S)-H(1S1)	0.9900
C(9)-C(10)	1.392(12)	C(1S)-H(1S2)	0.9900
C(9)-H(3)	0.9500	C(2S)-H(2S1)	0.9900
C(10)-C(11)	1.374(12)	C(2S)-H(2S2)	0.9900
C(10)-H(4)	0.9500	Cl(3S)-C(3S)	1.95(3)
C(11)-C(12)	1.402(11)	Cl(4S)-C(4S)	1.96(3)
C(11)-H(5)	0.9500	C(3S)-C(4S)	1.31(3)
C(12)-H(6)	0.9500	C(3S)-H(3S1)	0.9900
C(13)-C(18)	1.395(10)	C(3S)-H(3S2)	0.9900
C(13)-C(14)	1.397(11)	C(4S)-H(4S1)	0.9900

C(4S)-H(4S2)	0.9900	C(12)-C(7)-C(8)	119.6(7)
		C(12)-C(7)-P(1)	123.6(6)
C(3)-Pd(1)-P(1)	89.77(5)	C(8)-C(7)-P(1)	116.8(6)
C(3)-Pd(1)-P(1)#1	89.77(5)	C(9)-C(8)-C(7)	120.1(7)
P(1)-Pd(1)-P(1)#1	179.54(11)	C(9)-C(8)-H(2)	120.0
C(3)-Pd(1)-Br(2)	175.8(3)	C(7)-C(8)-H(2)	120.0
P(1)-Pd(1)-Br(2)	90.23(5)	C(8)-C(9)-C(10)	120.1(8)
P(1)#1-Pd(1)-Br(2)	90.23(5)	C(8)-C(9)-H(3)	120.0
N(2)-Se(1)-N(1)	94.1(4)	C(10)-C(9)-H(3)	120.0
C(19)-P(1)-C(7)	108.1(3)	C(11)-C(10)-C(9)	120.4(8)
C(19)-P(1)-C(13)	101.6(3)	C(11)-C(10)-H(4)	119.8
C(7)-P(1)-C(13)	104.7(3)	C(9)-C(10)-H(4)	119.8
C(19)-P(1)-Pd(1)	113.8(3)	C(10)-C(11)-C(12)	120.4(8)
C(7)-P(1)-Pd(1)	110.2(2)	C(10)-C(11)-H(5)	119.8
C(13)-P(1)-Pd(1)	117.5(3)	C(12)-C(11)-H(5)	119.8
C(1)-N(1)-Se(1)	106.8(8)	C(7)-C(12)-C(11)	119.4(8)
C(2)-N(2)-Se(1)	107.3(8)	C(7)-C(12)-H(6)	120.3
N(1)-C(1)-C(6)	124.9(11)	C(11)-C(12)-H(6)	120.3
N(1)-C(1)-C(2)	116.0(10)	C(18)-C(13)-C(14)	118.0(7)
C(6)-C(1)-C(2)	119.1(10)	C(18)-C(13)-P(1)	119.1(6)
N(2)-C(2)-C(3)	123.4(10)	C(14)-C(13)-P(1)	122.7(6)
N(2)-C(2)-C(1)	115.7(10)	C(15)-C(14)-C(13)	120.2(8)
C(3)-C(2)-C(1)	120.9(9)	C(15)-C(14)-H(8)	119.9
C(4)-C(3)-C(2)	118.3(10)	C(13)-C(14)-H(8)	119.9
C(4)-C(3)-Pd(1)	124.4(8)	C(16)-C(15)-C(14)	121.4(8)
C(2)-C(3)-Pd(1)	117.3(8)	C(16)-C(15)-H(9)	119.3
C(3)-C(4)-C(5)	121.9(11)	C(14)-C(15)-H(9)	119.3
C(3)-C(4)-H(24)	119.1	C(15)-C(16)-C(17)	119.1(8)
C(5)-C(4)-H(24)	119.1	C(15)-C(16)-H(10)	120.5
C(6)-C(5)-C(4)	121.4(11)	C(17)-C(16)-H(10)	120.5
C(6)-C(5)-H(23)	119.3	C(18)-C(17)-C(16)	119.6(8)
C(4)-C(5)-H(23)	119.3	C(18)-C(17)-H(11)	120.2
C(5)-C(6)-C(1)	118.5(11)	C(16)-C(17)-H(11)	120.2
C(5)-C(6)-Br(1)	120.7(9)	C(17)-C(18)-C(13)	121.7(8)
C(1)-C(6)-Br(1)	120.8(9)	C(17)-C(18)-H(12)	119.2

C(13)-C(18)-H(12)	119.2	C(2S)-C(1S)-H(1S2)	110.0
C(24)-C(19)-C(20)	118.9(7)	Cl(1S)-C(1S)-H(1S2)	110.0
C(24)-C(19)-P(1)	121.4(6)	H(1S1)-C(1S)-H(1S2)	108.4
C(20)-C(19)-P(1)	119.7(6)	C(1S)-C(2S)-Cl(2S)	107.4(19)
C(21)-C(20)-C(19)	119.9(8)	C(1S)-C(2S)-H(2S1)	110.2
C(21)-C(20)-H(14)	120.0	Cl(2S)-C(2S)-H(2S1)	110.2
C(19)-C(20)-H(14)	120.0	C(1S)-C(2S)-H(2S2)	110.2
C(20)-C(21)-C(22)	120.1(8)	Cl(2S)-C(2S)-H(2S2)	110.2
C(20)-C(21)-H(15)	120.0	H(2S1)-C(2S)-H(2S2)	108.5
C(22)-C(21)-H(15)	120.0	C(4S)-C(3S)-Cl(3S)	98.8(19)
C(23)-C(22)-C(21)	120.1(8)	C(4S)-C(3S)-H(3S1)	112.0
C(23)-C(22)-H(16)	120.0	Cl(3S)-C(3S)-H(3S1)	112.0
C(21)-C(22)-H(16)	120.0	C(4S)-C(3S)-H(3S2)	112.0
C(22)-C(23)-C(24)	121.0(9)	Cl(3S)-C(3S)-H(3S2)	112.0
C(22)-C(23)-H(17)	119.5	H(3S1)-C(3S)-H(3S2)	109.7
C(24)-C(23)-H(17)	119.5	C(3S)-C(4S)-Cl(4S)	102.3(19)
C(19)-C(24)-C(23)	119.9(8)	C(3S)-C(4S)-H(4S1)	111.3
C(19)-C(24)-H(18)	120.0	Cl(4S)-C(4S)-H(4S1)	111.3
C(23)-C(24)-H(18)	120.0	C(3S)-C(4S)-H(4S2)	111.3
C(2S)-C(1S)-Cl(1S)	108.4(19)	Cl(4S)-C(4S)-H(4S2)	111.3
C(2S)-C(1S)-H(1S1)	110.0	H(4S1)-C(4S)-H(4S2)	109.2
Cl(1S)-C(1S)-H(1S1)	110.0		

Symmetry transformations used to generate equivalent atoms: #1 x,-y+1/2,z

Table 4 Anisotropic displacement parameters ($Å^2$ x 10^3) for **7b**. The anisotropic displacement factor exponent takes the form: $-2\pi^2 [h^2 a^{*2} U^{11} + ... + 2 h k a^* b^* U^{12}]$

	U^{11}	U^{22}	U^{33}	U^{23}	U^{13}	U^{12}
Pd(1)	24(1)	28(1)	24(1)	0	1(1)	0
Br(1)	40(1)	56(1)	46(1)	0	17(1)	0
Br(2)	40(1)	37(1)	40(1)	0	13(1)	0
Se(1)	30(1)	67(1)	43(1)	0	-4(1)	0
P(1)	22(1)	28(1)	24(1)	0(1)	0(1)	1(1)
N(1)	27(5)	54(7)	47(6)	0	-1(5)	0
N(2)	33(6)	44(6)	38(6)	0	-2(5)	0
C(1)	26(6)	34(6)	37(6)	0	0(5)	0
C(2)	38(6)	24(5)	21(5)	0	1(5)	0
C(3)	31(6)	13(5)	36(6)	0	2(5)	0
C(4)	35(6)	34(6)	32(6)	0	3(5)	0
C(5)	41(7)	30(6)	35(6)	0	0(5)	0
C(6)	39(7)	34(6)	35(6)	0	5(5)	0
C(7)	23(4)	31(4)	24(4)	2(3)	-1(3)	0(3)
C(8)	32(4)	34(4)	27(4)	0(3)	3(3)	5(4)
C(9)	31(4)	44(5)	38(5)	5(4)	-3(4)	-1(4)
C(10)	46(5)	55(5)	23(4)	-4(4)	1(4)	-5(5)
C(11)	43(5)	47(5)	31(4)	-6(4)	3(4)	4(4)
C(12)	26(4)	37(5)	36(4)	0(4)	-3(3)	1(4)
C(13)	24(4)	30(4)	32(4)	-1(3)	1(3)	5(3)
C(14)	37(5)	57(6)	34(5)	5(4)	-3(4)	-9(5)
C(15)	25(4)	115(10)	43(5)	6(6)	-5(4)	-30(6)
C(16)	27(4)	93(8)	40(5)	16(5)	9(4)	-16(5)
C(17)	35(5)	58(6)	28(4)	2(4)	3(4)	-2(4)
C(18)	26(4)	41(5)	33(4)	-5(4)	1(3)	-2(4)
C(19)	27(4)	33(4)	22(4)	-3(3)	4(3)	0(3)
C(20)	25(4)	36(4)	33(4)	5(4)	0(3)	-1(3)
C(21)	32(4)	45(5)	35(4)	9(4)	9(4)	13(4)
C(22)	26(4)	71(7)	30(4)	12(4)	2(3)	7(4)
C(23)	27(4)	57(6)	38(5)	4(4)	2(4)	-3(4)

C(24)	28(4)	39(5)	30(4)	1(4)	2(3)	-3(4)
Cl(1S)	82(3)	81(3)	73(3)	0	12(2)	0
Cl(2S)	75(3)	76(3)	202(7)	0	-47(4)	0
C(1S)	108(10)	142(11)	124(11)	0	23(8)	0
C(2S)	108(10)	142(11)	124(11)	0	23(8)	0
Cl(3S)	92(4)	58(2)	102(4)	0	-29(3)	0
Cl(4S)	64(3)	126(5)	91(4)	0	-18(3)	0
C(3S)	108(10)	142(11)	124(11)	0	23(8)	0
C(4S)	108(10)	142(11)	124(11)	0	23(8)	0

Table 5 Hydrogen coordinates (x 10^4) and isotropic displacement parameters ($Å^2$ x 10^3) for **7b**

	x	y	z	U(eq)
H(24)	9732	2500	4651	40
H(23)	7997	2500	5148	42
H(2)	8765	1396	2796	37
H(3)	8466	897	2020	45
H(4)	9641	-256	1722	50
H(5)	11203	-840	2175	49
H(6)	11484	-385	2967	40
H(8)	7923	141	3353	51
H(9)	6377	-464	3809	73
H(10)	6530	-543	4629	64
H(11)	8298	-16	5008	48
H(12)	9848	583	4556	40
H(14)	11056	-811	3809	38
H(15)	12763	-1436	4173	45
H(16)	14393	-540	4412	51
H(17)	14301	960	4302	49
H(18)	12609	1612	3934	38
H(1S1)	3080	6974	3229	150
H(1S2)	3080	8026	3229	150
H(2S1)	4372	6973	2610	150
H(2S2)	4372	8027	2610	150
H(3S1)	3200	6970	1091	150
H(3S2)	3200	8030	1091	150
H(4S1)	4794	6971	607	150
H(4S2)	4794	8029	607	150

Table 6 Torsion angles [°] for **7b**

C(3)-Pd(1)-P(1)-C(19)	-114.7(4)
Br(2)-Pd(1)-P(1)-C(19)	69.5(3)
C(3)-Pd(1)-P(1)-C(7)	123.7(4)
Br(2)-Pd(1)-P(1)-C(7)	-52.1(3)
C(3)-Pd(1)-P(1)-C(13)	3.9(4)
Br(2)-Pd(1)-P(1)-C(13)	-172.0(3)
N(2)-Se(1)-N(1)-C(1)	0.000(2)
N(1)-Se(1)-N(2)-C(2)	0.000(2)
Se(1)-N(1)-C(1)-C(6)	180.000(3)
Se(1)-N(1)-C(1)-C(2)	0.000(2)
Se(1)-N(2)-C(2)-C(3)	180.000(2)
Se(1)-N(2)-C(2)-C(1)	0.000(2)
N(1)-C(1)-C(2)-N(2)	0.000(3)
C(6)-C(1)-C(2)-N(2)	180.000(3)
N(1)-C(1)-C(2)-C(3)	180.000(3)
C(6)-C(1)-C(2)-C(3)	0.000(4)
N(2)-C(2)-C(3)-C(4)	180.000(3)
C(1)-C(2)-C(3)-C(4)	0.000(3)
N(2)-C(2)-C(3)-Pd(1)	0.000(3)
C(1)-C(2)-C(3)-Pd(1)	180.000(2)
P(1)-Pd(1)-C(3)-C(4)	90.02(5)
P(1)#1-Pd(1)-C(3)-C(4)	-90.02(5)
P(1)-Pd(1)-C(3)-C(2)	-89.98(5)
P(1)#1-Pd(1)-C(3)-C(2)	89.98(5)
C(2)-C(3)-C(4)-C(5)	0.000(4)
Pd(1)-C(3)-C(4)-C(5)	180.000(3)
C(3)-C(4)-C(5)-C(6)	0.000(4)
C(4)-C(5)-C(6)-C(1)	0.000(4)
C(4)-C(5)-C(6)-Br(1)	180.000(2)
N(1)-C(1)-C(6)-C(5)	180.000(3)
C(2)-C(1)-C(6)-C(5)	0.000(4)
N(1)-C(1)-C(6)-Br(1)	0.000(4)
C(2)-C(1)-C(6)-Br(1)	180.000(2)

C(19)-P(1)-C(7)-C(12)	8.4(8)
C(13)-P(1)-C(7)-C(12)	-99.3(7)
Pd(1)-P(1)-C(7)-C(12)	133.4(6)
C(19)-P(1)-C(7)-C(8)	-172.0(6)
C(13)-P(1)-C(7)-C(8)	80.3(6)
Pd(1)-P(1)-C(7)-C(8)	-47.0(6)
C(12)-C(7)-C(8)-C(9)	1.1(12)
P(1)-C(7)-C(8)-C(9)	-178.5(6)
C(7)-C(8)-C(9)-C(10)	0.0(12)
C(8)-C(9)-C(10)-C(11)	-2.3(13)
C(9)-C(10)-C(11)-C(12)	3.4(14)
C(8)-C(7)-C(12)-C(11)	0.0(12)
P(1)-C(7)-C(12)-C(11)	179.6(6)
C(10)-C(11)-C(12)-C(7)	-2.3(13)
C(19)-P(1)-C(13)-C(18)	47.6(7)
C(7)-P(1)-C(13)-C(18)	160.0(6)
Pd(1)-P(1)-C(13)-C(18)	-77.3(7)
C(19)-P(1)-C(13)-C(14)	-138.2(7)
C(7)-P(1)-C(13)-C(14)	-25.8(8)
Pd(1)-P(1)-C(13)-C(14)	96.9(7)
C(18)-C(13)-C(14)-C(15)	-1.2(14)
P(1)-C(13)-C(14)-C(15)	-175.5(8)
C(13)-C(14)-C(15)-C(16)	0.9(17)
C(14)-C(15)-C(16)-C(17)	-0.3(18)
C(15)-C(16)-C(17)-C(18)	0.1(16)
C(16)-C(17)-C(18)-C(13)	-0.5(14)
C(14)-C(13)-C(18)-C(17)	1.1(13)
P(1)-C(13)-C(18)-C(17)	175.6(7)
C(7)-P(1)-C(19)-C(24)	116.9(6)
C(13)-P(1)-C(19)-C(24)	-133.2(6)
Pd(1)-P(1)-C(19)-C(24)	-5.9(7)
C(7)-P(1)-C(19)-C(20)	-63.5(7)
C(13)-P(1)-C(19)-C(20)	46.3(7)
Pd(1)-P(1)-C(19)-C(20)	173.7(5)
C(24)-C(19)-C(20)-C(21)	1.2(11)

P(1)-C(19)-C(20)-C(21)	-178.4(6)
C(19)-C(20)-C(21)-C(22)	-0.7(12)
C(20)-C(21)-C(22)-C(23)	0.4(12)
C(21)-C(22)-C(23)-C(24)	-0.6(13)
C(20)-C(19)-C(24)-C(23)	-1.4(11)
P(1)-C(19)-C(24)-C(23)	178.2(6)
C(22)-C(23)-C(24)-C(19)	1.1(12)
Cl(1S)-C(1S)-C(2S)-Cl(2S)	180.000(3)
Cl(3S)-C(3S)-C(4S)-Cl(4S)	180.0

Symmetry transformations used to generate equivalent atoms: #1 x,-y+1/2,z

Appendix four: Full crystallographic data of **8**

Table 1 Crystal data and structure refinement for **8**

Identification code	rb08042a	
Empirical formula	$C_{48}H_{34}Br_2Cl_2N_4P_2Pd_2Se_2$	
Formula weight	1330.17	
Temperature	173(2) K	
Wavelength	0.71073 Å	
Crystal system	Monoclinic	
Space group	P2/n	
Unit cell dimensions	a = 18.0613(8) Å	α = 90°.
	b = 15.5096(7) Å	β = 103.4100(10)°.
	c = 21.0807(10) Å	γ = 90°.
Volume	5744.2(5) Å^3	
Z	4	
Density (calculated)	1.538 Mg/m^3	
Absorption coefficient	3.466 mm^{-1}	
F(000)	2576	
Crystal size	0.229 x 0.134 x 0.095 mm^3	
Theta range for data collection	1.65 to 26.73°.	
Index ranges	-22<=h<=22, -19<=k<=19, -26<=l<=26	
Reflections collected	77661	
Independent reflections	12207 [R(int) = 0.0491]	
Completeness to theta = 25.00°	100.0 %	
Absorption correction	Semi-empirical from equivalents	
Max. and min. transmission	0.7343 and 0.5041	
Refinement method	Full-matrix least-squares on F^2	
Data / restraints / parameters	12207 / 0 / 529	
Goodness-of-fit on F^2	1.056	
Final R indices [I>2sigma(I)]	R1 = 0.0387, wR2 = 0.0875	
R indices (all data)	R1 = 0.0566, wR2 = 0.0926	
Largest diff. peak and hole	1.375 and -0.754 e.Å^{-3}	

Table 2 Atomic coordinates (x 10^4) and equivalent isotropic displacement parameters ($Å^2$ x 10^3) for **8**. U(eq) is defined as one third of the trace of the orthogonalized U^{ij} tensor

	x	y	z	U(eq)
Pd(1)	6801(1)	1441(1)	6883(1)	22(1)
Pd(2)	3229(1)	3539(1)	8134(1)	21(1)
Se(1)	4526(1)	2584(1)	7467(1)	33(1)
Se(2)	5555(1)	260(1)	7401(1)	41(1)
Br(1)	1312(1)	260(1)	9120(1)	50(1)
Cl(1)	4101(1)	4646(1)	8008(1)	31(1)
Br(2)	6272(1)	-1770(1)	9210(1)	64(1)
Cl(2)	6134(1)	2602(1)	7218(1)	27(1)
P(1)	2916(1)	4187(1)	8994(1)	24(1)
P(2)	6973(1)	2126(1)	5989(1)	26(1)
N(1)	4312(2)	1755(2)	6869(2)	33(1)
N(2)	3540(2)	2848(2)	7385(2)	26(1)
N(3)	5750(2)	-512(2)	8044(2)	44(1)
N(4)	6510(2)	664(2)	7596(2)	25(1)
C(1)	1445(2)	1749(3)	8354(2)	26(1)
C(2)	1875(2)	2373(2)	8093(2)	23(1)
C(3)	2675(2)	2514(2)	8357(2)	23(1)
C(4)	3015(2)	1932(3)	8823(2)	32(1)
C(5)	2614(3)	1253(3)	9046(2)	35(1)
C(6)	1849(3)	1163(3)	8831(2)	33(1)
C(7)	2060(2)	3802(2)	9232(2)	27(1)
C(8)	2104(2)	3246(3)	9757(2)	33(1)
C(9)	1451(3)	2958(3)	9927(2)	40(1)
C(10)	743(3)	3212(3)	9566(2)	43(1)
C(11)	683(2)	3753(3)	9034(2)	41(1)
C(12)	1345(2)	4046(3)	8865(2)	34(1)
C(13)	2733(2)	5339(3)	8857(2)	27(1)
C(14)	2278(2)	5587(3)	8262(2)	35(1)
C(15)	2080(3)	6435(3)	8135(2)	42(1)
C(16)	2361(3)	7049(3)	8604(3)	49(1)

C(17)	2830(3)	6814(3)	9189(3)	50(1)
C(18)	3019(2)	5958(3)	9321(2)	37(1)
C(19)	3672(2)	4074(3)	9719(2)	29(1)
C(20)	3603(3)	4358(3)	10333(2)	38(1)
C(21)	4204(3)	4280(3)	10866(2)	52(1)
C(22)	4867(3)	3905(3)	10806(2)	55(1)
C(23)	4945(3)	3606(3)	10208(2)	54(1)
C(24)	4353(2)	3702(3)	9665(2)	38(1)
C(25)	6469(2)	-413(3)	8355(2)	31(1)
C(26)	6910(2)	245(2)	8114(2)	26(1)
C(27)	7682(2)	426(2)	8423(2)	25(1)
C(28)	8004(2)	-118(3)	8920(2)	31(1)
C(29)	7595(3)	-791(3)	9154(2)	36(1)
C(30)	6848(3)	-917(3)	8895(2)	38(1)
C(31)	6920(2)	3304(3)	6006(2)	28(1)
C(32)	6487(3)	3760(3)	5494(2)	35(1)
C(33)	6493(3)	4662(3)	5514(2)	43(1)
C(34)	6920(3)	5084(3)	6040(2)	46(1)
C(35)	7347(3)	4628(3)	6557(2)	44(1)
C(36)	7350(2)	3732(3)	6547(2)	38(1)
C(37)	7866(3)	1899(4)	5752(3)	60(1)
C(38)	7924(3)	1218(4)	5339(3)	60(1)
C(39)	8597(3)	1015(4)	5183(3)	60(1)
C(40)	9227(3)	1475(4)	5459(3)	60(1)
C(41)	9201(3)	2164(4)	5859(3)	60(1)
C(42)	8509(3)	2388(4)	6012(3)	60(1)
C(43)	6221(2)	1806(2)	5295(2)	28(1)
C(44)	6267(3)	1964(3)	4657(2)	41(1)
C(45)	5667(3)	1764(3)	4140(2)	50(1)
C(46)	5019(3)	1398(3)	4249(2)	51(1)
C(47)	4971(3)	1227(3)	4873(2)	44(1)
C(48)	5560(2)	1439(3)	5401(2)	34(1)

Table 3 Bond lengths [Å] and angles [°] for **8**

Pd(1)-C(27)#1	2.012(4)	C(5)-C(6)	1.358(6)
Pd(1)-N(4)	2.088(3)	C(5)-H(5)	0.9500
Pd(1)-P(2)	2.2462(10)	C(7)-C(8)	1.389(6)
Pd(1)-Cl(2)	2.3641(10)	C(7)-C(12)	1.395(6)
Pd(1)-Pd(1)#1	3.1768(5)	C(8)-C(9)	1.385(6)
Pd(2)-C(3)	1.992(4)	C(8)-H(8)	0.9500
Pd(2)-N(2)	2.090(3)	C(9)-C(10)	1.385(7)
Pd(2)-P(1)	2.2563(10)	C(9)-H(9)	0.9500
Pd(2)-Cl(1)	2.3863(10)	C(10)-C(11)	1.384(7)
Se(1)-N(1)	1.780(3)	C(10)-H(10)	0.9500
Se(1)-N(2)	1.796(3)	C(11)-C(12)	1.400(6)
Se(2)-N(3)	1.782(3)	C(11)-H(11)	0.9500
Se(2)-N(4)	1.792(3)	C(12)-H(12)	0.9500
Br(1)-C(6)	1.882(4)	C(13)-C(18)	1.382(5)
Br(2)-C(30)	1.896(4)	C(13)-C(14)	1.386(6)
P(1)-C(19)	1.806(4)	C(14)-C(15)	1.374(6)
P(1)-C(13)	1.828(4)	C(14)-H(14)	0.9500
P(1)-C(7)	1.833(4)	C(15)-C(16)	1.382(7)
P(2)-C(43)	1.819(4)	C(15)-H(15)	0.9500
P(2)-C(37)	1.829(5)	C(16)-C(17)	1.372(7)
P(2)-C(31)	1.830(4)	C(16)-H(16)	0.9500
N(1)-C(1)#2	1.339(5)	C(17)-C(18)	1.384(6)
N(2)-C(2)#2	1.331(5)	C(17)-H(17)	0.9500
N(3)-C(25)	1.321(5)	C(18)-H(18)	0.9500
N(4)-C(26)	1.330(5)	C(19)-C(24)	1.387(6)
C(1)-N(1)#2	1.339(5)	C(19)-C(20)	1.401(6)
C(1)-C(6)	1.425(5)	C(20)-C(21)	1.376(6)
C(1)-C(2)	1.428(5)	C(20)-H(20)	0.9500
C(2)-N(2)#2	1.331(5)	C(21)-C(22)	1.363(7)
C(2)-C(3)	1.439(5)	C(21)-H(21)	0.9500
C(3)-C(4)	1.370(5)	C(22)-C(23)	1.381(7)
C(4)-C(5)	1.418(6)	C(22)-H(22)	0.9500
C(4)-H(4)	0.9500	C(23)-C(24)	1.381(6)

C(23)-H(23)	0.9500	C(44)-C(45)	1.383(7)
C(24)-H(24)	0.9500	C(44)-H(44)	0.9500
C(25)-C(30)	1.420(5)	C(45)-C(46)	1.368(7)
C(25)-C(26)	1.456(5)	C(45)-H(45)	0.9500
C(26)-C(27)	1.423(5)	C(46)-C(47)	1.363(7)
C(27)-C(28)	1.365(5)	C(46)-H(46)	0.9500
C(27)-Pd(1)#1	2.012(4)	C(47)-C(48)	1.388(6)
C(28)-C(29)	1.432(6)	C(47)-H(47)	0.9500
C(28)-H(28)	0.9500	C(48)-H(48)	0.9500
C(29)-C(30)	1.346(6)		
C(29)-H(29)	0.9500	C(27)#1-Pd(1)-N(4)	89.56(14)
C(31)-C(32)	1.373(5)	C(27)#1-Pd(1)-P(2)	86.37(11)
C(31)-C(36)	1.391(6)	N(4)-Pd(1)-P(2)	169.78(9)
C(32)-C(33)	1.400(6)	C(27)#1-Pd(1)-Cl(2)	177.09(11)
C(32)-H(32)	0.9500	N(4)-Pd(1)-Cl(2)	89.58(9)
C(33)-C(34)	1.363(6)	P(2)-Pd(1)-Cl(2)	94.02(4)
C(33)-H(33)	0.9500	C(27)#1-Pd(1)-Pd(1)#1	85.58(10)
C(34)-C(35)	1.376(6)	N(4)-Pd(1)-Pd(1)#1	72.25(8)
C(34)-H(34)	0.9500	P(2)-Pd(1)-Pd(1)#1	116.70(3)
C(35)-C(36)	1.389(6)	Cl(2)-Pd(1)-Pd(1)#1	96.80(2)
C(35)-H(35)	0.9500	C(3)-Pd(2)-N(2)	90.44(13)
C(36)-H(36)	0.9500	C(3)-Pd(2)-P(1)	86.13(10)
C(37)-C(38)	1.388(8)	N(2)-Pd(2)-P(1)	175.31(9)
C(37)-C(42)	1.389(8)	C(3)-Pd(2)-Cl(1)	168.91(11)
C(38)-C(39)	1.368(7)	N(2)-Pd(2)-Cl(1)	89.10(9)
C(38)-H(38)	0.9500	P(1)-Pd(2)-Cl(1)	93.66(4)
C(39)-C(40)	1.355(8)	N(1)-Se(1)-N(2)	92.83(15)
C(39)-H(39)	0.9500	N(3)-Se(2)-N(4)	92.87(15)
C(40)-C(41)	1.370(8)	C(19)-P(1)-C(13)	107.58(18)
C(40)-H(40)	0.9500	C(19)-P(1)-C(7)	104.90(18)
C(41)-C(42)	1.405(7)	C(13)-P(1)-C(7)	103.20(18)
C(41)-H(41)	0.9500	C(19)-P(1)-Pd(2)	110.83(14)
C(42)-H(42)	0.9500	C(13)-P(1)-Pd(2)	112.24(13)
C(43)-C(48)	1.386(6)	C(7)-P(1)-Pd(2)	117.33(12)
C(43)-C(44)	1.388(6)	C(43)-P(2)-C(37)	105.6(2)

C(43)-P(2)-C(31)	104.78(18)	C(9)-C(8)-H(8)	119.6
C(37)-P(2)-C(31)	104.5(2)	C(7)-C(8)-H(8)	119.6
C(43)-P(2)-Pd(1)	108.86(14)	C(8)-C(9)-C(10)	119.9(4)
C(37)-P(2)-Pd(1)	116.08(18)	C(8)-C(9)-H(9)	120.1
C(31)-P(2)-Pd(1)	115.92(13)	C(10)-C(9)-H(9)	120.1
C(1)#2-N(1)-Se(1)	106.8(3)	C(11)-C(10)-C(9)	120.5(4)
C(2)#2-N(2)-Se(1)	108.6(2)	C(11)-C(10)-H(10)	119.7
C(2)#2-N(2)-Pd(2)	130.8(3)	C(9)-C(10)-H(10)	119.7
Se(1)-N(2)-Pd(2)	118.58(16)	C(10)-C(11)-C(12)	119.4(4)
C(25)-N(3)-Se(2)	107.3(3)	C(10)-C(11)-H(11)	120.3
C(26)-N(4)-Se(2)	109.2(3)	C(12)-C(11)-H(11)	120.3
C(26)-N(4)-Pd(1)	133.9(3)	C(7)-C(12)-C(11)	120.4(4)
Se(2)-N(4)-Pd(1)	115.25(15)	C(7)-C(12)-H(12)	119.8
N(1)#2-C(1)-C(6)	124.4(4)	C(11)-C(12)-H(12)	119.8
N(1)#2-C(1)-C(2)	117.6(3)	C(18)-C(13)-C(14)	119.6(4)
C(6)-C(1)-C(2)	118.0(4)	C(18)-C(13)-P(1)	122.9(3)
N(2)#2-C(2)-C(1)	113.9(3)	C(14)-C(13)-P(1)	117.5(3)
N(2)#2-C(2)-C(3)	123.2(3)	C(15)-C(14)-C(13)	121.0(4)
C(1)-C(2)-C(3)	122.7(3)	C(15)-C(14)-H(14)	119.5
C(4)-C(3)-C(2)	114.8(3)	C(13)-C(14)-H(14)	119.5
C(4)-C(3)-Pd(2)	121.9(3)	C(14)-C(15)-C(16)	119.0(4)
C(2)-C(3)-Pd(2)	123.0(3)	C(14)-C(15)-H(15)	120.5
C(3)-C(4)-C(5)	123.2(4)	C(16)-C(15)-H(15)	120.5
C(3)-C(4)-H(4)	118.4	C(17)-C(16)-C(15)	120.5(4)
C(5)-C(4)-H(4)	118.4	C(17)-C(16)-H(16)	119.7
C(6)-C(5)-C(4)	121.7(4)	C(15)-C(16)-H(16)	119.7
C(6)-C(5)-H(5)	119.2	C(16)-C(17)-C(18)	120.5(5)
C(4)-C(5)-H(5)	119.2	C(16)-C(17)-H(17)	119.8
C(5)-C(6)-C(1)	118.9(4)	C(18)-C(17)-H(17)	119.8
C(5)-C(6)-Br(1)	122.0(3)	C(13)-C(18)-C(17)	119.4(4)
C(1)-C(6)-Br(1)	119.1(3)	C(13)-C(18)-H(18)	120.3
C(8)-C(7)-C(12)	119.0(4)	C(17)-C(18)-H(18)	120.3
C(8)-C(7)-P(1)	121.5(3)	C(24)-C(19)-C(20)	118.5(4)
C(12)-C(7)-P(1)	119.4(3)	C(24)-C(19)-P(1)	118.8(3)
C(9)-C(8)-C(7)	120.8(4)	C(20)-C(19)-P(1)	122.6(3)

C(21)-C(20)-C(19)	120.3(4)	C(36)-C(31)-P(2)	118.1(3)
C(21)-C(20)-H(20)	119.8	C(31)-C(32)-C(33)	119.5(4)
C(19)-C(20)-H(20)	119.8	C(31)-C(32)-H(32)	120.2
C(22)-C(21)-C(20)	120.4(5)	C(33)-C(32)-H(32)	120.2
C(22)-C(21)-H(21)	119.8	C(34)-C(33)-C(32)	120.2(4)
C(20)-C(21)-H(21)	119.8	C(34)-C(33)-H(33)	119.9
C(21)-C(22)-C(23)	120.4(4)	C(32)-C(33)-H(33)	119.9
C(21)-C(22)-H(22)	119.8	C(33)-C(34)-C(35)	120.3(4)
C(23)-C(22)-H(22)	119.8	C(33)-C(34)-H(34)	119.8
C(24)-C(23)-C(22)	119.9(5)	C(35)-C(34)-H(34)	119.8
C(24)-C(23)-H(23)	120.1	C(34)-C(35)-C(36)	120.4(4)
C(22)-C(23)-H(23)	120.1	C(34)-C(35)-H(35)	119.8
C(23)-C(24)-C(19)	120.5(4)	C(36)-C(35)-H(35)	119.8
C(23)-C(24)-H(24)	119.7	C(35)-C(36)-C(31)	119.2(4)
C(19)-C(24)-H(24)	119.7	C(35)-C(36)-H(36)	120.4
N(3)-C(25)-C(30)	124.7(4)	C(31)-C(36)-H(36)	120.4
N(3)-C(25)-C(26)	117.6(3)	C(38)-C(37)-C(42)	119.0(5)
C(30)-C(25)-C(26)	117.7(4)	C(38)-C(37)-P(2)	121.2(5)
N(4)-C(26)-C(27)	124.6(3)	C(42)-C(37)-P(2)	119.8(5)
N(4)-C(26)-C(25)	113.1(3)	C(39)-C(38)-C(37)	121.9(6)
C(27)-C(26)-C(25)	122.3(3)	C(39)-C(38)-H(38)	119.1
C(28)-C(27)-C(26)	115.4(4)	C(37)-C(38)-H(38)	119.1
C(28)-C(27)-Pd(1)#1	125.6(3)	C(40)-C(39)-C(38)	118.7(6)
C(26)-C(27)-Pd(1)#1	119.0(3)	C(40)-C(39)-H(39)	120.7
C(27)-C(28)-C(29)	123.5(4)	C(38)-C(39)-H(39)	120.7
C(27)-C(28)-H(28)	118.3	C(39)-C(40)-C(41)	122.0(5)
C(29)-C(28)-H(28)	118.3	C(39)-C(40)-H(40)	119.0
C(30)-C(29)-C(28)	121.0(4)	C(41)-C(40)-H(40)	119.0
C(30)-C(29)-H(29)	119.5	C(40)-C(41)-C(42)	119.6(6)
C(28)-C(29)-H(29)	119.5	C(40)-C(41)-H(41)	120.2
C(29)-C(30)-C(25)	119.8(4)	C(42)-C(41)-H(41)	120.2
C(29)-C(30)-Br(2)	122.6(3)	C(37)-C(42)-C(41)	118.8(6)
C(25)-C(30)-Br(2)	117.6(3)	C(37)-C(42)-H(42)	120.6
C(32)-C(31)-C(36)	120.4(4)	C(41)-C(42)-H(42)	120.6
C(32)-C(31)-P(2)	121.4(3)	C(48)-C(43)-C(44)	118.4(4)

C(48)-C(43)-P(2)	119.5(3)	C(47)-C(46)-H(46)	120.3
C(44)-C(43)-P(2)	121.9(3)	C(45)-C(46)-H(46)	120.3
C(45)-C(44)-C(43)	120.8(5)	C(46)-C(47)-C(48)	121.3(5)
C(45)-C(44)-H(44)	119.6	C(46)-C(47)-H(47)	119.4
C(43)-C(44)-H(44)	119.6	C(48)-C(47)-H(47)	119.4
C(46)-C(45)-C(44)	120.3(4)	C(43)-C(48)-C(47)	119.7(4)
C(46)-C(45)-H(45)	119.8	C(43)-C(48)-H(48)	120.1
C(44)-C(45)-H(45)	119.8	C(47)-C(48)-H(48)	120.1
C(47)-C(46)-C(45)	119.4(4)		

Symmetry transformations used to generate equivalent atoms: #1 -x+3/2,y,-z+3/2
#2 -x+1/2,y,-z+3/2

Table 4 Anisotropic displacement parameters ($Å^2$ x 10^3) for **8**. The anisotropic displacement factor exponent takes the form: $-2\pi^2$ [$h^2 a^{*2} U^{11}$ + ... + 2 h k a* b* U^{12}]

	U^{11}	U^{22}	U^{33}	U^{23}	U^{13}	U^{12}
Pd(1)	23(1)	23(1)	19(1)	3(1)	4(1)	1(1)
Pd(2)	19(1)	24(1)	19(1)	-4(1)	3(1)	-1(1)
Se(1)	24(1)	47(1)	26(1)	-11(1)	1(1)	8(1)
Se(2)	27(1)	49(1)	41(1)	22(1)	-2(1)	-4(1)
Br(1)	71(1)	37(1)	39(1)	15(1)	8(1)	-16(1)
Cl(1)	31(1)	34(1)	30(1)	-8(1)	9(1)	-13(1)
Br(2)	59(1)	58(1)	63(1)	39(1)	-11(1)	-24(1)
Cl(2)	24(1)	28(1)	32(1)	2(1)	11(1)	5(1)
P(1)	23(1)	27(1)	22(1)	-6(1)	5(1)	-1(1)
P(2)	27(1)	29(1)	22(1)	5(1)	7(1)	2(1)
N(1)	39(2)	34(2)	22(2)	-3(1)	3(2)	14(2)
N(2)	25(2)	30(2)	23(2)	-5(1)	6(1)	2(1)
N(3)	34(2)	46(2)	44(2)	24(2)	-2(2)	-13(2)
N(4)	24(2)	25(2)	27(2)	6(1)	5(1)	2(1)
C(1)	32(2)	28(2)	17(2)	-3(2)	1(2)	-8(2)
C(2)	29(2)	22(2)	16(2)	0(2)	3(2)	1(2)
C(3)	28(2)	22(2)	21(2)	-4(2)	7(2)	1(2)
C(4)	31(2)	37(2)	26(2)	4(2)	4(2)	5(2)
C(5)	46(3)	28(2)	27(2)	6(2)	2(2)	8(2)
C(6)	48(3)	26(2)	25(2)	4(2)	10(2)	-8(2)
C(7)	31(2)	24(2)	28(2)	-9(2)	12(2)	-3(2)
C(8)	36(2)	32(2)	31(2)	1(2)	10(2)	1(2)
C(9)	47(3)	35(2)	40(3)	3(2)	17(2)	-4(2)
C(10)	43(3)	32(2)	61(3)	-7(2)	26(2)	-13(2)
C(11)	28(2)	38(3)	55(3)	-7(2)	6(2)	-1(2)
C(12)	32(2)	33(2)	40(2)	-3(2)	12(2)	0(2)
C(13)	26(2)	30(2)	27(2)	-5(2)	8(2)	1(2)
C(14)	38(2)	32(2)	38(2)	-4(2)	12(2)	2(2)
C(15)	43(3)	42(3)	42(3)	9(2)	13(2)	11(2)
C(16)	52(3)	31(3)	67(3)	-4(2)	19(3)	10(2)

C(17)	57(3)	39(3)	53(3)	-12(2)	7(3)	4(2)
C(18)	33(2)	38(3)	39(2)	-10(2)	5(2)	1(2)
C(19)	29(2)	29(2)	26(2)	-4(2)	4(2)	-6(2)
C(20)	41(3)	43(3)	31(2)	-8(2)	8(2)	-3(2)
C(21)	66(4)	58(3)	26(2)	-8(2)	-2(2)	-9(3)
C(22)	52(3)	59(3)	38(3)	-4(2)	-19(2)	-3(3)
C(23)	38(3)	62(3)	50(3)	-9(3)	-10(2)	4(2)
C(24)	32(2)	43(3)	34(2)	-8(2)	-3(2)	3(2)
C(25)	31(2)	28(2)	31(2)	11(2)	-1(2)	0(2)
C(26)	30(2)	24(2)	25(2)	1(2)	9(2)	0(2)
C(27)	29(2)	23(2)	22(2)	-2(2)	5(2)	-1(2)
C(28)	29(2)	32(2)	30(2)	1(2)	0(2)	1(2)
C(29)	46(3)	27(2)	29(2)	6(2)	-5(2)	-4(2)
C(30)	44(3)	32(2)	35(2)	13(2)	1(2)	-8(2)
C(31)	31(2)	28(2)	29(2)	4(2)	12(2)	-3(2)
C(32)	45(3)	33(2)	26(2)	4(2)	4(2)	3(2)
C(33)	57(3)	37(3)	33(2)	14(2)	8(2)	5(2)
C(34)	66(3)	27(2)	47(3)	4(2)	18(3)	-5(2)
C(35)	54(3)	34(3)	41(3)	-3(2)	7(2)	-12(2)
C(36)	39(3)	39(3)	33(2)	6(2)	4(2)	-6(2)
C(37)	47(1)	84(2)	54(1)	10(1)	24(1)	11(1)
C(38)	47(1)	84(2)	54(1)	10(1)	24(1)	11(1)
C(39)	47(1)	84(2)	54(1)	10(1)	24(1)	11(1)
C(40)	47(1)	84(2)	54(1)	10(1)	24(1)	11(1)
C(41)	47(1)	84(2)	54(1)	10(1)	24(1)	11(1)
C(42)	47(1)	84(2)	54(1)	10(1)	24(1)	11(1)
C(43)	36(2)	24(2)	22(2)	1(2)	3(2)	6(2)
C(44)	63(3)	35(2)	28(2)	-1(2)	16(2)	-1(2)
C(45)	84(4)	42(3)	22(2)	-4(2)	11(2)	10(3)
C(46)	57(3)	46(3)	37(3)	-11(2)	-13(2)	12(3)
C(47)	38(3)	44(3)	45(3)	-4(2)	-1(2)	5(2)
C(48)	35(2)	35(2)	28(2)	4(2)	1(2)	4(2)

Table 5 Hydrogen coordinates ($x\ 10^4$) and isotropic displacement parameters ($Å^2\ x\ 10^3$) for **8**

	x	y	z	U(eq)
H(4)	3545	1986	9006	38
H(5)	2887	852	9353	42
H(8)	2588	3062	10001	39
H(9)	1488	2587	10292	47
H(10)	296	3013	9683	52
H(11)	196	3924	8786	49
H(12)	1307	4412	8498	41
H(14)	2100	5163	7936	42
H(15)	1754	6598	7731	50
H(16)	2229	7638	8522	59
H(17)	3026	7243	9505	60
H(18)	3342	5797	9726	45
H(20)	3138	4606	10382	46
H(21)	4157	4488	11279	62
H(22)	5278	3850	11178	66
H(23)	5405	3336	10170	64
H(24)	4414	3512	9252	46
H(28)	8529	-46	9121	38
H(29)	7853	-1153	9498	44
H(32)	6186	3465	5129	42
H(33)	6198	4981	5159	51
H(34)	6923	5697	6050	55
H(35)	7642	4927	6923	53
H(36)	7642	3417	6905	45
H(38)	7484	885	5160	72
H(39)	8622	560	4887	72
H(40)	9701	1315	5372	72
H(41)	9648	2490	6032	72
H(42)	8481	2864	6289	72

H(44)	6716	2213	4575	49
H(45)	5705	1881	3706	59
H(46)	4605	1265	3894	61
H(47)	4527	958	4948	53
H(48)	5510	1333	5833	40

Table 6 Torsion angles [°] for **8**

C(3)-Pd(2)-P(1)-C(19)	94.25(18)	P(2)-Pd(1)-N(4)-Se(2)	-33.1(6)
Cl(1)-Pd(2)-P(1)-C(19)	-74.64(14)	Cl(2)-Pd(1)-N(4)-Se(2)	77.68(15)
C(3)-Pd(2)-P(1)-C(13)	-145.44(17)	Pd(1)#1-Pd(1)-N(4)-Se(2)	174.96(18)
Cl(1)-Pd(2)-P(1)-C(13)	45.68(14)	N(1)#2-C(1)-C(2)-N(2)#2	-5.0(5)
C(3)-Pd(2)-P(1)-C(7)	-26.17(18)	C(6)-C(1)-C(2)-N(2)#2	175.0(3)
Cl(1)-Pd(2)-P(1)-C(7)	164.95(15)	N(1)#2-C(1)-C(2)-C(3)	170.8(3)
C(27)#1-Pd(1)-P(2)-C(43)	81.78(17)	C(6)-C(1)-C(2)-C(3)	-9.2(5)
N(4)-Pd(1)-P(2)-C(43)	15.1(5)	N(2)#2-C(2)-C(3)-C(4)	-176.7(4)
Cl(2)-Pd(1)-P(2)-C(43)	-95.32(14)	C(1)-C(2)-C(3)-C(4)	7.9(5)
Pd(1)#1-Pd(1)-P(2)-C(43)	164.99(13)	N(2)#2-C(2)-C(3)-Pd(2)	9.2(5)
C(27)#1-Pd(1)-P(2)-C(37)	-37.2(3)	C(1)-C(2)-C(3)-Pd(2)	-166.2(3)
N(4)-Pd(1)-P(2)-C(37)	-103.9(5)	N(2)-Pd(2)-C(3)-C(4)	93.1(3)
Cl(2)-Pd(1)-P(2)-C(37)	145.7(2)	P(1)-Pd(2)-C(3)-C(4)	-83.7(3)
Pd(1)#1-Pd(1)-P(2)-C(37)	46.0(2)	Cl(1)-Pd(2)-C(3)-C(4)	5.6(8)
C(27)#1-Pd(1)-P(2)-C(31)	-160.45(18)	N(2)-Pd(2)-C(3)-C(2)	-93.2(3)
N(4)-Pd(1)-P(2)-C(31)	132.8(5)	P(1)-Pd(2)-C(3)-C(2)	90.0(3)
Cl(2)-Pd(1)-P(2)-C(31)	22.44(15)	C(2)-C(3)-C(4)-C(5)	-1.6(6)
Pd(1)#1-Pd(1)-P(2)-C(31)	-77.25(15)	Pd(2)-C(3)-C(4)-C(5)	172.6(3)
N(2)-Se(1)-N(1)-C(1)#2	1.5(3)	C(3)-C(4)-C(5)-C(6)	-3.4(6)
N(1)-Se(1)-N(2)-C(2)#2	-4.2(3)	C(4)-C(5)-C(6)-C(1)	2.2(6)
N(1)-Se(1)-N(2)-Pd(2)	161.13(19)	C(4)-C(5)-C(6)-Br(1)	179.7(3)
C(3)-Pd(2)-N(2)-C(2)#2	49.3(3)	N(1)#2-C(1)-C(6)-C(5)	-176.1(4)
Cl(1)-Pd(2)-N(2)-C(2)#2	-141.8(3)	C(2)-C(1)-C(6)-C(5)	3.8(6)
C(3)-Pd(2)-N(2)-Se(1)	-112.25(19)	N(1)#2-C(1)-C(6)-Br(1)	6.3(6)
Cl(1)-Pd(2)-N(2)-Se(1)	56.67(17)	C(2)-C(1)-C(6)-Br(1)	-173.7(3)
N(4)-Se(2)-N(3)-C(25)	1.3(3)	C(19)-P(1)-C(7)-C(8)	-22.5(4)
N(3)-Se(2)-N(4)-C(26)	-1.4(3)	C(13)-P(1)-C(7)-C(8)	-135.0(3)
N(3)-Se(2)-N(4)-Pd(1)	165.9(2)	Pd(2)-P(1)-C(7)-C(8)	101.0(3)
C(27)#1-Pd(1)-N(4)-C(26)	63.8(4)	C(19)-P(1)-C(7)-C(12)	159.9(3)
P(2)-Pd(1)-N(4)-C(26)	130.2(4)	C(13)-P(1)-C(7)-C(12)	47.3(3)
Cl(2)-Pd(1)-N(4)-C(26)	-119.0(4)	Pd(2)-P(1)-C(7)-C(12)	-76.7(3)
Pd(1)#1-Pd(1)-N(4)-C(26)	-21.8(3)	C(12)-C(7)-C(8)-C(9)	-2.0(6)
C(27)#1-Pd(1)-N(4)-Se(2)	-99.53(19)	P(1)-C(7)-C(8)-C(9)	-179.6(3)

C(7)-C(8)-C(9)-C(10)	1.2(6)	Se(2)-N(3)-C(25)-C(26)	-1.0(5)
C(8)-C(9)-C(10)-C(11)	-0.1(7)	Se(2)-N(4)-C(26)-C(27)	-176.9(3)
C(9)-C(10)-C(11)-C(12)	-0.2(7)	Pd(1)-N(4)-C(26)-C(27)	19.1(6)
C(8)-C(7)-C(12)-C(11)	1.7(6)	Se(2)-N(4)-C(26)-C(25)	1.1(4)
P(1)-C(7)-C(12)-C(11)	179.4(3)	Pd(1)-N(4)-C(26)-C(25)	-162.9(3)
C(10)-C(11)-C(12)-C(7)	-0.6(6)	N(3)-C(25)-C(26)-N(4)	0.0(6)
C(19)-P(1)-C(13)-C(18)	-12.9(4)	C(30)-C(25)-C(26)-N(4)	178.2(4)
C(7)-P(1)-C(13)-C(18)	97.7(4)	N(3)-C(25)-C(26)-C(27)	178.0(4)
Pd(2)-P(1)-C(13)-C(18)	-135.1(3)	C(30)-C(25)-C(26)-C(27)	-3.8(6)
C(19)-P(1)-C(13)-C(14)	168.0(3)	N(4)-C(26)-C(27)-C(28)	-175.7(4)
C(7)-P(1)-C(13)-C(14)	-81.5(3)	C(25)-C(26)-C(27)-C(28)	6.5(6)
Pd(2)-P(1)-C(13)-C(14)	45.8(3)	N(4)-C(26)-C(27)-Pd(1)#1	5.2(5)
C(18)-C(13)-C(14)-C(15)	-2.8(6)	C(25)-C(26)-C(27)-Pd(1)#1	-172.6(3)
P(1)-C(13)-C(14)-C(15)	176.4(3)	C(26)-C(27)-C(28)-C(29)	-4.2(6)
C(13)-C(14)-C(15)-C(16)	2.1(7)	Pd(1)#1-C(27)-C(28)-C(29)	174.8(3)
C(14)-C(15)-C(16)-C(17)	-0.2(7)	C(27)-C(28)-C(29)-C(30)	-0.9(7)
C(15)-C(16)-C(17)-C(18)	-0.9(8)	C(28)-C(29)-C(30)-C(25)	3.9(7)
C(14)-C(13)-C(18)-C(17)	1.6(6)	C(28)-C(29)-C(30)-Br(2)	-177.6(3)
P(1)-C(13)-C(18)-C(17)	-177.5(4)	N(3)-C(25)-C(30)-C(29)	176.5(5)
C(16)-C(17)-C(18)-C(13)	0.2(7)	C(26)-C(25)-C(30)-C(29)	-1.6(7)
C(13)-P(1)-C(19)-C(24)	-117.0(3)	N(3)-C(25)-C(30)-Br(2)	-2.2(6)
C(7)-P(1)-C(19)-C(24)	133.6(3)	C(26)-C(25)-C(30)-Br(2)	179.8(3)
Pd(2)-P(1)-C(19)-C(24)	6.0(4)	C(43)-P(2)-C(31)-C(32)	-11.7(4)
C(13)-P(1)-C(19)-C(20)	62.0(4)	C(37)-P(2)-C(31)-C(32)	99.1(4)
C(7)-P(1)-C(19)-C(20)	-47.4(4)	Pd(1)-P(2)-C(31)-C(32)	-131.7(3)
Pd(2)-P(1)-C(19)-C(20)	-174.9(3)	C(43)-P(2)-C(31)-C(36)	170.1(3)
C(24)-C(19)-C(20)-C(21)	1.0(7)	C(37)-P(2)-C(31)-C(36)	-79.0(4)
P(1)-C(19)-C(20)-C(21)	-178.0(4)	Pd(1)-P(2)-C(31)-C(36)	50.1(4)
C(19)-C(20)-C(21)-C(22)	-1.6(8)	C(36)-C(31)-C(32)-C(33)	1.3(7)
C(20)-C(21)-C(22)-C(23)	0.5(8)	P(2)-C(31)-C(32)-C(33)	-176.8(3)
C(21)-C(22)-C(23)-C(24)	1.2(8)	C(31)-C(32)-C(33)-C(34)	-0.6(7)
C(22)-C(23)-C(24)-C(19)	-1.9(8)	C(32)-C(33)-C(34)-C(35)	-0.2(8)
C(20)-C(19)-C(24)-C(23)	0.8(7)	C(33)-C(34)-C(35)-C(36)	0.2(8)
P(1)-C(19)-C(24)-C(23)	179.8(4)	C(34)-C(35)-C(36)-C(31)	0.5(7)
Se(2)-N(3)-C(25)-C(30)	-179.1(4)	C(32)-C(31)-C(36)-C(35)	-1.2(7)

P(2)-C(31)-C(36)-C(35)	176.9(4)	C(37)-P(2)-C(43)-C(48)	144.0(4)
C(43)-P(2)-C(37)-C(38)	-31.9(5)	C(31)-P(2)-C(43)-C(48)	-105.9(3)
C(31)-P(2)-C(37)-C(38)	-142.1(5)	Pd(1)-P(2)-C(43)-C(48)	18.7(4)
Pd(1)-P(2)-C(37)-C(38)	88.8(5)	C(37)-P(2)-C(43)-C(44)	-39.8(4)
C(43)-P(2)-C(37)-C(42)	151.2(4)	C(31)-P(2)-C(43)-C(44)	70.3(4)
C(31)-P(2)-C(37)-C(42)	41.0(5)	Pd(1)-P(2)-C(43)-C(44)	-165.1(3)
Pd(1)-P(2)-C(37)-C(42)	-88.1(5)	C(48)-C(43)-C(44)-C(45)	0.3(6)
C(42)-C(37)-C(38)-C(39)	0.2(9)	P(2)-C(43)-C(44)-C(45)	-175.9(3)
P(2)-C(37)-C(38)-C(39)	-176.8(4)	C(43)-C(44)-C(45)-C(46)	-0.6(7)
C(37)-C(38)-C(39)-C(40)	2.3(8)	C(44)-C(45)-C(46)-C(47)	-0.5(7)
C(38)-C(39)-C(40)-C(41)	-3.6(9)	C(45)-C(46)-C(47)-C(48)	1.8(7)
C(39)-C(40)-C(41)-C(42)	2.5(9)	C(44)-C(43)-C(48)-C(47)	1.0(6)
C(38)-C(37)-C(42)-C(41)	-1.3(8)	P(2)-C(43)-C(48)-C(47)	177.3(3)
P(2)-C(37)-C(42)-C(41)	175.7(4)	C(46)-C(47)-C(48)-C(43)	-2.1(7)
C(40)-C(41)-C(42)-C(37)	0.0(8)		

Symmetry transformations used to generate equivalent atoms: #1 -x+3/2,y,-z+3/2
#2 -x+1/2,y,-z+3/2

Appendix five: Full crystallographic data of **10**

Table 1 Crystal data and structure refinement for **10**

Identification code	rb09006a	
Empirical formula	$C_{11}H_6BrN_3Se$	
Formula weight	339.06	
Temperature	173(2) K	
Wavelength	0.71073 Å	
Crystal system	Orthorhombic	
Space group	*P*bca	
Unit cell dimensions	*a* = 12.183(6) Å	α = 90°.
	b = 7.516(4) Å	β = 90°.
	c = 23.215(11) Å	γ = 90°.
Volume	2125.6(18) $Å^3$	
Z	8	
Density (calculated)	2.119 Mg/m^3	
Absorption coefficient	7.263 mm^{-1}	
F(000)	1296	
Crystal size	0.31 x 0.125 x 0.096 mm^3	
Theta range for data collection	1.75 to 25.49°.	
Index ranges	-14<=*h*<=14, -9<=*k*<=9, -28<=*l*<=28	
Reflections collected	23525	
Independent reflections	1977 [*R*(int) = 0.1081]	
Completeness to theta = 25.25°	100.0 %	
Absorption correction	Semi-empirical from equivalents	
Max. and min. transmission	0.5423 and 0.2117	
Refinement method	Full-matrix least-squares on F^2	
Data / restraints / parameters	1977 / 0 / 145	
Goodness-of-fit on F^2	1.138	
Final *R* indices [I>2sigma(I)]	*R*1 = 0.0526, *wR*2 = 0.1303	
R indices (all data)	*R*1 = 0.0735, *wR*2 = 0.1439	
Largest diff. peak and hole	1.723 and -0.685 e.$Å^{-3}$	

Table 2 Atomic coordinates (x 10^4) and equivalent isotropic displacement parameters ($Å^2$ x 10^3) for **10**. U(eq) is defined as one third of the trace of the orthogonalized U^{ij} tensor

	x	y	z	U(eq)
Se(1)	182(1)	9856(1)	5877(1)	28(1)
Br(1)	2698(1)	8069(1)	4335(1)	36(1)
N(1)	1008(5)	9191(8)	5276(3)	29(1)
N(2)	1327(5)	10102(8)	6349(2)	25(1)
N(3)	4073(6)	10769(10)	8048(3)	40(2)
C(1)	2032(5)	9192(8)	5455(3)	21(1)
C(2)	2218(5)	9689(9)	6047(3)	22(2)
C(3)	3320(6)	9760(9)	6277(3)	24(2)
C(4)	4149(6)	9352(10)	5905(3)	30(2)
C(5)	3973(6)	8834(10)	5326(3)	31(2)
C(6)	2944(6)	8760(10)	5102(3)	26(2)
C(7)	3540(6)	10192(9)	6895(3)	26(2)
C(8)	2850(6)	9618(11)	7326(3)	32(2)
C(9)	3142(7)	9943(11)	7892(3)	36(2)
C(10)	4727(7)	11290(11)	7625(3)	37(2)
C(11)	4501(6)	11041(10)	7048(3)	30(2)

Table 3 Bond lengths [Å] and angles [°] for **10**

Se(1)-N(2)	1.783(6)	C(6)-C(1)-C(2)	119.2(6)
Se(1)-N(1)	1.792(6)	N(2)-C(2)-C(1)	115.8(6)
Br(1)-C(6)	1.879(7)	N(2)-C(2)-C(3)	123.7(6)
N(1)-C(1)	1.315(9)	C(1)-C(2)-C(3)	120.5(6)
N(2)-C(2)	1.329(9)	C(4)-C(3)-C(2)	116.5(7)
N(3)-C(10)	1.326(10)	C(4)-C(3)-C(7)	121.6(6)
N(3)-C(9)	1.343(10)	C(2)-C(3)-C(7)	121.9(6)
C(1)-C(6)	1.419(9)	C(3)-C(4)-C(5)	123.4(7)
C(1)-C(2)	1.441(10)	C(3)-C(4)-H(4)	118.3
C(2)-C(3)	1.445(9)	C(5)-C(4)-H(4)	118.3
C(3)-C(4)	1.364(10)	C(6)-C(5)-C(4)	121.0(7)
C(3)-C(7)	1.497(10)	C(6)-C(5)-H(5)	119.5
C(4)-C(5)	1.415(11)	C(4)-C(5)-H(5)	119.5
C(4)-H(4)	0.9500	C(5)-C(6)-C(1)	119.4(7)
C(5)-C(6)	1.359(11)	C(5)-C(6)-Br(1)	121.5(5)
C(5)-H(5)	0.9500	C(1)-C(6)-Br(1)	119.1(5)
C(7)-C(8)	1.375(11)	C(8)-C(7)-C(11)	118.5(7)
C(7)-C(11)	1.380(10)	C(8)-C(7)-C(3)	121.3(7)
C(8)-C(9)	1.383(11)	C(11)-C(7)-C(3)	119.9(7)
C(8)-H(8)	0.9500	C(7)-C(8)-C(9)	118.6(7)
C(9)-H(9)	0.9500	C(7)-C(8)-H(8)	120.7
C(10)-C(11)	1.379(11)	C(9)-C(8)-H(8)	120.7
C(10)-H(10)	0.9500	N(3)-C(9)-C(8)	123.8(8)
C(11)-H(11)	0.9500	N(3)-C(9)-H(9)	118.1
		C(8)-C(9)-H(9)	118.1
N(2)-Se(1)-N(1)	93.9(3)	N(3)-C(10)-C(11)	124.0(7)
C(1)-N(1)-Se(1)	106.6(5)	N(3)-C(10)-H(10)	118.0
C(2)-N(2)-Se(1)	106.9(5)	C(11)-C(10)-H(10)	118.0
C(10)-N(3)-C(9)	116.3(7)	C(10)-C(11)-C(7)	118.8(7)
N(1)-C(1)-C(6)	124.0(7)	C(10)-C(11)-H(11)	120.6
N(1)-C(1)-C(2)	116.8(6)	C(7)-C(11)-H(11)	120.6

Symmetry transformations used to generate equivalent atoms

Table 4 Anisotropic displacement parameters ($Å^2$ x 10^3) for **10**. The anisotropic displacement factor exponent takes the form: $-2\pi^2$ [$h^2 a^{*2} U^{11}$ + ... + 2 h k a* b* U^{12}]

	U^{11}	U^{22}	U^{33}	U^{23}	U^{13}	U^{12}
Se(1)	17(1)	37(1)	29(1)	-3(1)	-2(1)	-1(1)
Br(1)	41(1)	38(1)	28(1)	-7(1)	1(1)	7(1)
N(1)	23(3)	34(3)	31(3)	-4(3)	-1(3)	2(3)
N(2)	21(3)	30(3)	24(3)	0(3)	-2(2)	0(3)
N(3)	35(4)	51(4)	33(4)	-2(3)	-10(3)	-4(3)
C(1)	20(4)	16(3)	27(4)	1(3)	3(3)	2(3)
C(2)	17(4)	19(3)	30(4)	2(3)	-3(3)	0(3)
C(3)	17(3)	25(4)	31(4)	6(3)	-4(3)	0(3)
C(4)	19(4)	33(4)	36(4)	-1(3)	2(3)	0(3)
C(5)	25(4)	33(4)	35(4)	2(3)	9(3)	4(3)
C(6)	26(4)	28(4)	24(4)	-5(3)	-1(3)	7(3)
C(7)	17(3)	21(4)	40(4)	7(3)	-4(3)	6(3)
C(8)	24(4)	37(4)	34(4)	-2(3)	-7(3)	2(3)
C(9)	33(4)	42(5)	31(4)	2(3)	-1(3)	3(4)
C(10)	32(5)	39(5)	39(5)	2(4)	-11(4)	-5(4)
C(11)	30(4)	23(4)	38(4)	4(3)	-1(3)	-2(3)

Table 5 Hydrogen coordinates (x 10^4) and isotropic displacement parameters ($Å^2$ x 10^3) for **10**

	x	y	z	U(eq)
H(4)	4883	9420	6042	35
H(5)	4584	8534	5091	37
H(8)	2188	9011	7236	38
H(9)	2656	9560	8187	43
H(10)	5393	11871	7724	44
H(11)	4998	11447	6761	36

Table 6 Torsion angles [°] for **10**

N(2)-Se(1)-N(1)-C(1)	0.0(5)	C(4)-C(5)-C(6)-Br(1)	-179.9(6)
N(1)-Se(1)-N(2)-C(2)	-0.2(5)	N(1)-C(1)-C(6)-C(5)	178.7(7)
Se(1)-N(1)-C(1)-C(6)	-179.1(6)	C(2)-C(1)-C(6)-C(5)	-0.5(10)
Se(1)-N(1)-C(1)-C(2)	0.1(8)	N(1)-C(1)-C(6)-Br(1)	-2.0(10)
Se(1)-N(2)-C(2)-C(1)	0.3(7)	C(2)-C(1)-C(6)-Br(1)	178.8(5)
Se(1)-N(2)-C(2)-C(3)	178.7(5)	C(4)-C(3)-C(7)-C(8)	-141.6(8)
N(1)-C(1)-C(2)-N(2)	-0.3(9)	C(2)-C(3)-C(7)-C(8)	36.2(10)
C(6)-C(1)-C(2)-N(2)	179.0(6)	C(4)-C(3)-C(7)-C(11)	32.4(10)
N(1)-C(1)-C(2)-C(3)	-178.8(6)	C(2)-C(3)-C(7)-C(11)	-149.9(7)
C(6)-C(1)-C(2)-C(3)	0.5(10)	C(11)-C(7)-C(8)-C(9)	1.0(11)
N(2)-C(2)-C(3)-C(4)	-177.8(7)	C(3)-C(7)-C(8)-C(9)	175.1(7)
C(1)-C(2)-C(3)-C(4)	0.6(10)	C(10)-N(3)-C(9)-C(8)	0.3(12)
N(2)-C(2)-C(3)-C(7)	4.3(11)	C(7)-C(8)-C(9)-N(3)	-1.0(12)
C(1)-C(2)-C(3)-C(7)	-177.3(6)	C(9)-N(3)-C(10)-C(11)	0.4(12)
C(2)-C(3)-C(4)-C(5)	-1.7(11)	N(3)-C(10)-C(11)-C(7)	-0.3(12)
C(7)-C(3)-C(4)-C(5)	176.2(7)	C(8)-C(7)-C(11)-C(10)	-0.4(11)
C(3)-C(4)-C(5)-C(6)	1.8(12)	C(3)-C(7)-C(11)-C(10)	-174.6(7)
C(4)-C(5)-C(6)-C(1)	-0.6(11)		

Symmetry transformations used to generate equivalent atoms:

Appendix six: Full crystallographic data of **13**

Table 1 Crystal data and structure refinement for **13**

Identification code	rb09019_0m	
Empirical formula	$C_{16}H_{10}N_4Se$	
Formula weight	337.24	
Temperature	173(2) K	
Wavelength	0.71073 Å	
Crystal system	Monoclinic	
Space group	*P*2(1)/c	
Unit cell dimensions	*a* = 15.3736(8) Å	*α* = 90°.
	b = 8.3764(4) Å	*β* = 93.1210(10)°.
	c = 20.5773(11) Å	*γ* = 90°.
Volume	2645.9(2) $Å^3$	
Z	8	
Density (calculated)	1.693 Mg/m^3	
Absorption coefficient	2.836 mm^{-1}	
F(000)	1344	
Crystal size	0.27 x 0.21 x 0.16 mm^3	
Theta range for data collection	1.98 to 27.26°.	
Index ranges	-19<=*h*<=19, -10<=*k*<=10, -26<=*l*<=26	
Reflections collected	36203	
Independent reflections	5929 [*R*(int) = 0.0224]	
Completeness to theta = 25.25°	100.0 %	
Absorption correction	None	
Max. and min. transmission	0.6566 and 0.5104	
Refinement method	Full-matrix least-squares on F^2	
Data / restraints / parameters	5929 / 0 / 379	
Goodness-of-fit on F^2	1.030	
Final *R* indices [I>2sigma(I)]	*R*1 = 0.0235, *wR*2 = 0.0613	
R indices (all data)	*R*1 = 0.0296, *wR*2 = 0.0644	
Largest diff. peak and hole	0.442 and -0.472 e.$Å^{-3}$	

Table 2 Atomic coordinates (x 10^4) and equivalent isotropic displacement parameters ($Å^2$ x 10^3) for **13**. U(eq) is defined as one third of the trace of the orthogonalized U^{ij} tensor

	x	y	z	U(eq)
Se(1)	10654(1)	2163(1)	10768(1)	37(1)
Se(1A)	4371(1)	7310(1)	524(1)	26(1)
N(1)	10480(1)	2897(2)	9960(1)	30(1)
N(2)	9592(1)	1346(2)	10806(1)	32(1)
N(3)	9243(1)	3755(2)	8025(1)	36(1)
N(4)	6874(1)	715(2)	10491(1)	27(1)
N(1A)	5000(1)	6004(2)	1048(1)	25(1)
N(2A)	5176(1)	7461(2)	-63(1)	24(1)
N(3A)	7099(1)	3160(2)	1895(1)	26(1)
N(4A)	7341(1)	6376(2)	-1194(1)	32(1)
C(1)	9668(1)	2512(2)	9761(1)	24(1)
C(2)	9172(1)	1646(2)	10238(1)	24(1)
C(3)	8280(1)	1199(2)	10086(1)	25(1)
C(4)	7942(1)	1613(2)	9486(1)	29(1)
C(5)	8422(1)	2418(2)	9022(1)	31(1)
C(6)	9271(1)	2882(2)	9128(1)	25(1)
C(7)	9718(1)	3686(2)	8594(1)	26(1)
C(8)	10552(1)	4315(3)	8655(1)	37(1)
C(9)	10907(1)	5004(3)	8116(1)	43(1)
C(10)	10432(1)	5038(3)	7534(1)	41(1)
C(11)	9605(1)	4406(3)	7515(1)	43(1)
C(12)	7732(1)	366(2)	10551(1)	25(1)
C(13)	8076(1)	-719(2)	11009(1)	31(1)
C(14)	7521(1)	-1432(2)	11424(1)	36(1)
C(15)	6649(1)	-1037(2)	11387(1)	35(1)
C(16)	6359(1)	22(2)	10912(1)	32(1)
C(1A)	5745(1)	5724(2)	765(1)	22(1)
C(2A)	5848(1)	6564(2)	152(1)	22(1)
C(3A)	6640(1)	6386(2)	-186(1)	22(1)
C(4A)	7271(1)	5434(2)	104(1)	24(1)

C(5A)	7162(1)	4602(2)	693(1)	24(1)
C(6A)	6420(1)	4687(2)	1031(1)	22(1)
C(7A)	6338(1)	3686(2)	1621(1)	23(1)
C(8A)	5543(1)	3233(2)	1857(1)	28(1)
C(9A)	5535(1)	2219(2)	2387(1)	31(1)
C(10A)	6315(1)	1663(2)	2666(1)	30(1)
C(11A)	7076(1)	2164(2)	2399(1)	29(1)
C(12A)	6777(1)	7138(2)	-825(1)	24(1)
C(13A)	6372(1)	8545(2)	-1029(1)	33(1)
C(14A)	6551(1)	9186(2)	-1625(1)	38(1)
C(15A)	7132(1)	8422(2)	-2003(1)	36(1)
C(16A)	7504(1)	7020(3)	-1767(1)	37(1)

Table 3 Bond lengths [Å] and angles [°] for **13**

Se(1)-N(2)	1.7749(15)	C(11)-H(11)	0.9500
Se(1)-N(1)	1.7796(15)	C(12)-C(13)	1.392(2)
Se(1A)-N(2A)	1.7802(14)	C(13)-C(14)	1.378(3)
Se(1A)-N(1A)	1.7826(14)	C(13)-H(13)	0.9500
N(1)-C(1)	1.333(2)	C(14)-C(15)	1.378(3)
N(2)-C(2)	1.330(2)	C(14)-H(14)	0.9500
N(3)-C(11)	1.332(2)	C(15)-C(16)	1.377(3)
N(3)-C(7)	1.346(2)	C(15)-H(15)	0.9500
N(4)-C(16)	1.336(2)	C(16)-H(16)	0.9500
N(4)-C(12)	1.351(2)	C(1A)-C(6A)	1.438(2)
N(1A)-C(1A)	1.334(2)	C(1A)-C(2A)	1.461(2)
N(2A)-C(2A)	1.333(2)	C(2A)-C(3A)	1.442(2)
N(3A)-C(11A)	1.333(2)	C(3A)-C(4A)	1.368(2)
N(3A)-C(7A)	1.346(2)	C(3A)-C(12A)	1.483(2)
N(4A)-C(16A)	1.333(2)	C(4A)-C(5A)	1.416(2)
N(4A)-C(12A)	1.344(2)	C(4A)-H(4A)	0.9500
C(1)-C(6)	1.443(2)	C(5A)-C(6A)	1.369(2)
C(1)-C(2)	1.465(2)	C(5A)-H(5A)	0.9500
C(2)-C(3)	1.440(2)	C(6A)-C(7A)	1.487(2)
C(3)-C(4)	1.359(2)	C(7A)-C(8A)	1.391(2)
C(3)-C(12)	1.482(2)	C(8A)-C(9A)	1.384(3)
C(4)-C(5)	1.410(2)	C(8A)-H(8A)	0.9500
C(4)-H(4)	0.9500	C(9A)-C(10A)	1.381(3)
C(5)-C(6)	1.369(2)	C(9A)-H(9A)	0.9500
C(5)-H(5)	0.9500	C(10A)-C(11A)	1.385(3)
C(6)-C(7)	1.487(2)	C(10A)-H(10A)	0.9500
C(7)-C(8)	1.385(2)	C(11A)-H(11A)	0.9500
C(8)-C(9)	1.388(3)	C(12A)-C(13A)	1.388(3)
C(8)-H(8)	0.9500	C(13A)-C(14A)	1.381(3)
C(9)-C(10)	1.367(3)	C(13A)-H(13A)	0.9500
C(9)-H(9)	0.9500	C(14A)-C(15A)	1.375(3)
C(10)-C(11)	1.375(3)	C(14A)-H(14A)	0.9500
C(10)-H(10)	0.9500	C(15A)-C(16A)	1.383(3)

C(15A)-H(15A)	0.9500	C(7)-C(8)-H(8)	120.4
C(16A)-H(16A)	0.9500	C(9)-C(8)-H(8)	120.4
		C(10)-C(9)-C(8)	119.49(18)
N(2)-Se(1)-N(1)	94.82(7)	C(10)-C(9)-H(9)	120.3
N(2A)-Se(1A)-N(1A)	94.57(6)	C(8)-C(9)-H(9)	120.3
C(1)-N(1)-Se(1)	106.99(12)	C(9)-C(10)-C(11)	117.81(18)
C(2)-N(2)-Se(1)	106.93(12)	C(9)-C(10)-H(10)	121.1
C(11)-N(3)-C(7)	118.25(16)	C(11)-C(10)-H(10)	121.1
C(16)-N(4)-C(12)	117.21(16)	N(3)-C(11)-C(10)	124.03(19)
C(1A)-N(1A)-Se(1A)	107.15(11)	N(3)-C(11)-H(11)	118.0
C(2A)-N(2A)-Se(1A)	106.85(11)	C(10)-C(11)-H(11)	118.0
C(11A)-N(3A)-C(7A)	118.17(15)	N(4)-C(12)-C(13)	122.38(16)
C(16A)-N(4A)-C(12A)	117.84(16)	N(4)-C(12)-C(3)	115.20(15)
N(1)-C(1)-C(6)	124.54(16)	C(13)-C(12)-C(3)	122.41(16)
N(1)-C(1)-C(2)	115.35(15)	C(14)-C(13)-C(12)	118.57(18)
C(6)-C(1)-C(2)	120.10(15)	C(14)-C(13)-H(13)	120.7
N(2)-C(2)-C(3)	123.55(15)	C(12)-C(13)-H(13)	120.7
N(2)-C(2)-C(1)	115.91(15)	C(13)-C(14)-C(15)	119.66(18)
C(3)-C(2)-C(1)	120.53(15)	C(13)-C(14)-H(14)	120.2
C(4)-C(3)-C(2)	116.28(15)	C(15)-C(14)-H(14)	120.2
C(4)-C(3)-C(12)	120.30(15)	C(16)-C(15)-C(14)	118.08(17)
C(2)-C(3)-C(12)	123.40(15)	C(16)-C(15)-H(15)	121.0
C(3)-C(4)-C(5)	123.36(16)	C(14)-C(15)-H(15)	121.0
C(3)-C(4)-H(4)	118.3	N(4)-C(16)-C(15)	124.01(18)
C(5)-C(4)-H(4)	118.3	N(4)-C(16)-H(16)	118.0
C(6)-C(5)-C(4)	123.88(17)	C(15)-C(16)-H(16)	118.0
C(6)-C(5)-H(5)	118.1	N(1A)-C(1A)-C(6A)	124.09(15)
C(4)-C(5)-H(5)	118.1	N(1A)-C(1A)-C(2A)	115.32(14)
C(5)-C(6)-C(1)	115.82(15)	C(6A)-C(1A)-C(2A)	120.59(14)
C(5)-C(6)-C(7)	119.02(16)	N(2A)-C(2A)-C(3A)	123.90(15)
C(1)-C(6)-C(7)	125.15(15)	N(2A)-C(2A)-C(1A)	116.06(14)
N(3)-C(7)-C(8)	121.12(16)	C(3A)-C(2A)-C(1A)	120.04(14)
N(3)-C(7)-C(6)	114.29(15)	C(4A)-C(3A)-C(2A)	116.60(15)
C(8)-C(7)-C(6)	124.59(16)	C(4A)-C(3A)-C(12A)	120.12(15)
C(7)-C(8)-C(9)	119.27(18)	C(2A)-C(3A)-C(12A)	123.25(15)

C(3A)-C(4A)-C(5A)	123.09(15)	C(11A)-C(10A)-H(10A)	121.1
C(3A)-C(4A)-H(4A)	118.5	N(3A)-C(11A)-C(10A)	123.84(17)
C(5A)-C(4A)-H(4A)	118.5	N(3A)-C(11A)-H(11A)	118.1
C(6A)-C(5A)-C(4A)	123.31(16)	C(10A)-C(11A)-H(11A)	118.1
C(6A)-C(5A)-H(5A)	118.3	N(4A)-C(12A)-C(13A)	121.64(16)
C(4A)-C(5A)-H(5A)	118.3	N(4A)-C(12A)-C(3A)	115.29(15)
C(5A)-C(6A)-C(1A)	116.29(15)	C(13A)-C(12A)-C(3A)	123.05(15)
C(5A)-C(6A)-C(7A)	119.70(15)	C(14A)-C(13A)-C(12A)	119.41(17)
C(1A)-C(6A)-C(7A)	123.96(14)	C(14A)-C(13A)-H(13A)	120.3
N(3A)-C(7A)-C(8A)	121.65(15)	C(12A)-C(13A)-H(13A)	120.3
N(3A)-C(7A)-C(6A)	114.58(14)	C(15A)-C(14A)-C(13A)	119.31(18)
C(8A)-C(7A)-C(6A)	123.66(15)	C(15A)-C(14A)-H(14A)	120.3
C(9A)-C(8A)-C(7A)	119.18(16)	C(13A)-C(14A)-H(14A)	120.3
C(9A)-C(8A)-H(8A)	120.4	C(14A)-C(15A)-C(16A)	117.73(17)
C(7A)-C(8A)-H(8A)	120.4	C(14A)-C(15A)-H(15A)	121.1
C(10A)-C(9A)-C(8A)	119.37(17)	C(16A)-C(15A)-H(15A)	121.1
C(10A)-C(9A)-H(9A)	120.3	N(4A)-C(16A)-C(15A)	124.06(18)
C(8A)-C(9A)-H(9A)	120.3	N(4A)-C(16A)-H(16A)	118.0
C(9A)-C(10A)-C(11A)	117.78(17)	C(15A)-C(16A)-H(16A)	118.0
C(9A)-C(10A)-H(10A)	121.1		

Symmetry transformations used to generate equivalent atoms:

Table 4 Anisotropic displacement parameters ($Å^2$ x 10^3) for **13**. The anisotropic displacement factor exponent takes the form: $-2\pi^2 [h^2 a^{*2} U^{11} + ... + 2 h k a^* b^* U^{12}]$

	U^{11}	U^{22}	U^{33}	U^{23}	U^{13}	U^{12}
Se(1)	29(1)	52(1)	27(1)	1(1)	-7(1)	-6(1)
Se(1A)	24(1)	25(1)	31(1)	-2(1)	4(1)	4(1)
N(1)	25(1)	39(1)	27(1)	0(1)	-1(1)	-3(1)
N(2)	31(1)	39(1)	26(1)	0(1)	-1(1)	-5(1)
N(3)	30(1)	50(1)	28(1)	8(1)	2(1)	-5(1)
N(4)	27(1)	27(1)	28(1)	-3(1)	5(1)	-5(1)
N(1A)	25(1)	24(1)	26(1)	-3(1)	3(1)	1(1)
N(2A)	24(1)	22(1)	27(1)	-2(1)	2(1)	-1(1)
N(3A)	26(1)	30(1)	22(1)	-2(1)	-2(1)	-1(1)
N(4A)	32(1)	40(1)	25(1)	2(1)	4(1)	7(1)
C(1)	22(1)	26(1)	25(1)	-3(1)	2(1)	2(1)
C(2)	26(1)	26(1)	21(1)	-1(1)	2(1)	1(1)
C(3)	24(1)	26(1)	25(1)	-1(1)	5(1)	0(1)
C(4)	20(1)	40(1)	29(1)	4(1)	1(1)	-2(1)
C(5)	24(1)	44(1)	25(1)	7(1)	0(1)	0(1)
C(6)	22(1)	28(1)	26(1)	1(1)	3(1)	1(1)
C(7)	25(1)	28(1)	27(1)	2(1)	4(1)	2(1)
C(8)	29(1)	48(1)	34(1)	7(1)	0(1)	-8(1)
C(9)	33(1)	53(1)	44(1)	11(1)	5(1)	-13(1)
C(10)	41(1)	46(1)	38(1)	13(1)	11(1)	-4(1)
C(11)	40(1)	59(1)	30(1)	12(1)	2(1)	-4(1)
C(12)	29(1)	24(1)	23(1)	-4(1)	5(1)	-3(1)
C(13)	36(1)	31(1)	25(1)	-1(1)	4(1)	-1(1)
C(14)	51(1)	32(1)	25(1)	2(1)	4(1)	-7(1)
C(15)	45(1)	32(1)	27(1)	-7(1)	12(1)	-15(1)
C(16)	32(1)	32(1)	32(1)	-8(1)	9(1)	-9(1)
C(1A)	23(1)	20(1)	23(1)	-5(1)	2(1)	-3(1)
C(2A)	24(1)	19(1)	22(1)	-4(1)	0(1)	-2(1)
C(3A)	24(1)	21(1)	22(1)	-3(1)	2(1)	-4(1)
C(4A)	22(1)	27(1)	24(1)	-2(1)	3(1)	-4(1)

C(5A)	22(1)	25(1)	25(1)	-2(1)	-1(1)	-1(1)
C(6A)	23(1)	21(1)	21(1)	-3(1)	0(1)	-3(1)
C(7A)	26(1)	21(1)	21(1)	-4(1)	0(1)	-1(1)
C(8A)	25(1)	30(1)	29(1)	1(1)	3(1)	0(1)
C(9A)	31(1)	32(1)	30(1)	1(1)	9(1)	-2(1)
C(10A)	40(1)	29(1)	22(1)	1(1)	4(1)	1(1)
C(11A)	31(1)	33(1)	23(1)	-2(1)	-2(1)	4(1)
C(12A)	24(1)	25(1)	22(1)	-3(1)	0(1)	-6(1)
C(13A)	42(1)	24(1)	35(1)	1(1)	11(1)	0(1)
C(14A)	50(1)	26(1)	37(1)	5(1)	6(1)	1(1)
C(15A)	46(1)	38(1)	23(1)	2(1)	3(1)	-5(1)
C(16A)	39(1)	48(1)	23(1)	0(1)	5(1)	7(1)

Table 5 Hydrogen coordinates ($x\ 10^4$) and isotropic displacement parameters ($Å^2\ x\ 10^3$) for **13**

	x	y	z	U(eq)
H(4)	7352	1346	9373	35
H(5)	8139	2652	8611	37
H(8)	10877	4276	9060	45
H(9)	11477	5448	8150	52
H(10)	10665	5483	7157	49
H(11)	9272	4437	7113	51
H(13)	8680	-962	11034	37
H(14)	7737	-2193	11735	43
H(15)	6260	-1483	11681	42
H(16)	5756	275	10881	38
H(4A)	7808	5325	-100	29
H(5A)	7627	3952	863	29
H(8A)	5012	3616	1656	33
H(9A)	4999	1908	2558	37
H(10A)	6328	959	3028	36
H(11A)	7614	1776	2586	35
H(13A)	5974	9063	-760	40
H(14A)	6276	10145	-1772	45
H(15A)	7273	8843	-2413	43
H(16A)	7901	6482	-2030	44

Table 6 Torsion angles [°] for **13**

N(2)-Se(1)-N(1)-C(1)	-0.07(13)	C(7)-C(8)-C(9)-C(10)	-0.5(3)
N(1)-Se(1)-N(2)-C(2)	-0.05(13)	C(8)-C(9)-C(10)-C(11)	1.3(3)
N(2A)-Se(1A)-N(1A)-C(1A)	-1.24(11)	C(7)-N(3)-C(11)-C(10)	-1.0(3)
N(1A)-Se(1A)-N(2A)-C(2A)	0.03(11)	C(9)-C(10)-C(11)-N(3)	-0.5(4)
Se(1)-N(1)-C(1)-C(6)	-179.51(14)	C(16)-N(4)-C(12)-C(13)	2.8(2)
Se(1)-N(1)-C(1)-C(2)	0.17(18)	C(16)-N(4)-C(12)-C(3)	-178.32(15)
Se(1)-N(2)-C(2)-C(3)	-178.48(14)	C(4)-C(3)-C(12)-N(4)	-30.2(2)
Se(1)-N(2)-C(2)-C(1)	0.16(19)	C(2)-C(3)-C(12)-N(4)	148.47(16)
N(1)-C(1)-C(2)-N(2)	-0.2(2)	C(4)-C(3)-C(12)-C(13)	148.77(18)
C(6)-C(1)-C(2)-N(2)	179.46(16)	C(2)-C(3)-C(12)-C(13)	-32.6(3)
N(1)-C(1)-C(2)-C(3)	178.45(16)	N(4)-C(12)-C(13)-C(14)	-1.5(3)
C(6)-C(1)-C(2)-C(3)	-1.9(2)	C(3)-C(12)-C(13)-C(14)	179.66(16)
N(2)-C(2)-C(3)-C(4)	179.12(17)	C(12)-C(13)-C(14)-C(15)	-1.3(3)
C(1)-C(2)-C(3)-C(4)	0.5(2)	C(13)-C(14)-C(15)-C(16)	2.6(3)
N(2)-C(2)-C(3)-C(12)	0.5(3)	C(12)-N(4)-C(16)-C(15)	-1.3(3)
C(1)-C(2)-C(3)-C(12)	-178.12(15)	C(14)-C(15)-C(16)-N(4)	-1.3(3)
C(2)-C(3)-C(4)-C(5)	0.7(3)	Se(1A)-N(1A)-C(1A)-C(6A)	-178.41(13)
C(12)-C(3)-C(4)-C(5)	179.44(17)	Se(1A)-N(1A)-C(1A)-C(2A)	2.09(17)
C(3)-C(4)-C(5)-C(6)	-0.7(3)	Se(1A)-N(2A)-C(2A)-C(3A)	-179.34(13)
C(4)-C(5)-C(6)-C(1)	-0.6(3)	Se(1A)-N(2A)-C(2A)-C(1A)	1.15(17)
C(4)-C(5)-C(6)-C(7)	178.36(17)	N(1A)-C(1A)-C(2A)-N(2A)	-2.3(2)
N(1)-C(1)-C(6)-C(5)	-178.52(17)	C(6A)-C(1A)-C(2A)-N(2A)	178.19(14)
C(2)-C(1)-C(6)-C(5)	1.8(2)	N(1A)-C(1A)-C(2A)-C(3A)	178.18(14)
N(1)-C(1)-C(6)-C(7)	2.6(3)	C(6A)-C(1A)-C(2A)-C(3A)	-1.3(2)
C(2)-C(1)-C(6)-C(7)	-177.07(16)	N(2A)-C(2A)-C(3A)-C(4A)	179.33(15)
C(11)-N(3)-C(7)-C(8)	1.8(3)	C(1A)-C(2A)-C(3A)-C(4A)	-1.2(2)
C(11)-N(3)-C(7)-C(6)	-177.73(18)	N(2A)-C(2A)-C(3A)-C(12A)	-2.4(2)
C(5)-C(6)-C(7)-N(3)	-5.5(2)	C(1A)-C(2A)-C(3A)-C(12A)	177.08(14)
C(1)-C(6)-C(7)-N(3)	173.40(17)	C(2A)-C(3A)-C(4A)-C(5A)	2.2(2)
C(5)-C(6)-C(7)-C(8)	175.07(19)	C(12A)-C(3A)-C(4A)-C(5A)	-176.07(15)
C(1)-C(6)-C(7)-C(8)	-6.1(3)	C(3A)-C(4A)-C(5A)-C(6A)	-0.8(3)
N(3)-C(7)-C(8)-C(9)	-1.0(3)	C(4A)-C(5A)-C(6A)-C(1A)	-1.8(2)
C(6)-C(7)-C(8)-C(9)	178.40(19)	C(4A)-C(5A)-C(6A)-C(7A)	175.72(15)

N(1A)-C(1A)-C(6A)-C(5A)	-176.71(15)	C(7A)-N(3A)-C(11A)-C(10A)	-1.3(3)
C(2A)-C(1A)-C(6A)-C(5A)	2.8(2)	C(9A)-C(10A)-C(11A)-N(3A)	0.6(3)
N(1A)-C(1A)-C(6A)-C(7A)	5.9(2)	C(16A)-N(4A)-C(12A)-C(13A)	0.3(3)
C(2A)-C(1A)-C(6A)-C(7A)	-174.65(14)	C(16A)-N(4A)-C(12A)-C(3A)	-178.51(16)
C(11A)-N(3A)-C(7A)-C(8A)	1.0(2)	C(4A)-C(3A)-C(12A)-N(4A)	25.1(2)
C(11A)-N(3A)-C(7A)-C(6A)	-175.43(15)	C(2A)-C(3A)-C(12A)-N(4A)	-153.13(16)
C(5A)-C(6A)-C(7A)-N(3A)	20.5(2)	C(4A)-C(3A)-C(12A)-C(13A)	-153.69(17)
C(1A)-C(6A)-C(7A)-N(3A)	-162.17(15)	C(2A)-C(3A)-C(12A)-C(13A)	28.1(2)
C(5A)-C(6A)-C(7A)-C(8A)	-155.81(17)	N(4A)-C(12A)-C(13A)-C(14A)	-0.2(3)
C(1A)-C(6A)-C(7A)-C(8A)	21.5(2)	C(3A)-C(12A)-C(13A)-C(14A)	178.52(17)
N(3A)-C(7A)-C(8A)-C(9A)	0.1(3)	C(12A)-C(13A)-C(14A)-C(15A)	-0.4(3)
C(6A)-C(7A)-C(8A)-C(9A)	176.13(16)	C(13A)-C(14A)-C(15A)-C(16A)	0.8(3)
C(7A)-C(8A)-C(9A)-C(10A)	-0.8(3)	C(12A)-N(4A)-C(16A)-C(15A)	0.2(3)
C(8A)-C(9A)-C(10A)-C(11A)	0.4(3)	C(14A)-C(15A)-C(16A)-N(4A)	-0.7(3)

Symmetry transformations used to generate equivalent atoms:

Appendix seven: Full crystallographic data of **16**

Table 1 Crystal data and structure refinement for **16**

Identification code	rb08044_0m	
Empirical formula	$C_{20}H_{14}N_2$	
Formula weight	282.33	
Temperature	173(2) K	
Wavelength	0.71073 Å	
Crystal system	Monoclinic	
Space group	*P*2(1)/n	
Unit cell dimensions	*a* = 9.096(6) Å	α = 90°.
	b = 5.954(4) Å	β = 103.849(7)°.
	c = 13.447(9) Å	γ = 90°.
Volume	707.0(8) $Å^3$	
Z	4	
Density (calculated)	2.652 Mg/m^3	
Absorption coefficient	0.157 mm^{-1}	
F(000)	592	
Crystal size	0.31 x 0.18 x 0.09 mm^3	
Theta range for data collection	2.46 to 28.62°.	
Index ranges	-12<=*h*<=11, -8<=*k*<=7, -17<=*l*<=17	
Reflections collected	9908	
Independent reflections	1740 [*R*(int) = 0.0296]	
Completeness to theta = 25.00°	100.0 %	
Absorption correction	None	
Max. and min. transmission	0.9866 and 0.9523	
Refinement method	Full-matrix least-squares on F^2	
Data / restraints / parameters	1740 / 0 / 100	
Goodness-of-fit on F^2	1.040	
Final *R* indices [I>2sigma(I)]	*R*1 = 0.0425, *wR*2 = 0.1004	
R indices (all data)	*R*1 = 0.0555, *wR*2 = 0.1075	
Largest diff. peak and hole	0.283 and -0.230 e.$Å^{-3}$	

Table 2 Atomic coordinates (x 10^4) and equivalent isotropic displacement parameters ($Å^2$ x 10^3) for **16**. U(eq) is defined as one third of the trace of the orthogonalized U^{ij} tensor

	x	y	z	U(eq)
N(1)	3903(1)	6284(2)	8372(1)	30(1)
C(1)	1817(1)	1562(2)	10045(1)	23(1)
C(2)	2660(2)	911(2)	10989(1)	27(1)
C(3)	2047(2)	-508(2)	11627(1)	27(1)
C(8)	-599(1)	1296(2)	8690(1)	26(1)
C(9)	308(1)	737(2)	9682(1)	22(1)
C(11)	2497(1)	3172(2)	9428(1)	24(1)
C(12)	1859(2)	5270(2)	9132(1)	28(1)
C(13)	2593(2)	6743(2)	8614(1)	29(1)
C(14)	4501(2)	4260(2)	8656(1)	29(1)
C(15)	3853(1)	2677(2)	9169(1)	26(1)

Table 3 Bond lengths [Å] and angles [°] for **16**

N(1)-C(13)	1.3365(19)	C(1)-C(2)-H(2)	119.4
N(1)-C(14)	1.3396(19)	C(3)-C(2)-H(2)	119.4
C(1)-C(2)	1.372(2)	C(8)#1-C(3)-C(2)	120.53(12)
C(1)-C(9)	1.4298(19)	C(8)#1-C(3)-H(3)	119.7
C(1)-C(11)	1.4952(17)	C(2)-C(3)-H(3)	119.7
C(2)-C(3)	1.4104(18)	C(3)#1-C(8)-C(9)	120.57(12)
C(2)-H(2)	0.9500	C(3)#1-C(8)-H(8)	119.7
C(3)-C(8)#1	1.3670(19)	C(9)-C(8)-H(8)	119.7
C(3)-H(3)	0.9500	C(8)-C(9)-C(1)	122.11(11)
C(8)-C(3)#1	1.3670(19)	C(8)-C(9)-C(9)#1	118.70(14)
C(8)-C(9)	1.4292(19)	C(1)-C(9)-C(9)#1	119.17(14)
C(8)-H(8)	0.9500	C(15)-C(11)-C(12)	116.82(12)
C(9)-C(9)#1	1.431(2)	C(15)-C(11)-C(1)	120.84(12)
C(11)-C(15)	1.3906(19)	C(12)-C(11)-C(1)	122.25(12)
C(11)-C(12)	1.395(2)	C(13)-C(12)-C(11)	119.52(12)
C(12)-C(13)	1.3858(18)	C(13)-C(12)-H(12)	120.2
C(12)-H(12)	0.9500	C(11)-C(12)-H(12)	120.2
C(13)-H(13)	0.9500	N(1)-C(13)-C(12)	123.90(13)
C(14)-C(15)	1.3810(19)	N(1)-C(13)-H(13)	118.1
C(14)-H(14)	0.9500	C(12)-C(13)-H(13)	118.1
C(15)-H(15)	0.9500	N(1)-C(14)-C(15)	124.30(13)
		N(1)-C(14)-H(14)	117.8
C(13)-N(1)-C(14)	116.06(11)	C(15)-C(14)-H(14)	117.8
C(2)-C(1)-C(9)	119.84(11)	C(14)-C(15)-C(11)	119.39(13)
C(2)-C(1)-C(11)	118.74(12)	C(14)-C(15)-H(15)	120.3
C(9)-C(1)-C(11)	121.41(11)	C(11)-C(15)-H(15)	120.3
C(1)-C(2)-C(3)	121.13(12)		

Symmetry transformations used to generate equivalent atoms: #1 -x,-y,-z+2

Table 4 Anisotropic displacement parameters ($Å^2$ x 10^3) for **16**. The anisotropic displacement factor exponent takes the form: $-2\pi^2$ [$h^2 a^{*2} U^{11}$ + ... + 2 h k a* b* U^{12}]

	U^{11}	U^{22}	U^{33}	U^{23}	U^{13}	U^{12}
N(1)	32(1)	30(1)	29(1)	2(1)	11(1)	-7(1)
C(1)	26(1)	19(1)	29(1)	-1(1)	13(1)	-1(1)
C(2)	26(1)	26(1)	31(1)	-1(1)	9(1)	-5(1)
C(3)	29(1)	27(1)	26(1)	2(1)	6(1)	-1(1)
C(8)	29(1)	23(1)	27(1)	1(1)	12(1)	-2(1)
C(9)	24(1)	17(1)	28(1)	-2(1)	12(1)	0(1)
C(11)	26(1)	23(1)	25(1)	-2(1)	8(1)	-5(1)
C(12)	28(1)	24(1)	35(1)	-2(1)	14(1)	-1(1)
C(13)	33(1)	22(1)	31(1)	1(1)	8(1)	-2(1)
C(14)	25(1)	34(1)	31(1)	0(1)	11(1)	-3(1)
C(15)	26(1)	24(1)	30(1)	1(1)	9(1)	0(1)

Table 5 Hydrogen coordinates (x 10^4) and isotropic displacement parameters ($Å^2$ x 10^3) for **16**

	x	y	z	U(eq)
H(2)	3674	1425	11217	33
H(3)	2646	-919	12282	33
H(8)	-191	2223	8247	31
H(12)	929	5687	9283	34
H(13)	2138	8163	8420	34
H(14)	5432	3890	8494	35
H(15)	4328	1262	9343	32

Table 6 Torsion angles [°] for **16**

C(9)-C(1)-C(2)-C(3)	-2.10(19)
C(11)-C(1)-C(2)-C(3)	176.58(11)
C(1)-C(2)-C(3)-C(8)#1	1.0(2)
C(3)#1-C(8)-C(9)-C(1)	-178.89(12)
C(3)#1-C(8)-C(9)-C(9)#1	2.5(2)
C(2)-C(1)-C(9)-C(8)	-177.67(12)
C(11)-C(1)-C(9)-C(8)	3.69(18)
C(2)-C(1)-C(9)-C(9)#1	0.9(2)
C(11)-C(1)-C(9)-C(9)#1	-177.76(13)
C(2)-C(1)-C(11)-C(15)	57.27(17)
C(9)-C(1)-C(11)-C(15)	-124.07(14)
C(2)-C(1)-C(11)-C(12)	-119.29(14)
C(9)-C(1)-C(11)-C(12)	59.37(17)
C(15)-C(11)-C(12)-C(13)	-0.65(18)
C(1)-C(11)-C(12)-C(13)	176.04(12)
C(14)-N(1)-C(13)-C(12)	0.30(19)
C(11)-C(12)-C(13)-N(1)	0.0(2)
C(13)-N(1)-C(14)-C(15)	0.0(2)
N(1)-C(14)-C(15)-C(11)	-0.7(2)
C(12)-C(11)-C(15)-C(14)	0.95(18)
C(1)-C(11)-C(15)-C(14)	-175.79(12)

Symmetry transformations used to generate equivalent atoms: #1 -x,-y,-z+2

Appendix eight: Full crystallographic data of **18**

Table 1 Crystal data and structure refinement for **18**

Identification code	rb09031	
Empirical formula	$C_6H_3BrNO_4Re$	
Formula weight	419.20	
Temperature	173(2) K	
Wavelength	0.71073 Å	
Crystal system	Triclinic	
Space group	*P*-1	
Unit cell dimensions	*a* = 5.8624(4) Å	α = 94.1040(10)°.
	b = 7.2614(5) Å	β = 103.2590(10)°.
	c = 12.5469(8) Å	γ = 103.6670(10)°.
Volume	500.67(6) $Å^3$	
Z	2	
Density (calculated)	2.781 Mg/m^3	
Absorption coefficient	16.107 mm^{-1}	
F(000)	376	
Crystal size	0.20 x 0.14 x 0.08 mm^3	
Theta range for data collection	2.91 to 28.70°.	
Index ranges	-7<=*h*<=7, -9<=*k*<=9, -16<=*l*<=16	
Reflections collected	7388	
Independent reflections	2407 [*R*(int) = 0.0966]	
Completeness to theta = 25.00°	99.7 %	
Absorption correction	None	
Max. and min. transmission	0.3553 and 0.1410	
Refinement method	Full-matrix least-squares on F^2	
Data / restraints / parameters	2407 / 0 / 119	
Goodness-of-fit on F^2	1.062	
Final *R* indices [I>2sigma(I)]	*R*1 = 0.0265, *wR*2 = 0.0674	
R indices (all data)	*R*1 = 0.0280, *wR*2 = 0.0680	
Largest diff. peak and hole	2.836 and -1.410 e.$Å^{-3}$	

Table 2 Atomic coordinates (x 10^4) and equivalent isotropic displacement parameters ($Å^2$ x 10^3) for **18**. U(eq) is defined as one third of the trace of the orthogonalized U^{ij} tensor

	x	y	z	U(eq)
Re(1)	5794(1)	7729(1)	7854(1)	25(1)
Br(1)	7213(1)	7589(1)	6029(1)	31(1)
O(1)	8674(8)	4710(6)	8595(5)	54(1)
O(2)	10370(7)	10942(6)	8943(4)	46(1)
O(3)	3402(8)	10964(6)	7034(5)	52(1)
O(4)	3944(8)	7769(6)	9944(4)	54(1)
N(1)	2691(7)	5500(5)	6977(4)	30(1)
C(1)	7588(9)	5773(7)	8337(5)	35(1)
C(2)	8636(9)	9744(7)	8547(5)	33(1)
C(3)	4157(9)	9750(7)	7308(5)	35(1)
C(4)	4655(9)	7729(7)	9170(5)	38(1)
C(5)	1031(8)	4347(6)	6511(4)	28(1)
C(6)	-1093(8)	2875(6)	5905(5)	38(1)

Table 3 Bond lengths [Å] and angles [°] for **18**

Re(1)-C(2)	1.917(5)	C(2)-Re(1)-N(1)	176.09(17)
Re(1)-C(4)	1.918(6)	C(4)-Re(1)-N(1)	92.05(19)
Re(1)-C(1)	2.006(5)	C(1)-Re(1)-N(1)	90.19(19)
Re(1)-C(3)	2.013(5)	C(3)-Re(1)-N(1)	91.38(18)
Re(1)-N(1)	2.139(4)	C(2)-Re(1)-Br(1)	90.53(16)
Re(1)-Br(1)	2.6125(5)	C(4)-Re(1)-Br(1)	177.58(15)
O(1)-C(1)	1.131(6)	C(1)-Re(1)-Br(1)	88.42(16)
O(2)-C(2)	1.151(6)	C(3)-Re(1)-Br(1)	88.14(16)
O(3)-C(3)	1.118(6)	N(1)-Re(1)-Br(1)	85.62(11)
O(4)-C(4)	1.142(8)	C(5)-N(1)-Re(1)	178.8(4)
N(1)-C(5)	1.129(6)	O(1)-C(1)-Re(1)	177.3(4)
C(5)-C(6)	1.446(6)	O(2)-C(2)-Re(1)	178.3(5)
C(6)-H(6A)	0.9800	O(3)-C(3)-Re(1)	175.1(5)
C(6)-H(6B)	0.9800	O(4)-C(4)-Re(1)	178.0(5)
C(6)-H(6C)	0.9800	N(1)-C(5)-C(6)	179.5(5)
		C(5)-C(6)-H(6A)	109.5
C(2)-Re(1)-C(4)	91.8(2)	C(5)-C(6)-H(6B)	109.5
C(2)-Re(1)-C(1)	90.3(2)	H(6A)-C(6)-H(6B)	109.5
C(4)-Re(1)-C(1)	90.9(2)	C(5)-C(6)-H(6C)	109.5
C(2)-Re(1)-C(3)	87.9(2)	H(6A)-C(6)-H(6C)	109.5
C(4)-Re(1)-C(3)	92.6(2)	H(6B)-C(6)-H(6C)	109.5
C(1)-Re(1)-C(3)	176.10(18)		

Symmetry transformations used to generate equivalent atoms:

Table 4 Anisotropic displacement parameters ($Å^2$ x 10^3) for **18**. The anisotropic displacement factor exponent takes the form: $-2\pi^2$ [$h^2 a^{*2} U^{11}$ + ... + 2 h k a* b* U^{12}]

	U^{11}	U^{22}	U^{33}	U^{23}	U^{13}	U^{12}
Re(1)	21(1)	27(1)	28(1)	1(1)	7(1)	6(1)
Br(1)	31(1)	32(1)	31(1)	2(1)	11(1)	8(1)
O(1)	50(2)	56(2)	68(3)	30(2)	21(2)	27(2)
O(2)	33(2)	48(2)	45(3)	1(2)	2(2)	-4(2)
O(3)	46(2)	40(2)	74(4)	14(2)	12(2)	22(2)
O(4)	56(2)	61(2)	45(3)	-1(2)	29(2)	2(2)
N(1)	28(2)	30(2)	34(2)	6(2)	10(2)	10(2)
C(1)	33(2)	36(2)	39(3)	12(2)	13(2)	10(2)
C(2)	32(2)	34(2)	33(3)	6(2)	11(2)	7(2)
C(3)	31(2)	30(2)	43(3)	0(2)	12(2)	6(2)
C(4)	36(2)	37(2)	40(3)	-1(2)	15(2)	4(2)
C(5)	24(2)	29(2)	34(3)	6(2)	10(2)	10(2)
C(6)	31(2)	31(2)	46(3)	0(2)	7(2)	2(2)

Table 5 Hydrogen coordinates (x 10^4) and isotropic displacement parameters ($Å^2$ x 10^3) for **18**

	x	y	z	U(eq)
H(6A)	-929	2531	5162	56
H(6B)	-2541	3351	5851	56
H(6C)	-1248	1744	6293	56

Table 6 Torsion angles [°] for **18**

C(2)-Re(1)-N(1)-C(5)	-93(20)	N(1)-Re(1)-C(2)-O(2)	-27(17)
C(4)-Re(1)-N(1)-C(5)	79(20)	Br(1)-Re(1)-C(2)-O(2)	-19(15)
C(1)-Re(1)-N(1)-C(5)	170(100)	C(2)-Re(1)-C(3)-O(3)	7(6)
C(3)-Re(1)-N(1)-C(5)	-14(20)	C(4)-Re(1)-C(3)-O(3)	99(6)
Br(1)-Re(1)-N(1)-C(5)	-102(20)	C(1)-Re(1)-C(3)-O(3)	-55(8)
C(2)-Re(1)-C(1)-O(1)	-46(12)	N(1)-Re(1)-C(3)-O(3)	-169(6)
C(4)-Re(1)-C(1)-O(1)	-138(12)	Br(1)-Re(1)-C(3)-O(3)	-84(6)
C(3)-Re(1)-C(1)-O(1)	16(14)	C(2)-Re(1)-C(4)-O(4)	88(15)
N(1)-Re(1)-C(1)-O(1)	130(12)	C(1)-Re(1)-C(4)-O(4)	178(100)
Br(1)-Re(1)-C(1)-O(1)	44(12)	C(3)-Re(1)-C(4)-O(4)	0(15)
C(4)-Re(1)-C(2)-O(2)	161(15)	N(1)-Re(1)-C(4)-O(4)	-92(15)
C(1)-Re(1)-C(2)-O(2)	70(15)	Br(1)-Re(1)-C(4)-O(4)	-107(14)
C(3)-Re(1)-C(2)-O(2)	-107(15)	Re(1)-N(1)-C(5)-C(6)	78(65)

Symmetry transformations used to generate equivalent atoms:

Appendix nine: Full crystallographic data of **19**

Table 1 Crystal data and structure refinement for **19** (α-form)

Identification code	rb09027_0m	
Empirical formula	$C_{24}H_{10}Br_2N_4O_8Re_2S$	
Formula weight	1046.64	
Temperature	173(2) K	
Wavelength	0.71073 Å	
Crystal system	Rhombohedral	
Space group	*R*-3	
Unit cell dimensions	*a* = 28.8050(16) Å	*α* = 90°.
	b = 28.8050(16) Å	*β* = 90°.
	c = 21.754(2) Å	*γ* = 120°.
Volume	15631(2) $Å^3$	
Z	18	
Density (calculated)	2.001 Mg/m^3	
Absorption coefficient	9.368 mm^{-1}	
F(000)	8676	
Crystal size	0.19 x 0.06 x 0.05 mm^3	
Theta range for data collection	1.88 to 27.10°.	
Index ranges	-36<=*h*<=36, -36<=*k*<=36, -27<=*l*<=27	
Reflections collected	73729	
Independent reflections	7675 [*R*(int) = 0.1241]	
Completeness to theta = 25.00°	100.0 %	
Absorption correction	None	
Max. and min. transmission	0.6725 and 0.2747	
Refinement method	Full-matrix least-squares on F^2	
Data / restraints / parameters	7675 / 0 / 370	
Goodness-of-fit on F^2	1.046	
Final *R* indices [I>2sigma(I)]	*R*1 = 0.0691, *wR*2 = 0.1708	
R indices (all data)	*R*1 = 0.1385, *wR*2 = 0.2043	
Largest diff. peak and hole	2.440 and -1.130 e.$Å^{-3}$	

Table 2 Atomic coordinates (x 10^4) and equivalent isotropic displacement parameters ($Å^2$ x 10^3) for **19** (α-form). U(eq) is defined as one third of the trace of the orthogonalized U^{ij} tensor

	x	y	z	U(eq)
Re(1)	12100(1)	4247(1)	5619(1)	51(1)
Re(1A)	7729(1)	2516(1)	10877(1)	58(1)
Br(1)	11370(1)	3867(1)	4761(1)	60(1)
Br(1A)	7633(1)	1566(1)	10750(1)	67(1)
S(1)	8804(2)	2935(3)	7031(2)	80(2)
N(1)	9436(6)	3183(6)	6945(6)	61(4)
N(2)	8763(6)	2987(7)	7769(6)	65(4)
N(3)	11439(5)	3974(5)	6315(5)	51(3)
N(4)	8289(5)	2769(5)	10099(5)	52(3)
C(1)	9659(7)	3321(7)	7518(6)	51(4)
C(2)	9271(6)	3196(6)	7987(6)	44(4)
C(3)	9425(7)	3295(6)	8614(7)	50(4)
C(4)	9958(7)	3536(6)	8732(6)	54(4)
C(5)	10350(6)	3666(6)	8270(6)	47(4)
C(6)	10217(7)	3560(6)	7654(6)	50(4)
C(7)	10630(7)	3686(7)	7197(7)	53(4)
C(8)	11094(6)	3657(7)	7309(7)	53(4)
C(9)	11488(7)	3807(6)	6873(7)	52(4)
C(10)	11002(7)	3999(6)	6189(6)	51(4)
C(11)	10602(6)	3869(6)	6603(7)	49(4)
C(12)	9011(7)	3121(6)	9109(7)	51(4)
C(13)	8538(6)	2655(6)	9080(7)	53(4)
C(14)	8191(7)	2490(7)	9584(7)	58(4)
C(15)	8766(7)	3229(7)	10123(7)	59(4)
C(16)	9134(7)	3415(7)	9657(7)	62(5)
C(17)	12049(7)	3546(7)	5658(7)	51(4)
C(18)	12608(7)	4461(8)	4953(8)	68(5)
C(19)	12645(8)	4538(8)	6228(9)	68(5)
C(20)	12124(7)	4946(9)	5604(7)	65(5)

C(17A)	8308(8)	2648(7)	11468(8)	67(5)
C(18A)	7836(8)	3222(9)	10933(8)	70(5)
C(19A)	7266(8)	2306(7)	11571(9)	76(6)
C(20A)	7111(9)	2280(8)	10322(10)	72(5)
O(1)	12031(5)	3148(6)	5655(6)	73(4)
O(2)	12893(5)	4561(6)	4538(6)	88(4)
O(3)	12967(7)	4734(7)	6584(7)	101(5)
O(4)	12139(6)	5352(6)	5624(5)	76(4)
O(1A)	8628(6)	2717(5)	11823(6)	79(4)
O(2A)	7893(7)	3648(6)	10934(6)	91(4)
O(3A)	6997(7)	2194(7)	11989(7)	122(7)
O(4A)	6752(7)	2149(7)	10019(8)	100(5)

Table 3 Bond lengths [Å] and angles [°] for **19** (α-form)

Re(1)-C(19)	1.90(2)	C(8)-H(8)	0.9500
Re(1)-C(18)	1.929(18)	C(9)-H(9)	0.9500
Re(1)-C(17)	1.952(18)	C(10)-C(11)	1.36(2)
Re(1)-C(20)	1.98(2)	C(10)-H(10)	0.9500
Re(1)-N(3)	2.244(13)	C(11)-H(11)	0.9500
Re(1)-Br(1)	2.6088(18)	C(12)-C(13)	1.35(2)
Re(1A)-C(19A)	1.90(2)	C(12)-C(16)	1.40(2)
Re(1A)-C(18A)	1.90(2)	C(13)-C(14)	1.40(2)
Re(1A)-C(20A)	1.97(3)	C(13)-H(13)	0.9500
Re(1A)-C(17A)	1.99(2)	C(14)-H(14)	0.9500
Re(1A)-N(4)	2.195(12)	C(15)-C(16)	1.37(2)
Re(1A)-Br(1A)	2.621(2)	C(15)-H(15)	0.9500
S(1)-N(1)	1.598(15)	C(16)-H(16)	0.9500
S(1)-N(2)	1.622(14)	C(17)-O(1)	1.122(18)
N(1)-C(1)	1.366(19)	C(18)-O(2)	1.157(19)
N(2)-C(2)	1.36(2)	C(19)-O(3)	1.12(2)
N(3)-C(10)	1.325(19)	C(20)-O(4)	1.15(2)
N(3)-C(9)	1.339(18)	C(17A)-O(1A)	1.14(2)
N(4)-C(14)	1.326(19)	C(18A)-O(2A)	1.15(2)
N(4)-C(15)	1.35(2)	C(19A)-O(3A)	1.13(2)
C(1)-C(2)	1.420(19)	C(20A)-O(4A)	1.12(2)
C(1)-C(6)	1.43(2)		
C(2)-C(3)	1.42(2)	C(19)-Re(1)-C(18)	93.2(8)
C(3)-C(4)	1.36(2)	C(19)-Re(1)-C(17)	92.6(8)
C(3)-C(12)	1.49(2)	C(18)-Re(1)-C(17)	90.9(8)
C(4)-C(5)	1.42(2)	C(19)-Re(1)-C(20)	87.8(8)
C(4)-H(4)	0.9500	C(18)-Re(1)-C(20)	91.6(8)
C(5)-C(6)	1.384(19)	C(17)-Re(1)-C(20)	177.5(7)
C(5)-H(5)	0.9500	C(19)-Re(1)-N(3)	93.1(6)
C(6)-C(7)	1.45(2)	C(18)-Re(1)-N(3)	173.6(6)
C(7)-C(8)	1.40(2)	C(17)-Re(1)-N(3)	89.8(6)
C(7)-C(11)	1.41(2)	C(20)-Re(1)-N(3)	87.7(6)
C(8)-C(9)	1.37(2)	C(19)-Re(1)-Br(1)	178.4(6)

C(18)-Re(1)-Br(1)	85.4(5)	C(4)-C(3)-C(12)	123.0(14)
C(17)-Re(1)-Br(1)	88.2(5)	C(2)-C(3)-C(12)	120.6(14)
C(20)-Re(1)-Br(1)	91.4(5)	C(3)-C(4)-C(5)	123.4(14)
N(3)-Re(1)-Br(1)	88.3(3)	C(3)-C(4)-H(4)	118.3
C(19A)-Re(1A)-C(18A)	90.0(8)	C(5)-C(4)-H(4)	118.3
C(19A)-Re(1A)-C(20A)	90.4(8)	C(6)-C(5)-C(4)	122.2(14)
C(18A)-Re(1A)-C(20A)	92.5(8)	C(6)-C(5)-H(5)	118.9
C(19A)-Re(1A)-C(17A)	86.3(8)	C(4)-C(5)-H(5)	118.9
C(18A)-Re(1A)-C(17A)	94.7(8)	C(5)-C(6)-C(1)	115.4(13)
C(20A)-Re(1A)-C(17A)	172.1(7)	C(5)-C(6)-C(7)	120.4(15)
C(19A)-Re(1A)-N(4)	177.9(7)	C(1)-C(6)-C(7)	124.2(13)
C(18A)-Re(1A)-N(4)	89.7(7)	C(8)-C(7)-C(11)	114.5(14)
C(20A)-Re(1A)-N(4)	91.7(6)	C(8)-C(7)-C(6)	123.5(14)
C(17A)-Re(1A)-N(4)	91.6(6)	C(11)-C(7)-C(6)	121.9(14)
C(19A)-Re(1A)-Br(1A)	93.5(6)	C(9)-C(8)-C(7)	121.6(15)
C(18A)-Re(1A)-Br(1A)	176.4(6)	C(9)-C(8)-H(8)	119.2
C(20A)-Re(1A)-Br(1A)	88.2(6)	C(7)-C(8)-H(8)	119.2
C(17A)-Re(1A)-Br(1A)	84.8(5)	N(3)-C(9)-C(8)	121.3(16)
N(4)-Re(1A)-Br(1A)	86.7(4)	N(3)-C(9)-H(9)	119.4
N(1)-S(1)-N(2)	101.2(7)	C(8)-C(9)-H(9)	119.4
C(1)-N(1)-S(1)	106.8(11)	N(3)-C(10)-C(11)	123.1(13)
C(2)-N(2)-S(1)	105.9(10)	N(3)-C(10)-H(10)	118.4
C(10)-N(3)-C(9)	118.7(13)	C(11)-C(10)-H(10)	118.4
C(10)-N(3)-Re(1)	120.4(9)	C(10)-C(11)-C(7)	120.7(14)
C(9)-N(3)-Re(1)	120.9(11)	C(10)-C(11)-H(11)	119.7
C(14)-N(4)-C(15)	115.6(13)	C(7)-C(11)-H(11)	119.7
C(14)-N(4)-Re(1A)	123.5(11)	C(13)-C(12)-C(16)	117.6(15)
C(15)-N(4)-Re(1A)	120.9(10)	C(13)-C(12)-C(3)	122.6(14)
N(1)-C(1)-C(2)	112.7(15)	C(16)-C(12)-C(3)	119.4(15)
N(1)-C(1)-C(6)	125.6(13)	C(12)-C(13)-C(14)	119.7(15)
C(2)-C(1)-C(6)	121.7(14)	C(12)-C(13)-H(13)	120.2
N(2)-C(2)-C(3)	125.7(13)	C(14)-C(13)-H(13)	120.2
N(2)-C(2)-C(1)	113.4(13)	N(4)-C(14)-C(13)	123.9(16)
C(3)-C(2)-C(1)	120.9(15)	N(4)-C(14)-H(14)	118.0
C(4)-C(3)-C(2)	116.4(14)	C(13)-C(14)-H(14)	118.0

N(4)-C(15)-C(16)	124.3(15)	O(2)-C(18)-Re(1)	176.1(17)
N(4)-C(15)-H(15)	117.9	O(3)-C(19)-Re(1)	176.6(19)
C(16)-C(15)-H(15)	117.9	O(4)-C(20)-Re(1)	176.7(14)
C(15)-C(16)-C(12)	118.9(17)	O(1A)-C(17A)-Re(1A)	177.6(17)
C(15)-C(16)-H(16)	120.6	O(2A)-C(18A)-Re(1A)	176.2(17)
C(12)-C(16)-H(16)	120.6	O(3A)-C(19A)-Re(1A)	178.4(19)
O(1)-C(17)-Re(1)	176.9(15)	O(4A)-C(20A)-Re(1A)	178.1(19)

Symmetry transformations used to generate equivalent atoms:

Table 4 Anisotropic displacement parameters ($Å^2$ x 10^3) for **19** (α-form). The anisotropic displacement factor exponent takes the form: $-2\pi^2$ [$h^2 a^{*2} U^{11}$ + ... + 2 h k a* b* U^{12}]

	U^{11}	U^{22}	U^{33}	U^{23}	U^{13}	U^{12}
Re(1)	47(1)	59(1)	43(1)	3(1)	2(1)	23(1)
Re(1A)	63(1)	56(1)	43(1)	-2(1)	11(1)	21(1)
Br(1)	59(1)	66(1)	46(1)	3(1)	-3(1)	24(1)
Br(1A)	70(1)	57(1)	64(1)	3(1)	14(1)	25(1)
S(1)	69(3)	149(5)	40(2)	8(3)	0(2)	68(4)
N(1)	67(9)	97(11)	36(7)	12(7)	0(6)	54(9)
N(2)	62(10)	103(12)	44(7)	17(8)	10(7)	50(9)
N(3)	58(8)	57(8)	38(7)	8(6)	-3(6)	30(7)
N(4)	55(9)	57(9)	37(7)	-5(6)	0(6)	22(7)
C(1)	76(12)	66(11)	36(8)	12(7)	15(7)	54(10)
C(2)	61(10)	45(9)	32(7)	14(6)	15(7)	32(8)
C(3)	52(10)	54(10)	41(8)	0(7)	6(7)	25(8)
C(4)	80(13)	59(10)	26(7)	2(7)	2(7)	36(10)
C(5)	45(9)	49(9)	37(7)	7(6)	0(6)	16(8)
C(6)	64(11)	59(10)	34(7)	11(7)	10(7)	37(9)
C(7)	69(11)	61(10)	44(8)	5(7)	-3(8)	44(9)
C(8)	56(10)	63(11)	43(8)	-3(7)	-4(7)	33(9)
C(9)	51(10)	55(10)	41(8)	13(7)	7(7)	20(8)
C(10)	63(11)	64(11)	30(7)	10(7)	1(7)	35(9)
C(11)	51(9)	59(10)	49(9)	7(7)	6(7)	37(8)
C(12)	69(11)	50(10)	38(8)	-1(7)	5(7)	33(9)
C(13)	55(10)	49(10)	43(8)	1(7)	11(7)	16(8)
C(14)	55(10)	53(10)	49(9)	5(8)	12(8)	15(9)
C(15)	69(12)	68(12)	38(8)	-4(8)	7(8)	32(10)
C(16)	63(11)	68(12)	49(9)	-7(8)	5(8)	27(10)
C(17)	53(10)	54(10)	55(9)	6(8)	9(7)	33(9)
C(18)	49(11)	72(13)	66(11)	-11(9)	12(9)	17(10)
C(19)	65(12)	75(13)	61(11)	2(10)	-4(9)	33(11)
C(20)	64(12)	95(16)	36(8)	-3(9)	3(8)	40(12)
C(17A)	83(14)	51(11)	53(10)	8(8)	16(10)	23(10)

C(18A)	79(14)	85(15)	48(10)	0(10)	1(9)	42(12)
C(19A)	78(14)	54(11)	63(11)	-25(9)	5(10)	9(10)
C(20A)	82(15)	53(12)	77(13)	2(10)	22(11)	29(11)
O(1)	50(7)	75(9)	93(10)	-1(7)	16(6)	31(7)
O(2)	67(9)	111(12)	70(9)	0(8)	23(7)	33(8)
O(3)	103(12)	110(12)	87(10)	-26(9)	-45(9)	49(10)
O(4)	112(11)	71(9)	52(7)	6(6)	11(7)	51(9)
O(1A)	97(11)	71(9)	67(8)	-6(7)	-16(8)	40(8)
O(2A)	127(13)	75(10)	68(9)	-1(8)	-7(8)	49(10)
O(3A)	99(12)	115(13)	83(11)	-15(9)	40(9)	2(10)
O(4A)	87(12)	110(13)	99(12)	-18(10)	-11(9)	46(10)

Table 5 Hydrogen coordinates (x 10^4) and isotropic displacement parameters ($Å^2$ x 10^3) for **19** (α-form)

	x	y	z	U(eq)
H(4)	10074	3622	9147	65
H(5)	10717	3831	8386	56
H(8)	11137	3531	7696	63
H(9)	11802	3793	6969	62
H(10)	10966	4113	5791	61
H(11)	10300	3901	6491	58
H(13)	8443	2441	8719	64
H(14)	7865	2157	9556	69
H(15)	8851	3438	10488	71
H(16)	9467	3737	9704	75

Table 6 Torsion angles [°] for **19** (α-form)

N(2)-S(1)-N(1)-C(1)	0.7(13)	C(1)-C(2)-C(3)-C(12)	-174.7(14)
N(1)-S(1)-N(2)-C(2)	-2.1(13)	C(2)-C(3)-C(4)-C(5)	-3(2)
C(19)-Re(1)-N(3)-C(10)	143.3(13)	C(12)-C(3)-C(4)-C(5)	175.0(15)
C(18)-Re(1)-N(3)-C(10)	-28(7)	C(3)-C(4)-C(5)-C(6)	1(3)
C(17)-Re(1)-N(3)-C(10)	-124.1(13)	C(4)-C(5)-C(6)-C(1)	1(2)
C(20)-Re(1)-N(3)-C(10)	55.6(13)	C(4)-C(5)-C(6)-C(7)	-178.4(15)
Br(1)-Re(1)-N(3)-C(10)	-35.9(12)	N(1)-C(1)-C(6)-C(5)	179.8(15)
C(19)-Re(1)-N(3)-C(9)	-33.6(13)	C(2)-C(1)-C(6)-C(5)	-1(2)
C(18)-Re(1)-N(3)-C(9)	155(6)	N(1)-C(1)-C(6)-C(7)	-1(3)
C(17)-Re(1)-N(3)-C(9)	59.0(13)	C(2)-C(1)-C(6)-C(7)	178.8(14)
C(20)-Re(1)-N(3)-C(9)	-121.3(13)	C(5)-C(6)-C(7)-C(8)	33(2)
Br(1)-Re(1)-N(3)-C(9)	147.2(12)	C(1)-C(6)-C(7)-C(8)	-146.3(17)
C(19A)-Re(1A)-N(4)-C(14)	143(19)	C(5)-C(6)-C(7)-C(11)	-144.6(16)
C(18A)-Re(1A)-N(4)-C(14)	-133.9(15)	C(1)-C(6)-C(7)-C(11)	36(2)
C(20A)-Re(1A)-N(4)-C(14)	-41.4(15)	C(11)-C(7)-C(8)-C(9)	1(2)
C(17A)-Re(1A)-N(4)-C(14)	131.5(14)	C(6)-C(7)-C(8)-C(9)	-176.6(16)
Br(1A)-Re(1A)-N(4)-C(14)	46.8(13)	C(10)-N(3)-C(9)-C(8)	1(2)
C(19A)-Re(1A)-N(4)-C(15)	-36(20)	Re(1)-N(3)-C(9)-C(8)	177.7(12)
C(18A)-Re(1A)-N(4)-C(15)	46.5(14)	C(7)-C(8)-C(9)-N(3)	-2(3)
C(20A)-Re(1A)-N(4)-C(15)	139.0(14)	C(9)-N(3)-C(10)-C(11)	1(2)
C(17A)-Re(1A)-N(4)-C(15)	-48.2(14)	Re(1)-N(3)-C(10)-C(11)	-176.1(12)
Br(1A)-Re(1A)-N(4)-C(15)	-132.9(13)	N(3)-C(10)-C(11)-C(7)	-1(3)
S(1)-N(1)-C(1)-C(2)	0.9(16)	C(8)-C(7)-C(11)-C(10)	0(2)
S(1)-N(1)-C(1)-C(6)	-179.6(13)	C(6)-C(7)-C(11)-C(10)	178.1(15)
S(1)-N(2)-C(2)-C(3)	-177.9(13)	C(4)-C(3)-C(12)-C(13)	-140.3(18)
S(1)-N(2)-C(2)-C(1)	2.8(17)	C(2)-C(3)-C(12)-C(13)	37(2)
N(1)-C(1)-C(2)-N(2)	-2.5(19)	C(4)-C(3)-C(12)-C(16)	32(2)
C(6)-C(1)-C(2)-N(2)	178.0(14)	C(2)-C(3)-C(12)-C(16)	-150.0(16)
N(1)-C(1)-C(2)-C(3)	178.1(14)	C(16)-C(12)-C(13)-C(14)	1(3)
C(6)-C(1)-C(2)-C(3)	-1(2)	C(3)-C(12)-C(13)-C(14)	173.8(16)
N(2)-C(2)-C(3)-C(4)	-176.2(15)	C(15)-N(4)-C(14)-C(13)	-2(3)
C(1)-C(2)-C(3)-C(4)	3(2)	Re(1A)-N(4)-C(14)-C(13)	178.1(13)
N(2)-C(2)-C(3)-C(12)	6(2)	C(12)-C(13)-C(14)-N(4)	1(3)

C(14)-N(4)-C(15)-C(16)	1(3)	N(3)-Re(1)-C(20)-O(4)	50(30)
Re(1A)-N(4)-C(15)-C(16)	-179.7(14)	Br(1)-Re(1)-C(20)-O(4)	139(30)
N(4)-C(15)-C(16)-C(12)	2(3)	C(19A)-Re(1A)-C(17A)-O(1A)	7(40)
C(13)-C(12)-C(16)-C(15)	-2(3)	C(18A)-Re(1A)-C(17A)-O(1A)	97(40)
C(3)-C(12)-C(16)-C(15)	-175.4(16)	C(20A)-Re(1A)-C(17A)-O(1A)	-59(42)
C(19)-Re(1)-C(17)-O(1)	-105(31)	N(4)-Re(1A)-C(17A)-O(1A)	-173(100)
C(18)-Re(1)-C(17)-O(1)	-12(31)	Br(1A)-Re(1A)-C(17A)-O(1A)	-87(40)
C(20)-Re(1)-C(17)-O(1)	154(25)	C(19A)-Re(1A)-C(18A)-O(2A)	-128(29)
N(3)-Re(1)-C(17)-O(1)	162(31)	C(20A)-Re(1A)-C(18A)-O(2A)	-38(29)
Br(1)-Re(1)-C(17)-O(1)	73(31)	C(17A)-Re(1A)-C(18A)-O(2A)	145(29)
C(19)-Re(1)-C(18)-O(2)	140(28)	N(4)-Re(1A)-C(18A)-O(2A)	54(29)
C(17)-Re(1)-C(18)-O(2)	48(28)	Br(1A)-Re(1A)-C(18A)-O(2A)	64(35)
C(20)-Re(1)-C(18)-O(2)	-132(28)	C(18A)-Re(1A)-C(19A)-O(3A)	-31(87)
N(3)-Re(1)-C(18)-O(2)	-48(33)	C(20A)-Re(1A)-C(19A)-O(3A)	-124(87)
Br(1)-Re(1)-C(18)-O(2)	-41(28)	C(17A)-Re(1A)-C(19A)-O(3A)	64(87)
C(18)-Re(1)-C(19)-O(3)	87(31)	N(4)-Re(1A)-C(19A)-O(3A)	52(100)
C(17)-Re(1)-C(19)-O(3)	178(100)	Br(1A)-Re(1A)-C(19A)-O(3A)	148(87)
C(20)-Re(1)-C(19)-O(3)	-4(31)	C(19A)-Re(1A)-C(20A)-O(4A)	30(65)
N(3)-Re(1)-C(19)-O(3)	-92(31)	C(18A)-Re(1A)-C(20A)-O(4A)	-60(65)
Br(1)-Re(1)-C(19)-O(3)	58(46)	C(17A)-Re(1A)-C(20A)-O(4A)	95(65)
C(19)-Re(1)-C(20)-O(4)	-43(30)	N(4)-Re(1A)-C(20A)-O(4A)	-150(65)
C(18)-Re(1)-C(20)-O(4)	-136(30)	Br(1A)-Re(1A)-C(20A)-O(4A)	123(65)
C(17)-Re(1)-C(20)-O(4)	58(39)		

Symmetry transformations used to generate equivalent atoms:

Table 1 Crystal data and structure refinement for **19** (β-form)

Identification code	rb09032_0m	
Empirical formula	$C_{25}H_{12}Br_2Cl_2N_4O_8Re_2S$	
Formula weight	1131.57	
Temperature	173(2) K	
Wavelength	0.71073 Å	
Crystal system	Triclinic	
Space group	*P*-1	
Unit cell dimensions	*a* = 6.1496(13) Å	*α* = 109.581(2)°.
	b = 15.569(3) Å	*β* = 91.113(2)°.
	c = 17.686(4) Å	*γ* = 99.489(2)°.
Volume	1568.5(6) $Å^3$	
Z	2	
Density (calculated)	2.396 Mg/m^3	
Absorption coefficient	10.548 mm^{-1}	
F(000)	1048	
Crystal size	0.20 x 0.13 x 0.07 mm^3	
Theta range for data collection	2.16 to 27.48°.	
Index ranges	-7<=*h*<=7, -20<=*k*<=20, -22<=*l*<=22	
Reflections collected	22148	
Independent reflections	7068 [*R*(int) = 0.0448]	
Completeness to theta = 25.00°	99.2 %	
Absorption correction	None	
Max. and min. transmission	0.5172 and 0.2210	
Refinement method	Full-matrix least-squares on F^2	
Data / restraints / parameters	7068 / 0 / 397	
Goodness-of-fit on F^2	1.131	
Final *R* indices [I>2sigma(I)]	*R*1 = 0.0660, *wR*2 = 0.1880	
R indices (all data)	*R*1 = 0.0718, *wR*2 = 0.1916	
Largest diff. peak and hole	4.381 and -3.280 e.$Å^{-3}$	

Table 2 Atomic coordinates (x 10^4) and equivalent isotropic displacement parameters ($Å^2$ x 10^3) for **19** (β-form). U(eq) is defined as one third of the trace of the orthogonalized U^{ij} tensor

	x	y	z	U(eq)
Re(1)	280(1)	7707(1)	5349(1)	24(1)
Re(1A)	4541(1)	3597(1)	11913(1)	23(1)
Br(1A)	2093(2)	4475(1)	11317(1)	30(1)
Br(1)	3647(2)	8931(1)	6187(1)	34(1)
S(1)	8743(6)	423(2)	7098(2)	33(1)
N(1)	10996(19)	969(8)	6893(7)	30(2)
N(2)	8240(20)	1166(8)	7929(7)	29(2)
N(3)	2175(19)	7646(7)	4292(7)	26(2)
N(4)	6048(17)	3232(8)	10750(6)	23(2)
C(1)	11460(20)	1790(9)	7491(8)	23(2)
C(2)	9890(20)	1901(9)	8089(8)	25(3)
C(3)	10140(20)	2741(9)	8779(8)	25(2)
C(4)	12000(30)	3387(10)	8832(9)	35(3)
C(5)	13560(20)	3283(10)	8256(8)	33(3)
C(6)	13340(20)	2509(9)	7571(8)	25(3)
C(7)	14960(20)	2441(9)	6960(8)	27(3)
C(8)	3750(20)	6768(10)	3118(8)	30(3)
C(9)	2420(20)	6828(9)	3729(8)	27(3)
C(10)	3290(20)	8419(10)	4191(9)	32(3)
C(11)	15330(20)	1590(9)	6403(8)	27(3)
C(12)	8560(20)	2869(9)	9410(7)	24(3)
C(13)	7720(20)	2178(9)	9729(8)	27(3)
C(14)	6560(20)	2390(9)	10391(8)	27(3)
C(15)	6700(20)	3878(9)	10408(9)	27(3)
C(16)	7930(20)	3719(9)	9755(8)	28(3)
C(17)	1760(20)	6740(12)	5548(9)	35(3)
C(18)	-1210(20)	7849(9)	6319(8)	27(3)
C(19)	-2210(20)	6765(11)	4723(10)	33(3)
C(20)	-1080(20)	8723(10)	5186(8)	28(3)
C(17A)	6870(20)	4751(11)	12377(9)	34(3)

C(18A)	3150(30)	3958(12)	12915(10)	38(3)
C(19A)	6350(20)	2929(10)	12313(8)	31(3)
C(20A)	2160(20)	2466(11)	11456(9)	31(3)
O(1)	2580(30)	6172(10)	5641(9)	61(4)
O(2)	-2010(20)	7975(8)	6911(7)	44(3)
O(3)	-3570(20)	6215(10)	4410(8)	53(3)
O(4)	-1806(17)	9308(7)	5099(7)	35(2)
O(1A)	8140(20)	5379(9)	12654(8)	51(3)
O(2A)	2310(20)	4209(9)	13496(7)	51(3)
O(3A)	7500(20)	2539(9)	12554(7)	46(3)
O(4A)	811(18)	1840(7)	11218(7)	39(2)
C(1S)	3410(30)	9945(14)	8402(11)	48(4)
Cl(1)	1946(9)	10540(5)	9189(4)	72(2)
Cl(2)	5636(8)	9571(3)	8782(4)	57(1)

Table 3 Bond lengths [Å] and angles [°] for **19** (β-form)

Re(1)-C(18)	1.926(13)	C(8)-C(7)#1	1.400(19)
Re(1)-C(19)	1.956(16)	C(8)-H(8)	0.9500
Re(1)-C(17)	2.002(16)	C(9)-H(9)	0.9500
Re(1)-C(20)	2.004(15)	C(10)-C(11)#1	1.36(2)
Re(1)-N(3)	2.205(11)	C(10)-H(10)	0.9500
Re(1)-Br(1)	2.6081(16)	C(11)-C(10)#1	1.36(2)
Re(1A)-C(19A)	1.916(15)	C(11)-H(11)	0.9500
Re(1A)-C(18A)	1.933(16)	C(12)-C(16)	1.382(19)
Re(1A)-C(20A)	2.014(16)	C(12)-C(13)	1.406(17)
Re(1A)-C(17A)	2.017(16)	C(13)-C(14)	1.357(19)
Re(1A)-N(4)	2.208(10)	C(13)-H(13)	0.9500
Re(1A)-Br(1A)	2.6137(15)	C(14)-H(14)	0.9500
S(1)-N(2)	1.610(12)	C(15)-C(16)	1.37(2)
S(1)-N(1)	1.615(12)	C(15)-H(15)	0.9500
N(1)-C(1)	1.341(17)	C(16)-H(16)	0.9500
N(2)-C(2)	1.345(17)	C(17)-O(1)	1.14(2)
N(3)-C(10)	1.351(18)	C(18)-O(2)	1.134(17)
N(3)-C(9)	1.362(17)	C(19)-O(3)	1.082(19)
N(4)-C(14)	1.345(17)	C(20)-O(4)	1.131(18)
N(4)-C(15)	1.351(16)	C(17A)-O(1A)	1.106(19)
C(1)-C(2)	1.434(18)	C(18A)-O(2A)	1.138(19)
C(1)-C(6)	1.439(17)	C(19A)-O(3A)	1.161(19)
C(2)-C(3)	1.442(18)	C(20A)-O(4A)	1.121(18)
C(3)-C(4)	1.375(19)	C(1S)-Cl(1)	1.749(19)
C(3)-C(12)	1.478(17)	C(1S)-Cl(2)	1.778(19)
C(4)-C(5)	1.40(2)	C(1S)-H(1S1)	0.9900
C(4)-H(4)	0.9500	C(1S)-H(1S2)	0.9900
C(5)-C(6)	1.379(19)		
C(5)-H(5)	0.9500	C(18)-Re(1)-C(19)	90.4(6)
C(6)-C(7)	1.474(18)	C(18)-Re(1)-C(17)	90.1(6)
C(7)-C(8)#1	1.400(19)	C(19)-Re(1)-C(17)	91.3(6)
C(7)-C(11)	1.416(18)	C(18)-Re(1)-C(20)	89.6(5)
C(8)-C(9)	1.355(19)	C(19)-Re(1)-C(20)	91.6(6)

C(17)-Re(1)-C(20)	177.1(6)	N(1)-C(1)-C(6)	126.0(12)
C(18)-Re(1)-N(3)	175.4(5)	C(2)-C(1)-C(6)	120.8(12)
C(19)-Re(1)-N(3)	94.0(5)	N(2)-C(2)-C(1)	113.5(11)
C(17)-Re(1)-N(3)	90.8(5)	N(2)-C(2)-C(3)	125.7(12)
C(20)-Re(1)-N(3)	89.2(5)	C(1)-C(2)-C(3)	120.8(12)
C(18)-Re(1)-Br(1)	89.7(4)	C(4)-C(3)-C(2)	115.4(12)
C(19)-Re(1)-Br(1)	178.6(4)	C(4)-C(3)-C(12)	122.5(12)
C(17)-Re(1)-Br(1)	87.3(5)	C(2)-C(3)-C(12)	121.9(11)
C(20)-Re(1)-Br(1)	89.8(4)	C(3)-C(4)-C(5)	124.3(13)
N(3)-Re(1)-Br(1)	85.9(3)	C(3)-C(4)-H(4)	117.9
C(19A)-Re(1A)-C(18A)	91.2(6)	C(5)-C(4)-H(4)	117.9
C(19A)-Re(1A)-C(20A)	91.9(6)	C(6)-C(5)-C(4)	122.3(13)
C(18A)-Re(1A)-C(20A)	90.6(6)	C(6)-C(5)-H(5)	118.9
C(19A)-Re(1A)-C(17A)	89.3(6)	C(4)-C(5)-H(5)	118.9
C(18A)-Re(1A)-C(17A)	88.6(6)	C(5)-C(6)-C(1)	116.4(12)
C(20A)-Re(1A)-C(17A)	178.5(6)	C(5)-C(6)-C(7)	120.8(12)
C(19A)-Re(1A)-N(4)	91.6(5)	C(1)-C(6)-C(7)	122.8(12)
C(18A)-Re(1A)-N(4)	177.1(6)	C(8)#1-C(7)-C(11)	114.8(12)
C(20A)-Re(1A)-N(4)	89.7(5)	C(8)#1-C(7)-C(6)	121.5(12)
C(17A)-Re(1A)-N(4)	91.1(5)	C(11)-C(7)-C(6)	123.7(12)
C(19A)-Re(1A)-Br(1A)	178.0(4)	C(9)-C(8)-C(7)#1	121.3(13)
C(18A)-Re(1A)-Br(1A)	90.6(5)	C(9)-C(8)-H(8)	119.3
C(20A)-Re(1A)-Br(1A)	87.4(4)	C(7)#1-C(8)-H(8)	119.3
C(17A)-Re(1A)-Br(1A)	91.4(4)	C(8)-C(9)-N(3)	123.5(12)
N(4)-Re(1A)-Br(1A)	86.5(3)	C(8)-C(9)-H(9)	118.2
N(2)-S(1)-N(1)	101.5(6)	N(3)-C(9)-H(9)	118.2
C(1)-N(1)-S(1)	106.0(9)	N(3)-C(10)-C(11)#1	123.8(13)
C(2)-N(2)-S(1)	105.8(9)	N(3)-C(10)-H(10)	118.1
C(10)-N(3)-C(9)	115.8(11)	C(11)#1-C(10)-H(10)	118.1
C(10)-N(3)-Re(1)	121.9(9)	C(10)#1-C(11)-C(7)	120.5(12)
C(9)-N(3)-Re(1)	122.3(9)	C(10)#1-C(11)-H(11)	119.8
C(14)-N(4)-C(15)	116.7(11)	C(7)-C(11)-H(11)	119.8
C(14)-N(4)-Re(1A)	122.0(8)	C(16)-C(12)-C(13)	116.2(12)
C(15)-N(4)-Re(1A)	121.0(9)	C(16)-C(12)-C(3)	120.3(12)
N(1)-C(1)-C(2)	113.1(11)	C(13)-C(12)-C(3)	123.4(13)

C(14)-C(13)-C(12)	120.0(12)	O(2)-C(18)-Re(1)	176.2(14)
C(14)-C(13)-H(13)	120.0	O(3)-C(19)-Re(1)	175.4(14)
C(12)-C(13)-H(13)	120.0	O(4)-C(20)-Re(1)	178.7(12)
N(4)-C(14)-C(13)	123.3(12)	O(1A)-C(17A)-Re(1A)	177.8(15)
N(4)-C(14)-H(14)	118.3	O(2A)-C(18A)-Re(1A)	176.5(15)
C(13)-C(14)-H(14)	118.3	O(3A)-C(19A)-Re(1A)	178.3(14)
N(4)-C(15)-C(16)	122.9(12)	O(4A)-C(20A)-Re(1A)	178.4(13)
N(4)-C(15)-H(15)	118.5	Cl(1)-C(1S)-Cl(2)	110.6(10)
C(16)-C(15)-H(15)	118.5	Cl(1)-C(1S)-H(1S1)	109.5
C(15)-C(16)-C(12)	120.5(12)	Cl(2)-C(1S)-H(1S1)	109.5
C(15)-C(16)-H(16)	119.7	Cl(1)-C(1S)-H(1S2)	109.5
C(12)-C(16)-H(16)	119.7	Cl(2)-C(1S)-H(1S2)	109.5
O(1)-C(17)-Re(1)	178.1(16)	H(1S1)-C(1S)-H(1S2)	108.1

Symmetry transformations used to generate equivalent atoms: #1 -x+2,-y+1,-z+1

Table 4 Anisotropic displacement parameters ($Å^2$ x 10^3) for **19** (β-form). The anisotropic displacement factor exponent takes the form: $-2\pi^2$ [$h^2 a^{*2} U^{11}$ + ... + 2 h k a* b* U^{12}]

	U^{11}	U^{22}	U^{33}	U^{23}	U^{13}	U^{12}
Re(1)	23(1)	27(1)	24(1)	10(1)	7(1)	8(1)
Re(1A)	25(1)	23(1)	22(1)	8(1)	7(1)	8(1)
Br(1A)	29(1)	26(1)	38(1)	12(1)	5(1)	11(1)
Br(1)	32(1)	35(1)	31(1)	7(1)	2(1)	4(1)
S(1)	33(2)	24(2)	32(2)	1(1)	9(1)	-1(1)
N(1)	30(6)	28(6)	30(6)	6(5)	12(5)	5(4)
N(2)	37(6)	19(5)	30(6)	6(4)	14(5)	5(4)
N(3)	36(6)	19(5)	28(5)	10(4)	11(5)	10(4)
N(4)	24(5)	26(5)	21(5)	10(4)	7(4)	8(4)
C(1)	23(6)	21(6)	24(6)	7(5)	3(5)	4(5)
C(2)	30(6)	25(6)	22(6)	10(5)	5(5)	5(5)
C(3)	30(6)	21(6)	23(6)	5(5)	9(5)	8(5)
C(4)	44(8)	19(6)	33(7)	0(5)	17(6)	-2(6)
C(5)	37(7)	29(7)	26(7)	3(5)	7(6)	-3(6)
C(6)	28(6)	21(6)	29(6)	9(5)	6(5)	8(5)
C(7)	30(6)	22(6)	30(7)	7(5)	8(5)	12(5)
C(8)	38(7)	23(6)	27(6)	4(5)	7(5)	7(5)
C(9)	22(6)	25(6)	35(7)	11(5)	11(5)	5(5)
C(10)	40(8)	29(7)	32(7)	12(6)	8(6)	13(6)
C(11)	39(7)	14(5)	26(6)	5(5)	7(5)	5(5)
C(12)	23(6)	31(7)	15(5)	7(5)	-1(4)	-6(5)
C(13)	43(7)	14(5)	26(6)	9(5)	4(5)	7(5)
C(14)	36(7)	18(6)	31(7)	12(5)	9(5)	4(5)
C(15)	29(6)	20(6)	36(7)	13(5)	2(5)	6(5)
C(16)	35(7)	21(6)	31(7)	12(5)	8(5)	8(5)
C(17)	31(7)	50(9)	33(7)	25(7)	10(6)	10(6)
C(18)	39(7)	26(6)	27(6)	17(5)	12(5)	14(5)
C(19)	23(6)	42(8)	43(8)	25(7)	12(6)	10(6)
C(20)	20(6)	38(7)	28(6)	16(6)	8(5)	4(5)
C(17A)	29(7)	40(8)	32(7)	10(6)	11(6)	11(6)

C(18A)	36(8)	43(9)	38(8)	19(7)	8(6)	7(6)
C(19A)	37(7)	31(7)	28(7)	11(6)	11(6)	11(6)
C(20A)	23(6)	48(9)	31(7)	20(6)	7(5)	15(6)
O(1)	88(10)	51(8)	66(9)	30(7)	22(7)	52(8)
O(2)	58(7)	46(7)	42(6)	26(5)	22(5)	24(6)
O(3)	43(7)	64(9)	51(7)	24(6)	2(6)	-3(6)
O(4)	37(5)	28(5)	43(6)	15(4)	8(4)	12(4)
O(1A)	40(6)	42(7)	53(7)	-5(6)	4(5)	4(5)
O(2A)	64(8)	53(7)	42(7)	14(6)	33(6)	26(6)
O(3A)	54(7)	53(7)	40(6)	22(5)	1(5)	26(6)
O(4A)	39(6)	26(5)	50(6)	11(5)	9(5)	2(4)
C(1S)	53(10)	55(11)	43(9)	20(8)	8(8)	20(8)
Cl(1)	51(3)	80(4)	78(4)	7(3)	5(2)	32(3)
Cl(2)	47(2)	43(2)	95(4)	37(2)	11(2)	16(2)

Table 5 Hydrogen coordinates (x 10^4) and isotropic displacement parameters ($Å^2$ x 10^3) for **19** (β-form)

	x	y	z	U(eq)
H(4)	12253	3940	9289	42
H(5)	14813	3763	8341	40
H(8)	3806	6176	2734	36
H(9)	1609	6270	3766	32
H(10)	3095	9003	4556	39
H(11)	14598	1022	6443	32
H(13)	7967	1563	9480	32
H(14)	6086	1919	10613	33
H(15)	6293	4469	10631	33
H(16)	8351	4197	9537	33
H(1S1)	3986	10356	8102	58
H(1S2)	2395	9401	8025	58

Table 6 Torsion angles [°] for **19** (β-form)

N(2)-S(1)-N(1)-C(1)	-0.1(11)	C(1)-C(2)-C(3)-C(12)	-179.2(12)
N(1)-S(1)-N(2)-C(2)	-0.3(11)	C(2)-C(3)-C(4)-C(5)	2(2)
C(18)-Re(1)-N(3)-C(10)	-29(7)	C(12)-C(3)-C(4)-C(5)	178.7(15)
C(19)-Re(1)-N(3)-C(10)	138.7(12)	C(3)-C(4)-C(5)-C(6)	0(3)
C(17)-Re(1)-N(3)-C(10)	-130.0(12)	C(4)-C(5)-C(6)-C(1)	-2(2)
C(20)-Re(1)-N(3)-C(10)	47.1(12)	C(4)-C(5)-C(6)-C(7)	177.3(14)
Br(1)-Re(1)-N(3)-C(10)	-42.7(11)	N(1)-C(1)-C(6)-C(5)	-176.9(14)
C(18)-Re(1)-N(3)-C(9)	147(6)	C(2)-C(1)-C(6)-C(5)	1.8(19)
C(19)-Re(1)-N(3)-C(9)	-45.7(12)	N(1)-C(1)-C(6)-C(7)	3(2)
C(17)-Re(1)-N(3)-C(9)	45.7(12)	C(2)-C(1)-C(6)-C(7)	-177.9(12)
C(20)-Re(1)-N(3)-C(9)	-137.2(11)	C(5)-C(6)-C(7)-C(8)#1	-24(2)
Br(1)-Re(1)-N(3)-C(9)	132.9(11)	C(1)-C(6)-C(7)-C(8)#1	156.0(13)
C(19A)-Re(1A)-N(4)-C(14)	39.0(11)	C(5)-C(6)-C(7)-C(11)	157.3(14)
C(18A)-Re(1A)-N(4)-C(14)	-149(11)	C(1)-C(6)-C(7)-C(11)	-23(2)
C(20A)-Re(1A)-N(4)-C(14)	-53.0(11)	C(7)#1-C(8)-C(9)-N(3)	2(2)
C(17A)-Re(1A)-N(4)-C(14)	128.3(11)	C(10)-N(3)-C(9)-C(8)	3(2)
Br(1A)-Re(1A)-N(4)-C(14)	-140.3(10)	Re(1)-N(3)-C(9)-C(8)	-173.2(11)
C(19A)-Re(1A)-N(4)-C(15)	-134.2(11)	C(9)-N(3)-C(10)-C(11)#1	-3(2)
C(18A)-Re(1A)-N(4)-C(15)	38(11)	Re(1)-N(3)-C(10)-C(11)#1	172.5(11)
C(20A)-Re(1A)-N(4)-C(15)	133.8(11)	C(8)#1-C(7)-C(11)-C(10)#1	-5(2)
C(17A)-Re(1A)-N(4)-C(15)	-44.9(11)	C(6)-C(7)-C(11)-C(10)#1	174.2(13)
Br(1A)-Re(1A)-N(4)-C(15)	46.5(10)	C(4)-C(3)-C(12)-C(16)	43(2)
S(1)-N(1)-C(1)-C(2)	0.5(14)	C(2)-C(3)-C(12)-C(16)	-141.0(13)
S(1)-N(1)-C(1)-C(6)	179.3(11)	C(4)-C(3)-C(12)-C(13)	-132.9(15)
S(1)-N(2)-C(2)-C(1)	0.7(14)	C(2)-C(3)-C(12)-C(13)	43.3(19)
S(1)-N(2)-C(2)-C(3)	-179.9(11)	C(16)-C(12)-C(13)-C(14)	-6.5(19)
N(1)-C(1)-C(2)-N(2)	-0.8(17)	C(3)-C(12)-C(13)-C(14)	169.4(13)
C(6)-C(1)-C(2)-N(2)	-179.7(12)	C(15)-N(4)-C(14)-C(13)	2(2)
N(1)-C(1)-C(2)-C(3)	179.7(12)	Re(1A)-N(4)-C(14)-C(13)	-171.9(11)
C(6)-C(1)-C(2)-C(3)	0.8(19)	C(12)-C(13)-C(14)-N(4)	4(2)
N(2)-C(2)-C(3)-C(4)	177.8(14)	C(14)-N(4)-C(15)-C(16)	-3(2)
C(1)-C(2)-C(3)-C(4)	-3(2)	Re(1A)-N(4)-C(15)-C(16)	170.1(10)
N(2)-C(2)-C(3)-C(12)	1(2)	N(4)-C(15)-C(16)-C(12)	0(2)

C(13)-C(12)-C(16)-C(15)	4.7(19)	Br(1)-Re(1)-C(20)-O(4)	13(53)
C(3)-C(12)-C(16)-C(15)	-171.3(13)	C(19A)-Re(1A)-C(17A)-O(1A)	-54(36)
C(18)-Re(1)-C(17)-O(1)	126(43)	C(18A)-Re(1A)-C(17A)-O(1A)	38(36)
C(19)-Re(1)-C(17)-O(1)	35(43)	C(20A)-Re(1A)-C(17A)-O(1A)	95(42)
C(20)-Re(1)-C(17)-O(1)	-149(38)	N(4)-Re(1A)-C(17A)-O(1A)	-145(36)
N(3)-Re(1)-C(17)-O(1)	-59(43)	Br(1A)-Re(1A)-C(17A)-O(1A)	128(36)
Br(1)-Re(1)-C(17)-O(1)	-145(43)	C(19A)-Re(1A)-C(18A)-O(2A)	153(25)
C(19)-Re(1)-C(18)-O(2)	-169(19)	C(20A)-Re(1A)-C(18A)-O(2A)	-115(25)
C(17)-Re(1)-C(18)-O(2)	100(19)	C(17A)-Re(1A)-C(18A)-O(2A)	63(25)
C(20)-Re(1)-C(18)-O(2)	-77(19)	N(4)-Re(1A)-C(18A)-O(2A)	-19(34)
N(3)-Re(1)-C(18)-O(2)	-1(23)	Br(1A)-Re(1A)-C(18A)-O(2A)	-28(25)
Br(1)-Re(1)-C(18)-O(2)	13(19)	C(18A)-Re(1A)-C(19A)-O(3A)	-115(47)
C(18)-Re(1)-C(19)-O(3)	-54(19)	C(20A)-Re(1A)-C(19A)-O(3A)	154(47)
C(17)-Re(1)-C(19)-O(3)	36(19)	C(17A)-Re(1A)-C(19A)-O(3A)	-27(47)
C(20)-Re(1)-C(19)-O(3)	-144(19)	N(4)-Re(1A)-C(19A)-O(3A)	64(47)
N(3)-Re(1)-C(19)-O(3)	127(19)	Br(1A)-Re(1A)-C(19A)-O(3A)	85(51)
Br(1)-Re(1)-C(19)-O(3)	39(32)	C(19A)-Re(1A)-C(20A)-O(4A)	80(45)
C(18)-Re(1)-C(20)-O(4)	103(53)	C(18A)-Re(1A)-C(20A)-O(4A)	-11(45)
C(19)-Re(1)-C(20)-O(4)	-167(53)	C(17A)-Re(1A)-C(20A)-O(4A)	-69(55)
C(17)-Re(1)-C(20)-O(4)	18(60)	N(4)-Re(1A)-C(20A)-O(4A)	172(45)
N(3)-Re(1)-C(20)-O(4)	-73(53)	Br(1A)-Re(1A)-C(20A)-O(4A)	-102(45)

Symmetry transformations used to generate equivalent atoms: #1 -x+2,-y+1,-z+1

Appendix ten: 2D NMR data

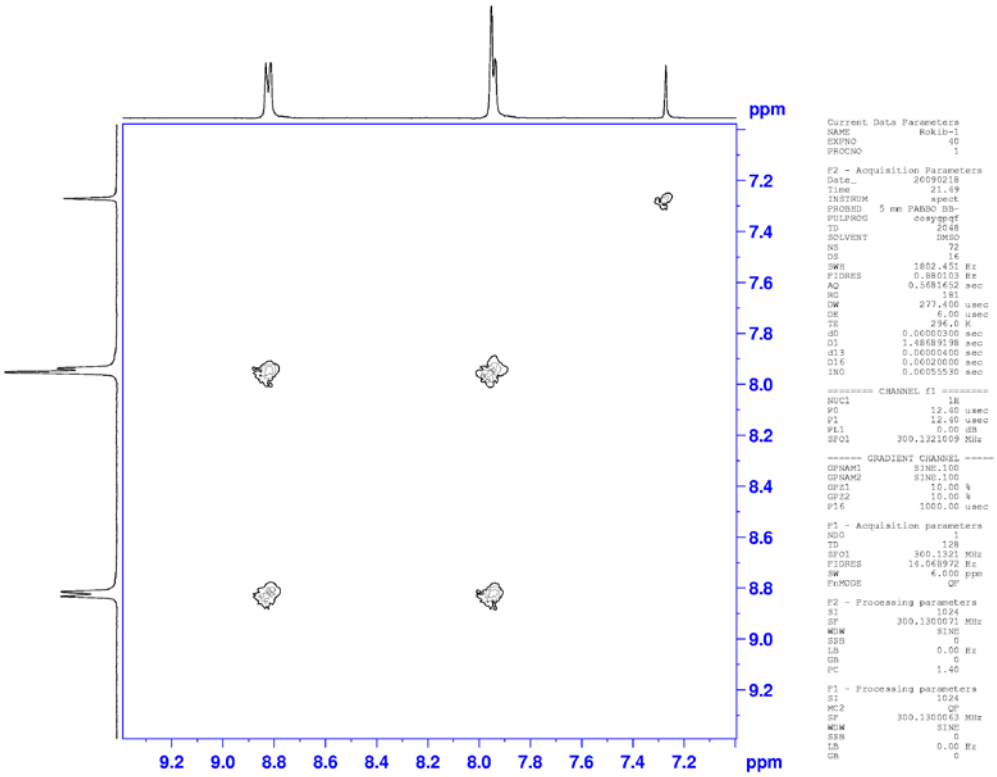

Figure A 10.1 COSY of **9**

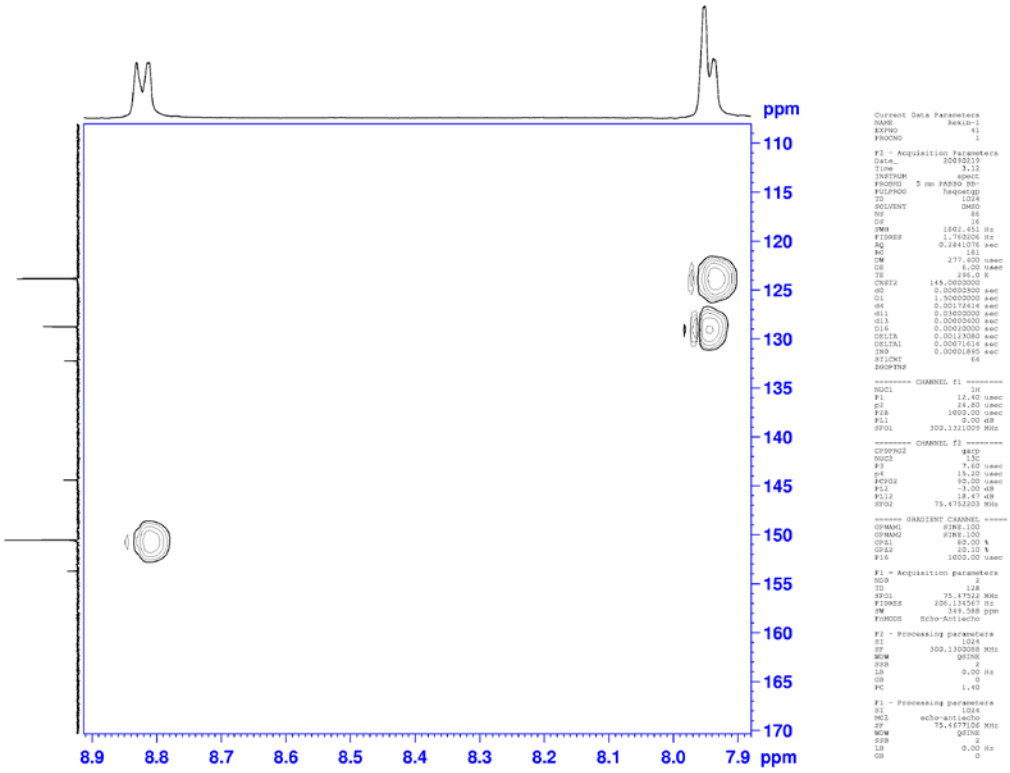

Figure A 10.2 HSQC of **9**

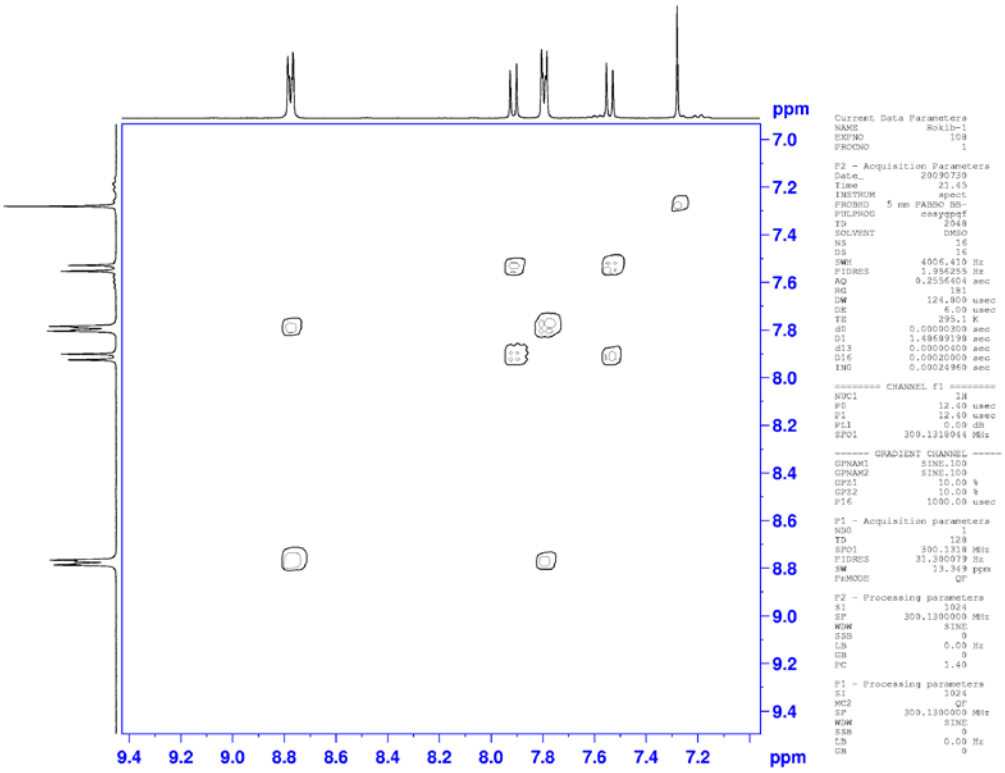

Figure A 10.3 COSY of **10**

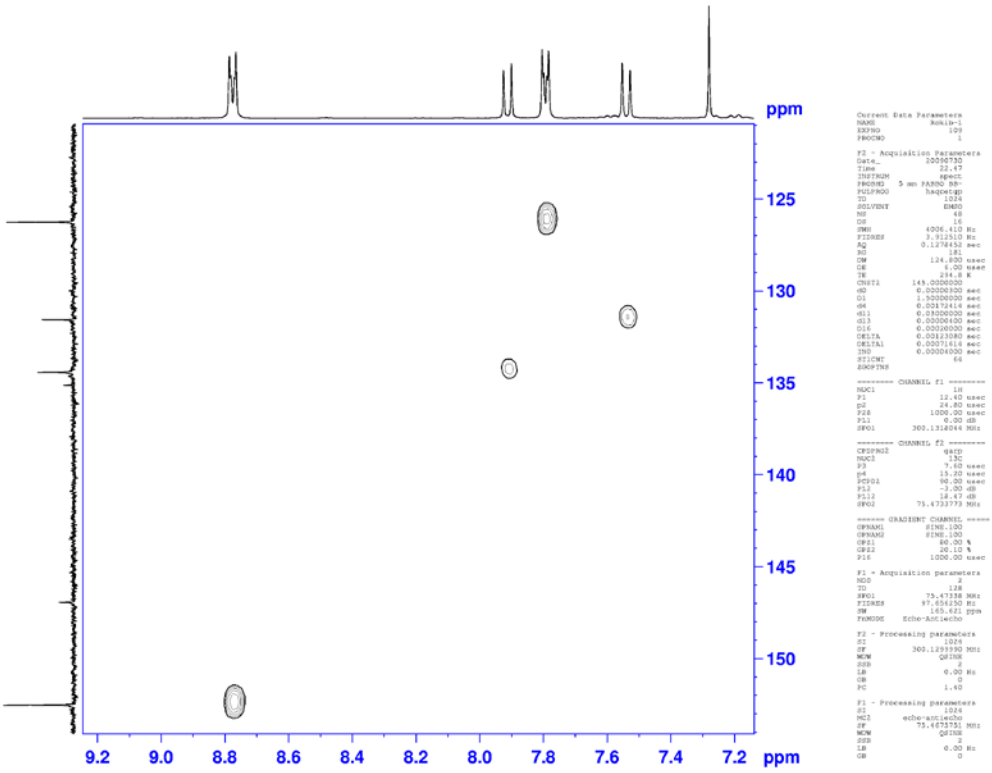

Figure A 10.4 HSQC of **10**

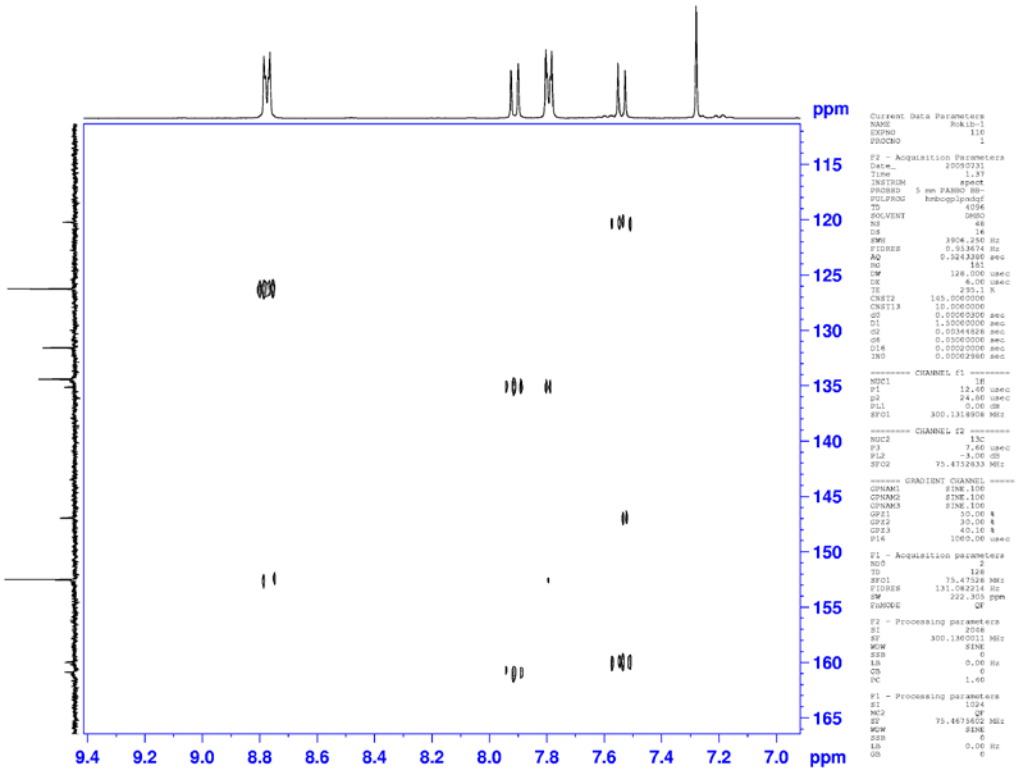

Figure A 10.5 HMBC of **10**

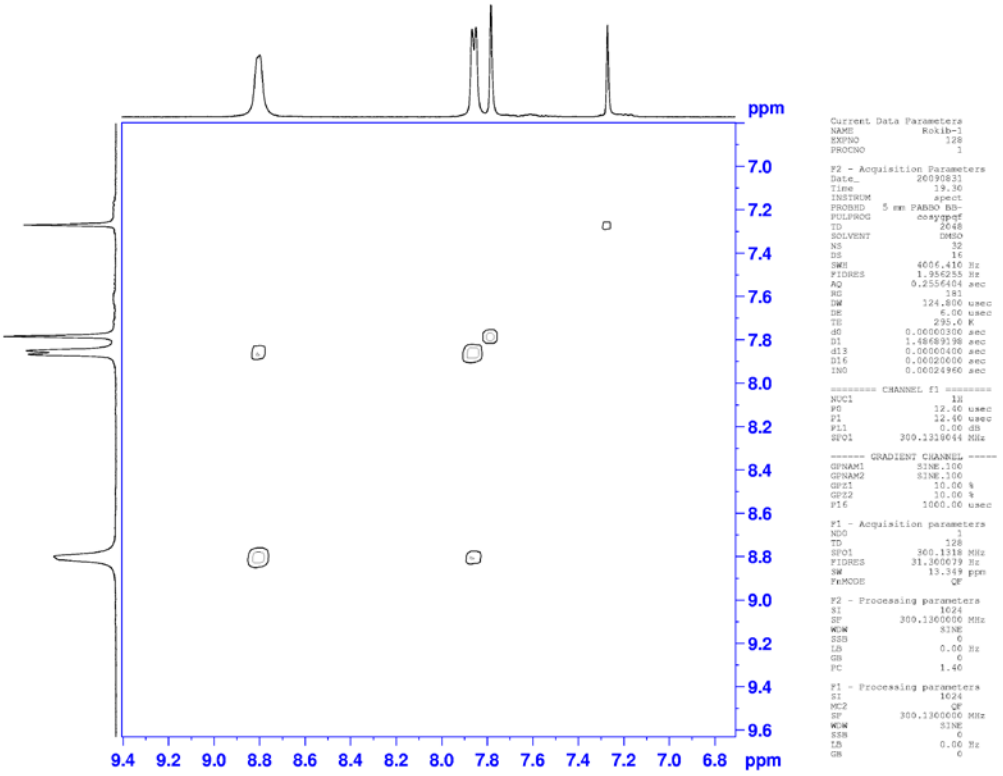

Figure A 10.6 COSY of **11**

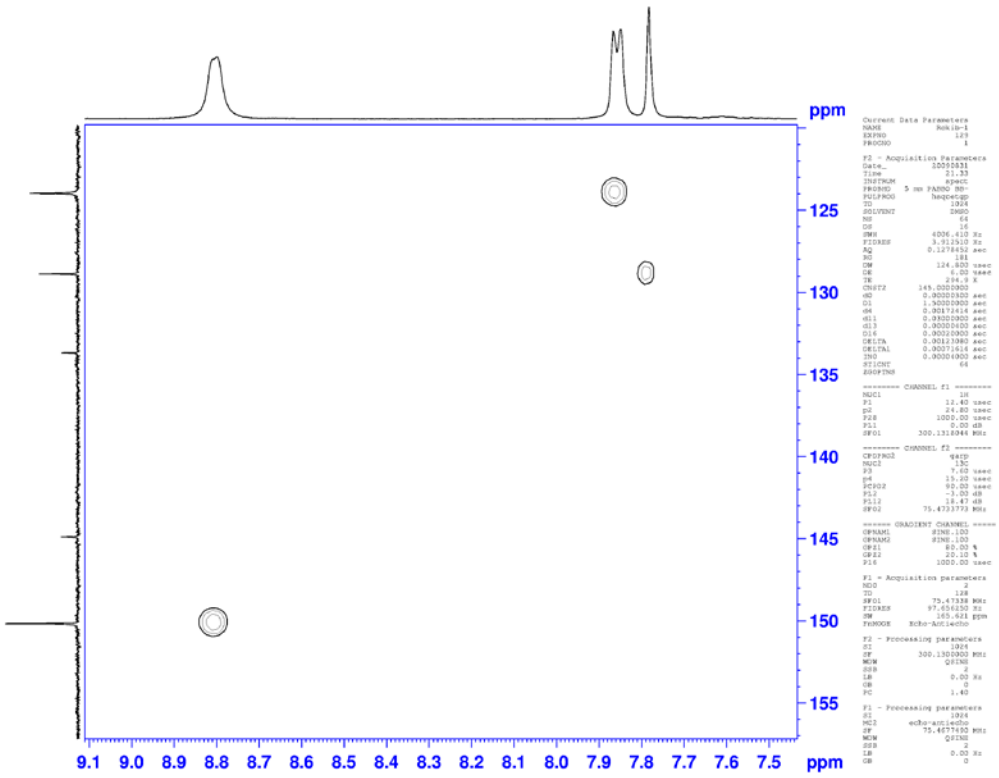

Figure A 10.7 HSQC of **11**

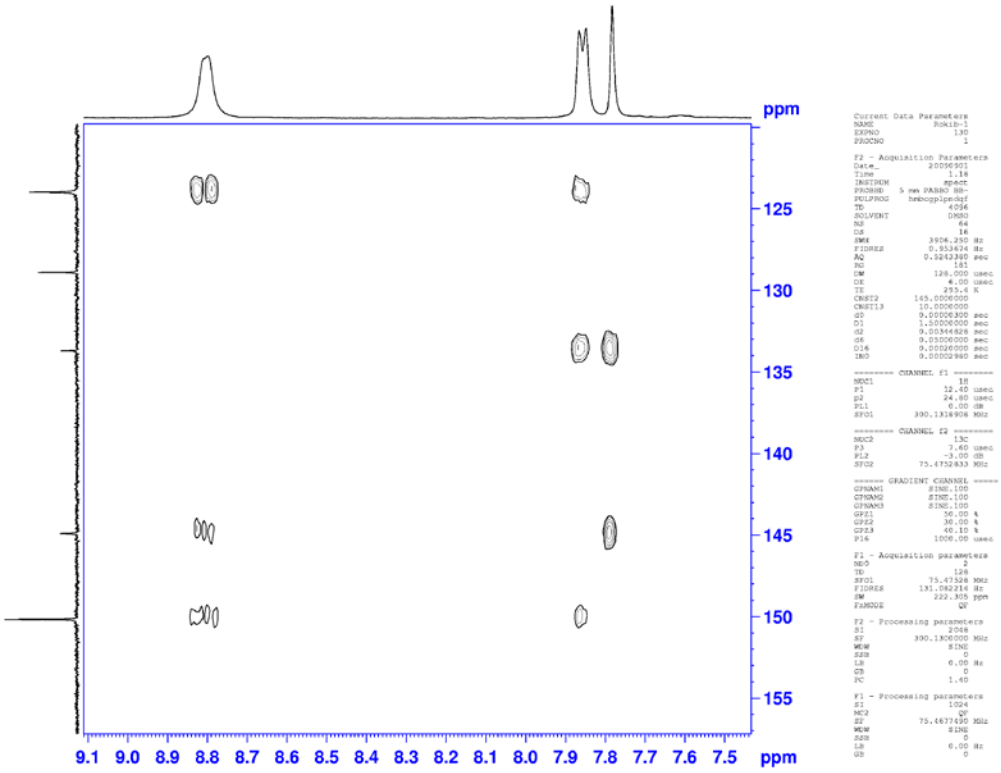

Figure A 10.8 HMBC of **11**

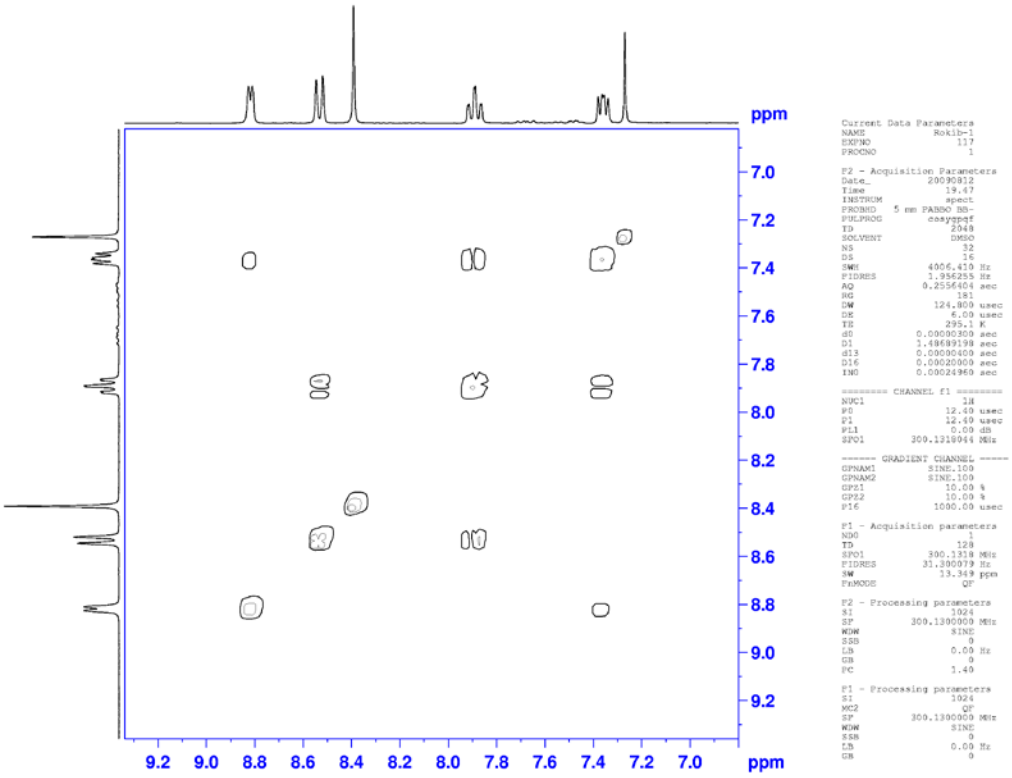

Figure A 10.9 COSY of **13**

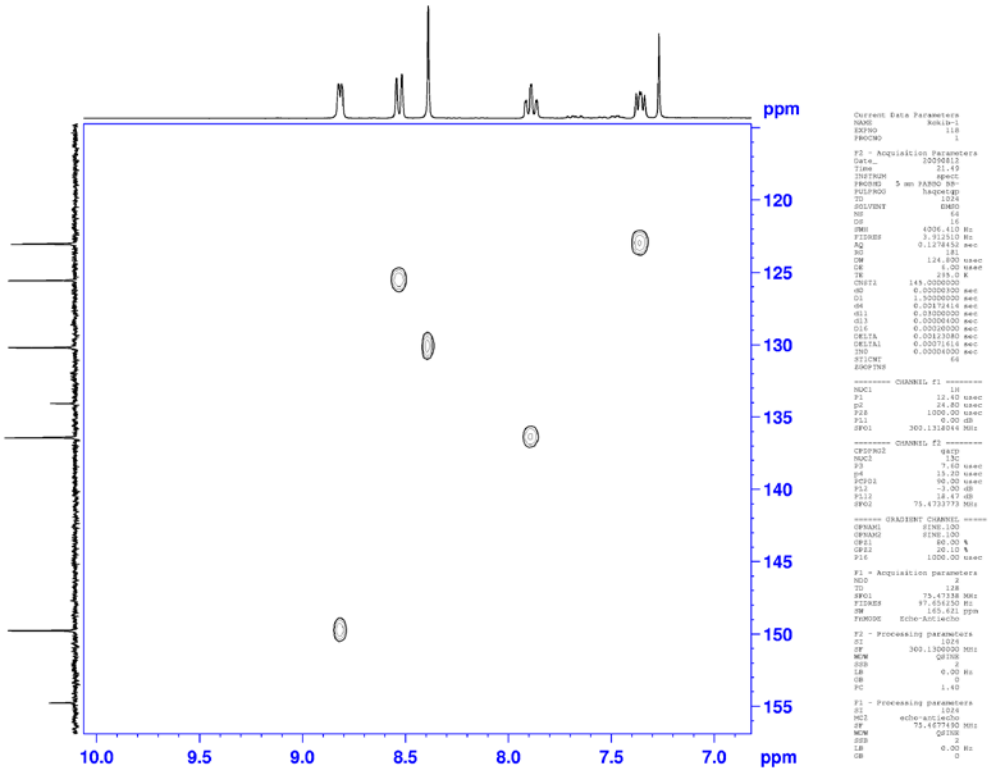

Figure A 10.10 HSQC of **13**

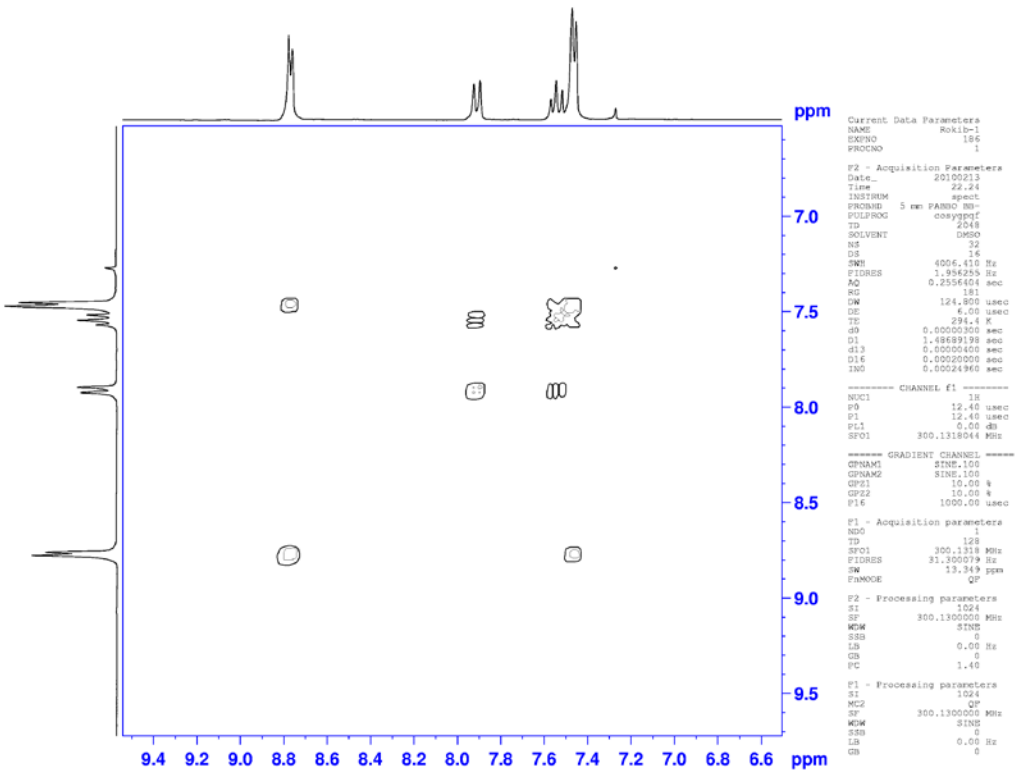

Figure A 10.11 COSY of **16**

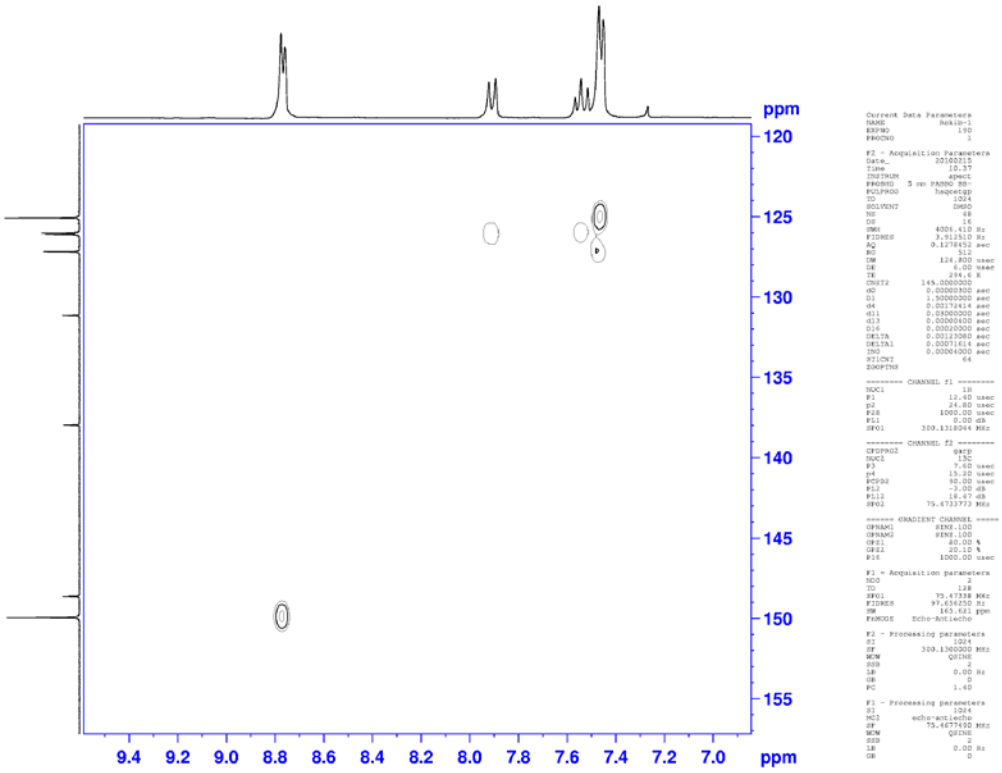

Figure A 10.12 HSQC of **16**

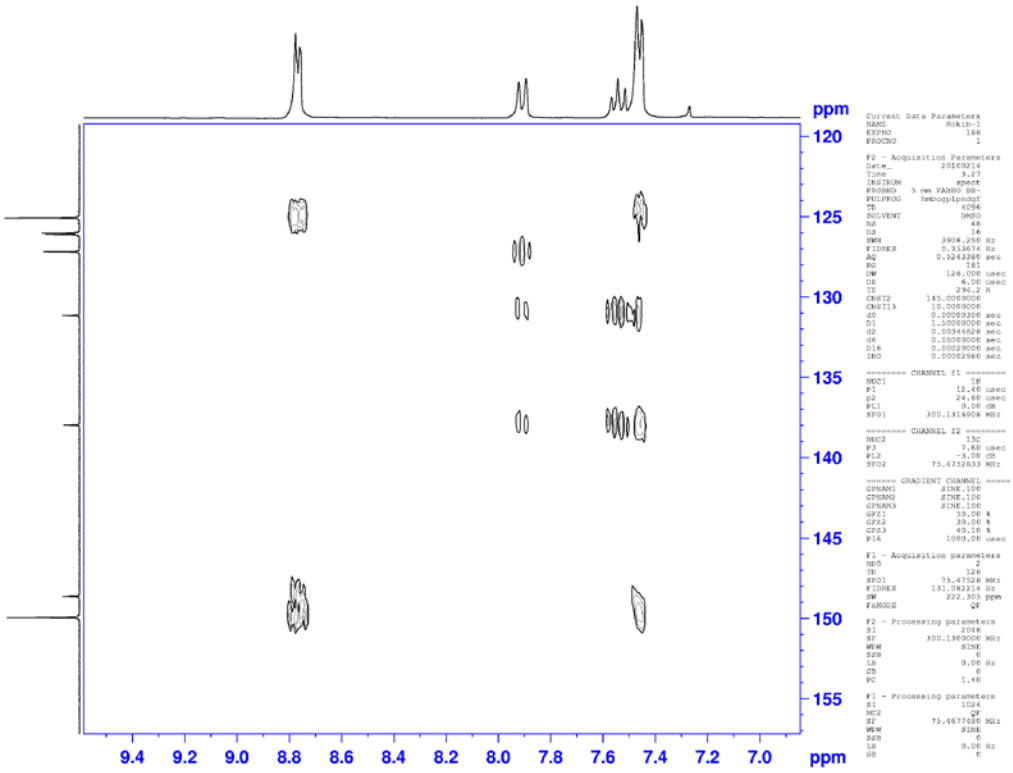

Figure A 10.13 HMBC of **16**

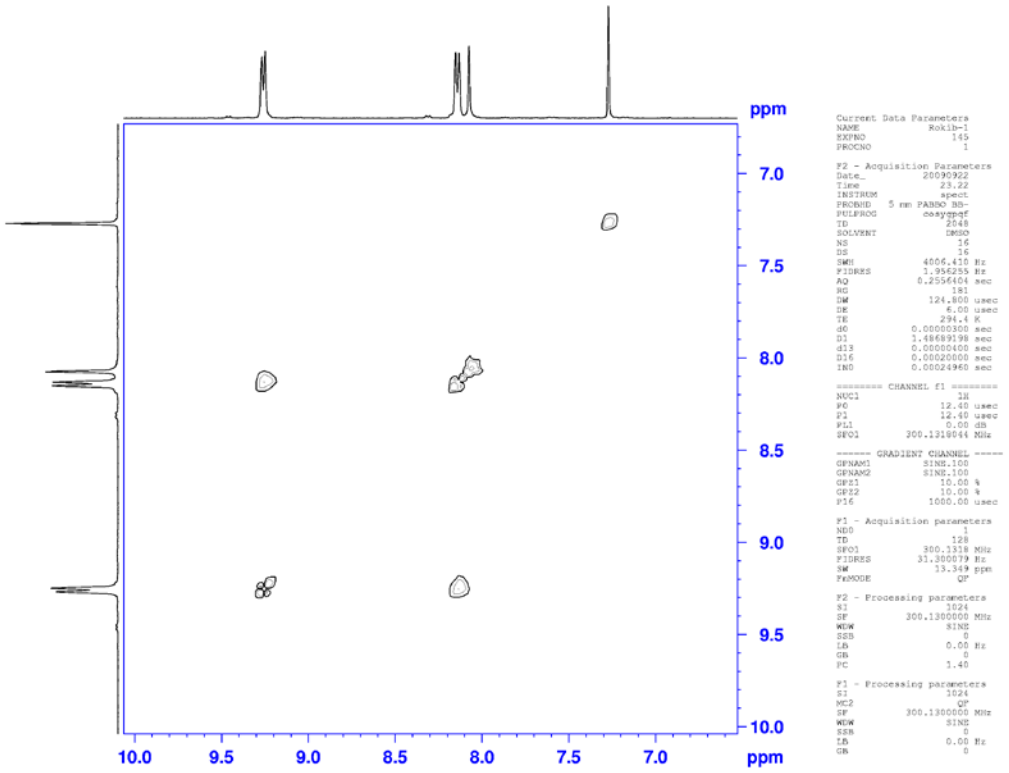

Figure A 10.14 COSY of **19**

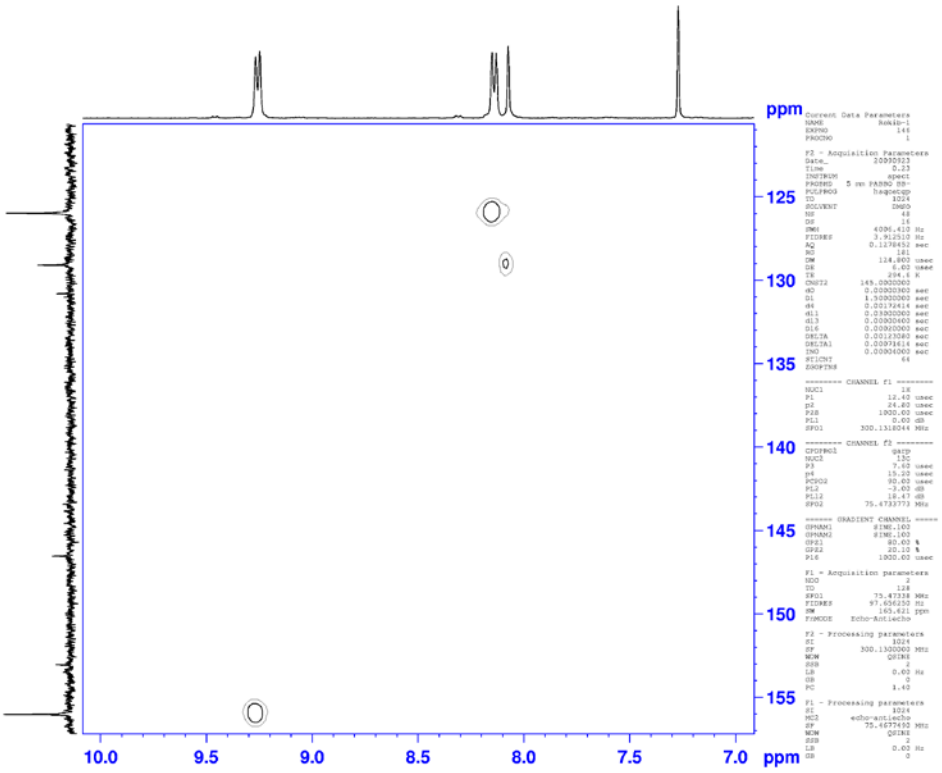

Figure A 10.15 HSQC of **19**

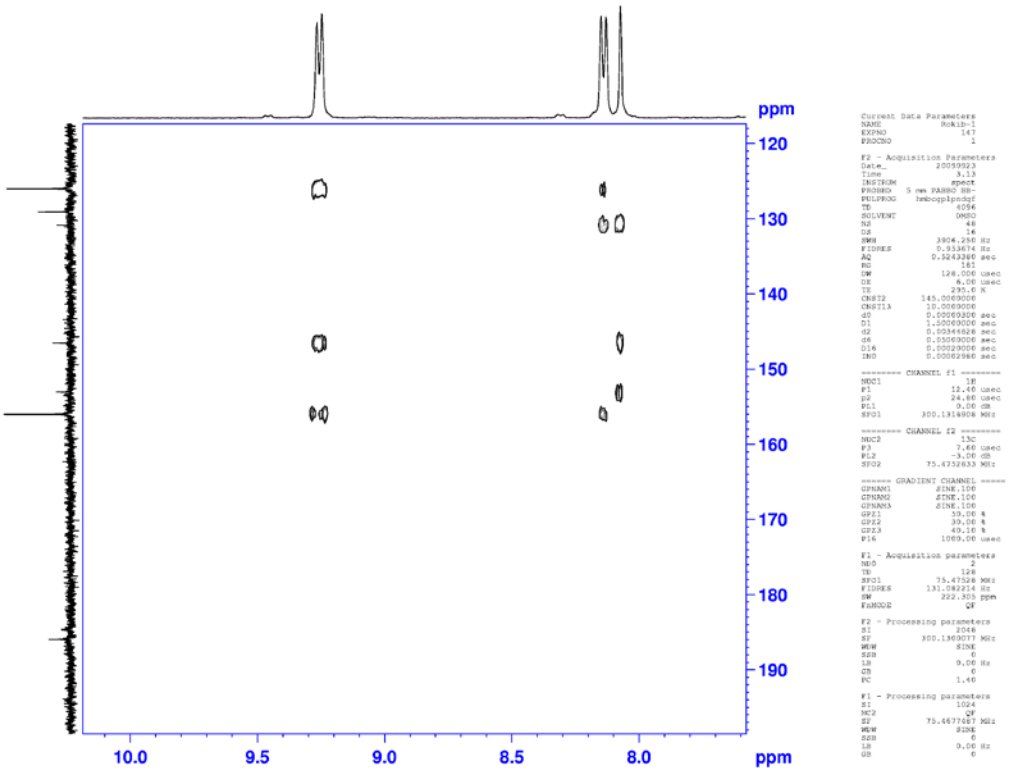

Figure A 10.16 HMBC of **19**

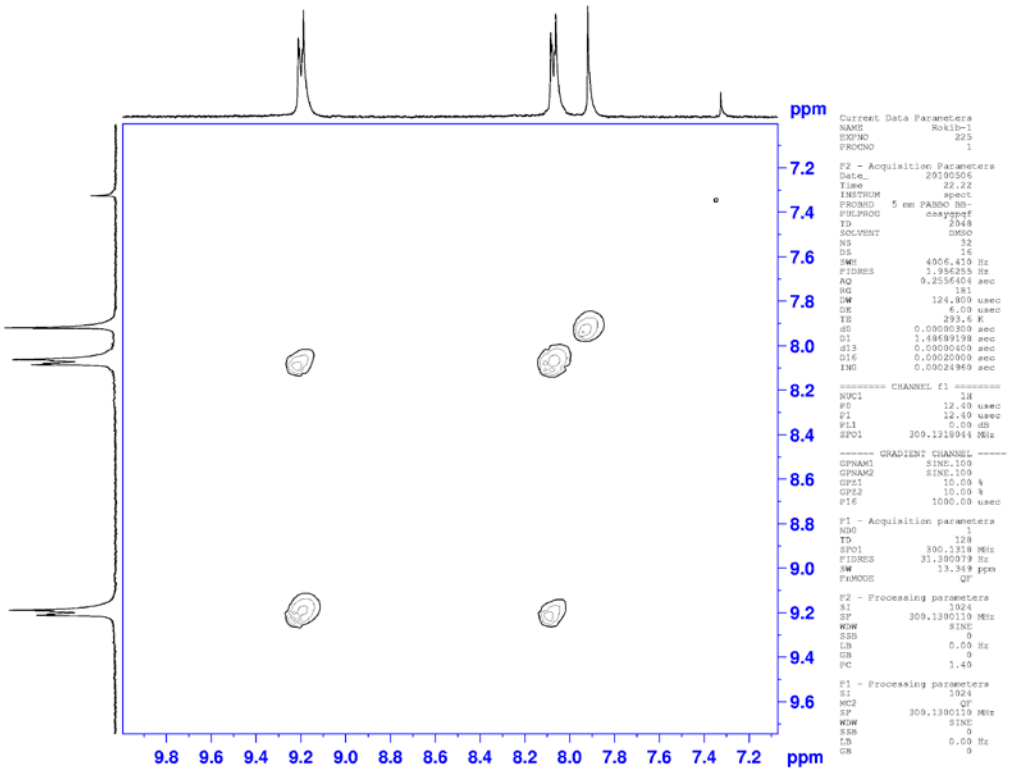

Figure A 10.17 COSY of **20**

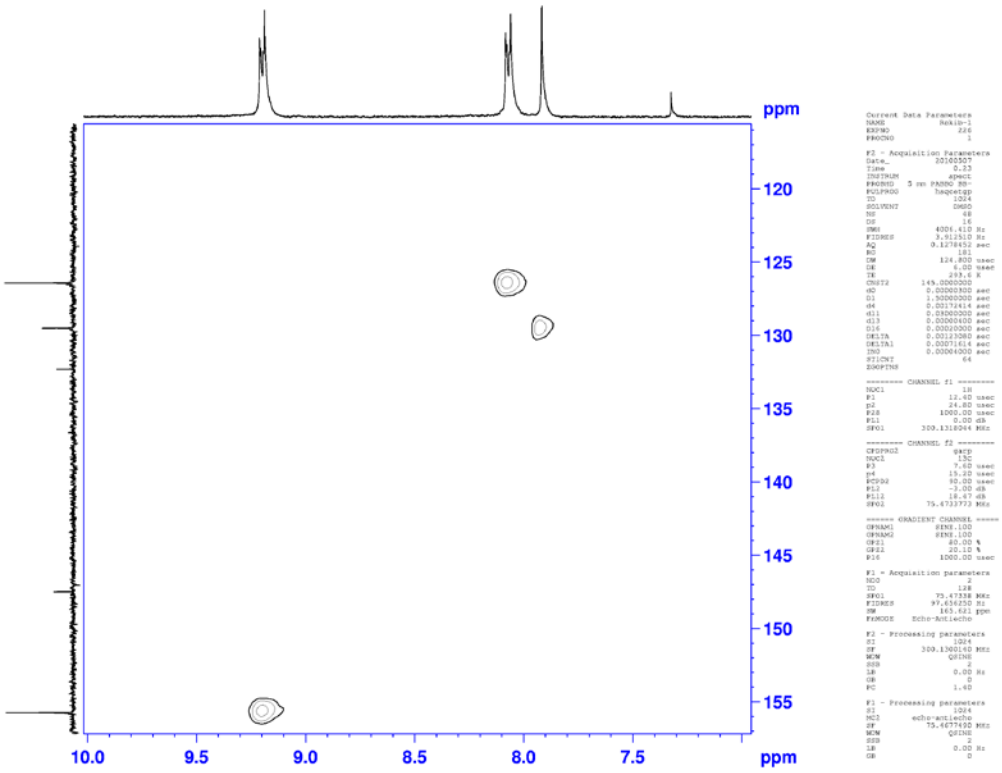

Figure A 10.18 HSQC of **20**

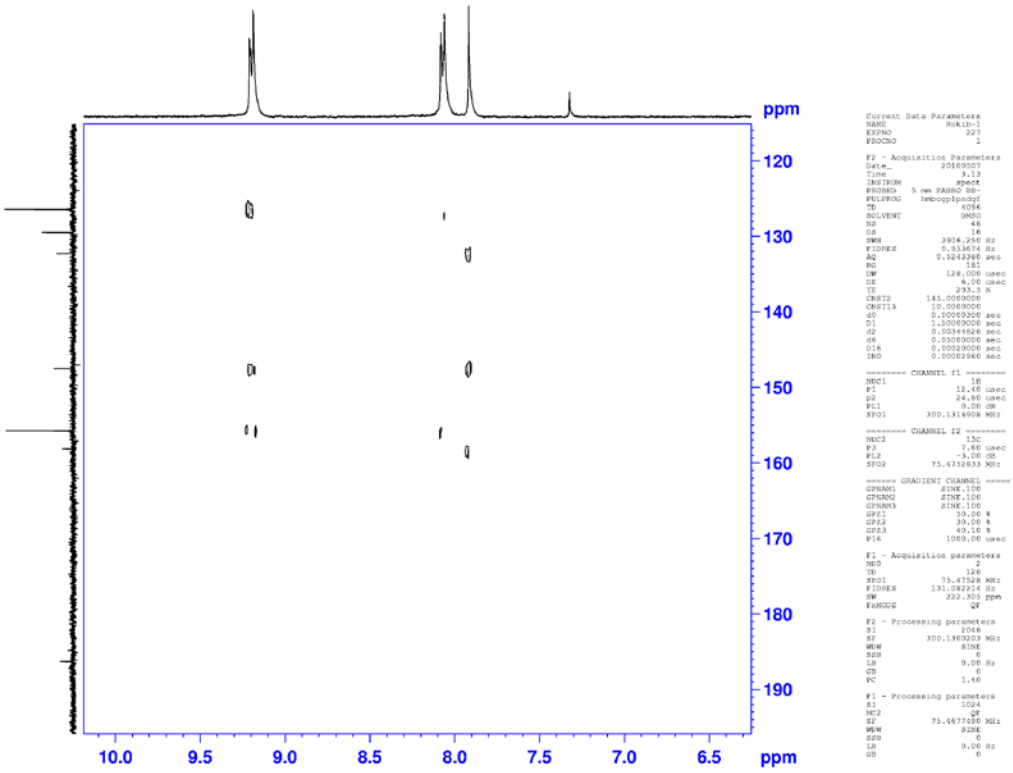

Figure A 10.19 HMBC of **20**

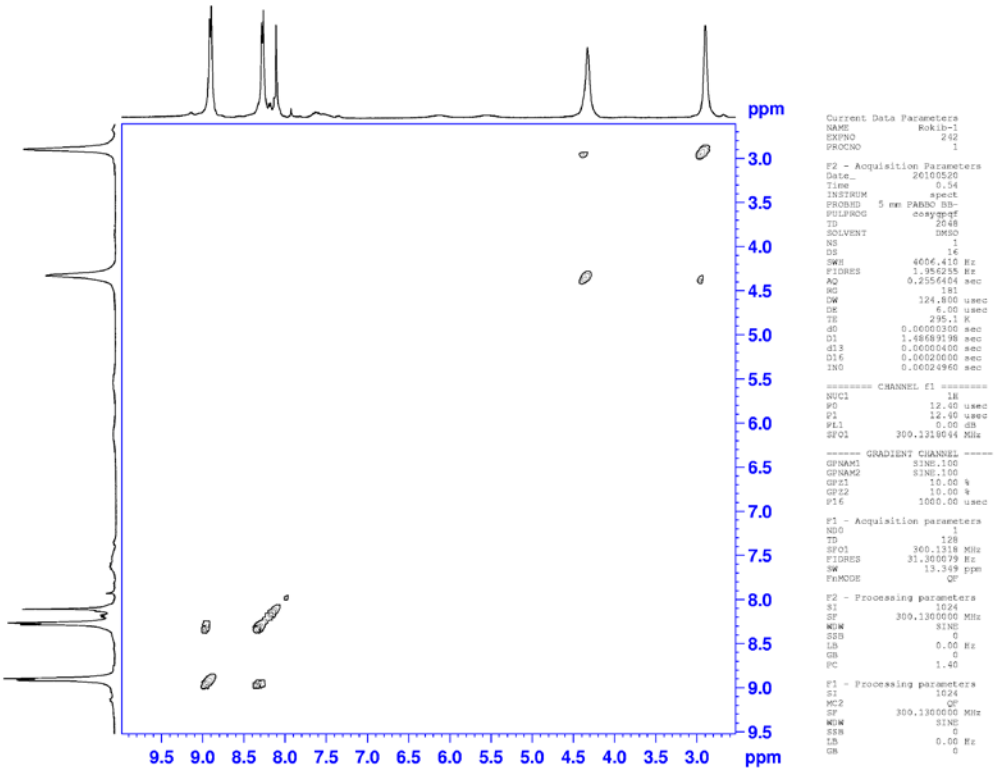

Figure A 10.20 COSY of **23**

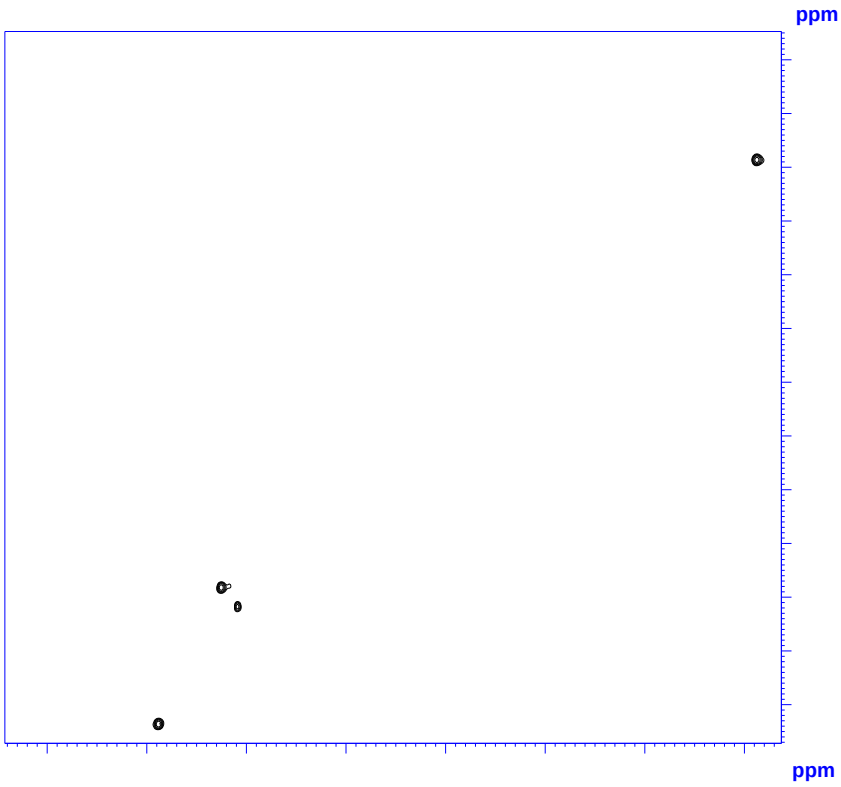

Figure A 10.21 HSQC of **23**

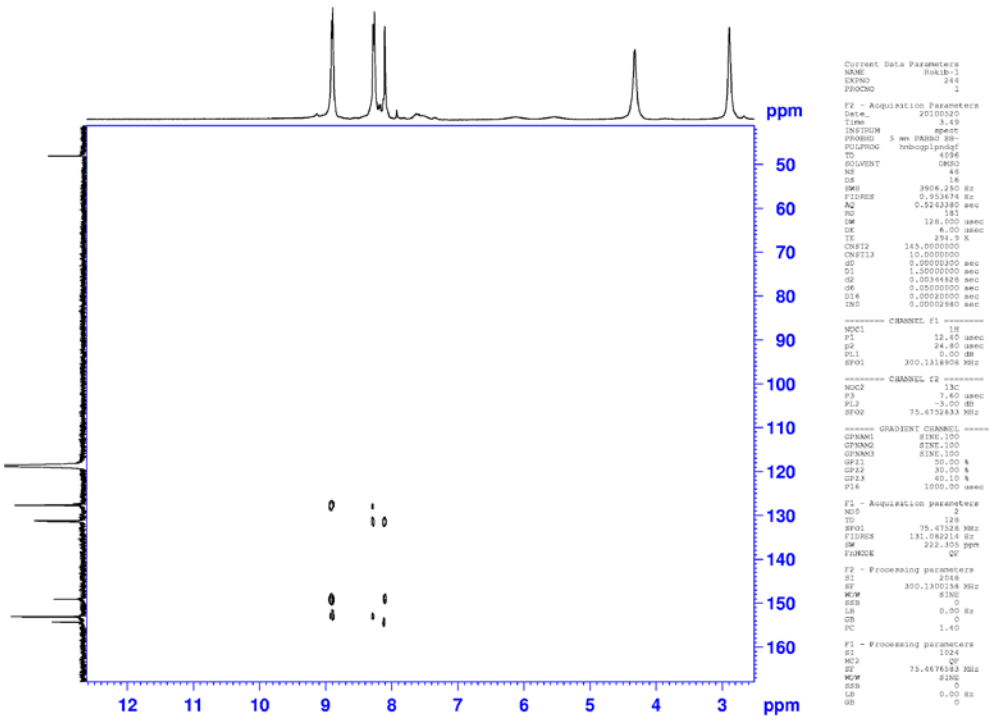

Figure A 10.22 HMBC of **23**

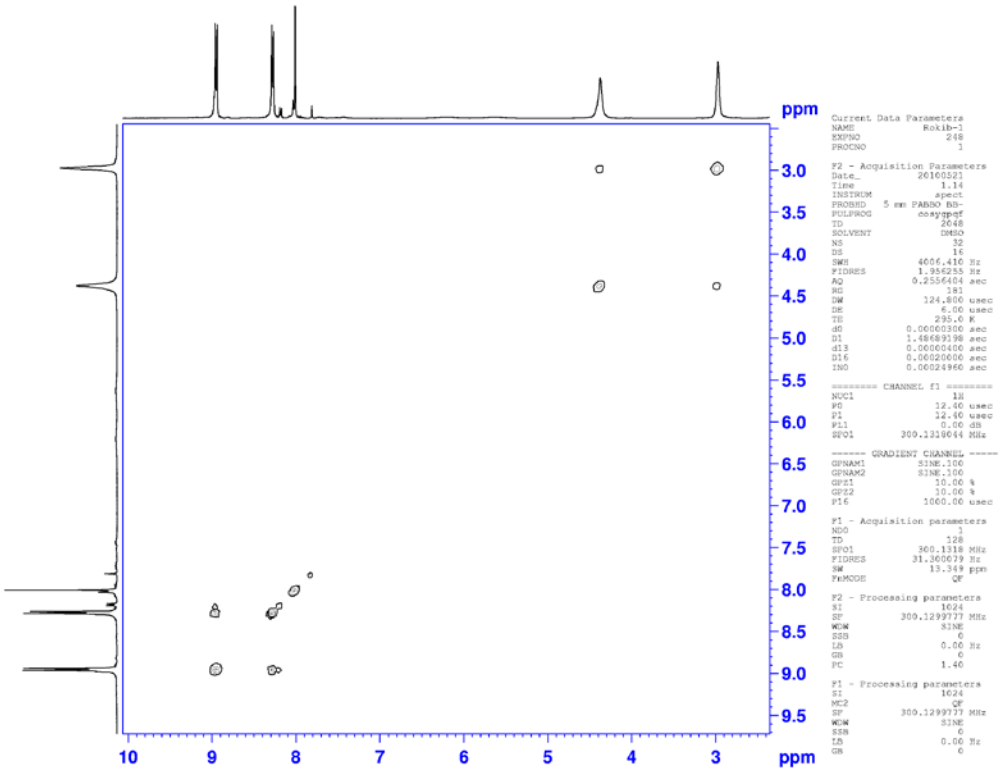

Figure A 10.23 COSY of **24**

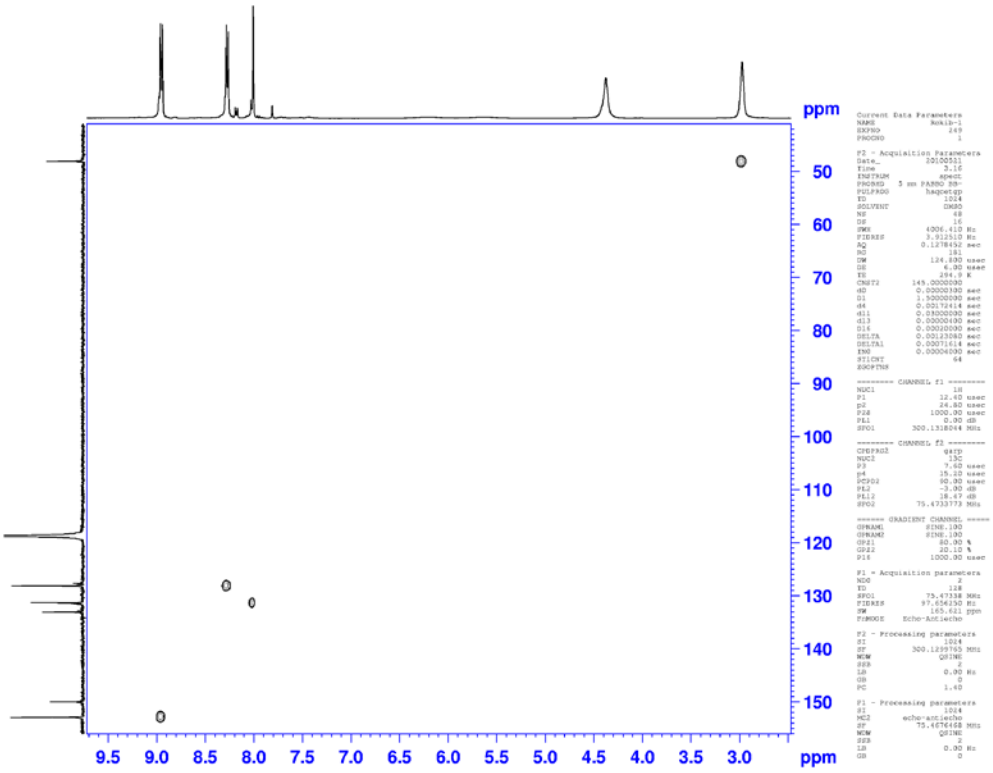

Figure A 10.24 HSQC of **24**

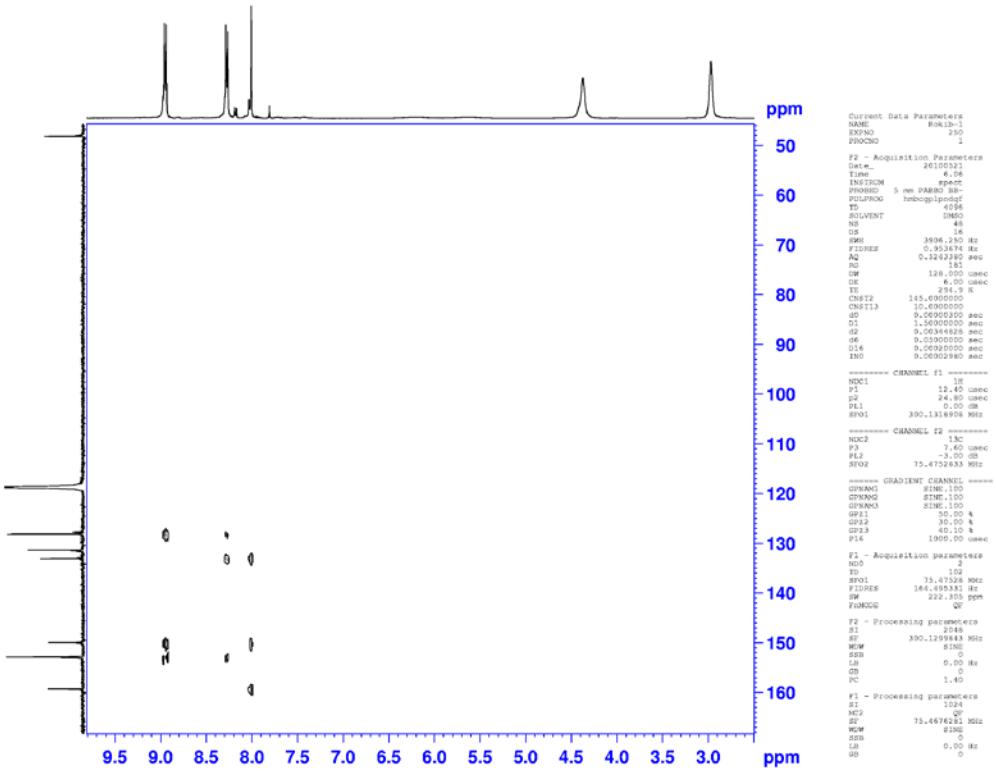

Figure A 10.25 HMBC of **24**